THE UNIVERSITY OF QUEENSLAND

AUSTRALIA

Characterising moisture within unbound granular pavements using multi-offset Ground Penetrating Radar

Wayne Bernard Muller

BEng., GCEng.

A thesis submitted for the degree of Doctor of Philosophy at

The University of Queensland in 2016

School of Civil Engineering

Abstract

Moisture has a significant influence on the performance and durability of unbound granular (UBG) pavements with thin bituminous surfacings, which form the vast majority of all-weather Australian roads. Techniques for measuring pavement moisture content are therefore important to quantify its influence on structural performance, enable early detection of problem areas, and to assess the condition of flood-affected pavements. Conventional techniques, however, require invasive probes or physical sampling which are impractical for large-scale investigations. Ground Penetrating Radar (GPR) techniques show promise, yet existing methods achieve only qualitative estimates, involve simplifications that limit accuracy or require complicated or laborious data analysis. The aim of this research was to develop a semi-automated approach using multi-offset GPR to quantitatively estimate the moisture content and depth of UBG pavement layers while maintaining data analysis simplicity.

The research made use of a new type of 3-dimensional (3D) GPR technology able to continuously collect ground-coupled multi-offset gathers across the road while travelling at up to traffic speeds. To enable development of analysis methods prior to equipment completion, numerical simulations were used to model the expected response for typical pavement configurations. These data were used to test a semi-automated approach using interface tracking and conventional multi-offset geophysical analysis methods. They were also used to develop two novel self-correcting analysis techniques, Interface Matching (IM) and Ray-path Modelling (RM), which use migration and tomographic approaches, respectively.

A permittivity characterisation approach, later called modified free-space (MFS), was also adapted for laboratory characterisation of UBG materials. It was used to calibrate petro-physical relations for these materials that enable pavement moisture estimates from the GPR measurements. As the MFS approach departs from conventional free-space methods, numerical modelling and a series of laboratory experiments were used to assess measurement accuracy and to determine the influence of sample edges, aspect ratio, and depth and antenna separation on the measurements. These investigations demonstrated that the MFS approach was suitable using the proposed equipment, sample sizes and for the range of relative permittivity values likely to be encountered. It also produced results that compared well with established apparatus over the frequency range relevant to pavement GPR.

Measurements using this approach were also compared with conventional time-domain reflectometry (TDR) and common-offset GPR measurements of moisture-varying and density-varying UBG samples. The comparison showed similar results for most samples, although TDR reported lower relative permittivity values for drier and lower-density materials.

Upon completion of the 3D GPR equipment, a revised analysis approach called Ray-path Modelling-Semblance (RM-S) was developed. It was used to analyse multi-offset measurements collected along a recently-constructed site to predict the depth, relative permittivity and volumetric moisture content of UBG pavement layers. The predictions were validated by comparing to physical measurements of layer depth and moisture content along the site, which showed a good correlation. Moisture variability along the site and over time was determined by comparing predictions from a scan collected at the end of construction and another approximately 11 months later. The comparison showed that the permittivity of upper layers was relatively consistent along the site at the time of construction and that lower pavement layers had a greater permittivity. By the time of the second scan the permittivity differential between upper and lower layers had reduced along most of the site, however in places the permittivity increased due to moisture ingress. These temporal trends compared well with results determined using embedded TDR sensors and common-offset GPR measurements of buried reflectors, although the new approach produced somewhat higher permittivity estimates. The analysis approach was also shown to be repeatable, based on a comparison of layer depth and moisture predictions determined for consecutive scans along the site.

The key outcomes of the research were the successful development and validation of:

1. A new semi-automated analysis approach using multi-offset GPR that enables quasi-continuous determination of the depth, relative permittivity and moisture content of UBG pavement layers; and

2. A novel laboratory technique for permittivity characterisation of civil engineering materials at GPR frequencies that enables measurement of larger samples and is better suited to measuring coarse-grained, compacted and un-bonded pavement materials compared to existing alternatives.

Declaration by author

This thesis is composed of my original work, and contains no material previously published or written by another person except where due reference has been made in the text. I have clearly stated the contribution by others to jointly-authored works that I have included in my thesis.

I have clearly stated the contribution of others to my thesis as a whole, including statistical assistance, survey design, data analysis, significant technical procedures, professional editorial advice, and any other original research work used or reported in my thesis. The content of my thesis is the result of work I have carried out since the commencement of my research higher degree candidature and does not include a substantial part of work that has been submitted to qualify for the award of any other degree or diploma in any university or other tertiary institution. I have clearly stated which parts of my thesis, if any, have been submitted to qualify for another award.

I acknowledge that an electronic copy of my thesis must be lodged with the University Library and, subject to the policy and procedures of The University of Queensland, the thesis be made available for research and study in accordance with the Copyright Act 1968 unless a period of embargo has been approved by the Dean of the Graduate School.

I acknowledge that copyright of all material contained in my thesis resides with the copyright holder(s) of that material. Where appropriate I have obtained copyright permission from the copyright holder to reproduce material in this thesis.

Publications during candidature

Peer-reviewed journal papers (accepted or published)

Muller, W.B. and Scheuermann A., Optimising a modified free-space permittivity characterisation method for civil engineering applications. Journal of Geophysics and Engineering 13(2):S9-S18, April 2016.

Muller, W.B., Permittivity characterisation of unbound granular pavement materials using a modified free-space approach. Transportation Research Record: Journal of the Transportation Research Board, 2578, 93-101, Washington, D.C., 2016.

Muller, W.B., Bhuyan H. and Scheuermann A., A comparison of modified free-space (MFS), GPR and TDR techniques for permittivity characterisation of unbound granular pavement materials, Near Surface Geophysics, 14(6), 537-550, December 2016.

Peer-reviewed conference proceedings papers

Muller, W.B., Scheuermann A. and Reeves B., Quantitative moisture measurement of road pavements using 3D noise-modulated GPR. 14th International Conference on Ground Penetrating Radar (GPR) 2012, Shanghai. IEEE, 517-523, June 2012.

Muller, W.B. and Dérobert X. A comparison of phase-shift and one-port coaxial cell permittivity measurements for GPR applications. 7th International Workshop of Advanced GPR (IWAGPR-2013), Nantes. IEEE, 1-6, July 2013

Muller, W.B., Self-correcting pavement layer depth estimates using 3D multi-offset ground penetrating radar (GPR). 15th International conference on Ground Penetrating Radar (GPR-2014), Brussels. IEEE, 887-892, July 2014.

Publications included in this thesis

Muller, W.B., Scheuermann, A. and Reeves, B., Quantitative moisture measurement of road pavements using 3D noise-modulated GPR, Proceedings of the 14th International Conference on Ground Penetrating Radar (GPR) 2012, Shanghai. IEEE, 517-523, June 2012 – incorporated as Attached Paper I.

Contributor	Statement of contribution
Muller, W.B.	Undertook simulations (100%) Developed analysis approach (100%) Designed laboratory experiments (60%) Wrote the paper (100%)
Scheuermann, A.	Designed laboratory experiments (10%)
Reeves, B.	Designed laboratory experiments (30%)

Muller, W.B., Self-correcting pavement layer depth estimates using 3D multi-offset ground penetrating radar (GPR), Proceedings of the 15th International conference on Ground Penetrating Radar (GPR-2014), Brussels. IEEE, 887-892, July 2014 – incorporated as Attached Paper II.

Contributor	Statement of contribution
Muller, W.B.	Undertook simulations (100%) Developed and applied analysis techniques (100%) Wrote the paper (100%)

Muller, W.B. and Dérobert, X. A comparison of phase-shift and one-port coaxial cell permittivity measurements for GPR applications, 7th International Workshop of Advanced GPR (IWAGPR-2013), Nantes. IEEE, 1-6, July 2013 – incorporated as Attached Paper III.

Contributor	Statement of contribution
Muller, W.B.	Designed laboratory experiments (80%) Undertook simulations (100%) Wrote the paper (90%)
Dérobert, X.	Designed laboratory experiments (20%) Wrote and edited paper (10%)

Muller W.B. and Scheuermann A., Optimising a modified free-space permittivity characterisation method for civil engineering applications, Journal of Geophysics and Engineering 13(2):S9-S18, April 2016 – incorporated as Attached Paper IV.

Contributor	Statement of contribution
Muller, W.B.	Undertook simulations (100%) Designed laboratory experiments (90%) Wrote the paper (90%)
Scheuermann, A.	Designed laboratory experiments (10%) Wrote and edited paper (10%)

Muller, W.B., Permittivity characterisation of unbound granular pavement materials using a modified free-space approach, Transportation Research Record: Journal of the Transportation Research Board, 2578, 93-101, Washington, D.C., 2016 – incorporated as Attached Paper V.

Contributor	Statement of contribution
Muller, W.B.	Undertook laboratory measurements (100%) Analysed the data and results (100%) Wrote the paper (100%)

Muller W.B., Bhuyan H. and Scheuermann A., A comparison of modified free-space (MFS), GPR and TDR techniques for permittivity characterisation of unbound granular pavement materials, Near Surface Geophysics, 14(6), 537-550, December 2016 – incorporated as Attached Paper VI.

Contributor	Statement of contribution
Muller, W.B.	Designed laboratory experiments (85%) Undertook measurements and analysed results (80%) Wrote the paper (90%)
Bhuyan H.	Designed laboratory experiments (5%) Undertook measurements and analysed results (20%) Wrote and edited paper (5%)
Scheuermann, A.	Designed laboratory experiments (10%) Wrote and edited paper (5%)

Contributions by others to the thesis

Dr Alexander Scheuermann advised on all aspects of the work, in particular in relation to the electrical properties of materials and TDR.

Dr Bryan Reeves designed and operated the NM-GPR equipment used in the thesis and provided extensive guidance and suggestions regarding the use of GPR and electrical engineering aspects of the work.

Statement of parts of the thesis submitted to qualify for the award of another degree

None.

Acknowledgements

Many of the papers included in this thesis were funded by the Department of Transport and Main Roads, primarily under its National Asset Centre of Excellence (NACOE) program of research.

I wish to express a special thanks to current and former colleagues including Peter Evans, Ian Reeves, Julie Mitchell, Phil Tweddell and Tony Platz who all played roles in supporting the research, and colleagues at the ARRB Group, in particular Carlos Rial and Dr Erik Denneman, who also supported the work.

I would like to express my gratitude to my very helpful advisors Dr-Ing Alexander Scheuermann, Dr Bryan Reeves and Professor Peter Dux. I also wish to thank those at Radar Portal Systems who provided technical support and access to the radar equipment used for much of this work, in particular John Reeves, Grigory Gaborenko and Simon Long. A very special thanks also goes to Dr Monica Behrend who provided many helpful suggestions to improve and finalise the thesis.

Most of all, thanks to my very supportive wife Margaret; and my very active and clever children – Emily, Christian and Elizabeth. As promised Margaret, the Ph.D. is done; now it's your turn…

Disclaimer – The views expressed in this thesis are solely those of the author and do not represent the policy or position of the Department of Transport and Main Roads, the ARRB Group Ltd or other organisations named.

Keywords

Road pavement moisture, unbound granular road pavements, ground penetrating radar, permittivity characterisation, time domain reflectometry.

Australian and New Zealand Standard Research Classifications (ANZSRC)

ANZSRC code: 090505 Infrastructure Engineering and Asset Management, 70%

ANZSRC code: 040401 Electrical and Electromagnetic Methods in Geophysics, 30%

Fields of Research (FoR) Classification

FoR code: 0905 Civil Engineering, 70%

FoR code: 0404 Geophysics, 30%

Table of Contents

List of Figures

List of Abbreviations

2D	Two-dimensional
3D	Three-dimensional
ADC	Analog to digital converter
ARRB	Australian Road Research Board
CMP	Common midpoint
CRIM	Complex refractive index model
DOS	Degree of saturation
EM	Electromagnetic
ETS	Equivalent time sampling
FDTD	Finite difference time domain
FWD	Falling weight deflectometer
GPR	Ground penetrating radar
GSSI	Geophysical Survey Systems Incorporated
HMA	Hot mix asphalt
IM	Interface matching (an analysis method proposed in Paper II)
LTPP	Long-term pavement performance
Matlab	Mathematical software and programming language by Mathworks Inc.
MFS	Modified free-space
NM-GPR	Noise modulated ground penetrating radar
NMO	Normal move-out
RM	Ray-path modelling (an analysis method proposed in Paper II)

RM-S	Ray-path modelling – semblance (an analysis method proposed in Paper VII)
TDR	Time-domain reflectometry
TSD	Traffic speed deflectometer
UBG	Unbound granular
VNA	Vector network analyser
WARR	Wide angle reflection and refraction

1 INTRODUCTION

This research investigates an approach combining multi-offset 3-dimensional (3D) ground penetrating radar (GPR) and a laboratory characterisation technique to continuously calibrate depth estimates and predict the permittivity and moisture content of pavement layers constructed from unbound granular (UBG) materials. The research is presented as a report incorporating a number of peer-reviewed papers and one submitted paper written during candidature. It comprises:

1. An outline of the problem statement, necessity for the work, the research question and the thesis objectives, methodology and structure;
2. A review of the current state of knowledge;
3. A summary of incorporated papers; and
4. A discussion of potential uses of the developed techniques and avenues for future research.

1.1 Problem statement

Granular pavements are widely used within Australia, with more than 80% of sealed roads consisting of unbound flexible pavements with thin bituminous surfacings (Bodin and Kraft, 2015, Oliver, 1999, Martin, 2005, Vuong and Hazell, 2003). These pavements are typically moisture-sensitive (Charlier et al., 2009, Saevarsdottir and Erlingsson, 2013) and as a result it is imperitive to prevent and predict moisture infiltration as this affects pavement serviceabilty and longevity (Vuong, 2007). The potential impact of moisture on these roads is considerable. During 2010 and 2011, flooding damaged more than 9,100 kilometres of Queensland state-controlled roads (The International Bank for Reconstruction and Development and Queensland Reconstruction Authority, 2011) equating to approximately 27.3% of the total length of that network. Repair costs exceeded $7 billion, of which 85% was road-related and was primarily due to pavement damage, loss of seals and culvert damage (Pritchard, 2013). In addition to damage caused directly by floodwaters, heavy vehicle loading of wet and weakened roads was a major contributor to pavement distress, an example of which is shown in Figure 1-1.

Figure 1-1: Heavy vehicle damage of a flood-affected UBG pavement on the Thompson Developmental road, Queensland, May 2011 (Photo credit: Steve Hogan, Department of Transport and Main Roads)

A challenge faced by engineers after these events is to determine when to re-open roads to heavy vehicles. However, the extent of moisture ingress and its effect on structural capacity are not quick or easy to determine using conventional methods. Physical sampling is slow, damages the road and only provides spot measurements at a small number of locations. Embedded sensors measure at fixed locations and need to be installed ahead of time, making it difficult and thus impractical to achieve good spatial coverage across expansive road networks. Furthermore, conventional surface-based deflection measurement techniques used to monitor the influence of moisture on structural capacity – for example the falling weight deflectometer (FWD) – require the test apparatus to remain stationary during measurement. As a result, data collection is slow and thus similarly problematic when long lengths of road need to be assessed quickly after flood events.

Another area where knowledge of pavement moisture conditions is often lacking is during the investigation of pavement failures. Moisture is regularly implicated as a cause or contributor to pavement distress. This is often inferred from visual assessments of surface distress, with perhaps a few physical samples for verification. More extensive sampling would be prudent, but the likely benefits must be weighed against the additional costs and the potential disruption to road users. As a result, at times it may be difficult, expensive or impractical to determine the true extent of subsurface moisture ingress. Furthermore, it may be unclear where to position a limited number of physical samples to target the worst-affected or most representative locations.

More complete knowledge of pavement moisture conditions would also be useful for new UBG pavements, as an excessive degree of saturation (DOS) within these materials can result in premature failure under traffic loading (Austroads, 2003). An example of DOS-related pavement failures along a recently rehabilitated pavement is shown in Figure 1-2. As current methods of detecting DOS issues rely on random physical sampling, problem areas can easily be overlooked prior to covering with the next pavement layer or bitumen sealing and opening to traffic.

Figure 1-2: Early pavement failure due to excessive moisture and elevated DOS conditions within UBG layers of a recently rehabilitated pavement. Warrego Highway near Dalby, Queensland (Photo credit: Dave Christian, Department of Transport and Main Roads)

1.2 Motivation, objectives and methodology

This research was motivated by the need for an improved non-invasive and quantitative method of measuring pavement moisture and by an opportunity to achieve this, along with improved layer depth estimates, using a new type of three-dimensional (3D) ground penetrating radar (GPR) technology.

GPR is a non-destructive technique that operates by emitting electromagnetic (EM) waves into the road and measuring the travel time and strength of reflections returning from pavement layer interfaces and other features. The velocity of EM waves within pavement layers primarily depends on the relative permittivity (ε_r) of these materials, which can vary along or across the road or vertically within layers. The term 'relative' indicates that the permittivity is being reported as a dimensionless ratio compared to the properties of free-space. The 'apparent permittivity' is that calculated from the velocity of EM waves propagating within these materials (Huisman et al., 2003). While relative permittivity is more properly described as a complex and frequency-dependent parameter, for many practical GPR applications it is approximated as a real and fixed value, also called the 'dielectric constant'. For brevity, in this thesis the term 'permittivity' is used to denote the 'apparent relative permittivity', except where noted.

GPR has been used for decades within the road industry for a range of pavement applications (Saarenketo and Scullion, 2000, Maser, 1996). A common use is to estimate the depth of pavement layers (Al-Qadi and Lahouar, 2005, Loizos and Plati, 2007, Plati and Loizos, 2012). These estimates need to be calibrated to account for variations in pavement permittivity and the EM wave velocity to achieve accurate results (Lahouar et al., 2002, Loizos and Plati, 2007, Evans et al., 2007). The permittivity of pavement layers is strongly influenced by water content (Plati and Loizos, 2013, Rmeili and Scullion, 1997). As a result, techniques used to calibrate layer-depth predictions can also be used to estimate in situ pavement moisture conditions (Grote et al., 2005, Plati and Loizos, 2013, Al-Qadi et al., 2004). While some calibration methods require prior knowledge of layer thickness or assume homogenous layers, in most practical situations this information is unknown or the material properties vary, limiting the suitability of these techniques or the accuracy of the results.

An approach that avoids these particular issues is multi-offset GPR. It involves collecting measurements with transmitting and receiving antennas at a series of offsets (separations) at regular intervals along the road. The measurements are analysed using geophysical techniques similar to those used for seismic reflection to determine the depth of pavement layers and the velocity of EM waves within these materials based on the change of arrival time of layer interface reflections measured at different offsets. As the approach involves measuring through the full depth of layers, permittivity estimates using this approach represent an average and therefore account for material inhomogeneity (Al-Qadi et al., 2003, Lahouar et al., 2002). A disadvantage is that data collection and analysis is more involved compared to the conventional common-offset GPR approach, which involves collecting measurements using one antenna pair with a fixed separation. While a number of studies have used pairs of common-offset antennas to enable rapid collection of a simplified multi-offset dataset (Leng and Al-Qadi, 2014, Hamrouche and Saarenketo, 2014, Lahouar et al., 2002) or have used 3D GPR systems to achieve a greater number of antenna offsets or wider coverage across the road lane (Zhao and Al-Qadi, 2016, De Pue et al., 2016), most have used air coupled antennas. This is problematic as surface-refraction issues limit calibration sensitivity (Davis et al., 1994).

At the commencement of research a new type of 3D Noise-Modulated GPR (NM-GPR) equipment was planned by Brisbane-based company Radar Portal Systems. The equipment is the second-generation (Reeves, 2014) of an existing NM-GPR technology (Reeves, 2010a). One benefit of the updated equipment is the ability to collect a series of adjacent partially-overlapping ground-coupled multi-offset measurements. These measurements can be collected quasi-continuously while travelling along the road at up to traffic speeds.

Considering the need for a more flexible and responsive method of measuring pavement moisture along with a reliable means of determining layer depths, the opportunity presented by local GPR development, and the anticipated challenge of analysing numerous measurements collected using this new equipment, a research question was posed:

> Can a semi-automatic approach be developed to analyse multi-offset measurements collected using this new 3D GPR to enable quantitative moisture predictions and reliable layer depth estimates for UBG pavements that is also simple to use?

To answer this question, a number of investigations needed to be undertaken and challenges had to be addressed. For one, the updated GPR equipment had not yet been built so there was no data on which to test or develop automated analysis methods. Furthermore, it was unclear if multi-offset measurements collected on typical pavements using the proposed antenna layout would be suitable for reliable automated analysis. The multi-fold (overlapping) nature of measurements presented the possibility of using calibration approaches based on tomographic or migration methods (Stork, 1992), however these needed to be developed and tested on realistic data.

Laboratory measurements were also required to calibrate petro-physical relations for UBG materials. These are used to enable moisture content predictions from the multi-offset measurements of layer permittivity. The calibrations typically involve characterising the permittivity of samples prepared to a range of moisture conditions in the laboratory. However, available measurement techniques lacked precision, achieved small or uncertain sampling volumes or were otherwise unsuitable for assessing representative volumes of these materials. A free-space approach was identified as potentially suitable, but required modifications that might affect accuracy and validity of the measurements. A detailed laboratory assessment of this approach and comparison to results using established methods was therefore required.

Finally, once the analysis techniques had been developed and calibrations made they would need to be combined, adapted for use on real multi-offset data and applied in the field. The accuracy and reproducibility of layer depth, permittivity and moisture content predictions would then need to be assessed.

To address the research question and these challenges, the following objectives and methodology was established:

1. **Investigate and develop semi-automated multi-offset analysis methods:** Undertake numerical modelling to determine the multi-offset response for typical pavement structures. Use these simulations to develop and test semi-automated geophysical analysis methods. Assess the accuracy of the developed methods by comparing predictions of layer depth and permittivity to the modelled values.

2. **Develop and validate a laboratory characterisation method to calibrate petro-physical relations for UBG pavement materials:** Adapt the identified free-space permittivity characterisation approach for use on compacted UBG material samples. Assess the accuracy of the approach by comparing to results using established apparatus on materials with a range of permittivity values and by testing materials with known properties. Investigate aspects of the test setup that may influence the accuracy of results including sample thickness, aspect ratio, edge effects and near-field antenna effects. Undertake numerical modelling to better understand the nature of wave propagation within samples and apparatus. Compare permittivity results using this approach to those from conventional time-domain-reflectometry (TDR) and GPR travel time measurements for moisture-varying and density-varying UBG samples. Use the developed approach to determine an appropriate moisture-permittivity relation for UBG materials.

3. **Field trial and validate the developed approach to predict the moisture content, depth and permittivity of UBG pavement layers:** Adapt the developed multi-offset analysis methods for use in the field with the new NM-GPR equipment. Use the approach with moisture-permittivity relationships determined in the laboratory to predict the depth, permittivity and volumetric moisture content of UBG pavement layers along a test site. Validate predictions of layer depth and moisture by comparing to results of physical sampling. Compare permittivity predictions to results based on embedded TDR sensors and GPR measurements of diffraction hyperbolas of buried reflectors. Assess the reproducibility of results using the approach by comparing layer depth and moisture predictions for repeat runs along the site.

1.3 Thesis structure

1.3.1 Overview

This thesis consists of five chapters and one appendix. **Chapter 1** sets out the problem statement, research needs and motivation, research question, challenges, objectives, methodology and thesis structure. **Chapter 2** presents a literature review summarising the current state of knowledge. It discusses the influence of moisture on UBG pavements with thin bituminous surfacings and techniques to quantify the amount of moisture within and under the road and its influence on pavement structural response. To better understand electromagnetic (EM) moisture measurement techniques, an overview regarding the interaction of EM waves, soils and moisture is given. An overview of GPR technology, its use for pavement moisture measurement and the use of multi-offset techniques for this and other applications is then provided. TDR techniques and their use for pavement moisture monitoring are also discussed. A review of laboratory-based permittivity characterisation techniques is then presented, with a particular focus on free-space methods. Petro-physical models used to relate pavement permittivity and moisture content are also briefly discussed. **Chapter 3** presents an overview of the incorporated papers. It outlines the problem each paper set out to address along with the aims and main contributions to the research objectives of this study. **Chapter 4** discusses a number of potential applications for the developed techniques. These include use in combination with conventional TDR techniques to improve spatial coverage and use alongside the recently-developed traffic speed deflectometer (TSD) to achieve far more rapid and comprehensive pavement investigations. A number of avenues to further develop or improve the methods are also discussed. **Chapter 5** presents the conclusion to the thesis, providing an overview of the key research achievements. The referenced works are then listed, after which the seven incorporated papers are presented in **Appendix A**.

1.3.2 Paper topics and linkages

The incorporated papers primarily deal with the development of semi-automated multi-offset analysis methods; development, validation or use of the modified free-space (MFS) permittivity characterisation approach on compacted UBG and other materials; and the adaptation, implementation and validation of these methods for use in the field.

Papers I to VI have either been published or accepted for publication. Paper VII has been submitted to a journal for peer review. Figure 1-3 provides an overview of the main topics covered in each paper. It also illustrates how these contributions link together to meet the overall aim of the study – to develop a semi-automated method of predicting layer depth, permittivity and volumetric moisture content for UBG pavement layers using multi-offset 3D GPR while maintaining analytical simplicity.

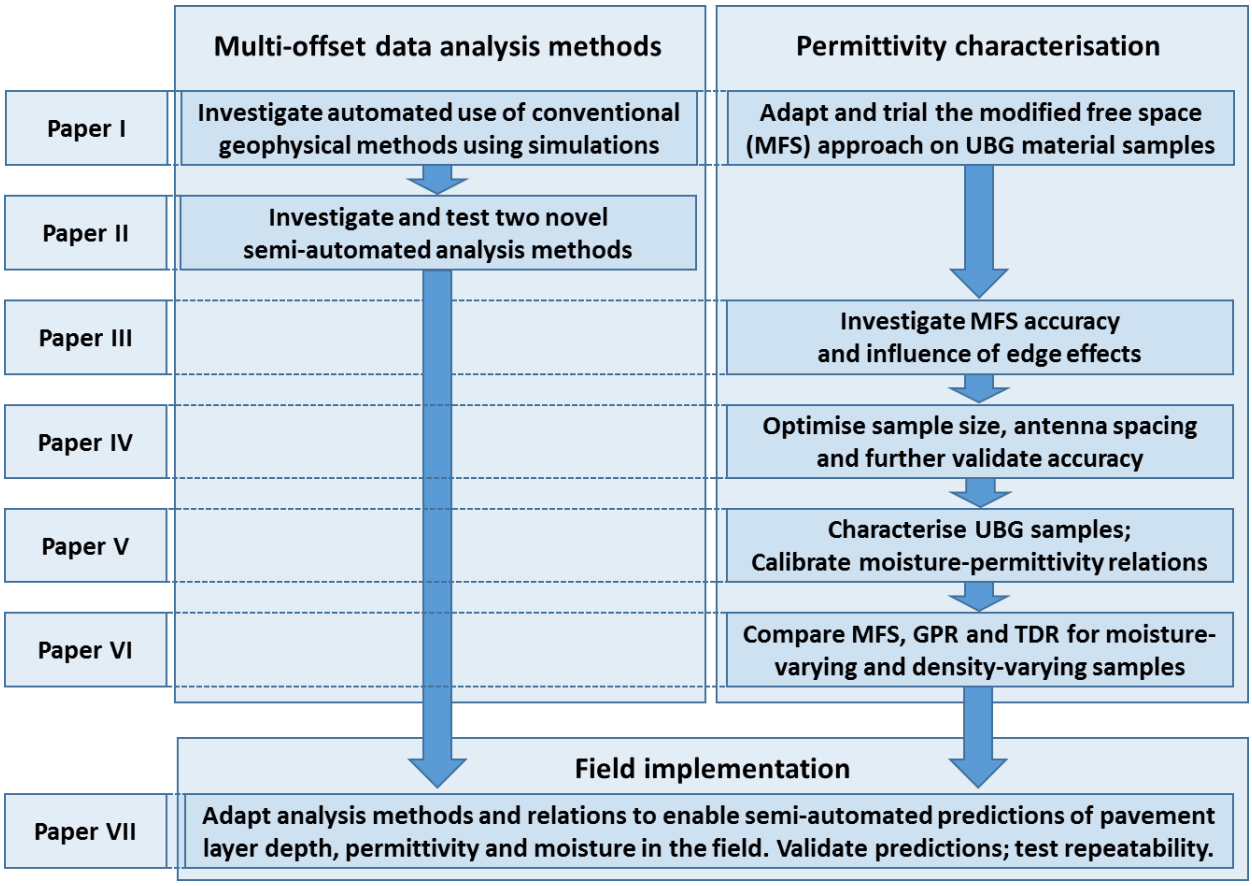

Figure 1-3: Linkages between incorporated papers to meet the research aim

2 MEASURING MOISTURE AND ITS INFLUENCE ON PAVEMENTS: A LITERATURE REVIEW

To better understand the influence of moisture on unbound granular (UBG) pavements with thin bituminous surfacings, Section 2.1 commences with an overview of its effects on the performance and durability of this pavement type. To quantify this influence, Section 2.2 discusses available techniques to measure moisture within and under the road and to detect changes in structural response due to moisture variations. Of available moisture-measurement methods, high-frequency electromagnetic (EM) techniques are particularly useful. To better understand these techniques, Section 2.3 provides an overview regarding the interaction of EM waves, water and soils. Ground penetrating radar (GPR) and time-domain reflectometry (TDR) are two such EM methods used in this thesis. An overview of GPR technology, equipment types and its use for moisture measurement is given in Section 2.4, with a particular focus on multi-offset techniques. An overview of TDR technology and its use for pavement moisture monitoring is given in Section 2.5. To relate these EM measurements to pavement moisture conditions, calibrations need to be developed in the laboratory by characterising material samples. Section 2.6 presents a review of available laboratory-based permittivity characterisation methods, with a focus on free-space techniques. Petro-physical relations used to describe the measured response are also discussed. Section 2.7 then summarises the main observations from the literature review.

2.1 Thin bituminous pavements and the influence of moisture

Low-cost thin bituminous pavements are widely used within Australia and elsewhere (Bodin and Kraft, 2015, Oliver, 1999, Martin, 2005, Vuong and Hazell, 2003). They typically consist of compacted UBG base and sub-base layers protected by a thin ‘chip seal’ or asphalt surfacing (see Figure 2-1). As unbound materials contain no binder they have no tensile strength, however can withstand shear due to friction which resists inter-particle slip and rotation (Thom, 2008). In addition to particle shape, size and frictional characteristics, the particle size distribution and packing also affect the shear strength, with well-compacted broadly-graded materials achieving greater strength by increasing the number of contact points and making failure planes more difficult to develop (Thom, 2008).

Figure 2-1: A typical thin bituminous pavement with UBG layers (Photo credit: Dave Christian, Department of Transport and Main Roads)

Moisture is nearly always the principal cause of problems in unbound materials and as a result measures need to be taken to keep the water content within suitable limits (Thom, 2008). During road construction the subgrade and pavement layers are constructed wet, typically at 90 - 95 % saturation to aid compaction (Thom, 2008). Later, when in use, high stresses due to vehicle loading are transmitted from the road surface into the unbound granular layers and the underlying subgrade materials (Charlier et al., 2009). If kept relatively dry, matric suction develops within the pore spaces of these materials due to meniscus effects at the water-air interface resulting in an increase of the effective stress (Dawson, 2009). The negative pore pressures that result are highly beneficial to the performance of the unbound material, however these benefits only accrue if the material contains a significant fine particle fraction (Thom, 2008). The measurable effect of these negative pore pressures is an apparent cohesion that is loading-rate dependent, however for most pavement engineering applications loading occurs too quickly for pore pressures to dissipate (Thom, 2008).

These effects and the corresponding influence on mechanical performance can be related to the material plasticity, a property that occurs within unbound materials containing a proportion of particles in the clay size range (<2 μm), which can be useful for distinguishing between moisture-sensitive materials and those that are not (Thom, 2008). Such small particles lead to low permeability and high suction but also a high equilibrium degree of saturation (Thom, 2008). The percentage of fines (particles <425 μm) within the material and their plasticity can also have a significant influence on shear strength, workability and stability of the unbound pavement material (Vuong et al., 2008). A material containing a high clay content, for example, may lead to instability and rutting, particularly when excess moisture is present (Vuong et al., 2008). On the other hand, it may be advantageous to add a fine plastic component to a crushed rock material to achieve a more suitable grading, improve cohesion, workability and reduce permeability of the compacted material (Vuong et al., 2008). As a result, it is often necessary to reach a compromise between having enough fines for some suction to occur, but not so much as to prevent drainage (Thom, 2008) or lead to other problems.

While the pavement moisture content should be relatively constant for sealed and well-maintained pavements, in cracked pavements water entry during rainfall periods may result in part of the layer closest to the surface having a high water content or becoming fully saturated (Erlingsson et al., 2009b). At high water contents, the shear strength of unbound materials reduces due to the formation of positive pore pressures within water-filled voids under applied loads that reduce normal forces between aggregate particles making inter-particle slip easier (Thom, 2008). High water contents may also reduce the material shear strength by increasing particle spacing, resulting in fewer contact points (Thom, 2008).

The response of granular pavement layers under traffic loading can be characterised by both a recoverable (resilient) deformation and residual (permanent) deformation (Lekarp et al., 2000). The resilient behaviour of these materials is affected by a range of factors including stress level, density, grading, fines content, maximum grain size, aggregate type, particle shape, moisture content, stress history and the number of load applications (Lekarp et al., 2000). It is most affected, however, by the level of applied stresses and the amount of moisture present within the material (Lekarp et al., 2000, Richter, 2006) with high water content typically resulting in a significant reduction in resilient modulus (Richter, 2006).

The in situ moduli (stiffness) of pavement layers also vary on a seasonal basis due to changes in environmental conditions within the pavement structure (Richter, 2006). This is important as deflection, stresses and strains induced in the pavement by traffic loading vary with the moduli of pavement layers (Richter, 2006). As a result, the performance of thin bituminous pavements strongly depends on variations in moisture conditions due to the sensitivity of unbound layers and subgrade materials to water content (Charlier et al., 2009).

2.2 Measuring moisture and its influence on roads

As UBG pavements and the supporting subgrade materials are moisture-sensitive, techniques used to measure the amount of moisture within these materials and its influence on structural response are important to enable better-informed pavement assessment, monitoring and management. An overview of these methods follows.

2.2.1 Soil and pavement moisture measurement techniques

A range of techniques exist for measuring soil moisture (Vereecken et al., 2008, Robinson et al., 2008, Dobriyal et al., 2012, Tarantino et al., 2008), many of which can be applied to granular pavement materials. These include: contact-based methods such as capacitance sensors, TDR, heat pulse sensors, fibre-optic sensors and gravimetric techniques; and contact-free methods such as remote-sensing and hydrogeophysical techniques, which include GPR and electromagnetic induction (Vereecken et al., 2008).

In relation to roads, gravimetric assessment (oven drying of samples) is the simplest and most widely used technique, although it requires destructive sampling and cannot make real-time in situ measurements (Erlingsson et al., 2009a). A number of non-destructive methods including neutron-scattering, TDR, GPR and capacitance techniques are also used (Erlingsson et al., 2009a). While nuclear methods such as neutron-scattering can achieve accurate moisture measurements (Erlingsson et al., 2009a, Dobriyal et al., 2012) strict rules around using radioactive materials, the need for an operator and slow data acquisition have reduced use of these methods (Robinson et al., 2008).

Investigating a range of non-nuclear alternatives, Sebesta et al. (2013) concluded that gravimetric and dielectric-based devices (that is, EM methods) offered the greatest potential for rapid moisture measurement of road base and subgrade materials. TDR is considered the standard EM method for determining soil moisture (Robinson et al., 2008) and is the most common technique used for monitoring water content in pavement structures and subgrades (Erlingsson et al., 2009a) (see Section 2.5.2). However, a key disadvantage for this and other contact-based methods is the need for embedded sensors, which become difficult and expensive to install at regular intervals along long lengths of road. The development of low-cost sensors (Yang, 2014) and wireless sensor networks (Robinson et al., 2008, Vereecken et al., 2008) may in future make large-scale implementation of embedded sensors a more practical proposition.

Of available contact-free methods, GPR presents a number of key advantages for pavement moisture quantification (see Section 2.4.4). The ability to quickly and non-invasively investigate subsurface moisture conditions is perhaps its greatest advantage, enabling quasi-continuous measurements at up to traffic speeds. A number of quantitative moisture measurement approaches are also possible using GPR (Huisman et al., 2003). Nonetheless, while GPR has been used for decades within the road industry (Saarenketo and Scullion, 2000, Saarenketo, 2009) its use to date for quantitative pavement moisture assessment remains limited. A more detailed discussion of GPR equipment and its use for soil and pavement moisture quantification is given in Section 2.4. As TDR is also used in this study, a more detailed overview of that technology can be found in Section 2.5.

2.2.2 Measuring variations in structural response due to moisture

Deflection measurements are currently the only reliable non-destructive method for determining the structural strength of flexible pavements (Ferne et al., 2009). These techniques have also been used to monitor the influence of moisture on pavement structural response. The falling weight deflectometer (FWD), for instance, has been used to monitor changes due to moisture variations (Salour and Erlingsson, 2013, Al-Qadi et al., 2004), seasonal variations (Richter, 2006) and flood damage (Zhang et al., 2008). The deflectograph has also been used to monitor the influence of seasonal variations (Paige-Green, 2009).

Perhaps the most promising technology for large-scale deflection measurements is the traffic speed deflectometer (TSD), a new approach enabling continuous measurement of pavement structural response under load at collection speeds of up to 80 kilometres per hour (Ferne et al., 2009, Krarup et al., 2006, Muller and Roberts, 2013). This approach has significant potential to provide network-level measurements with which to compare over time or to detect changes in pavement structural response due to moisture variations. The use to date of this technology in combination with GPR and its potential use with the techniques developed in this thesis are discussed in Chapter 4.

2.3 Electromagnetic waves, water and soils

Of available soil moisture measurement methods, high-frequency EM measurements are the most promising category (Huisman et al., 2003). To better understand these methods and their underlying principles, the following section presents an overview regarding the interaction of EM waves with dielectric materials such as soils and pavement materials and the influence of moisture.

2.3.1 Wave equations

An EM wave, like other wave types, is an energy transfer mechanism. EM energy moves within a dielectric material (electrical insulator) as a disturbance that separates or aligns charged particles within the material and then releases them as the wave passes. Charges within the material are displaced or polarised in relation to their original position, however, if the separating charges within the material are free to move and can physically interact with the waves, for example water within material pores, this process converts some of the EM energy into heat (Cassidy, 2009).

To describe the propagation of these waves mathematically, homogenous wave equations for the electric and magnetic fields can be derived from Maxwell's equations, which for the electric field $\tilde{E}$ is (Ulaby et al., 2010):

$$\nabla^2 \tilde{E} - \gamma^2 \tilde{E} = 0 \qquad \text{Eqn. 1}$$

where the propagation constant (γ) is given by:

$$\gamma^2 = -\omega^2 \mu \varepsilon_c \qquad \text{Eqn. 2}$$

and where ε_c is the complex permittivity:

$$\varepsilon_c = \varepsilon - j\frac{\sigma}{\omega} \qquad \text{Eqn. 3}$$

Here the term ε_c contains contributions from the electrical permittivity (ε) and conductivity (σ), parameters which can each be complex. Because of the j term in Equation 3, the real component of ε is in-phase with the imaginary component of σ, and vice versa.

Because ε_c is complex it can be separated into real (ε') and imaginary (ε'') components:

$$\varepsilon_c = \varepsilon' - j\varepsilon'' \qquad \text{Eqn. 4}$$

where ε' contains contributions from permittivity and conductivity in-phase with the electric field and ε'' contains the contributions 90º ($\pi/2$) out of phase.

2.3.2 Attenuation and velocity

Combining Equations 2 and 4 (Ulaby et al., 2010):

$$\gamma^2 = -\omega^2\mu(\varepsilon' - j\varepsilon'') \qquad \text{Eqn. 5}$$

As γ is complex it can be expressed as:

$$\gamma = \alpha + j\beta \qquad \text{Eqn. 6}$$

Expanding Equation 6 and separating real and imaginary components enables evaluation of α and β:

$$\alpha = \omega\left(\frac{\mu\varepsilon_c'}{2}\left[\sqrt{1+\left(\frac{\varepsilon''}{\varepsilon'}\right)^2} - 1\right]\right)^{1/2} \qquad \text{Eqn. 7}$$

$$\beta = \omega\left(\frac{\mu\varepsilon_c'}{2}\left[\sqrt{1+\left(\frac{\varepsilon''}{\varepsilon'}\right)^2} + 1\right]\right)^{1/2} \qquad \text{Eqn. 8}$$

where α is the attenuation constant, measured in Nepers per metre (Np/m), which characterises signal attenuation and where β is the phase constant, measured in radians per metre (rad/m).

A uniform plane-wave solution to the homogeneous wave equation for the electric field, travelling in a lossy-medium in the positive z-direction, can be expressed in terms of an attenuation component ($e^{-\alpha z}$) and a propagation component ($e^{-j\beta z}$) as (Ulaby et al., 2010):

$$\tilde{E}(z) = \hat{x} E_{x0} e^{-\alpha z} e^{-j\beta z} \qquad \text{Eqn. 9}$$

where:

$\hat{x}$ = unit vector in the x-direction

E_{x0} = amplitude of the propagating E-field with respect to the x-direction.

and the phase velocity (v) of the wave is given by:

$$v = \frac{\omega}{\beta} \qquad \text{Eqn. 10}$$

For simplicity, the permittivity and permeability are normally expressed as relative permittivity (ε_r) and relative permeability (μ_r), by dividing by the properties of free space:

$$\varepsilon_r = \varepsilon_c / \varepsilon_0 = \varepsilon_r' - j\varepsilon_r'' \qquad \text{Eqn. 11}$$

$$\mu_r = \mu / \mu_0 \qquad \text{Eqn. 12}$$

where:

ε_0 = electrical permittivity of free space, 8.854 x 10^{-12} F/m.

μ_0 = magnetic permeability of free space, 4π x 10^{-7} H/m.

Substituting for the *phase-constant* (β) from Equation 8 into Equation 10 gives:

$$v = \frac{c}{\sqrt{\varepsilon_r' \mu_r \frac{1 + \sqrt{1 + (\varepsilon_r'' / \varepsilon_r')^2}}{2}}} \qquad \text{Eqn. 13}$$

where:

c = speed of light in a vacuum ≈ 2.99 x 10^8 m/s

The material loss tangent ($\tan\delta$) is defined as (Daniels, 2004, Millard et al., 2001):

$$\tan\delta = \varepsilon''/\varepsilon' = \varepsilon_r''/\varepsilon'_r \qquad \text{Eqn. 14}$$

The phase velocity of the propagating wave can then be expressed as:

$$v = \frac{c}{\sqrt{\varepsilon'_r \mu_r \frac{1+\sqrt{1+\tan^2\delta}}{2}}} \qquad \text{Eqn. 15}$$

For most practical GPR applications the materials under test are non-magnetic ($\mu_r \approx 1$) and the imaginary component of permittivity is small in relation to the real component ($\varepsilon'' << \varepsilon'$), enabling the simplification:

$$v \approx \frac{c}{\sqrt{\varepsilon_r}} \qquad \text{Eqn. 16}$$

While this approximation is usually acceptable for dry and low-loss materials, dipolar relaxation and conductivity losses due to moisture may give rise to a ε'' component that would affect the phase velocity, the reasons for which are discussed in the following section. However, based on Eqn. 13, the imaginary component of permittivity would need to be large relative to the real component to have much influence on the phase velocity.

2.3.3 Soil dielectric properties and the influence of moisture

The permittivity and conductivity of subsurface materials are usually termed their dielectric properties (Cassidy, 2009). Permittivity is normally considered a complex and frequency-dependent quantity, with the real component representing energy storage and the imaginary component representing loss (Cassidy, 2009). Conductivity characterises free change movement when an electric field is applied (Annan, 2009).

The dielectric response of natural and man-made materials is complicated as they exhibit both dielectric and conducting properties, are controlled by the microscopic-scale behaviour of their components and because dielectric losses occur at different frequencies due to a range of mechanisms, leading to a frequency-dependent response (Daniels, 2004). These mechanisms include atomic, dipolar and Maxwell-Wagner relaxation effects, which combine to produce an overall material response (Cassidy, 2009).

Water within these materials often has a significant influence on this response, for a number of reasons. For one, the non-uniform charge distribution of the water molecule produces a permanent electric dipole moment that tends to rotate it in the direction of the electric field (Kaatze and Hübner, 2010). Consequently water is highly polarizable, resulting in a large relative permittivity (of around 80), which is also temperature dependent (Annan, 2005). The relative permittivity of water is markedly different to the typical range for most geological materials used for road construction, which is usually around 4 to 8. Consequently, a small amount of water within these materials can significantly increase the bulk permittivity and thus slow the velocity of EM waves passing through pavement layers (see Eqn. 15 and Eqn. 16). The contribution of water to the overall material permittivity also varies depending on the degree to which water molecules are free to rotate or are bonded to material surfaces, which changes as the amount of water within the material increases (Saarenketo, 1998). The polar nature of the water molecule also enables dissolution of ionic materials, disassociating them to form positively and negatively charged ions that conduct electricity by being mobile in water (Annan, 2005). Under the influence of an applied EM field, free charges flow though the material resulting in signal attenuation and energy loss (Cassidy, 2009), with all real materials generally exhibiting some loss primarily attributable to electrical conductivity (Annan, 2005). In more conductive environments with a high degree of free charges, for example saline conditions or materials with a high clay content, the majority of energy may be lost as heat in the conduction process (Cassidy, 2009).

While at low frequencies molecular rotation is able to keep up with the applied alternating electric field enabling the dipoles to fully contribute to the real permittivity (National Physical Laboratory, 2003), as the frequency increases material polarization can no longer keep up. This phase lag between polarisation and the changing electric field leads to a frequency-dependent dielectric loss represented as a complex permittivity, with the real part representing the polarisation component in phase with the electric field and the imaginary part representing the component with a $\pi/2$ phase difference (Kaatze and Hübner, 2010). While there is no typical complex effective permittivity spectrum valid for all materials, the measured response of a damp, lossy soil provides a good indication of what to expect (Cassidy, 2009). Typically, over the frequency range relevant to pavement GPR (500 MHz to 3 GHz), real permittivity decreases gradually and imaginary permittivity increases gradually with increasing frequency.

The dielectric response of soils and other materials is often determined in the laboratory using broadband characterisation techniques (see Section 2.6). Guidance for these methods can be found in a number of texts (Behari, 2005, Chen et al., 2004, National Physical Laboratory, 2003). In relation to civil engineering materials, researchers have used a number of approaches to investigate dielectric properties and the influence of moisture (see Section 2.6). These include the use of broadband surface probes to investigate small volumes of fine-grained materials such as clays and silts (Saarenketo, 1998, Wagner et al., 2014) and measurement of larger samples of bound coarse-grained conglomerates such as asphalt (Shang and Umana, 1999, Shang et al., 1999, Adous et al., 2006, Al-Qadi, 1992, Al-Qadi et al., 1991) and concrete (Robert, 1998, Davis et al., 2003, Millard et al., 2001) using custom-developed broadband coaxial cells. However, there appears to be little information specifically related to the broadband-response of moist coarse-grained and compacted unbound granular pavement materials. Furthermore, concrete and asphalt do not contain the fine-graded fraction nor the fines plasticity that UBG materials do to achieve workability, cohesion and impermeably. As some amount of clay or clay-like secondary minerals are usually present, which may in turn influence on the dielectric properties of the UBG materials (particularly when wet), it is unclear how reliably measurements of these other material types could be compared.

While time-domain methods such as TDR and GPR have been used to determine the bulk apparent permittivity of UBG and other pavement material types (see Sections 2.4.4 and 2.5.2), these methods are not normally used to determine a frequency-dependent response. Nonetheless, it is possible to obtain such information using GPR inversion methods (Davis et al., 2003), time-domain spectroscopy techniques (Arcone and Boitnott, 2010) or TDR quarter-wavelength analysis (Thomas et al., 2008).

This section has given a brief overview regarding the propagation of EM waves, their interaction with soil and pavement materials and the influence of moisture on the dielectric properties of these materials. The review now turns to the techniques themselves: GPR, TDR and a number of laboratory permittivity characterisation methods, whose measurements are affected by moisture and these other material parameters.

2.4 Ground Penetrating Radar (GPR)

A brief review of GPR technology and its use for measuring moisture within pavements and other materials follows. More detailed overviews can be found elsewhere within the literature (Jol, 2009, Daniels, 2004, Goodman and Piro, 2013, Annan, 2009).

2.4.1 Equipment and operation

GPR is a well-accepted geophysical technique that uses EM waves to probe low-loss dielectric materials, primarily natural geological materials but also wood, concrete, asphalt and other materials (Annan, 2009). The equipment typically comprises a control unit connected via cables to one or more transmitting and receiving antennas placed on or near the ground surface. The antennas are used to emit EM signals into the ground and detect the resulting response. At the boundary between two media, some of the energy is reflected and the remainder is transmitted, with the strength of reflections depending on the contrast of intrinsic impedance between the materials (Daniels, 2004). For road pavements, reflections typically occur at the interface of pavement layers, provided there is a sufficient permittivity contrast between the layers and a sufficient thickness of the contrasting materials to cause a reflection. The GPR control unit then samples the resulting response detected at the receiving antenna. These measurements are typically triggered at regular intervals along the road using a wheel encoder to ensure linearly proportional measurements.

GPR equipment can be categorised by various aspects of its configuration or operation. Antennas are often categorised as either ground-coupled, which are placed directly on or near the ground surface, or air-coupled, which are suspended at some height above the ground surface. Most GPR surveys use the common-offset survey mode, where the separation between the transmitter and receiver is fixed (Daniels, 2004). Alternatively the antenna spacing may be varied between measurements to produce multi-offset modes of operation such as common-midpoint (CMP) or wide-angle reflection and refraction (WARR) (Huisman et al., 2003), an approach that is primarily used to estimate the radar signal velocity (Annan, 2009). Multi-fold reflection surveys, where subsurface features are illuminated from different transmitter positions as the response is recorded at a number of locations, are also possible but are seldom performed as they are time consuming and are complex to analyse (Annan, 2009).

GPR control systems also vary in terms of the signal modulation that is employed, although the output from most systems is an equivalent time-domain signal (Daniels, 2004). Numerical techniques used to model wave propagation for impulse GPR systems can therefore also be used to determine the expected response for systems using other forms of signal modulation.

The record of signal strength versus time measured by GPR can be displayed as a trace or A-scan, representing the polarity and magnitude of the electric-field (E-field) intensity on one axis and the two-way travel time on the other. More often traces are combined sequentially to produce a radargram (B-scan), in which the vertical axis represents the two-way travel time, the horizontal axis represents the position along the road and a colour or grayscale palette represents the measured signal intensity and polarity (see Figure 2-2). If an average EM wave velocity within the material is then assumed, the approximate depth to these features can be estimated. However, as the velocity of waves varies within subsurface materials these estimates need to be calibrated for accurate depth predictions.

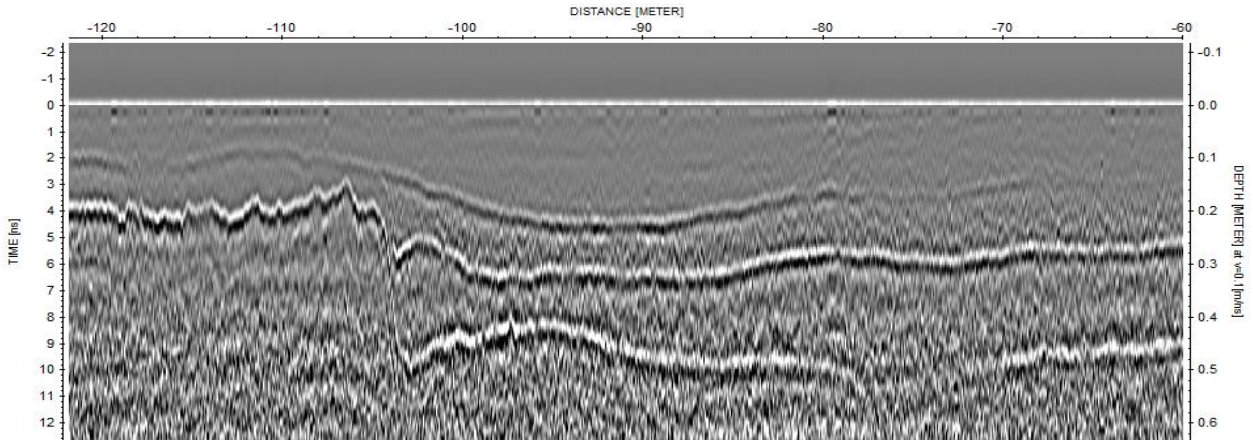

Figure 2-2: Greyscale radargram (B-scan) collected along a road pavement

A 3-dimenational (3D) GPR is a multi-channel system that uses an antenna array to simultaneously collect radargrams for a number of adjacent antenna pairs. These measurements may be achieved either by using a GPR control unit with multiple dedicated receiver channels or by multiplexing the one receiver across a number of antenna pairs within the array.

The current research made use of a 3D noise-modulated GPR system for field measurements. A conventional single-channel impulse GPR system was used for field and laboratory investigations. A vector network analyser (VNA) was also used in the laboratory to measure material samples, which for reflected signals viewed in the time domain is equivalent to a mono-static stepped-frequency GPR. To better understand the different approaches, a discussion of these signal modulation techniques follows.

Impulse GPR

Most GPR systems are a particular implementation of ultra-wideband impulse radar technology (Daniels, 2004, Koppenjan, 2009, Annan, 2005). They operate by transmitting a time-domain pulse and receiving the reflected energy as a function of time (Koppenjan, 2009) and generally come into the category of amplitude modulation (Daniels, 2004). The equipment consists of a timing unit, transmitter electronics (pulse generator), transducer element(s) and digitising circuitry, specifically an analogue to digital converter (ADC) (Koppenjan, 2009). While in a perfect system the return signal would be digitised quickly using a high dynamic range ADC, to date such sampling capabilities have not existed, although this is changing (Annan, 2009).

To get around this limitation, an approach called equivalent time sampling (ETS) or stroboscopic sampling has been used in the majority of commercial GPR systems (Annan, 2005, Koppenjan, 2009, Pasculli and Manacorda, 2015). This repetitive sampling method involves collecting single samples in succession after each transmitted pulse and then precisely adjusting the sampling delay to capture the entire received waveform (Koppenjan, 2009). Advantages of this approach include the relative simplicity of generating impulse waveforms and use of low-cost parts, whereas the disadvantages include undesirable ringing, inefficient use of transmit power (low duty cycle) and the limitation of resolution based on the pulse width (Koppenjan, 2009). An example of a portable impulse GPR system and a skid-mounted ground-coupled common-offset antenna are shown in Figure 2-3.

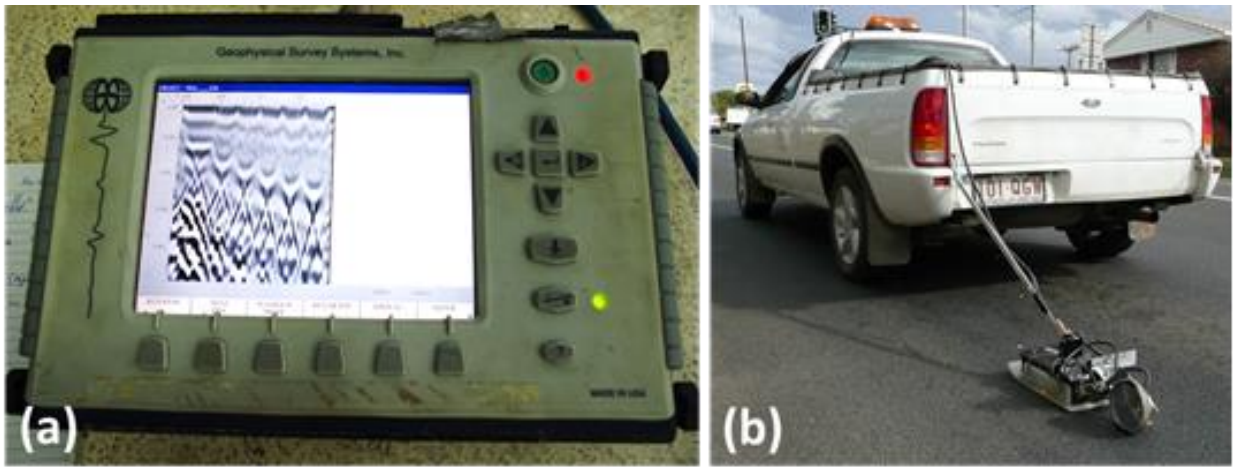

Figure 2-3: (a) Geophysical Survey Systems Inc. (GSSI) SIR-3000 impulse GPR control unit; and (b) a skid-mounted GSSI 900 MHz ground coupled antenna and encoder wheel

Stepped-frequency GPR

Stepped-frequency GPR has been the focus of considerable research (Noon et al., 1994). Detailed overviews of the approach are given by Noon et al. (1994) and Koppenjan (2009). Unlike impulse systems, stepped-frequency GPR's operate in the frequency-domain. They transmit and receive a series of narrowband frequency tones that are stepped across the required bandwidth over a finite time (Noon et al., 1994). At each step a copy of signal is diverted prior to transmission, mixed with the return signal, the combination is low-pass filtered and the resulting voltage is sampled with a low-speed ADC (Koppenjan, 2009).

A complex inverse fast Fourier transformation is then used to produce an equivalent time-domain version of the measured response (Daniels, 2004). The stepped-frequency approach has a range of benefits over impulse systems including waveform controllability, improved time jitter, signal transmission efficiency, greater dynamic range, a wider choice of antennas, better ability to control ringing and to account for material dispersion (Noon et al., 1994). This approach also has agility to skip over frequencies that could interfere with commercial broadcast stations (Stickley et al., 2000), however, these advantages come at the cost of increased system cost and complexity (Noon et al., 1994, Reeves, 2010a).

A number of authors have used commercial VNA's as a stepped-frequency GPR, for example Kong et al. (2012) and Liu and Sato (2014). A similar approach to these has been used in Paper VI to enable visual comparisons of impulse GPR and VNA measurements.

Noise-modulated GPR

Noise-modulated GPR, also called coded GPR, involves transmitting a pseudo-random noise signal (Reeves, 2010b), also called a pseudo-random code, pseudo-random binary sequence or M-sequence (Sachs, 2004). These signals appear random, however, their autocorrelation is pulse-like (Sachs, 2004). The GPR system receives the reflected signal which is demodulated by cross-correlating with the code. The approach spreads the radiated power evenly throughout the spectrum and is sometimes categorised as a frequency-domain method (Daniels, 2004), however, as the response is sampled in the time-domain it could also be considered a time-domain method. Benefits of this style of system are low frequency detection signals and simplicity, although data acquisition speeds may be too slow for GPR applications (Annan, 2005), at least using a conventional approach.

The first generation Noise-Modulated Ground Penetrating Radar (NM-GPR) system developed by Reeves (2010a, 2010b) achieved multi-channel implementation of this approach using rapid low-fidelity sampling. The updated NM-GPR equipment used in this research made a number of changes to improve signal quality and limit cross-talk (Reeves, 2014) and also added the ability to collect multi-offset measurements. The updated system is typically used with 3D ground-coupled antenna arrays designed for traffic-speed road scanning, an example which is shown in Figure 2-4.

Figure 2-4: Second generation NM-GPR system incorporating a traffic-speed 3D ground-coupled antenna array

Advantages of the NM-GPR approach include system simplicity and the use of a short digital sequence, which enables optimisation of average transmit and peak power, allows the transmitter to be tuned to detect weak return signals from deeper targets, uses lower power, can be switched across multiple antennas, and can also be filtered to reduce power levels for specific frequency bands (to enable regulatory compliance) (Reeves, 2014). A disadvantage of the current design is that closely spaced targets within the length of the transmitted code are limited by a 45 dB dynamic range limit relative to the highest amplitude return (Reeves, 2014).

2.4.2 Permittivity calibration and multi-offset GPR

As the velocity of EM waves largely depends on the pavement permittivity, which may vary along or across the road or vertically within pavement layers and is strongly influenced by moisture content, GPR layer depth predictions need to be calibrated to account for these changes. Several permittivity calibration methods exist. The most straight-forward involves digging holes, determining the as-built depth of pavement layers and then adjusting the assumed permittivity until the depth of features seen in the radargram matches the sampling findings. This approach is commonly used, however, it is also slow, damages the pavement and only enables calibration at a limited number of locations.

Two non-invasive permittivity calibration methods are the surface reflection coefficient approach (see Section 2.4.4) and multi-offset GPR. As noted previously, the multi-offset approach involves collecting GPR measurements at regular intervals along the road using two or more antenna offsets. Geophysical analysis techniques are then used to determine the wave velocity within pavement layers based on the arrival times of layer interface reflections measured at different offsets. The conventional approach to collecting these data involves physically separating antennas, which is slow and tedious. A similar dataset can be achieved by using a multi-channel or 3D GPR system to record the response of an arrangement of two or more fixed antennas or the response of several antenna pairs within an array which is then towed along the road.

The two antenna configurations most commonly used for multi-offset measurements are CMP and WARR (Huisman et al., 2003). The CMP approach involves separating the antennas equidistant from a point in the middle. The WARR approach involves keeping one antenna stationary (either the transmitter or receiver) and moving the other relative to it. The response at each offset is then recorded, either measurement-by-measurement if physically separating antennas or simultaneously using a multi-channel system. The measurements are then combined to produce the multi-offset response, an example of which is shown in Figure 2-5 (b). This synthetic example was determined by modelling the propagation of EM waves within a pavement model over time using the finite difference time domain (FDTD) approach. The instantaneous electric field strength at one moment in time, and the position of transmitters and receivers in the model, are illustrated in Figure 2-5 (a). As illustrated in this figure, the increasing antenna separation results in longer travel paths and later arrivals of the airwave, groundwave and reflected EM waves. For horizontal reflectors, this change in travel time with increasing offset is called normal move-out (NMO) (Burger et al., 2006). A procedure called NMO correction can be applied to convert the measured response into that which would have been measured for zero offset across the array, straightening the hyperbolic move-out response to provide an accurate image of the reflector (Everett, 2013), which requires knowledge of the wave velocity.

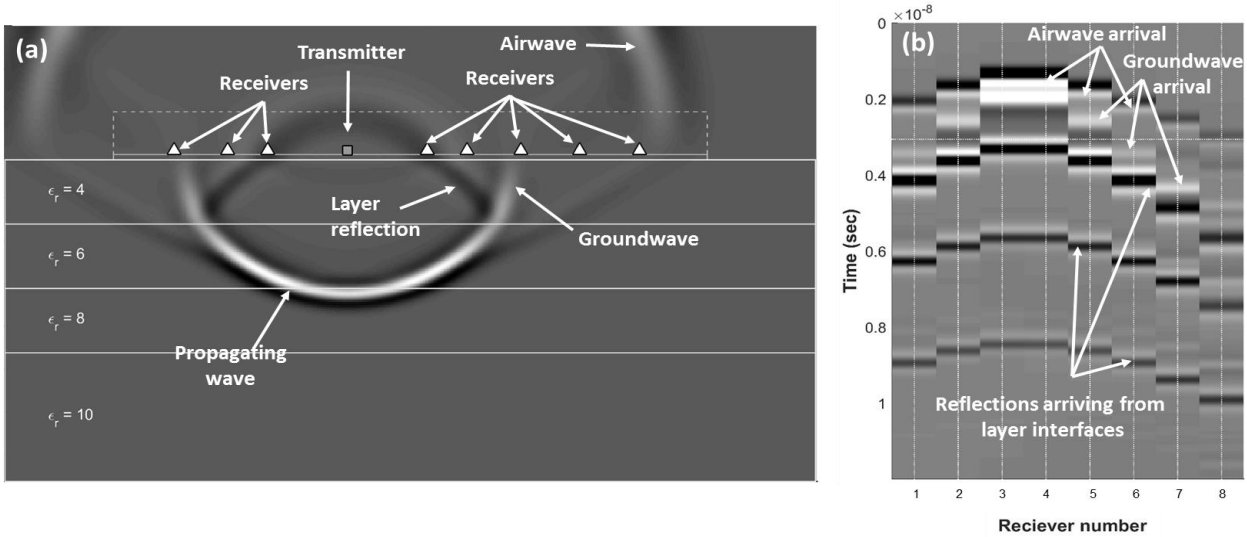

Figure 2-5: (a) Simulated wave propagation within a pavement model. Signals emitted by the transmitter (square) propagate directly or reflect from layer boundaries and are detected at the receiver positions (triangles); (b) the recorded responses at each receiver position are then combined to form the multi-offset response

A conventional geophysical approach for determining the velocity of reflected waves within subsurface layers is the x^2–t^2 or Green method (Burger et al., 2006). In this approach multi-offset data are displayed on squared offset (x^2) and two-way travel-time axes (t^2), on which horizontal reflectors appear as straight lines with the gradient equal to $1/V_{RMS}^2$ and the zero offset intercept equal to the zero offset travel time squared, where V_{RMS} is the root-mean squared velocity (Reynolds, 1997). In the case of multiple horizontal layers and small source-receiver offsets compared to reflector depth, the Dix Equation (Dix, 1955) enables the x^2–t^2 method to be used to determine the interval velocity of individual layers (Burger et al., 2006). Another approach involves generating a velocity semblance spectrum, where semblance is a measure of coherence in the stacking process (Reynolds, 1997), for example by stacking numerous NMO-corrected measurements using a range of trial velocities (Greaves et al., 1996) or by several other computational trial-and-error methods for NMO correction (Burger et al., 2006). Travel-time tomography, also called reflection tomography, is another approach involving adjustment of the layer depths and wave velocities within a model of the subsurface so that the difference between ray-traced estimates and measured travel times are minimised (Stork, 1992).

Another option is migration velocity analysis, which involves altering the velocity field so that the multiple images of the same reflector collected at different offsets (for instance using a multi-fold configuration) are consistent after pre-stack depth migration (Stork, 1992). The velocity values determined via each of these methods varies slightly and depends on their underlying assumptions. It is also possible to determine the near-surface EM wave velocity based on the groundwave arrival times at different offsets, an approach that has been used in a number of studies to monitor near-surface soil moisture (Lunt et al., 2005, Huisman and Bouten, 2002, Grote et al., 2003, Huisman and Bouten, 2003).

2.4.3 Use of multi-offset GPR for soil moisture quantification

Multi-offset GPR techniques have been widely used for soil moisture quantification, with numerous examples in the literature employing a range of approaches (Du and Rummel, 1994, Sperl et al., 1997, Greaves et al., 1996, Chanzy et al., 1996, Huisman and Bouten, 2002, Huisman and Bouten, 2003, Charlton, 2000, Charlton, 2001, Hubbard et al., 2002, Toy et al., 2010, Jacob et al., 2010, Steelman and Endres, 2012, Mangel et al., 2012, Iwasaki et al., 2016). One interesting approach was that by Gerhards et al. (2008) who configured two 400 MHz common-offset antennas to enable rapid collection multi-offset data and then used a ray-tracing algorithm to estimate the depth, moisture content and dipping angle of a soil layer. This approach was later adapted for use with three antennas (Wollschläger et al., 2010) and was used for monitoring changes in soil moisture over time (Pan et al., 2012).

2.4.4 Use of GPR for pavement moisture quantification

Many researchers have investigated GPR as a means of detecting moisture for road applications (Berthelot et al., 2010, Chen and Scullion, 2007, Chen and Scullion, 2008, Diefenderfer et al., 2006, Elseifi et al., 2001, Emilsson et al., 2002, Evans et al., 2008, Fernandes and Pais, 2014, Grote et al., 2005, Jaselskis et al., 2003, Li et al., 2010, Liu and Guo, 2002, Pedret Rodés et al., 2015, Plati and Loizos, 2013, Saarenketo and Vesa, 2000, Walubita et al., 2009, Benedetto, 2007, Benedetto and Pensa, 2007, Benedetto et al., 2013, Al-Qadi et al., 2004). Only a few have used quantitative techniques to estimate the amount of water present, a review of which follows.

One approach involves measuring the two-way travel time of EM waves through water saturated samples prepared in the laboratory (Liu and Guo, 2003, Fernandes and Pais, 2014)) or cored from existing pavements (Evans et al., 2008). Measurements of the two-way travel time of EM waves to fixed subsurface features or through known layer depths have also been used to monitor moisture during pavement infiltration experiments (Benedetto and Pensa, 2007, Benedetto, 2007, Grote et al., 2005). In most practical field situations, however, the depth of pavement layers is not known with sufficient accuracy to enable use of this approach without cores or trenching.

The surface reflection coefficient method is another approach used by researchers for moisture quantification. It involves using an air-coupled antenna to measure the reflection amplitude of the pavement surface which is compared to a reference measurement of a metal plate placed on the road surface, representing a total reflector, from which the surface dielectric permittivity can be calculated (Saarenketo, 2006). This approach can potentially also be extended onto the next layer by comparing the reflection amplitude of the top of that layer to the previous interface (Saarenketo and Scullion, 2000). In an early report, Scullion et al. (1992) used the surface reflection coefficient approach with the complex refractive index model (CRIM) to estimate moisture content within road base materials along a road. The authors noted that the assumption of constant density was a likely source of error and that the accuracy of the CRIM model had not been determined. Al-Qadi et al. (2004) used a similar approach to estimate moisture within granular materials for fixed pavement segments over time. The researchers noted that the predictions may have underestimated the permittivity and might not be accurate without calibration cores to account for a number of analysis parameters and attenuation within the overlying hot mixed asphalt (HMA) surfacing layer. Li et al. (2010) also used this approach and a volumetric mixing model to predict moisture within HMA, which compared well with a calibrated nuclear gauge. Plati and Loizos (2013) used surface reflection techniques with 1 GHz and 2 GHz horn antennas to determine permittivity and estimate density and moisture content along a HMA pavement. The researchers found that the lower frequency antenna reported higher permittivity values, which was attributed to the greater penetration depth identifying additional areas of moisture in the body of the HMA layer.

However, while surface reflection coefficient methods are quick and relatively simple to perform, they have a number of disadvantages that become problematic for moisture quantification. The approach is normally undertaken assuming homogenous pavement layers without moisture or defects present (Lahouar et al., 2002, Al-Qadi et al., 2003, Saarenketo and Scullion, 2000) and without signal attenuation (Saarenketo and Scullion, 2000) and therefore become more difficult to use on older and more variable materials (Al-Qadi et al., 2003, Lahouar et al., 2002), on lossy materials such as fresh concrete containing moisture and conductive salts (Maser et al., 2003) or wet base course (Scullion et al., 1992). These methods are also adversely affected when the thickness of the upper pavement layer is small compared with the wavelength and the reflection amplitude is also affected by surface roughness (Davis et al., 1994). Additionally, the material depth influencing the response is somewhat unclear, although microwave penetration depths have been estimated for asphalt materials at high-frequencies (Jaselskis et al., 2003).

Multi-offset methods have been used for pavement moisture assessments by a few investigators. Emilsson et al. (2002) configured an array of four conventional ground-coupled impulse antennas in a mobile WARR arrangement to enable continuous data collection along approximately 10 kilometres of road. Three different arrays were configured using 250, 500 and 800 MHz antennas towed at 20 to 40 km/hr. The Topp equation (Topp et al., 1980) was used to predict the in situ moisture content from the calculated permittivity, which compared well with physical sampling in the two example locations presented. Grote et al. (2005) used a separable 900 MHz ground-coupled antenna to manually collect CMP measurements during a pavement infiltration experiment. However, the use of multi-offset methods in that study appears ancillary, with the researchers instead focusing on common-offset measurements of travel time and amplitude data through the known layer thicknesses for moisture monitoring over time. While not specifically pavement-related, a number of studies have used multi-offset methods to monitor moisture within concrete using reflection techniques (du Plooy et al., 2013, Villain et al., 2010), direct wave measurements (Dérobert et al., 2008), tomography (Leucci, 2012) or cross-power spectral density measurements to determine the EM wave velocity (Klysz and Balayssac, 2007, Lai et al., 2011).

2.4.5 Other uses of multi-offset techniques

While the use of multi-offset methods has been somewhat limited for pavement moisture quantification, this approach has been used by many authors to determine the depth and permittivity of pavement layers (Davis et al., 1994, Mesher et al., 1995, Edwards and Mason, 2011, Hamrouche and Saarenketo, 2014, Fauchard et al., 2003, Zhao and Al-Qadi, 2016, Liu and Sato, 2014, De Pue et al., 2016, Al-Qadi et al., 2003, Leng and Al-Qadi, 2014, Hugenschmidt, 2000, Lahouar et al., 2002). To enable efficient data collection using off-the-shelf equipment, some authors have combined the response of a common-offset ground-coupled and an air-coupled antenna (Al-Qadi et al., 2003, Lahouar et al., 2002) or a pair of air-coupled antennas (Leng and Al-Qadi, 2014, Hamrouche and Saarenketo, 2014) to achieve multi-offset configurations with few offsets. A number have also used air-coupled 3D GPR systems to collect multi-offset measurements (Zhao and Al-Qadi, 2016, De Pue et al., 2016) or used 3D antenna arrays placed physically on the road surface at a number of fixed locations (Liu and Sato, 2014).

2.4.6 Advantages and limitations

The key advantage of the multi-offset approach is the ability to determine the mean velocity of EM waves within pavement layers without invasive sampling or a priori knowledge of layer depths. This in turn enables calibration of layer depth estimates and determination of the bulk relative permittivity of pavement layers, from which the moisture content or other pavement parameters or their variation may be inferred, for example changes in density for new asphalt pavements (Al-Qadi et al., 2010). As the approach accounts for material inhomogeneity within layers, it enables more accurate layer depth estimates for older and more variable pavement materials compared to the surface reflection coefficient approach (Lahouar et al., 2002) as that approach is better suited to new or defect-free pavements that are non-attenuative (Saarenketo and Scullion, 2000).

Another advantage of the multi-offset approach is that permittivity estimates can also be determined based on the change in groundwave arrival times measured at different offsets, provided ground-coupled antennas are used. There are a number of other advantages of using ground coupled antennas for these measurements, including the maximisation of penetration depth and the minimisation of surface refraction issues.

Davis et al. (1994) discusses the influence of refraction at the ground surface on multi-offset measurements. Those authors note the difficulty of accurately measuring the change in travel times at different offsets using air-launched antennas and conclude that the increased reliability of determining EM velocities and layer thickness using ground coupled antennas far outweighed the disadvantages of having transducers in contact with the pavement. Furthermore, surface refraction leads to a number of challenges when applying conventional semblance techniques to air-coupled multi-offset measurements (De Pue et al., 2016).

There are a number of additional limitations and challenges when using multi-offset GPR methods. For one thing, data analysis is usually more complicated compared to ground-coupled common-offset or air-launched surface reflection coefficient-based investigations. Another challenge relates to the nature of data collected using mobile multi-offset antenna configurations. While data collection may be much faster using multi-channel or 3D GPR systems, a disadvantage compared to physically separating antennas is that the measurements may be relatively sparse. This presents challenges when applying conventional semblance methods (Yi et al., 2015) and may make it more difficult to correctly identify or follow the same reflection feature between antenna pairs, which is critical for ensuring correct data interpretation (Emilsson et al., 2002). Another limitation of the multi-offset approach is that it relies on the presence of continuous, and preferably flat and horizontal, subsurface reflectors. While this seems a reasonable assumption for most road pavements, at times the strength of layer interface reflections may be weak or intermittent due to a poor permittivity contrast between layers or varying signal attenuation within these materials. Abrupt lateral changes in layer profile may also be encountered, for example where the outer-wheel path has been excavated and repaired, or the interfaces may dip along or across the road, further increasing the data analysis challenge.

Another limitation is that the multi-offset approach can only be used to analyse layers down to the lowest coherent reflection, typically the subgrade interface. It would therefore not be possible to calculate subgrade moisture using this approach. On the other hand, it might be conceivable to provide an indication of subgrade moisture based on the reflectivity of that interface compared to the layer above or by using the Brewster angle to identify phase changes in the multi-offset response (Reppert et al., 2000).

2.5 Time-domain reflectometry (TDR)

TDR has been widely used for pavement moisture monitoring, with many examples reported within Queensland (Baran, 1994, O'May, 2007, Vuong, 2007) and elsewhere (Jiang and Tayabji, 1999a, Rada et al., 1995, Jiang and Tayabji, 1999b, Richter, 2002, Richter, 2006, Diefenderfer et al., 2000, Ekblad and Isacsson, 2007, Hore-Lacy et al., 2014, Liang et al., 2006, Wright et al., 2001, van der Aa and Boer, 1997). It has also been used in this study. A brief review of the TDR approach and its uses to date for pavement and subgrade moisture monitoring follows. More detailed reviews of the TDR technique and its use for moisture monitoring of soils can be found elsewhere (Chung and Lin, 2009, Robinson et al., 2003, Jones et al., 2002).

2.5.1 Equipment and approach

A TDR measurement system typically consists of a transmission line (wave-guide or probe), coaxial connecting cable and a TDR instrument that generates fast-rise-time voltage pulses (Rainwater et al., 1999). A number of probe designs can be used for these measurements including two-wire or three-wire designs (Whalley, 1993) and other sensor types (Robinson et al., 2003, Scheuermann et al., 2009) that are embedded into the soil during the measurements. Sharp pulses are supplied to the sensor via the coaxial line (Kaatze and Hübner, 2010). The voltage pulse propagates along the transmission line (probe) through the dielectric material surrounding it and impedance changes at the beginning and end cause a reflected pulse (Rainwater et al., 1999). The velocity of this signal is primarily a function of the permittivity of the material through which it travels (Robinson et al., 2005). Thus the 'apparent' permittivity of soil surrounding the probe can be determined from the average EM wave velocity along the probe, determined from the arrival times of reflections from the start and end of the probe and Equation 16. The corresponding volumetric moisture content can then be estimated using the Topp equation (Topp et al., 1980) or other petro-physical relations (see Section 2.6.3).

The TDR technique is reasonably simple to operate and is analogous to short-pulse radar systems (Topp et al., 1980). A network of passive TDR probes can also be configured using a multiplexer to enable measurement using a single TDR instrument (Robinson et al., 2008). The TDR control unit and the type of three-prong sensor used in this research are shown in Figure 2-6.

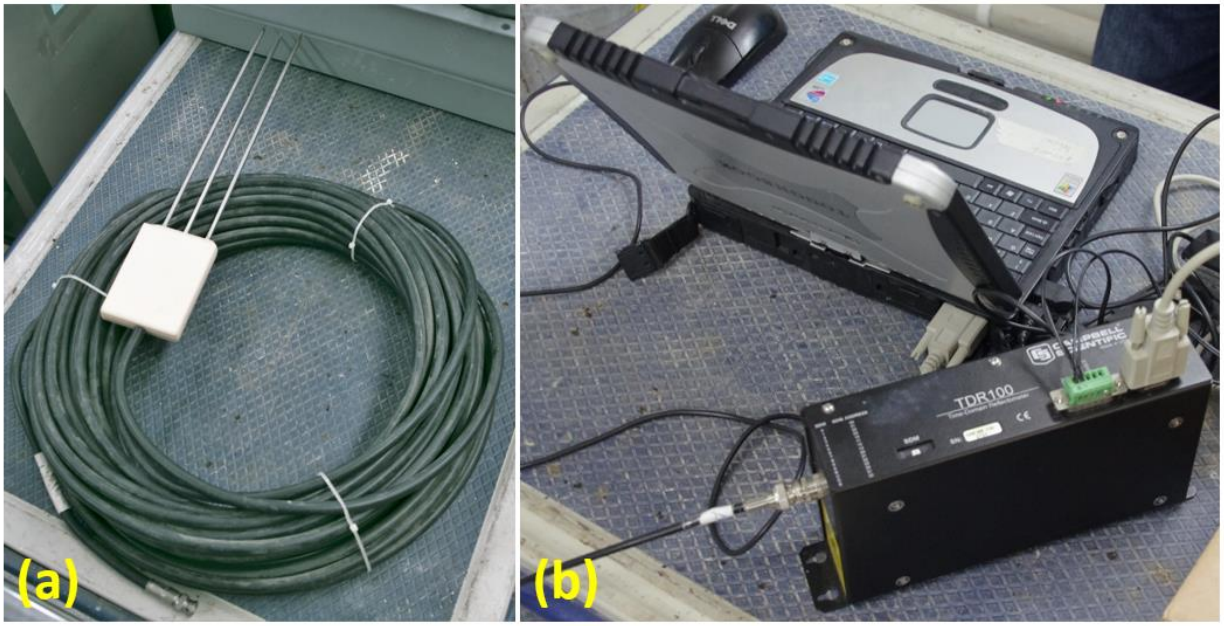

Figure 2-6: (a) Three-prong CS610-L TDR probe sensor; and (b) A Campbell Scientific TDR100 TDR control unit connected to a laptop for data viewing and analysis

2.5.2 Uses of TDR for measuring road moisture

The TDR approach has been used by many investigators for pavement moisture monitoring applications. Baran (1994) used the approach on samples of compacted crushed-rock pavement materials, finding that the Topp equation (Topp et al., 1980) was unsuitable for densely-compacted materials. The approach was also used in the US Long Term Pavement Performance (LTPP) program (Rada et al., 1995) where a number of alternative methods of analysing TDR measurements were investigated for a range of moisture and density levels. In that program the method of tangents was determined to produce apparent permittivity predictions with the least scatter compared to a number of regression relationships (Klemunes, 1998). Algorithms were later developed to enable automated moisture monitoring over time within unbound base, sub-base and subgrade materials (Jiang and Tayabji, 1999b, Richter, 2006). TDR has also been used for LTPP programs located elsewhere (Kim, 2010).

TDR has also been used for monitoring moisture within crushed concrete pavements and sand sub-base materials (van der Aa and Boer, 1997), sub-base or subgrade materials (Diefenderfer et al., 2000, Liang et al., 2006), materials located under geomembranes (Elseifi et al., 2001), crushed aggregate materials with varying gradings (Ekblad and Isacsson, 2007), drainable base materials and permeable pavement systems (Taamneh and Liang, 2010, Brown, 2013) and as part of accelerated pavement testing programs (Lim et al., 2014, Vuong, 2007).

2.5.3 Advantages and limitations

A key advantage of TDR is that it is well established, considered the standard EM method for determining soil moisture (Robinson et al., 2008). The approach is typically more accurate compared to capacitance methods due to its higher effective frequency and can often be used without a site-specific calibration (Chung and Lin, 2009). Another advantage is its temporal sampling resolution, enabling frequent measurements at the same locations over hours, days, months or years. This ability is useful for monitoring seasonal moisture changes (Baran, 1994, Jiang and Tayabji, 1999b, Erlingsson et al., 2009a) and the influence of rainfall or flooding events on pavement and subgrade moisture conditions (Elseifi et al., 2001). The small sampling volume of TDR probes enables small-scale processes to be monitored, although on the other hand, a large number of probes are required to map soil water content at larger scales with an adequate spatial sampling density (Huisman et al., 2002).

A key disadvantage is the need for embedded probes, which increases the cost and effort of installation and reduces the number of sites or locations within a site that can be practically monitored. At times key features within the measured response may be indistinct, requiring manual interpretation and making automated analysis more difficult to achieve and less reliable. The operational or effective frequency range of the TDR measurements is also somewhat unclear, although there are techniques to estimate it (Chung and Lin, 2009, Robinson et al., 2003). This parameter is important when comparing TDR to other methods, particularly for dispersive materials whose real permittivity changes as a function of frequency (Robinson et al., 2005). In addition, while TDR measurements are usually calibrated on known materials such as air and water to ensure measurement accuracy, a number of different analysis methods are in use (Klemunes, 1998, Heimovaara, 1993), which may produce somewhat different results and complicate the comparison with other techniques.

Furthermore, the measurements are not only affected by material parameters such as water content, dry density, bulk electrical conductivity, temperature and dielectric dispersion, but are also influenced by the length of the attached coaxial cable (Tarantino et al., 2008, Logsdon, 2000) and cable resistance (Chung and Lin, 2009) and are also sensitive to air gaps near the sensor (Whalley, 1993).

2.6 Laboratory permittivity characterisation methods

While GPR and TDR are useful for collecting permittivity measurements in the field, more detailed and accurate measurements can often be achieved in the laboratory using a number of sophisticated characterisation techniques. A brief review of these permittivity characterisation methods, their use to date on civil engineering materials and the petro-physical relations used to describe the measured repose follows.

2.6.1 Characterisation options

A number of techniques are available for permittivity characterisation of material samples in the laboratory. Detailed overviews of these methods (Chen et al., 2004, National Physical Laboratory, 2003, Krupka, 2006) and their use for measuring moisture within materials (Kaatze and Hübner, 2010) and soils (Behari, 2005) can be found in the literature. Not all of the available methods are suitable for use on pavement materials nor do all measure at or around the frequency range relevant to GPR (typically 100 MHz to 3 GHz), which is important for dispersive materials whose permittivity response is frequency-dependent.

While at lower frequencies material samples can be treated as a lumped impedance circuit and measured using an impedance analyser, at higher frequencies complex reflection and / or complex transmission coefficients are usually measured using a vector network analyser (VNA) and are called wave techniques (Krupka, 2006). To measure over the frequency range relevant to GPR, wave techniques are required. For isotropic material samples the complex permittivity and permeability can be determined from measurements of the complex reflection (S_{11}) and transmission (S_{21}) coefficients (Krupka, 2006). These measurements are collectively called scattering parameters or S-parameters. They are measured using a VNA connected to either an open-ended probe, a closed measurement cell or apparatus enabling measurements in a free-space environment (Krupka, 2006).

The VNA generates a sinusoidal test signal (Hiebel, 2007) that is applied to the sample under test. It then measures the amplitude and phase of the wave quantities and uses these values to calculate a complex S-parameter, where the wave quantities are the incident and reflected waves (Hiebel, 2007). The S_{11} measurement denotes the signal originating from port 1 on the VNA that is reflected back from the sample to that same port. The S_{21} measurement denotes the signal originating from port 1 that passes through the sample and is measured at port 2 of the VNA.

VNA measurements using broadband surface probes is one approach that has been used by researchers to characterise fine-grained soils and granular materials (Saarenketo, 1998, Berthelot et al., 2010), concrete (Filali et al., 2008) and asphalt materials (Chang et al., 2011). The probes are easy to handle, enable non-invasive characterisation, are commercially available and offer a broad frequency-measurement range (Kaatze and Hübner, 2010). They are one of the best techniques for measuring lossy dielectrics (Krupka, 2006). However, the sampling volume is relatively small compared to the maximum aggregate size within UBG materials (typically 20 mm, although sometimes greater) and so it may be more difficult to achieve representative measurements of bulk material properties. Wagner et al. (2014), for instance, estimated that the sensitive region near an open-ended coaxial line probe they developed was approximately ±7 mm laterally and ±7 mm perpendicular to the probe. Air gaps between specimens and probes are also hard to avoid for solid specimens using this approach (Krupka, 2006). As such, surface preparation is likely to be a challenge for use on UBG materials, particularly considering their un-bonded and coarse grained nature. Chang et al. (2011), for example, reported machine cutting and polishing asphalt samples to achieve a sufficiently smooth surface for broadband surface probe measurements.

Capacitance-based surface probes (Berthelot et al., 2010) operating at or around 50 MHz (Saarenketo, 1998, Loizos and Plati, 2007) have also been used to measure clays or silts and also granular and bound material samples (Loizos and Plati, 2007, Saarenketo, 1998, Saarenketo and Vesa, 2000, Berthelot et al., 2010). The approach measures at a fixed frequency that is notably lower compared to the centre frequencies of typical pavement GPR antennas (approx. 500 MHz to 3.0 GHz). Permittivity results using this approach have been observed to differ when compared to commercial broadband surface probe measurements of gravel base and clay materials (Berthelot et al., 2010). The penetration depth of these measurements is also unclear (Loizos and Plati, 2007).

Coaxial transmission line or 2-port coaxial cell measurements are another approach available for permittivity characterisation of civil engineering materials. This approach is especially useful for broad frequency band measurements, but solid materials are more difficult to measure due to the formation of air gaps between the sample and metal parts of the apparatus which, if neglected, can lead to substantial errors in permittivity determination (Krupka, 2006). Large coaxial cells have been developed and used for testing bound materials such as concrete or asphalt (Soutsos et al., 2001, Millard et al., 2001, Shang and Umana, 1999, Shang et al., 1999, Robert, 1998), however this equipment is not available off-the-shelf and would be difficult and time-consuming to develop. There is also a risk of damaging or distorting this apparatus when installing and compacting UBG materials to replicate realistic field conditions. One-port coaxial cells have also been developed and used for testing concrete (Huang, 2001) and asphalt (Adous et al., 2006). While some designs enable easier sample installation compared to two-port designs by avoiding the centre conductor (Adous et al., 2006), they still face many of the same challenges as the two-port methods.

Resonance methods have also been used to characterise asphalt and granular pavement materials (Fauchard et al., 2000, Fauchard et al., 2003). These methods are especially useful for measuring very low-loss materials and offer the highest possible accuracy for measuring real permittivity (Krupka, 2006). A disadvantage is that the approach only produces measurements at a few discrete frequencies and samples need to be placed within a resonant chamber, risking damage to the apparatus when compacting materials to replicate field conditions. Furthermore, as the equipment is not available off-the-shelf, custom apparatus would need to be developed and validated, which is likely to be time-consuming and complicated.

2.6.2 Free-space methods

Free-space methods are another category of permittivity characterisation approach with a number of potential benefits. They are often used at millimetre wave frequencies instead of transmission line cells and open-ended probes to measure a sample situated between two antennas or placed in front of one antenna (Krupka, 2006). Free-space methods have been used in the laboratory to characterise the dielectric properties of asphalt (Pellinen et al., 2015, Olkkonen, 2016) and the influence of moisture within it (Al-Qadi et al., 1991), to measure bitumen (Aziz et al., 2010) and to measure concrete or mortar samples (Hasar, 2009, Jamil et al., 2013, Büyüköztürk et al., 2006).

To ensure accurate measurements and avoid diffraction from sample edges, the size of samples in the direction perpendicular to the incident wave needs to be larger than the EM beam width (Krupka, 2006). Consequently many studies have used beam focussing apparatus and have measured only at high frequencies (typically > 10 GHz) to ensure a narrow beam width. As this is well above the range relevant to GPR, it is unclear how easily laboratory results using this approach could be compared.

Surface reflection measurements collected at GPR frequencies have also been used with inversion methods to estimate dielectric properties of mortar (Davis et al., 2003), moist soils (Lambot, 2004) and road layers (Mahmoudzadeh et al., 2013). While this is a valuable avenue of research, there can be problems involving reflections between the antenna and sample or within the sample (Davis et al., 2003). In addition, the analysis techniques are relatively complicated and are still being developed.

Within the agricultural sector, a relatively simple free-space transmission approach has been developed (Trabelsi et al., 2008, Trabelsi and Nelson, 2010) and used for a number of years to characterise the permittivity and moisture content of grain and seeds (Trabelsi and Nelson, 2010, Trabelsi et al., 1997, Trabelsi and Nelson, 2006, Trabelsi and Nelson, 2003). The approach involves using a VNA to collect S-parameter measurements connected to a pair of antennas at a fixed spacing with and without a sample of known thickness placed in between. Assuming the signal is a plane-wave travelling in low-loss conditions, the real and imaginary components of permittivity can be calculated at each measurement frequency via (Trabelsi et al., 2000):

$$\varepsilon_r' \approx \left(1+\frac{\Delta\Phi\lambda_0}{360d}\right)^2 \qquad \text{Eqn. 17}$$

$$\varepsilon_r'' \approx \frac{\Delta A\lambda_0\sqrt{\varepsilon_r'}}{8.686\pi d} \qquad \text{Eqn. 18}$$

where:

ΔA = attenuation (decibels) due to dielectric insertion;

λ_0 = free-space wavelength for a given frequency;

$\Delta\Phi$ = measured phase shift (degrees); and

d = material thickness (metres).

The main sources of error in the approach are due to multiple reflections, edge effects and mismatches, although phase measurements are less sensitive to these factors and multiple reflections can be minimised provided there is at least a 10 dB attenuation through the sample thickness (Trabelsi et al., 2000). One challenge with the approach is phase ambiguity, however, this can be overcome either from a priori knowledge of the expected range of dielectric values or by measurement at several frequencies (Trabelsi et al., 2000).

To demonstrate the derivation of Equation 17, consider the antenna measurement setup illustrated in Figure 2-7 with the antenna separation (L) and material thickness (d) (both in metres).

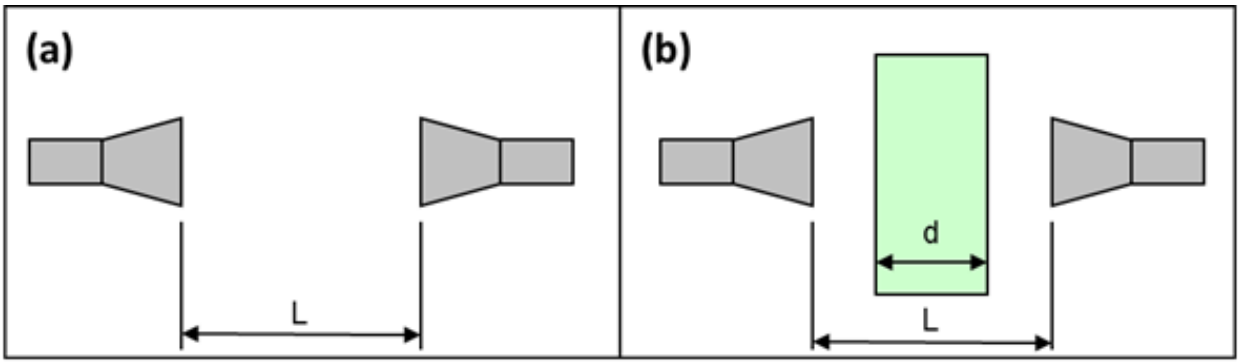

Figure 2-7: Antenna arrangement for free-space transmission measurements collecting (a) the reference measurement with the sample absent; and (b) a measurement with sample of known thickness d placed between the antennas

The phase-shift ($\Delta\Phi$) (in degrees) measured at each frequency by a VNA attached to these antennas can be determined by adding up the phase change contributions between antennas within the sample thickness (d) and the remaining air gap (Figure 2-7(b)) and subtracting the phase variation between antennas when only air is present (Figure 2-7(a)).

That is:

$$\Delta\Phi = (L-d)\frac{360}{\lambda_0} + d\frac{360}{\lambda_m} - L\frac{360}{\lambda_0} \qquad \text{Eqn. 19}$$

where:

λ_m = wavelength of EM wave for a given frequency within the sample material.

Cancelling the terms containing L, rearranging and noting that the EM wave frequency (f) is related to velocity and wavelength in free space and within the material via the relation $f = c/\lambda_0 = v/\lambda_m$ we see that the wave velocity (v) within the material can be determined for each frequency via:

$$v = \frac{c}{\left(\frac{\Delta\Phi\lambda_0}{360d} + 1\right)} \qquad \text{Eqn. 20}$$

Equation 17 can then be obtained by combining Equation 20 with Equation 16. As the calculation of the real component of relative permittivity is based on the velocity of EM waves passing through the sample, albeit measured in terms of phase-change, the approach determines the mean permittivity through the sample thickness.

2.6.3 Petro-physical relations

To enable moisture predictions from EM techniques such as GPR and TDR, relationships need to be established between the amount of moisture present within a material and the corresponding dielectric permittivity and other parameters. The simplest and most widely used relation is the Topp equation (Topp et al., 1980), an empirical relationship that enables the volumetric moisture content of soils to be estimated from the apparent permittivity of soils measured using TDR:

$$\theta_v = -5.3\times10^{-2} + 2.92\times10^{-2}\varepsilon_a - 5.5\times10^{-4}\varepsilon_a{}^2 + 4.3\times10^{-6}\varepsilon_a{}^3 \qquad \text{Eqn. 21}$$

where:

θ_v = volumetric water content

ε_a = apparent dielectric constant (apparent relative permittivity) measured by the TDR device. For low-loss homogenous materials $\varepsilon_a \approx \varepsilon_r'$.

A number of investigators have proposed variants of this approach for fine and coarse-grained pavement subgrade soils (Jiang and Tayabji, 1999b). Variants have also been proposed for high-density materials such as compacted crushed-rock road pavement materials (Baran, 1994, Ekblad and Isacsson, 2007).

Reviewing available methods, Wright et al. (2001) found the relation proposed by Baran (1994) produced the lowest prediction error for unbound aggregate sub-base materials compared to a number of other models, which over the range 5 < ε_a < 25 is:

$$\theta_v = 6\times10^{-6}\varepsilon_a^3 - 5.98\times10^{-4}\varepsilon_a^2 + 2.3831\times10^{-2}\varepsilon_a - 6.2164\times10^{-2} \qquad \text{Eqn. 22}$$

An alternative approach involves using dielectric mixing models that account for the permittivity of individual volumetric components within the soil or pavement material when predicting the overall response. These include three-phase mixing models (water, soil and air) for soils (Roth et al., 1990) and the CRIM model which along with other mixing models has been used to model the response of concrete (Halabe et al., 1993) and asphalt materials (Al-Qadi et al., 2010). Effective medium approaches have also been developed to model the response of sandy and alluvial soils (Fiori et al., 2005) and concrete (Halabe et al., 1993) for GPR applications. This approach involves determining an effective permittivity of a soil by considering the influence of scatterers within a background medium on the average displacement field within the material (Behari, 2005). While some versions of this approach assume spherical scatterers, others can be calibrated to account for arbitrary scatterer shapes (Behari, 2005) and make different assumptions regarding grain size distributions (Halabe et al., 1993).

2.7 Summary

The literature shows that moisture has a significant influence on resilient modulus of unbound materials and the structural performance of these pavements under traffic loading. Water content also has a significant, and at times complicated, influence on the dielectric properties of soils and pavement materials. High-frequency EM methods such as GPR and TDR are particularly useful for measuring pavement moisture.

The GPR approach offers a number of benefits including the ability to collect non-invasive and mobile measurements along the road. Multi-offset GPR measurements can be used to quantitatively determine subsurface moisture, but to date this approach has not been widely used for measuring pavement moisture. Multi-channel or 3D GPR systems can be used to collect these measurements quasi-continuously along the road by combining the response of two or more fixed antennas. However, the measurements may be relatively sparse, presenting challenges when applying conventional analysis methods and when considering semi-automated analysis procedures.

While there are many examples in the literature where multi-offset measurements have been achieved using a pairs of conventional common-offset antennas to calibrate the depth or permittivity of a single pavement layer, there are few examples of analysing multiple pavement layers or automating analysis of these data. In addition, while most researchers have focussed on air-coupled multi-offset GPR techniques to enable rapid data collection, refraction at the ground surface limits the sensitivity of permittivity calibration and presents a number of challenges when applying conventional analysis techniques.

TDR techniques have been widely used for monitoring pavement and subgrade moisture. This approach is particularly useful for monitoring a limited number of fixed locations over time. However, the need for embedded probes reduces the appeal of this approach for large-scale pavement monitoring. In addition, at times key features within the measured repose are indistinct and may be influenced by soil parameters other than water content or by equipment parameters, complicating data interpretation and comparisons with other methods.

Various broadband laboratory-based permittivity characterisation methods are available, however many are unsuitable for practical measurement of UBG materials for the reasons outlined. While the identified free-space transmission approach appears suitable for characterising UBG samples, it requires adaptation to operate over the frequency range relevant to GPR and to measure samples compacted within containers. The accuracy of the approach also needs to be established. Furthermore, as free-space methods are sensitive to edge effects, sample size and antenna setup, the influence of these aspects need to be investigated. Results using this approach also need to be compared with conventional GPR and TDR measurements, particularly if those methods are to be used for field validation of multi-offset GPR permittivity estimates. Furthermore, the influence of sample density and other parameters that may affect the results should also be investigated for these different methods.

A number of petro-physical relations have been developed by previous researchers to relate dielectric properties of soils and pavement materials to their internal moisture conditions and other parameters. Empirically-based polynomial relations are the simplest approach, requiring only the measured apparent permittivity of bulk material as an input for estimating the volumetric moisture content.

Volumetric mixing models such as CRIM or the effective medium approach may better account for the influence of individual constituents on the overall material response. However, these methods require additional information such as the permittivity and volumetric proportion of individual components as well as the porosity or specific gravity of these materials, details that are unknown for existing pavements and would require physical sampling and laboratory characterisation to determine. Furthermore, for many real-world uses an estimate of moisture content may be sufficient and its relative change along or across the road or over time is often of greater interest. Moreover, for large-scale GPR investigations the need for physical sampling to calibrate models may negate the benefits of using a non-destructive approach. For these reasons, empirical polynomial relations have been used in this research. Nonetheless, for new pavements where sample materials can be easily obtained for laboratory characterisation or where a greater understanding of the observed pavement response is desired and the additional sampling and characterisation effort is warranted, these more sophisticated models may be preferable.

3 SUMMARY OF ATTACHED PAPERS

This chapter summarises the seven incorporated papers that present the research. For each paper, an overview of the problem statement the paper set-out to address, the research aim(s), the approach used and the main contribution(s) to meeting the research objectives are outlined, which are to:

1. *Investigate and develop semi-automated multi-offset analysis methods;*
2. *Develop and validate a laboratory characterisation method to calibrate moisture-permittivity relations for unbound granular (UBG) pavement materials; and*
3. *Field trial and validate the approach to predict the moisture content and depth of UBG pavement layers.*

3.1 Paper I: Preliminary multi-offset analysis and permittivity characterisation

Muller, W.B., Scheuermann, A. and Reeves, B., Quantitative moisture measurement of road pavements using 3D noise-modulated GPR, Proceedings of the 14th International Conference on Ground Penetrating Radar (GPR) 2012, Shanghai. IEEE, 517-523, June 2012.

Development of the new 3-dimensional (3D) ground penetrating radar (GPR) equipment enables quasi-continuous multi-offset measurements while travelling along the road. Analysis of these data, however, presents a considerable challenge and necessitated development of a semi-automated approach. At the time of Paper I the new GPR equipment had not been developed and therefore there were no data on which to test potential analysis strategies. To enable development of analysis methods prior to equipment completion, numerical modelling was needed to simulate the expected multi-offset response for typical pavements. An analysis approach using layer interface tracking and automated implementation of conventional geophysical methods was envisaged. It was unclear, however, if the proposed antenna configuration would produce data for typical pavements that would be suitable to implement this approach.

Laboratory investigations were also needed to calibrate the petro-physical relations for predicting the volumetric moisture content of pavement materials from the GPR measurements. A free-space approach was identified as potentially suitable for characterisation of compacted UBG samples, but needed to be adapted for use on these materials and tested.

Considering this situation and needs, the two main aims of this paper were to:

1. Use numerical modelling to determine the expected multi-offset response for typical pavement configurations and develop interface tracking algorithms to follow the shape layer reflections within the multi-offset response and apply conventional geophysical analysis methods; and

2. Adapt and trial the proposed free-space permittivity characterisation approach, later called modified free-space (MFS), to characterise moist compacted samples of UBG materials and compare the results with conventional common-offset GPR measurements.

In the first half of Paper I, the finite difference time domain (FDTD) approach was used to model the expected multi-offset response of the planned 3D Noise-Modulated GPR (NM-GPR) equipment for a typical layered pavement. Noise was added to make the data more realistic. A Matlab (The Mathworks Inc., 2015) software script was developed to automatically identify and track the groundwave and to determine its velocity based on the arrival times determined at different antenna offsets. This result was used to undertake a preliminary normal move-out (NMO) correction of the data to produce an approximate cross-section across the road. The operator then selected interfaces that were used as seed points to automatically track interfaces across the multi-offset response. The wave velocity was determined using the $x^2 - t^2$ (Burger et al., 2006, Reynolds, 1997) approach and the Dix equation (Dix, 1955) was applied to determine interval velocities within individual layers.

A key contribution of this part of Paper I to the research objectives was to demonstrate that the proposed combination of layer tracking and conventional multi-offset analysis methods could be successfully applied to numerical simulations modelling the forthcoming NM-GPR equipment. Furthermore, it demonstrated that the approach produced results that matched the modelled values reasonably well.

In the second half of Paper I, a portable vector network analyser (VNA) was used to measure the phase-change occurring through UBG material samples compacted within a number of form-ply boxes compared to a reference measurement through an empty sample box. A Matlab script was developed to collect the VNA measurements of amplitude and phase, unwrap the phase measurements, determine the phase-shift compared to the reference measurement and make predictions of real and imaginary permittivity (using Equations 20 and 21). The results were compared to literature relations and to GPR permittivity estimates based on the measured two-way travel time through samples, showing similar results.

A key contribution of this part of Paper I was to demonstrate practical implementation of the proposed free-space approach on moist and compacted UBG samples. The results compared favourably with GPR measurements of permittivity based on the measured two-way travel time of electromagnetic (EM) waves passing through the same samples.

3.2 Paper II: Development of semi-automated multi-offset analysis methods

Muller, W.B., Self-correcting pavement layer depth estimates using 3D multi-offset ground penetrating radar (GPR), Proceedings of the 15th International conference on Ground Penetrating Radar (GPR-2014), Brussels. IEEE, 887-892, July 2014.

A limitation of using the $x^2 – t^2$ method and Dix equation for multi-offset analysis is that this approach neglects refraction at interface boundaries and assumes that a straight-line path is a permissible approximation for small source-receiver distances (Burger et al., 2006), also referred to as the small-spread approximation (De Pue et al., 2016). The source-receiver offset distance is considered in relation to the depth of subsurface targets and ideally should not exceed the target depth (Burger et al., 2006). However, for the proposed NM-GPR configuration some antenna offsets are wide in relation to shallow pavement layers, resulting in potential inaccuracies using this approach.

To improve accuracy of the multi-offset analysis, ray-path modelling (ray-tracing) methods are one option. Reflection tomography is one such approach, which involves tracing rays through a reference model to predict travel times for reflectors within the model, comparing to actual arrival times and then adjusting the model to minimise the difference (Stork, 1992).

Another approach is migration velocity analysis, which for seismic applications that use multiple shot points makes use of the fact that the same subsurface features are illuminated from different angles. Thus when the correct velocity model is used to migrate these data they should produce identical results (Stork, 1992). The planned NM-GPR configuration would also illuminate the pavement layer interfaces from different transmitter positions and hence this approach provides a potential means of calibrating the wave velocity and the permittivity of pavement layers.

The aim of Paper II was therefore to investigate semi-automated implementation of these two analysis methods and to assess their suitability for refining initial estimates of layer depth and permittivity determined using the approach described in Paper I.

The first technique was labelled Interface Matching (IM) and is a form of migration velocity analysis. As interface reflections had already been tracked using the approach in Paper I, their travel times and antenna offsets were known. The proposal was therefore to incrementally adjust the assumed layer permittivity estimates for each wide angle reflection and refraction (WARR) gather across the array until the calculated layer depths matched within the WARR overlaps and formed a line across the array. A simplified two-dimensional (2D) ray-path model with flat layers was used for these calculations. For the first layer, the layer depths were calculated using the permittivity values determined using the approach in Paper I. A line of best fit was determined for receivers physically closest to each transmitter (as these were least affected by changes in the trial permittivity). The permittivity values were then incrementally updated and the line of best fit was recalculated. This procedure was repeated until the error was minimised between the calculated layer depths and the line of best fit. The algorithm then went on to solve for the second layer, including the layer depth and permittivity values determined for the completed layers(s) and also considering refraction at the layer interface boundaries.

The second approach was an implementation of refection tomography called ray-path modelling (RM). Starting with the depth and permittivity values and tracked interface times determined using the approach in Paper I, the RM approach used a combination of lateral and longitudinal ray-path models to predict the two-way travel times at each antenna offset (see Figure 3-1).

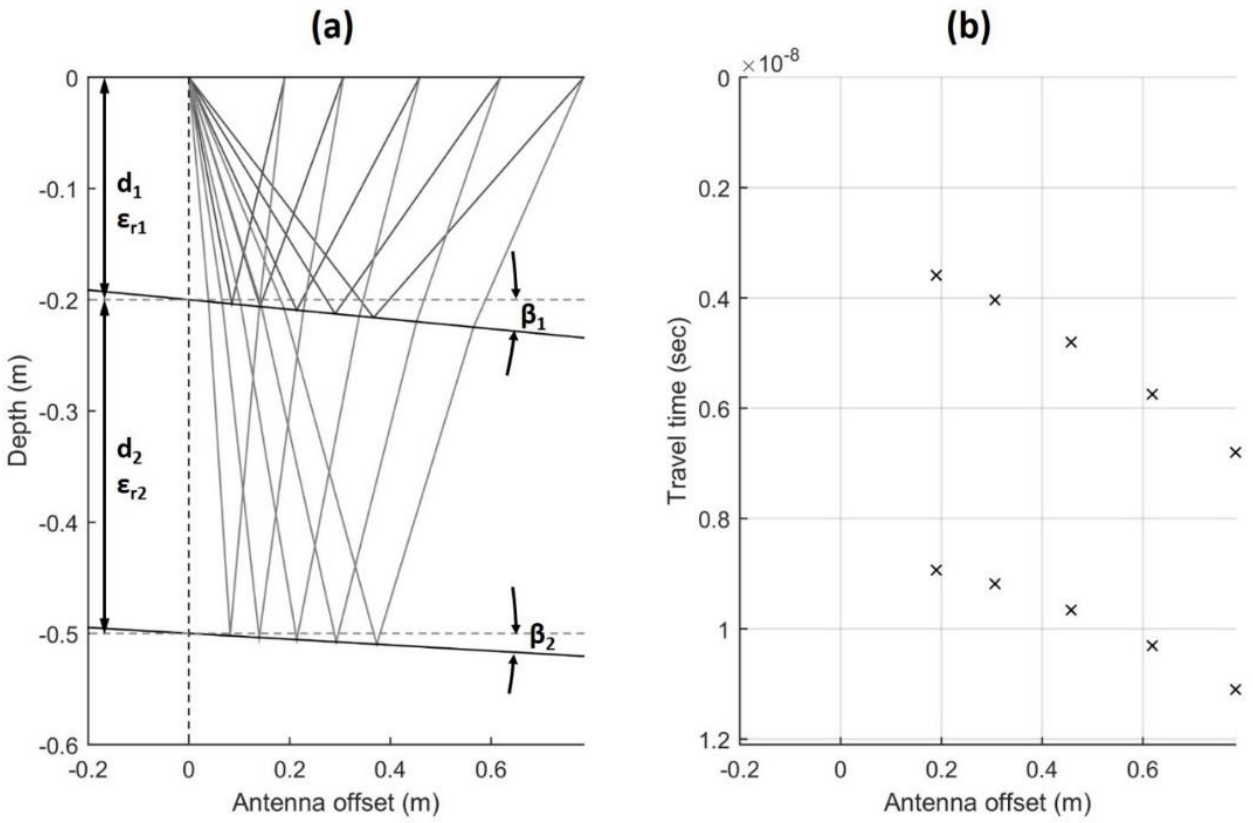

Figure 3-1: (a) An example lateral ray-path model applied to a two-layer pavement and (b) the corresponding two-way travel time predictions at different offsets

The procedure started on a selected WARR gather and worked through all layers before moving on to analyse the next adjacent WARR gather. For each gather, the analysis procedure involved determining the layer depth, permittivity and dipping angle for the uppermost layer by numerically optimising these parameters until the difference between travel times predicted by the ray-path model at each antenna offset and those determined from interface tracking were minimised. These parameters were then fixed for the first layer within the model and were included in the analysis as the algorithm solved for the next layer.

The main contribution of Paper II was to demonstrate the developed IM and RM methods using numerical simulations. While largely successful, there were a number of issues with the developed methods including slow speed of analysis, compounding errors with an increasing number of layers and occasional instability in the numerical analysis.

3.3 Paper III: MFS validation and investigation of edge effects

Muller, W.B. and Dérobert, X. A comparison of phase-shift and one-port coaxial cell permittivity measurements for GPR applications, 7th International Workshop of Advanced GPR (IWAGPR-2013), Nantes. IEEE, 1-6, July 2013.

While the results from initial testing of the phase-shift method in Paper I appeared promising, the approach departs significantly from conventional free-space measurement norms in its use of unfocussed antennas and ground-coupling with the sample under test. This in turn raises concerns regarding the accuracy of measurements and the potential influence of sample edges.

The aims of Paper III were therefore to:

1. Investigate the accuracy of permittivity measurements using the proposed free-space approach by comparing to results using an established one-port coaxial cell for a range of material samples; and

2. Undertake a laboratory experiment and numerical modelling to investigate the influence of sample edges on the measurements.

The research was undertaken by the author in Nantes, France, during a study period at the *Institut français des sciences et technologies des transports, de l'aménagement et des réseaux* (IFSTTAR). Due to an equipment shipping issue, the original antennas were unavailable and a temporary arrangement needed to be configured to enable the comparisons to proceed. The somewhat rudimentary configuration led to a number of unwanted reflections within the measured response which in turn required additional filtering to enable use of the data.

In the first experiment the phase-shift approach was used to characterise samples of various types of plastic, stone and a manufactured material to cover a range of permittivity values. The results were then compared to measurements determined on samples of the same materials using the one-port cell described by Adous et al. (2006) to assess the accuracy of measurements.

A second experiment was undertaken to investigate the influence of sample edges on the phase-shift measurements. It involved collecting a series of measurements using the same antennas and portable VNA while incrementally sliding material samples along in between the fixed antennas to determine how the position of the sample and its edges affected the measurements. FDTD numerical modelling was also undertaken to compare with these measurements and more fully understand EM wave propagation within the samples.

One main finding of Paper III and contribution to the research was validation of the accuracy of the MFS measurements, which compared well to the one-port coaxial cell results for the materials tested. The permittivity results were within 10% of the cell measurements, and within 7% if one particularly thin limestone sample is excluded. The second investigation revealed that sample edges only influenced the MFS measurements when placed very close to the antenna feed point, however, this influence quickly reduced as the samples were moved further along. Based on these observations it was concluded that edge effects did not have a significant influence on these measurements when the antennas were placed centrally on the samples for the size of samples tested.

3.4 Paper IV: MFS equipment investigation and further validation work

Muller W.B. and Scheuermann A., Optimising a modified free-space permittivity characterisation method for civil engineering applications, Journal of Geophysics and Engineering 13(2):S9-S18, April 2016.

An issue regarding the use of ground-coupled antennas for free-space measurements is the potential influence of near-field effects. The calculation of real permittivity in the MFS approach (see Equation 17) assumes plane waves (Trabelsi et al., 2000), and thus far-field conditions. While there are several ‘rules of thumb’ for estimating the distance to the far-field, recent numerical investigations by Diamanti and Annan (2013) indicate that this may be much further than previously thought. As a result, the MFS antennas are unlikely to be sufficiently separated to achieve far-field operation. Nonetheless, the previous laboratory tests in Papers I and III indicated that permittivity estimates using this approach compared well with GPR and one-port coaxial cell measurements.

The question therefore arises: How much of an influence do near-field effects have on the accuracy or reliability of the MFS measurements and is this a significant issue for the proposed approach?

Another aspect of the MFS approach requiring clarification was the optimum sample size, aspect ratio and depth that should be used. A sample size of 300 x 300 x 100 mm was initially selected because a shallow sample box size would be less prone to bursting during compaction and this size kept the sample weight within reasonable manual handling limits. It was unclear, however, if this was optimal in terms of EM wave propagation or reflections within the sample.

To address these questions, Paper IV presented a laboratory study using a combination of numerical modelling, laboratory experiments and sample testing. Numerical modelling was used to better understand wave propagation within the sample boxes and to optimise the sample size. The laboratory experiments primarily focussed on estimating the influence of near-field effects based on the linearity of the measured response for different antenna spacing's and sample thicknesses. Measurements on samples of nylon were also compared to results using the broadband probe developed by Wagner et al. (2014) and measurements were also conducted on distilled and tap water, with known properties, to further validate the accuracy of measurements using this approach.

The key findings and contribution to the research of Paper IV were that:

- The 3:1 sample aspect ratio was nearly ideal as it maximised the difference in arrival time between the direct wave and unwanted effects such as reflections from the box sides and the double bounce from the top of the sample, allowing the direct wave to be more easily isolated and analysed.
- Numerical modelling revealed significant issues with using an empty sample box as the reference measurement due to reflections from the box sides. As a result, the MFS approach was changed to use a ply sheet as the reference.
- Provided the sample depth was at least 100 mm thick, near-field effects did not appear to significantly influence the measurements.
- The MFS permittivity results for nylon compared well with the broadband probe measurement and with the literature values when measuring samples of reverse osmosis-distilled water that were 100 mm and 170 mm thick.

- Despite the numerical modelling finding regarding the optimum aspect ratio, measurements of reverse osmosis-distilled water of sample size 250 x 250 x 170 mm appeared more stable with frequency compared to measurements of a 300 x 300 x 100 mm sample.

3.5 Paper V: Moisture-permittivity investigations for UBG materials

Muller, W.B., Permittivity characterisation of unbound granular pavement materials using a modified free-space approach, Transportation Research Record: Journal of the Transportation Research Board, 2578, 93-101, Washington, D.C., 2016.

The main contribution of Paper V was to present results from six rounds of MFS laboratory testing, using material from four South-East Queensland quarries. The original box size of 300 x 300 x 100 mm was used for the majority of these measurements. An illustration of the MFS configuration used in Paper V is shown in Figure 3-2.

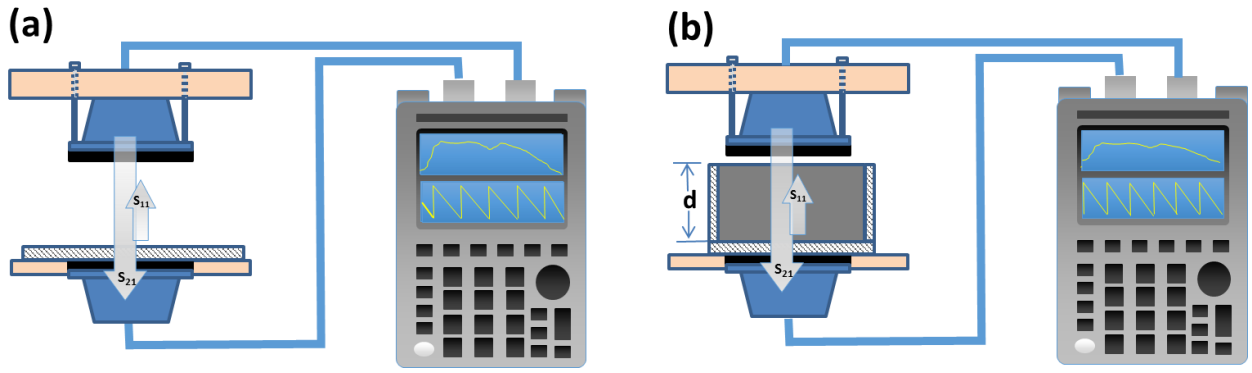

Figure 3-2: The MFS test configuration used for sample characterisation for Paper V. A portable VNA is attached to a fixed pair of bow-tie dipole antennas and is used to measure the transmitted (S_{21}) and reflected (S_{11}) scattering parameters of (a) a plywood sheet (a reference representing an empty sample box), and (b) the boxed and compacted UBG sample

While the results from individual quarries varied slightly, the overall trend of permittivity results was found to be relatively similar to those relations determined by previous researchers for compacted pavement materials using the time-domain reflectometry (TDR) approach. An empirical moisture-permittivity relation was also proposed based on the MFS measurements from these quarries.

3.6 Paper VI: Effect of sample moisture and density on MFS, TDR and GPR

Muller W.B., Bhuyan H. and Scheuermann A., A comparison of modified free-space (MFS), GPR and TDR techniques for permittivity characterisation of unbound granular pavement materials, Near Surface Geophysics, 14(6), 537-550, December 2016.

The permittivity of soil and pavement materials change, not only with material type and volumetric moisture content, but also with sample density, temperature and other attributes. Previous investigators have used TDR sensors embedded within pavement samples (Baran, 1994, Ekblad and Isacsson, 2007, Diefenderfer et al., 2000) or conventional common-offset GPR measurements through known sample depths (Liu and Guo, 2003, Fernandes and Pais, 2014, Evans et al., 2008) to determine pavement permittivity or the average wave velocity and to relate this to the moisture content of samples. It was uncertain, however, how permittivity measurements using these different methods compare to each other and to measurements using the MFS approach. Additionally, it was unclear how variations in density might influence these different methods. This information is important to assess whether reliable comparisons can be made using the combination of multi-offset GPR and MFS to measurements using conventional TDR and GPR measurements and to better understand if, when or why the results vary.

With this in mind, the aim of Paper VI was to undertake a laboratory experiment to compare permittivity results using MFS, TDR and common-offset GPR methods on moisture-varying and density-varying UBG samples.

A key finding and contribution of this paper was that the MFS and GPR measurements compared well for moisture-varying and density-varying samples. The TDR measurements also compared well for higher density and wetter samples, although it predicted lower permittivity results compared to GPR and also varied from the trend of MFS results for drier and lower-density samples. The MFS transmission and reflection measurements were also converted into an equivalent time-domain response and were visually compared to the GPR measurements, illustrating a similar response and hence indicating the signal analysis had been undertaken correctly. However, the response was not as clear or refined as the measurement produced using the commercial GPR equipment.

The variation in direct wave arrival times for MFS measurements shown in the time-domain were also used as a secondary means of estimating sample permittivity, which in general compared well with the phase-shift measurements.

One problem with the approach was the inclusion of nylon spacers during measurement of density-varying samples, which with hindsight was a mistake that increased data analysis complexity and decreased data quality. Another issue was that density-varying samples were prepared to a constant gravimetric moisture content prior to compaction. Thus when compacted to different density levels there was a slight change in volumetric moisture content which may have also contributed to the observed differences. As a result, and due to permittivity discrepancies noted when comparing to TDR for the driest and lowest density samples, Paper VI recommended a more extensive study to further investigate the influence of sample moisture and density on these measurement methods that also addresses these problems with the experimental approach.

3.7 Paper VII: Field implementation

Muller, W.B., Semi-automatic determination of layer depth, permittivity and moisture for unbound granular pavements using multi-offset 3D GPR, Submitted 11 August 2016 to the Journal of Applied Geophysics

The aim of Paper VII was to: combine the multi-offset analysis techniques and moisture-permittivity relation developed in Papers I to VI; apply them in the field to enable predictions of pavement layer depth, permittivity and volumetric moisture content; and validate the predictions. Originally one site investigation was planned. However, after undertaking an initial visit a number of data quality issues were observed in the multi-offset GPR measurements that made adaptation of the analysis methods difficult and required a re-think of the approach. A second investigation was undertaken nearly a year later. In the meantime a number of variants of the RM method had been trialled on data collected during the initial site visit aimed at developing a more robust analysis approach better able to deal with data imperfections. The resulting analysis approach, ray-path modelling-semblance (RM-S), combines elements of the original RM and IM methods and coherence measures to enable more reliable semi-automated analysis of the multi-offset GPR measurements.

The RM-S approach was used to analyse measurements collected along the site during both investigations to predict the depth, permittivity and moisture content of pavement layers. Physical measurements of layer depths and samples of the in situ moisture content of pavement and subgrade materials were undertaken at eight locations along the site during the second site visit (S1 to S8, see Figure 3-3) to validate the predictions. The pavement permittivity was determined during both site visits at one location using embedded TDR probes. Conventional common-offset impulse GPR measurements were undertaken along the site for comparison and to determine the pavement permittivity based on the shape of diffraction hyperbolas from buried reflectors. Repeat runs along the site using the 3D NM-GPR were also undertaken during the second site visit. These measurements were later analysed and compared to assess the reproducibility of RM-S predictions.

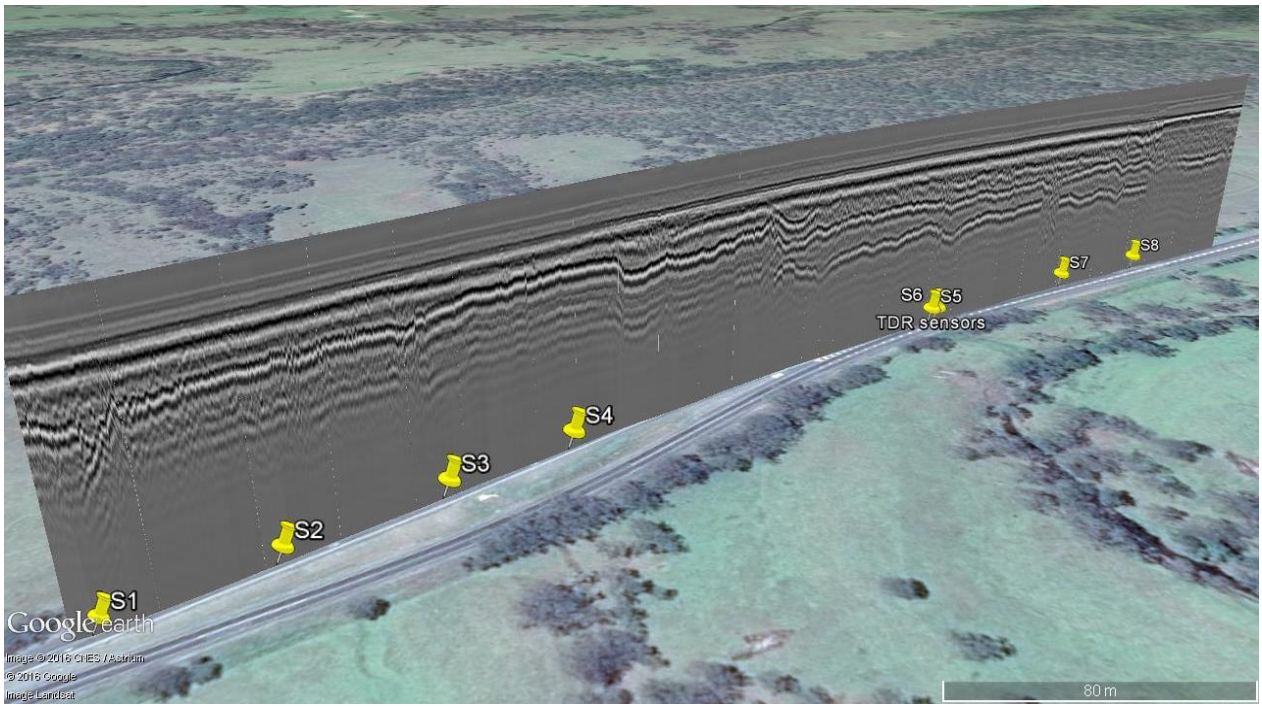

Figure 3-3: NM-GPR scan of the Fisher Park truck stop during Site Visit 2 collected 19 May 2016. Sampled locations S1 to S8 and the TDR installations are also indicated. Source: Google Earth™[1], "map title, scale" map data; (Image: CNES/Astrium, DigitalGlobe, Landsat, Google)

[1] Google Earth is a registered trademark of Google Inc. USA

The main findings, observations and contributions of Paper VII were:

1. The RM-S approach was successfully applied to multi-offset data collected in the field, enabling predictions of the depth, permittivity and volumetric moisture content along the site and for several pavement layers. For this study the multi-offset analysis was undertaken at 1 metre intervals.

2. Overall, the layer depth and volumetric moisture content predictions compared well and were consistent with the findings of physical sampling.

3. A comparison of RM-S predictions from the two site visits enabled pavement moisture variations along the site to be detected and for moisture changes to be monitored over time. The comparison indicated that at the completion of construction (Site Visit 1) the permittivity of upper layers was less than that of lower layers and was relatively consistent along the site. Approximately 11 months later (Site Visit 2) the permittivity differential between upper and lower layers had decreased, presumably due to moisture equalisation over this period. In places the upper layer permittivity also increased, presumably due to moisture ingress. Permittivity measurements determined using TDR and common-offset GPR measurements showed similar trends over this period, however RM-S produced somewhat higher results.

4. A comparison of layer depth and moisture predictions using the RM-S approach for repeat runs along the site during Site Visit 2 indicated that the approach generated relatively reproducible results, however the variability of permittivity predictions increased in lower layers, presumably due to compounding inaccuracies or errors in the analysis.

5. As the RM-S approach reports an average volumetric water content down to or between detected layer interfaces, it may provide a misleading result where a notable moisture gradient exists within these layers. For example, at location S4 physical sampling revealed a much lower volumetric water content within the upper 100 mm (5.0 %) compared to the lower 75 mm (19.6 %) of the pavement. As no intermediate layer reflection was visible in this location, the RM-S approach predicted a volumetric moisture content of approximately 12 % down to the subgrade interface. This example also highlights the potential variability that can occur within pavement layers due to moisture ingress.

4 PROPOSED USES AND FUTURE RESEARCH

This research successfully developed, demonstrated and validated an innovative semi-automatic approach using multi-offset ground penetrating radar (GPR) to achieve quantitative estimates of moisture content and layer depth predictions for unbound granular (UBG) pavements. A novel free-space characterisation method was also developed, investigated and validated. These research outcomes have a number of direct applications for measuring pavement layer depth, moisture and characterising materials. The developed methods also have significant potential for use in combination with conventional time-domain reflectometry (TDR) probes and the recently-developed traffic speed deflectometer (TSD) device. An overview of potential uses of the developed methods follows.

4.1 Pavement layer depth and moisture

The initial application of these techniques will most likely focus on the investigation of layer depth and moisture within roads at project-level scales, for example: assessing layer depth as part of pavement rehabilitation investigations; identifying the extent and severity of suspected pavement moisture ingress problems; and for forensic investigation of the causes of pavement failures. Initially a number of additional comparisons should be undertaken to further assess the accuracy and repeatability of layer depth and moisture content predictions using the ray-path modelling-semblance (RM-S) approach for a wider range of pavement types, for older and more variable pavements and to further develop confidence in the approach.

One potential use would be to investigate the longitudinal, lateral and vertical distribution of moisture within pavement layers. Seasonal moisture variations could also be monitored by comparing measurements over time, as demonstrated in Paper VII. Measurement of lateral moisture variations may also be possible using variants of the RM-S approach. An example is shown in Figure 4-1, illustrating an early version of the RM-S approach applied to adjacent antenna pairs across the array. In this example the approach had not been fully refined, resulting in overestimate of lower layer permittivity and moisture content. Nonetheless, it demonstrates that separate moisture estimates can be determined across the array by analysing the measurements as adjacent pairs of wide angle reflection and refraction (WARR) gathers.

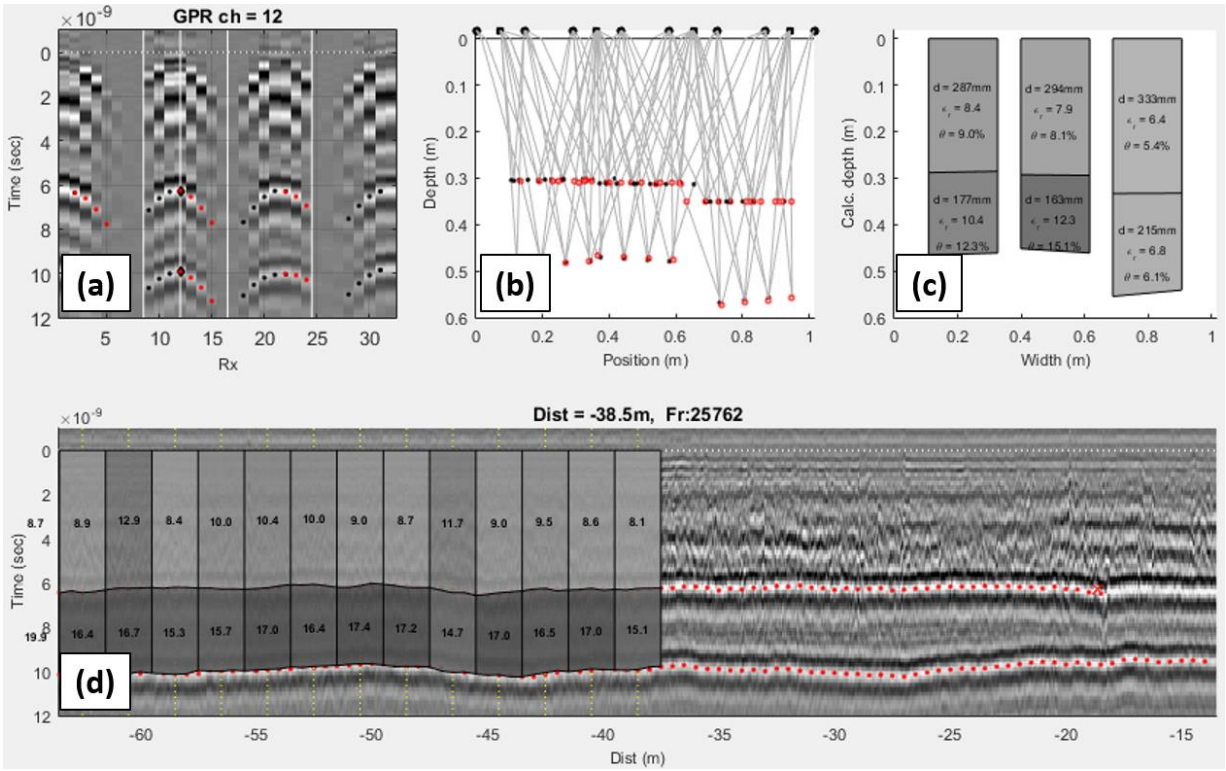

Figure 4-1: The RM-S approach applied to adjacent antenna pairs: (a) The measured multi-offset response compared to travel time predictions from the ray-path model (dots); (b) the ray-path models determined for each wide angle reflection and refraction (WARR) pair; (c) layer depth, permittivity and moisture content predictions for the three adjacent antenna pairs across the array; and (d) volumetric moisture content predictions for analysed locations for the central antenna pair, with tracked layer interfaces also shown

This version of the approach may also be useful for assessing the effectiveness of different pavement designs or drainage strategies, for example, by determining whether moisture is retained within the pavement, where it is located and how quickly it is drained. Furthermore, this could be achieved without the inconvenience or cost of installing sensors or physical sampling.

The approach may also be useful in combination with a network of embedded TDR probes arranged as monitoring stations to improve spatial coverage and develop a more complete picture of pavement moisture within the network. That is, TDR would be used to continuously monitor the pavement and subgrade moisture at a number of fixed stations. These data would then be supplemented by results using the RM-S approach, collected intermittently between these locations.

Such a combination would utilise both the temporal sampling strengths of TDR and the spatial sampling benefits of RM-S to enable better informed asset monitoring and management.

4.2 Combined use with the TSD

There are also a number of potential uses of the developed techniques in combination with the recently developed Traffic Speed Deflectometer (TSD). The TSD is a mobile device that uses a combination of Doppler-vibrometers and complementary sensors to measure the velocity of the deflecting road surface at fixed offsets ahead of loaded rear wheel (Ferne et al., 2009, Baltzer et al., 2010, Kelley and Moffat, 2011). The corresponding deflection profile of the road surface (deflection bowl) can be determined either by curve fitting and numerical integration (Muller and Roberts, 2013) or by fitting a pavement model or other model types to the TSD measurements (Krarup et al., 2006, Pedersen, 2012, Zofka et al., 2014). The measurements are collected essentially continuously at up to 80 kilometres per hour, which greatly increases the speed of data collection compared to conventional methods and enables far more practical measurement of pavement structural response at large scales. A number of field trials within Australia using first-generation (Muller and Roberts, 2013, Roberts et al., 2014) and second-generation (Muller and Wix, 2014, Wix et al., 2016) TSD equipment together with a simplified data analysis approach have demonstrated that this device can produce deflection predictions similar to conventional falling weight deflectometer (FWD) measurements (Muller and Roberts, 2013, Roberts et al., 2014, Muller, 2015). Since 2014 a second-generation TSD and this analysis approach have been used to scan state-controlled roads within Queensland, New South Wales and in New Zealand, covering more than 60,000 lane-kilometres (Wix et al., 2016).

The research presented in this thesis, if used to its full extent, will enhance use of the TSD in a number of ways. For one, the ability to determine pavement layer depth and moisture content would enable variations in these parameters to be identified and compared to changes in structural response. As TSD and multi-offset NM-GPR measurements can both be collected at traffic-speeds these data could be collected over long lengths of road for comparison and analysis. Ideally both sets of data would be collected simultaneously, that is, by mounting the 3D NM-GPR equipment on the TSD.

This information is important because without it investigators would be uncertain if deflection changes occurring at a fixed location are due to moisture changes, pavement deterioration, TSD calibration issues (Wix et al., 2016) or some other influence. Furthermore, the 3-dimensional (3D) GPR data would also be useful to determine if the changes were simply due to the vehicle following a slightly different lateral alignment from one year to the next or may be due to a pavement repair performed in between scans. Pavement moisture information would also help investigators determine if this attribute has changed from one year to the next, to enable better explanation of any observed differences. While simple visual comparisons of TSD and NM-GPR data have previously been demonstrated (Muller and Reeves, 2012, Muller, 2015) (see Figure 4-2), this research enables calibrated layer depth estimates and quantitative moisture predictions for comparison with the pavement structural response, offering potential for a more detailed and better informed analysis of existing pavement conditions.

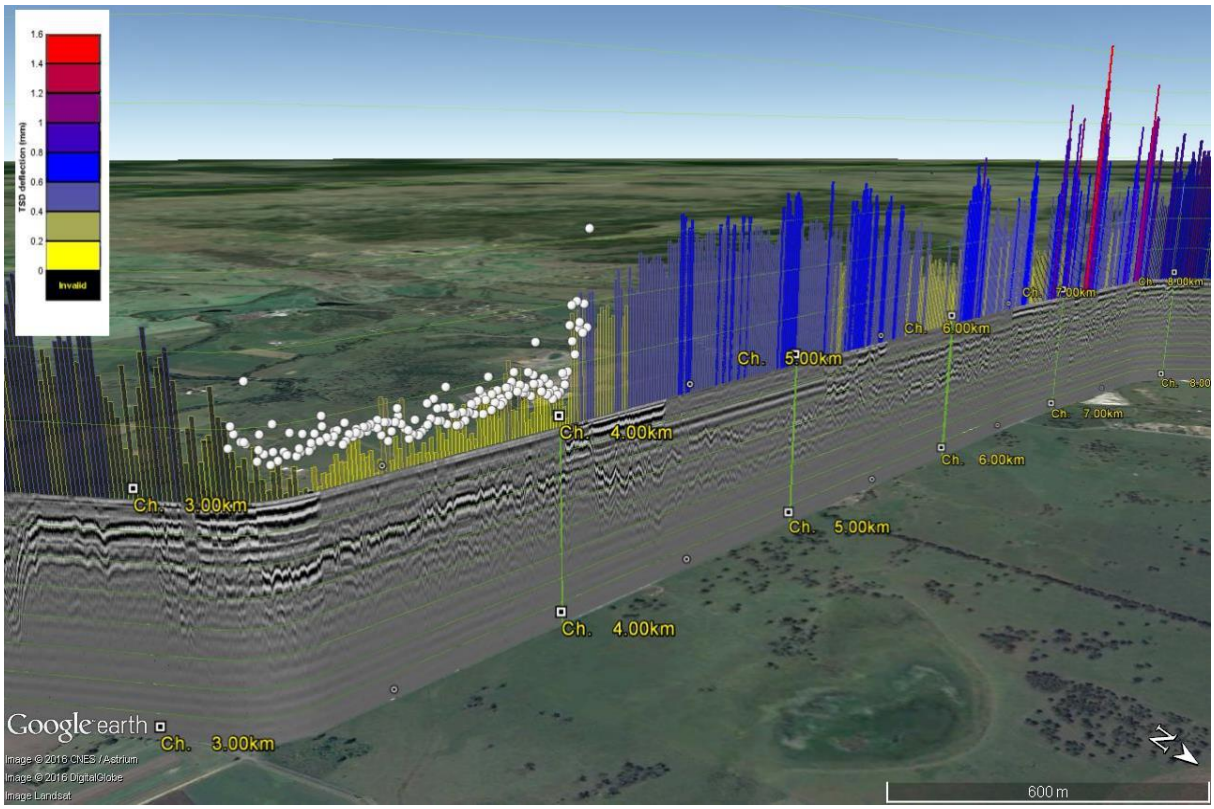

Figure 4-2: TSD (coloured bars), FWD (white dots) and GPR radargram measurements compared geospatially within Google Earth™[2]. Source: Google Earth™, "map title, scale" map data; (Image: CNES/Astrium, DigitalGlobe, Landsat, Google)

[2] Google Earth is a registered trademark of Google Inc. USA

Recent comparisons of TSD data have also demonstrated the repeatability of these measurements from one year to the next (Muller, 2015). A further example of this is shown in Figure 4-3.

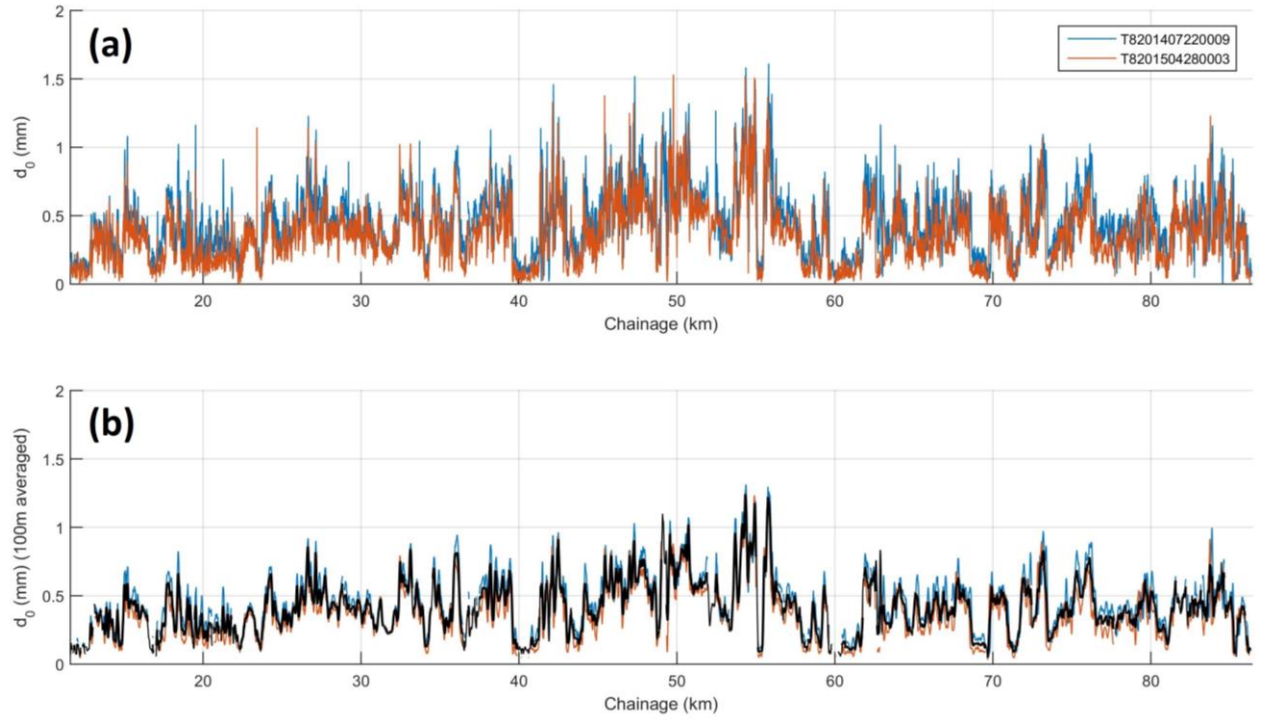

Figure 4-3: (a) TSD data collected on 22 July 2014 (blue) and on 28 April 2015 (red), auto-aligned to the Department of Transport and Main Roads chainage system; and (b) the same data 100 metre averaged (mean value shown as a black line)

These observations are important as they show that a repeatable network-level structural benchmark can be collected using TSD. If then combined with network-level measurements of layer depth and pavement moisture content determined using multi-offset GPR this may be useful for large-scale pavement assessment or monitoring.

An example of where this may be useful is during the assessment of flood-affected pavements. Large-scale TSD and multi-offset GPR measurements collected prior to these events could be used as a benchmark of ‘normal’ pavement deflection and moisture conditions with which to compare. Calibrated layer depths, which could be determined wherever layer interface reflections were visible prior to flooding, would also be useful for analysing or targeting FWD measurements. It might even be possible to fly a small and lightweight multi-offset GPR, for example the T02 trailer used in Paper VII, to flood-affected locations to scan saturated roads.

Provided the pavement layer interfaces were still sufficiently visible to be detected and tracked, the RM-S analysis approach could be used to determine the amount of moisture present within the road after flooding which then could be compared with the benchmark results to determine the difference. This may also be useful to guide or target the collection of FWD measurements, which could then be compared with the TSD measurements. In this case FWD would be preferable to TSD as the equipment is more likely to be available in regional areas at short notice and is less likely to damage wet and weakened pavements compared to a large and heavy semi-trailer.

Another way the research may enhance use of the TSD measurements is in relation to pavement structural analysis. As deflection bowls similar to FWD can be produced from TSD measurements (Muller and Roberts, 2013, Muller and Wix, 2014), back-analysis of layer moduli should also be possible. As pavement structure information is required for the forward-calculation portion of the analysis (Goktepe et al., 2006), the developed methods may be useful to determine calibrated estimates of layer depth without cores or trenches. While many authors have used GPR to interpret FWD measurements, target their location or provide layer depth information as an input for back-analysis (Noureldin et al., 2003, Maser, 1996, Lenngren et al., 2000, Saarenketo and Scullion, 2000, Scullion et al., 1992, Scullion and Saarenketo, 2000, Ahmed et al., 2014), the advantage of using TSD combined with multi-offset NM-GPR is that both datasets can be collected at traffic speeds. Furthermore, and as noted previously, the multi-offset approach should also be more reliable on older and more variable pavement materials compared to surface reflection coefficient-based methods.

The research is also timely as investigations into the combined used of TSD and GPR have been gaining interest in Europe (Cook, 2015, Rabe, 2013, Herronen et al., 2015) and specifications are currently being developed for the combined use of these methods (Wright et al., 2016).

4.3 Potential research avenues

The current research could be extended or refined in a number of ways. For one, additional validation studies are required to further assess the accuracy of layer depth and moisture predictions for a greater number of sites and a wider range of pavement types. While the site investigation results presented in Paper VII were promising, the scans were undertaken while the site was new and thus the materials were consistent.

The number of physical samples collected for layer depth and moisture content validation was also relatively limited, which was necessary considering that the test site was an operating truck stop and a brand new pavement. Further field investigations, including statistical analysis of a larger number of sites and validation points, are therefore recommended to develop further confidence in the method and to identify areas where it could be further refined or improved. It would also be useful to assess the reliability of permittivity and layer depth estimates using this approach compared to conventional impulse GPR and surface-reflection coefficient techniques, in particular considering the potential influence of layer inhomogeneity and equipment operating temperature on the results.

Another future task is to further develop and refine the RM-S approach. In particular, to improve analysis speed and investigate variants that increase analysis flexibility. The approach also needs to be adapted for use on the larger NM-GPR trailer, which uses 8 transmitters and 16 receivers. It may be possible to consider data from this system as two adjacent T02 trailers which are analysed separately. Alternatively, the WARR gathers could be analysed as adjacent pairs or by using some other combination. A further task will be to investigate the nature of the groundwave arrival to see whether it can be used to assess near-surface pavement permittivity.

Additional investigations using the modified free-space (MFS) method are also recommended. The laboratory study outlined in Paper VI identified a difference between permittivity estimates determined using TDR and those from MFS and GPR for dry and low-density samples. A more extensive investigation is recommended to further assess these differences. Other aspects that may also warrant investigation include: undertaking a direct comparison between multi-offset GPR measurements and the laboratory-based methods investigated in Paper VI; investigating the influence of temperature and other sample attributes on the MFS measurements; and studying whether the high-frequency signal loss observed in Paper V could be used as an additional means of moisture detection or quantification.

5 CONCLUSION

This research set out to develop an approach using a new type of 3-dimensional (3D) ground penetrating radar (GPR) to determine the moisture content and depth of unbound granular (UBG) pavement layers. To this end, a research question was posed:

> Can a semi-automatic approach be developed to analyse multi-offset measurements collected using this new 3D GPR to enable quantitative moisture predictions and reliable layer depth estimates for UBG pavements that is also simple to use?

To address this question, the research effort focussed on three main objectives, to:

1. Investigate and develop semi-automated multi-offset analysis methods;
2. Develop and validate a laboratory characterisation method to calibrate petro-physical relations for UBG pavement materials; and
3. Field trial and validate the developed approach to predict the moisture content, depth and permittivity of UBG pavement layers.

Seven incorporated papers were produced during candidature, generating a number of important findings. When combined, these papers demonstrate that the research objectives were met, with the main outcomes of the work being the successful:

1. Development, field implementation and validation of a semi-automated multi-offset GPR analysis approach; and
2. Development, laboratory validation and use of a novel approach for permittivity characterisation of civil engineering materials.

The research is significant as it provides a more practical method of using multi-offset GPR techniques to monitor pavement moisture continuously along the road and to estimate layer depths. Furthermore, the approach can be used to estimate moisture within several pavement layers, although the variability of predictions does increase with the number of layers.

Semi-automated implementation of these analysis methods also enables the multi-offset approach to be used as a viable alternative to well-established surface reflection coefficient methods for continuous permittivity calibration of pavement layers. As the approach is based on measuring the mean velocity of electromagnetic (EM) passing through the full depth of existing pavement layers, it accounts for material inhomogeneity within layers and thus should enable more reliable layer depth estimates for older and more variable pavements. Furthermore, the accuracy of measurements should be less influenced by material loss mechanisms within pavement layers compared to techniques that rely on accurate measurement of signal amplitude.

The variant of the free-space approach produced in the work, modified free space (MFS), enables characterisation of the bulk permittivity of coarse-grained un-bonded civil engineering materials. It enables measurement of larger and more representative sample volumes, uses a simple and low-cost antenna arrangement, operates at GPR frequencies and avoids the potential risk of damaging delicate apparatus by measuring materials compacted within low-cost sample boxes.

The work is timely when viewed in context of the recent development of high-speed deflection measurement devices such as the traffic-speed deflectometer (TSD) and efforts to combine measurements using this approach with GPR. The developed techniques also have potential to enable new investigation methods or to improve current practice in relation to forensic pavement studies, flooded pavement assessment and pavement moisture quantification and monitoring, a few examples of which have been described.

The research presented in the seven incorporated papers and drawn together in this thesis has successfully addressed the research question that was posed in the affirmative. That is, by developing a novel multi-offset analysis approach that was successfully applied in the field and was demonstrated to reliably predict the depth and moisture content of UBG pavement layers along a test site. Furthermore, the approach only requires the operator to select the start and end points along the road for a number of layer interfaces reflections within the GPR response for a single antenna pair, after which the analysis is fully automatic. It therefore also satisfies the aim of achieving data analysis simplicity.

REFERENCES

ADOUS, M., QUÉFFÉLEC, P. & LAGUERRE, L. 2006. Coaxial/cylindrical transition line for broadband permittivity measurement of civil engineering materials. *Measurement Science and Technology,* 17**,** 2241-2246.

AHMED, M., TAREFDER, R. & MAJI, A. 2014. Variation of FWD modulus due to incorporation of GPR predicted layer thicknesses. *15th International conference on Ground Penetrating Radar (GPR-2014).* Brussels: IEEE.

AL-QADI, I., LENG, Z., LAHOUAR, S. & BAEK, J. 2010. In-place hot-mix asphalt density estimation using Ground-Penetrating Radar. *Transportation Research Record: Journal of the Transportation Research Board,* 2152**,** 19-27.

AL-QADI, I. L. 1992. Using microwave measurements to detect moisture in asphaltic concrete. *Journal of Testing and Evaluation,* 20**,** 43-50.

AL-QADI, I. L., GHODGAONKAR, D. K., VARADAN, V. K. & VARADAN, V. V. 1991. Effect of moisture on asphaltic concrete at microwave frequencies. *IEEE Transactions on Geoscience and Remote Sensing,* 29**,** 710-717.

AL-QADI, I. L. & LAHOUAR, S. 2005. Measuring layer thicknesses with GPR – Theory to practice. *Construction and Building Materials,* 19**,** 763-772.

AL-QADI, I. L., LAHOUAR, S. & LOULIZI, A. 2003. GPR: From the state-of-the-art to the state-of-the-practice. *International Symposium Non-Destructive Testing in Civil Engineering (NDT-CE 2003).* Berlin: NDT.net.

AL-QADI, I. L., LAHOUAR, S., LOULIZI, A., ELSEIFI, M. A. & WILKES, J. A. 2004. Effective approach to improve pavement drainage layers. *Journal of Transportation Engineering,* 130**,** 658-664.

ANNAN, A. P. 2005. Ground-Penetrating Radar. *In:* BUTLER, D. K. (ed.) *Near-Surface Geophysics.* Netherlands: Society of Exploration Geophysicists.

ANNAN, A. P. 2009. Electromagnetic Principles of Ground Penetrating Radar. *In:* JOL, H. M. (ed.) *Ground Penetrating Radar Theory and Applications.* Amsterdam: Elsevier.

ARCONE, S. A. & BOITNOTT, G. E. 2010. Complex permittivity of common minerals and one soil at low water contents. *13th International conference on Ground Penetrating Radar (GPR-2010).* Leece: IEEE.

AUSTROADS 2003. *Control of moisture in pavements during construction*. APRG Technical Note 13. ARRB Transport Research, Sydney.

AZIZ, M. B. A., MUNIANDY, R., ABDULLAH, K., MAHMUD, A. R., KHALID, K. & ISMAIL, A. 2010. Preliminary determination of asphalt properties using microwave techniques. *ARPN Journal of Engineering and Applied Sciences,* 5**,** 70-81.

BALTZER, S., PRATT, D., WELIGAMAGE, J., ADAMSEN, J. & HILDEBRAND, G. 2010. Continuous bearing capacity profile of 18,000km Australian road network in 5 months. *24th ARRB Conference.* Melbourne: ARRB Group.

BARAN, E. 1994. Use of time domain reflectometry for monitoring moisture changes in crushed rock pavements. *Symposium and workshop on time domain reflectometry in environmental, infrastructure and mining applications.* Evanston, USA: United States Bureau of Mines.

BEHARI, J. 2005. *Microwave dielectric behavior of wet soils,* Netherlands & New Delhi, Springer & Anamaya Publishers.

BENEDETTO, A. 2007. Prediction of structural damages of road pavement using GPR. *4th International Workshop on Advanced Ground Penetrating Radar.* Naples: IEEE.

BENEDETTO, A. & PENSA, S. 2007. Indirect diagnosis of pavement structural damages using surface GPR reflection techniques. *Journal of Applied Geophysics,* 62**,** 107-123.

BENEDETTO, A., TOSTI, F., ORTUANI, B., GIUDICI, M. & MELE, M. 2013. Soil moisture mapping using GPR for pavement applications. *7th International Workshop on Advanced Ground Penetrating Radar (IWAGPR-2013)* Nantes: IEEE.

BERTHELOT, C., PODBOROCHYNSKI, D., SAARENKETO, T., MARJERISON, B. & PRANG, C. 2010. Ground-penetrating radar evaluation of moisture and frost across typical Saskatchewan road soils. *Advances in Civil Engineering,* 2010**,** 1-9.

BODIN, D. & KRAFT, J. 2015. *Effect of moisture content and laboratory preparation conditions on the permanent deformation of unbound granular materials*. Technical Report AP-T287-15. Austroads, Sydney.

BROWN, R. A. B., MICHAEL 2013. Assessment of Clogging Dynamics in Permeable Pavement Systems with Time Domain Reflectometers. *Journal of Environmental Engineering,* 139**,** 1255-1265.

BURGER, H. R., SHEEHAN, A. F. & JONES, C. H. 2006. *Introduction to Applied Geophysics: Exploring the shallow subsurface,* New York, W.W. Norton & Company Inc.

BÜYÜKÖZTÜRK, O., YU, T. & ORTEGA, J. 2006. A methodology for determining complex permittivity of construction materials based on transmission-only coherent, wide-bandwidth free-space measurements. *Cement and Concrete Composites,* 28**,** 349-359.

CASSIDY, N. J. 2009. Electrical and magnetic properties of rocks, soils and fluids. *In:* JOL, H. M. (ed.) *Ground Penetrating Radar: Theory and Applications.* Amsterdam: Elsevier.

CHANG, C. M., CHEN, J. S. & WU, T. B. 2011. Dielectric modeling of asphalt mixtures and relationship with density. *Journal of Transportation Engineering,* 137**,** 104-111.

CHANZY, A., TARUSSOV, A., JUDGE, A. & BONN, F. 1996. Soil water content determination using a digital ground-penetrating radar. *Soil Science Society of America Journal,* 60**,** 1318-1326.

CHARLIER, R., HORNYCH, P., SRŠEN, M., HERMANSSON, Å., BJARNASON, G., ERLINGSSON, S. & PAVŠIČ, P. 2009. Water influence on bearing capacity and pavement performance: Field observations. *In:* DAWSON, A. (ed.) *Water in road structures: Movement, drainage and effects.* Nottingham: Springer Science+Business Media B.V.

CHARLTON, M. 2000. Small-scale soil-moisture variability estimated using ground penetrating radar. *In:* NOON, D. A., STICKLEY, G. F. & LONGSTAFF, D. (eds.) *8th International conference on Ground Penetrating Radar (GPR-2000).* Gold Coast, Australia: SPIE.

CHARLTON, M. 2001. Characterization of ground-penetrating radar (GPR) response in a variety of Earth materials under different moisture conditions. *In:* NGUYEN, C. (ed.) *Subsurface and Surface Sensing Technologies and Applications III.* San Diego, USA: SPIE.

CHEN, D. H. & SCULLION, T. 2007. Using nondestructive testing technologies to assist in selecting the optimal pavement rehabilitation strategy. *Journal of Testing and Evaluation,* 35**,** 211-219.

CHEN, D. H. & SCULLION, T. 2008. Forensic investigations of roadway pavement failures. *Journal of Performance of Constructed Facilities,* 22**,** 35-44.

CHEN, L. F., ONG, C. K., NEO, C. P., VARADAN, V. V. & VARADAN, V. K. 2004. *Microwave electronics: Measurement and materials characterization,* Chichester, UK, John Wiley & Sons, Ltd.

CHUNG, C. C. & LIN, C. P. 2009. Apparent dielectric constant and effective frequency of TDR measurements: Influencing factors and comparison. *Vadose Zone Journal,* 8**,** 548-556.

COOK, A. 2015. Measuring overlay thickness. *Highways.* Sevenoaks, UK: Alad Ltd.

DANIELS, D. J. (ed.) 2004. *Ground penetrating radar,* London: Institution of Electrical Engineers (IEE).

DAVIS, J., HUANG, Y., MILLARD, S. G. & BUNGEY, J. H. 2003. Determination of dielectric properties of insitu concrete at radar frequencies. *International Symposium Non-Destructive Testing in Civil Engineering (NDT-CE 2003).* Berlin: NDT.net.

DAVIS, J. L., ROSSITER, J. R., MESHER, D. E. & DAWLEY, C. B. 1994. Quantitative measurement of pavement structures using radar. *5th International conference on Ground Penetrating Radar (GPR'94).* Kitchener, Canada: Waterloo Centre for Groundwater Research.

DAWSON, A. 2009. Introduction. *In:* DAWSON, A. (ed.) *Water in Road Structures: Movement, Drainage and Effects.* Netherlands: Springer.

DE PUE, J., VAN MEIRVENNE, M. & CORNELIS, W. M. 2016. Accounting for surface refraction in velocity semblance analysis with air-coupled GPR. *IEEE Journal of selected topics in Applied Earth Observations and Remote Sensing,* 9**,** 60-73.

DÉROBERT, X., IAQUINTA, J., KLYSZ, G. & BALAYSSAC, J. 2008. Use of capacitive and GPR techniques for the non-destructive evaluation of cover concrete. *NDT&E International,* 41**,** 44-52.

DIAMANTI, N. & ANNAN, A. P. 2013. Characterizing the energy distribution around GPR antennas. *Journal of Applied Geophysics,* 99**,** 83-90.

DIEFENDERFER, B., AL-QADI, I. & LOULIZI, A. 2000. Laboratory calibration and in situ measurements of moisture by using time-domain reflectometry probes. *Transportation Research Record: Journal of the Transportation Research Board,* 1699**,** 142-150.

DIEFENDERFER, B. K., MOKAREM, D. W. & SHARP, S. R. 2006. *Use of nondestructive evaluation to detect moisture in flexible pavements*. Report no. VTRC 06-R37. Virginia Transportation Research Council, Charlottesville, USA.

DIX, C. H. 1955. Seismic velocities form surface measurements. *Geophysics,* 20**,** 68-86.

DOBRIYAL, P., QURESHI, A., BADOLA, R. & HUSSAIN, S. A. 2012. A review of the methods available for estimating soil moisture and its implications for water resource management. *Journal of Hydrology,* 458-459**,** 110-117.

DU PLOOY, R., VILLAIN, G., PALMA LOPES, S., IHAMOUTEN, A., DÉROBERT, X. & THAUVIN, B. 2013. Electromagnetic non-destructive evaluation techniques for the monitoring of water and chloride ingress into concrete: a comparative study. *Materials and Structures,* 48**,** 369-386.

DU, S. & RUMMEL, P. 1994. Reconnaissance studies of moisture in the subsurface with GPR. *5th International conference on Ground Penetrating Radar (GPR'94).* Kitchener, Canada: Waterloo Centre for Groundwater Research, University of Waterloo.

EDWARDS, L. & MASON, Q. 2011. *Evaluation of nondestructive methods for determining pavement thickness*. Report no. ERDC/GSL TR-11-41. US Army Corp of Engineers, Engineer Research and Development Center, Vicksburg, USA.

EKBLAD, J. & ISACSSON, U. 2007. Time-domain reflectometry measurements and soil-water characteristic curves of coarse granular materials used in road pavements. *Canadian Geotechnical Journal,* 44**,** 858-872.

ELSEIFI, M., AL-QADI, I., LOULIZI, A. & WILKES, J. 2001. Performance of geocomposite membrane as pavement moisture barrier. *Transportation Research Record: Journal of the Transportation Research Board,* 1772**,** 168-173.

EMILSSON, J., ENGLUND, P. & FRIBORG, J. 2002. Simple method for estimation of water content of roadbeds using multi-offset GPR. *In:* KOPPENJAN, S. & LEE, H. (eds.) *9th International conference on Ground Penetrating Radar (GPR-2002).* Santa Barbara, USA: SPIE.

ERLINGSSON, S., BALTZER, S., BAENA, J. & BJARNASON, G. 2009a. Measurement Techniques for Water Flow. *In:* DAWSON, A. (ed.) *Water in Road Structures: Movement, Drainage and Effects.* Netherlands: Springer.

ERLINGSSON, S., BRENČIČ, M. & DAWSON, A. 2009b. Water Flow Theory for Saturated and Unsaturated Pavement Material. *In:* DAWSON, A. (ed.) *Water in Road Structures: Movement, Drainage and Effects.* Netherlands: Springer.

EVANS, R., FROST, M., STONECLIFFE-JONES, M. & DIXON, N. 2007. Assessment of in situ dielectric constant of pavement materials. *Transportation Research Record: Journal of the Transportation Research Board,* 2037**,** 128-135.

EVANS, R. D., FROST, M. W., DIXON, N. & STONECLIFFE-JONES, M. 2008. The response of ground penetrating radar (GPR) to changes in temperature and moisture condition of pavement materials. *In:* ELLIS, E., YU, H., MCDOWELL, G., DAWSON, A. & THOM, N. (eds.) *Advances in Transportation Geotechnics.* Nottingham, UK: CRC Press, Taylor Francis Group.

EVERETT, M. E. 2013. *Near-Surface Applied Geophysics,* Cambridge, UK, Cambridge University Press.

FAUCHARD, C., DÉROBERT, X., CARIOU, J. & CÔTE, P. 2003. GPR performances for thickness calibration on road test sites. *NDT&E International,* 36**,** 67-75.

FAUCHARD, C., DEROBERT, X. & COTE, P. GPR performances on a road test site. *In:* NOON, D. A., STICKLEY, G. F. & LONGSTAFF, D., eds. 8th International conference on Ground Penetrating Radar (GPR-2000), 2000 Gold Coast, Australia. SPIE, 421-426.

FERNANDES, F. M. & PAIS, J. 2014. Assessment of moisture in road pavements. *15th International conference on Ground Penetrating Radar (GPR-2014).* Brussels: IEEE.

FERNE, B. W., LANGDALE, P., ROUND, N. & FAIRCLOUGH, R. 2009. Development of a Calibration Procedure for the U.K. Highways Agency Traffic-Speed Deflectometer. *Transportation Research Record,* 2093**,** 111-117.

FILALI, B., BOONE, F., RHAZI, J. & BALLIVY, G. 2008. Design and calibration of a large open-ended coaxial probe for the measurement of the dielectric properties of concrete. *IEE Transactions on Microwave Theory and Techniques,* 56**,** 2322-2328.

FIORI, A., BENEDETTO, A. & ROMANELLI, M. 2005. Application of the effective medium approximation for determining water contents through GPR in coarse-grained soil materials. *Geophysical Research Letters,* 32**,** 1-4.

GERHARDS, H., WOLLSCHLÄGER, U., YU, Q., SCHIWEK, P., PAN, X. & ROTH, K. 2008. Continuous and simultaneous measurement of reflector depth and average soil-water content with multichannel ground-penetrating radar. *Geophysics,* 73**,** J15-J23.

GOKTEPE, A. B., AGAR, E. & LAV, A. H. 2006. Advances in backcalculating the mechanical properties of flexible pavements. *Advances in Engineering Software,* 37**,** 421-431.

GOODMAN, D. & PIRO, S. 2013. GPR Image Construction and Image Processing. *GPR Remote Sensing in Archaeology.* Heidelberg, New York, Dordrecht & London: Springer.

GREAVES, R. J., LESMES, D. P., LEE, J. M. & TOKSÖZ, M. N. 1996. Velocity variations and water content estimated from multi-offset, ground-penetrating radar. *Geophysics,* 61**,** 683-695.

GROTE, K., HUBBARD, S., HARVEY, J. & RUBIN, Y. 2005. Evaluation of infiltration in layered pavements using surface GPR reflection techniques. *Journal of Applied Geophysics,* 57**,** 129-153.

GROTE, K., HUBBARD, S. & RUBIN, Y. 2003. Field-scale estimation of volumetric water content using ground-penetrating radar ground wave techniques. *Water Resources Research,* 39.

HALABE, U. B., SOTOODEHNIA, A., MASER, K. R. & KAUSEL, E. A. 1993. Modeling of the Electromagnetic Properties of Concrete. *American Concrete Institute Materials Journal,* 90**,** 552-563.

HAMROUCHE, R. & SAARENKETO, T. 2014. Improvement of a coreless method to calculate the average dielectric value of the whole asphalt layer of a road pavement. *15th International conference on Ground Penetrating Radar (GPR-2014).* Brussels: IEEE.

HASAR, U. C. 2009. Non-destructive testing of hardened cement specimens at microwave frequencies using a simple free-space method. *NDT&E International,* 42**,** 550-557.

HEIMOVAARA, T. J. 1993. Design of triple-wire Time Domain Reflectometry probes in practice and theory. *Soil Science Society of America Journal,* 57**,** 1410-1417.

HERRONEN, T., MATINTUPA, A. & SAARENKETO, T. 2015. Experiences with integrated analysis of TSD, GPR and laser scanner data. *International Symposium Non-Destructive Testing in Civil Engineering (NDT-CE 2015).* Berlin: NDT.net.

HIEBEL, M. 2007. *Fundamentals of Vector Network Analysis*, Rohde & Schwarz.

HORE-LACY, W., BODIN, D. & SCHEUERMANN, A. 2014. Time domain reflectometry based moisture monitoring system for unbound granular pavements. *26th ARRB Conference.* Sydney, Australia: ARRB Group Ltd.

HUANG, Y. 2001. Design, calibration and data interpretation for a one-port large coaxial dielectric measurement cell. *Measurement Science and Technology,* 12**,** 111–115.

HUBBARD, S., GROTE, K. & RUBIN, Y. 2002. Mapping the volumetric soil water content of a California vineyard using high-frequency GPR ground wave data. *The Leading Edge,* 21**,** 552.

HUGENSCHMIDT, J. 2000. Multi-offset analysis for man-made structures. *In:* NOON, D. A., STICKLEY, G. F. & LONGSTAFF, D. (eds.) *8th International conference on Ground Penetrating Radar (GPR-2000).* Gold Coast, Australia: SPIE.

HUISMAN, J. A. & BOUTEN, W. 2002. Mapping surface soil water content with the ground wave of ground-penetrating radar. *In:* KOPPENJAN, S. & LEE, H. (eds.) *9th international conference on Ground Penetrating Radar (GPR-2002).* Santa Barbara, USA SPIE.

HUISMAN, J. A. & BOUTEN, W. 2003. Accuracy and reproducibility of mapping surface soil water content with the ground wave of ground-penetrating radar. *Journal of Environmental & Engineering Geophysics,* 8**,** 67-75.

HUISMAN, J. A., HUBBARD, S. S., REDMAN, J. D. & ANNAN, A. P. 2003. Measuring soil water content with Ground Penetrating Radar: A review. *Vadose Zone Journal,* 2**,** 476-491.

HUISMAN, J. A., SNEPVANGERS, J. J. J. C., BOUTEN, W. & HEUVELINK, G. B. M. 2002. Mapping spatial variation in surface soil water content: Comparison of ground-penetrating radar and time domain reflectometry. *Journal of Hydrology,* 269**,** 194-207.

IWASAKI, T., KURODA, S., SAITO, H., TOBE, Y., SUZUKI, K., FUJIMAKI, H. & INOUE, M. 2016. Monitoring infiltration process seamlessly using array Ground Penetrating Radar. *Agricultural & Environmental Letters,* 1.

JACOB, R. W., HERMANCE, J. F. & VAN DER KRUK, J. 2010. GPR reflection and dispersion analysis methods for water content: Multi-year study of GPR estimates and soil core measurements of water content. *13th International conference on Ground Penetrating Radar (GPR-2010).* Lecce, Italy: IEEE.

JAMIL, M., HASSAN, M. K., AL-MATTARNEH, H. M. A. & ZAIN, M. F. M. 2013. Concrete dielectric properties investigation using microwave nondestructive techniques. *Materials and Structures,* 46**,** 77-87.

JASELSKIS, E. J., GRIGAS, J. & BRILINGAS, A. 2003. Dielectric properties of asphalt pavement. *Journal of Materials in Civil Engineering,* 15**,** 427-434.

JIANG, Y. J. & TAYABJI, S. D. 1999a. *Analysis of time domain reflectometry data from LTPP seasonal monitoring program test sections - Final report*. Report no. FHWA-RD-99-115. Federal Highway Administration, McLean, USA.

JIANG, Y. J. & TAYABJI, S. D. 1999b. Evaluation of in situ moisture content at long-term pavement performance seasonal monitoring program sites. *Transportation Research Record: Journal of the Transportation Research Board,* 1655**,** 118-126.

JOL, H. M. (ed.) 2009. *Ground penetrating radar: Theory and applications,* Amsterdam; Oxford, UK: Elsevier Science.

JONES, S. B., WRAITH, J. M. & OR, D. 2002. Time domain reflectometry measurement principles and applications. *Hydrological Processes,* 16**,** 141-153.

KAATZE, U. & HÜBNER, C. 2010. Electromagnetic techniques for moisture content determination of materials. *Measurement Science and Technology,* 21**,** 1-26.

KELLEY, J. & MOFFAT, M. 2011. *Review of the Traffic Speed Deflectometer - Final Project Report*. Research report no. AP-R395-12. Austroads, Sydney.

KIM, B. 2010. Laboratory calibration of time-domain reflectometry and analysis of soil water content in Korea LTPP sections. *KSCE Journal of Civil Engineering,* 14**,** 503-511.

KLEMUNES, J., JR 1998. *Determining soil volumetric moisture content using time domain reflectometry*. Report no. FHWA-RD-97-139. Federal Higways Administration, McLean, USA.

KLYSZ, G. & BALAYSSAC, J. 2007. Determination of volumetric water content of concrete using ground-penetrating radar. *Cement and Concrete Research,* 37**,** 1164-1171.

KONG, F. N., BHASIN, R. K., WANG, L. Z. & ZHANG, Y. G. 2012. Development of handheld GPR using FieldFox network analyzer and its application in detecting structure of Qian Tang River Dike, Hang Zhou, China. *14th International conference on Ground Penetrating Radar (GPR-2012).* Shanghai: IEEE.

KOPPENJAN, S. K. 2009. Ground Penetrating Radar Systems and Design. *In:* JOL, H. M. (ed.) *Ground Penetrating Radar: Theory and Applications.* Amsterdam: Elsevier.

KRARUP, J., RASMUSSEN, S., AAGAARD, L. & HJORTH, P. G. 2006. Output from the Greenwood Traffic Speed Deflectometer. *22nd ARRB Conference.* Canberra: ARRB Group Ltd.

KRUPKA, J. 2006. Frequency domain complex permittivity measurements at microwave frequencies. *Measurement Science and Technology,* 17**,** R55-R70.

LAHOUAR, S., AL-QADI, I. L., LOULIZI, A., CLARK, T. M. & LEE, D. T. 2002. Approach to determining in situ dielectric constant of pavements - Development and implementation at Interstate 81 in Virginia. *Transportation Research Record***,** 81-87.

LAI, W. L., KIND, T. & WIGGENHAUSER, H. 2011. Using ground penetrating radar and time–frequency analysis to characterize construction materials. *NDT&E International,* 44**,** 111-120.

LAMBOT, S. 2004. Estimating soil electric properties from monostatic ground-penetrating radar signal inversion in the frequency domain. *Water Resources Research,* 40.

LEKARP, F., ISACSSON, U. & DAWSON, A. 2000. State of the Art. 1: Resilient response of unbound aggregates. *Journal of Transportation Engineering,* 126**,** 66-75.

LENG, Z. & AL-QADI, I. L. 2014. An innovative method for measuring pavement dielectric constant using the extended CMP method with two air-coupled GPR systems. *NDT&E International,* 66**,** 90-98.

LENNGREN, C., BERGSTROM, J. & ERSSON, B. 2000. Using ground penetrating radar for assessing highway pavement thickness. *In:* NGUYEN, C. (ed.) *Subsurface Sensing Technologies and Applications II.* Bellingham: SPIE.

LEUCCI, G. 2012. Ground Penetrating Radar: An application to estimate volumetric water content and reinforced bar diameter in concrete structures. *Journal of Advanced Concrete Technology,* 10**,** 411-422.

LI, C., MIAO, L. & YUE, J. 2010. Research on detection to moisture content of flexible pavement by GPR. *GeoShanghai International Conference.* Shanghai: ASCE.

LIANG, R., AL-AKHRAS, K. & RABAB'AH, S. 2006. Field monitoring of moisture variations under flexible pavement. *Transportation Research Record: Journal of the Transportation Research Board,* 1967**,** 160-172.

LIM, A., HORE-LACY, W., ALDERSON, A. & BODIN, D. 2014. *Characterisation and performance evaluation of granular bases project: Pavement construction report*. Technical report no. AP-T267-14. Austroads, Sydney.

LIU, H. & SATO, M. 2014. in situ measurement of pavement thickness and dielectric permittivity by GPR using an antenna array. *NDT&E International,* 64**,** 65-71.

LIU, L. & GUO, T. Dielectric property of asphalt pavement specimens in dry, water-saturated, and frozen conditions. *In:* KOPPENJAN, S. & LEE, H., eds. 9th International conference on Ground Penetrating Radar (GPR-2002), 2002 Santa Barbara, USA. SPIE, 410-415.

LIU, L. & GUO, T. 2003. Determining the condition of hot mix asphalt specimens in dry, water-saturated, and frozen conditions using GPR. *Journal of Environmental & Engineering Geophysics,* 8**,** 46-52.

LOGSDON, S. D. 2000. Effect of cable length on time domain reflectometry calibration for high surface area soils. *Soil Science Society of America Journal,* 64**,** 54-61.

LOIZOS, A. & PLATI, C. 2007. Accuracy of pavement thicknesses estimation using different ground penetrating radar analysis approaches. *NDT&E International,* 40**,** 147-157.

LUNT, I., HUBBARD, S. & RUBIN, Y. 2005. Soil moisture content estimation using ground-penetrating radar reflection data. *Journal of Hydrology,* 307**,** 254-269.

MAHMOUDZADEH, M. R., GOT, J. B., LAMBOT, S. & GRÉGOIRE, C. Road inspection using full-wave inversion of far-field ground-penetrating radar data. 7th International workshop on Advanced Ground Penetrating Radar (IWAGPR-2013), 2013 Nantes. IEEE, 1-6.

MANGEL, A., MOYSEY, S., RYAN, J. & TARBUTTON, J. 2012. Multi-offset ground-penetrating radar imaging of a lab-scale infiltration test. *Hydrology and Earth System Sciences,* 16**,** 4009-4022.

MARTIN, T. 2005. Structural deterioration of sealed granular pavements in Australia. *Road & Transport Research,* 14**,** 3-15.

MASER, K. R. 1996. Condition assessment of transportation infrastructure using Ground-Penetrating Radar. *Journal of Infrastructure Systems,* 2**,** 94-101.

MASER, K. R., HOLLAND, T. J., ROBERTS, R. & POPOVICS, J. 2003. Technology for quality assurance of new pavement thickness. *International Symposium Non-Destructive Testing in Civil Engineering (NDT-CE 2003).* Berlin: NDT.net.

MESHER, D. E., DAWLEY, C. B., DAVIS, J. L. & ROSSITER, J. R. 1995. Evaluation of new ground-penetrating radar technology to quantify pavement structures. *Transportation Research Record***,** 17-26.

MILLARD, S. G., AL-QADI, I. L., SHAW, M. R., RIAD, S. M., SHAARI, A. & BUNGEY, J. H. 2001. Coaxial transmission lines: Development of test procedures for concrete. *Journal of Materials in Civil Engineering,* 13**,** 202-208.

MULLER, W. & REEVES, B. 2012. Comparing Traffic Speed Deflectometer and Noise-Modulated Ground Penetrating Radar data for rapid road pavement investigations. *14th International conference on Ground Penetrating Radar (GPR-2012).* Shanghai: IEEE.

MULLER, W. & WIX, R. 2014. Preliminary field validation of the updated Traffic Speed Deflectometer (TSD) device. *26th ARRB Conference.* Sydney: ARRB Group Ltd.

MULLER, W. B. 2015. A comparison of TSD, FWD and GPR field measurements. *International Symposium Non-Destructive Testing in Civil Engineering (NDT-CE 2015).* Berlin: NDT.net.

MULLER, W. B. & ROBERTS, J. 2013. Revised approach to assessing Traffic Speed Deflectometer (TSD) data and field validation of deflection bowl predictions. *International Journal of Pavement Engineering,* 14**,** 388–402.

NATIONAL PHYSICAL LABORATORY 2003. *A guide to the characterisation of dielectric materials at RF and microwave frequencies,* London, NPL, Institute of Measurement and Control.

NOON, D. A., LONGSTAFF, D. & YELF, R. J. 1994. Advances in the development of step frequency ground penetrating radar. *5th International conference on Ground Penetrating Radar (GPR '94).* Kitchener, Canada: Waterloo Centre for Groundwater Research.

NOURELDIN, A. S., ZHU, K., LI, S. & HARRIS, D. 2003. Network pavement evaluation with Falling-Weight Deflectometer and Ground-Penetrating Radar. *Transportation Research Record,* 1860**,** 90-99.

O'MAY, D. V. 2007. *A study of pavement performance on the Gatton Bypass Duplication.* Bachelor of Engineering, University of Southern Queensland.

OLIVER, J. 1999. *The Performance of Sprayed Seals*. Research Report 326 (extract). ARRB Transport Research,

OLKKONEN, M.-K. 2016. Permittivity scanning of asphalt in a transmission configuration across 7–17 GHz employing a phase compensation method. *NDT & E International,* 83**,** 143-151.

PAIGE-GREEN, P. 2009. Lessons learned during regular monitoring of in situ pavement bearing capacity conditions. *In:* TUTUMLUER, E. & AL-QADI, I. L. (eds.) *8th International conference on the Bearing Capacity of Roads, Railways and Airfields (BCRRA-2009).* Champaign, USA.

PAN, X., KLENK, P., ROTH, K., ZHANG, J., HUANG, P. & HE, D. 2012. Multi-channel GPR to assess the influence of shallow structural heterogeneity on spatio-temporal variations of near-surface soil water content. *14th International conference on Ground Penetrating Radar (GPR-2012).* Shanghai: IEEE.

PASCULLI, D. & MANACORDA, G. Real-time, pseudo real-time and stroboscopic sampling in time-domain GPRs. 8th International Workshop on Advanced Ground Penetrating Radar (IWAGPR-2015), 7-10 July 2015 2015 Florence. IEEE, 1-4.

PEDERSEN, L. 2012. *Viscoelastic Modelling of Road Deflections for use with the Traffic Speed Deflectometer.* Doctor of Philosophy, Technical University of Denmark.

PEDRET RODÉS, J., RODES, J. P., PEREZ-GRACIA, V. & MARTINEZ-REGUERO, A. 2015. Evaluation of the GPR frequency spectra in asphalt pavement assessment. *Construction and Building Materials,* 96**,** 181-188.

PELLINEN, T., HUUSKONEN-SNICKER, E., ESKELINEN, P. & OLMOS MARTINEZ, P. 2015. Representative volume element of asphalt pavement for electromagnetic measurements. *Journal of Traffic and Transportation Engineering (English Edition),* 2**,** 30-39.

PLATI, C. & LOIZOS, A. 2012. Using ground-penetrating radar for assessing the structural needs of asphalt pavements. *Nondestructive Testing and Evaluation,* 27**,** 273-284.

PLATI, C. & LOIZOS, A. 2013. Estimation of in-situ density and moisture content in HMA pavements based on GPR trace reflection amplitude using different frequencies. *Journal of Applied Geophysics,* 97**,** 3-10.

PRITCHARD, R. W. 2013. 2011 to 2012 Queensland Floods and Cyclone Events: Lessons Learnt for Bridge Transport Infrastructure. *Australian Journal of Structural Engineering,* 14**,** 167-176.

RABE, R. 2013. Structural pavement monitoring with non-destructive measuring devices - Experience from a pilot project in Germany. *Ninth international conference on the Bearing Capacity of Road, Railways and Airfields (BCRRA 2013).* Trondheim, Norway.

RADA, G. R., ELKINS, G. E., HENDERSON, B., VAN SAMBEEK, R. I. & LOPEZ, I., A 1995. *LTPP seasonal monitoring program: Instrumentation installation and data collection guideline*. Report no. FHWA-RD-94-10. FHWA, McLean, USA.

RAINWATER, N. R., DRUMM, E. C., YODER, R. E. & WILSON, G. V. 1999. Comprehensive monitoring systems for measuring subgrade moisture conditions. *Journal of Transportation Engineering,* 125**,** 439-448.

REEVES, B. 2010a. Automatic road surface assessment and high speed 3D GPR technology. *NDE/NDT for Highways and Bridges, Structural Materials Technology (SMT).* New York City: The American Society for Nondestructive Testing.

REEVES, B. 2010b. *Noise augmented radar system*. United States patent application 11/815,546.

REEVES, B. 2014. Noise Modulated GPR: Second generation technology. *15th International conference on Ground Penetrating Radar (GPR-2014).* Brussels: IEEE.

REPPERT, P. M., MORGAN, F. D. & TOKSÖZ, M. N. 2000. Dielectric constant determination using ground-penetrating radar reflection coefficients. *Journal of Applied Geophysics,* 43**,** 189-197.

REYNOLDS, J. M. 1997. *An introduction to applied and environmental geophysics,* Chichester, John Wiley & Sons Ltd.

RICHTER, C. A. 2002. *Seasonal variations in the moduli of unbound pavement layers.* Doctor of Philosphy, University of Maryland, College Park.

RICHTER, C. A. 2006. *Seasonal Variations in the Moduli of Unbound Pavement Layers*. Report no. FHWA-HRT-04-079. Federal Highways Administration (FHWA), McLean, USA.

RMEILI, E. & SCULLION, T. 1997. Detecting stripping in asphalt concrete layers using Ground Penetrating Radar. *Transportation Research Record,* 1568**,** 165-174.

ROBERT, A. 1998. Dielectric permittivity of concrete between 50 MHz and 1 GHz and GPR measurements for building materials evaluation. *Journal of Applied Geophysics,* 40**,** 89-94.

ROBERTS, J., AI, U., TOOLE, T. & MARTIN, T. 2014. *Traffic Speed Deflectometer: Data review and lessons learnt*. Technical report no. AP-T279-14. Austroads, Sydney.

ROBINSON, D. A., CAMPBELL, C. S., HOPMANS, J. W., HORNBUCKLE, B. K., JONES, S. B., KNIGHT, R., OGDEN, F., SELKER, J. & WENDROTH, O. 2008. Soil moisture measurement for ecological and hydrological watershed-scale observatories: A review. *Vadose Zone Journal,* 7**,** 358-389.

ROBINSON, D. A., JONES, S. B., WRAITH, J. M., OR, D. & FRIEDMAN, S. P. 2003. A review of advances in dielectric and electrical conductivity measurement in soils using time domain reflectometry. *Vadose Zone Journal,* 2**,** 444-475.

ROBINSON, D. A., SCHAAP, M. G., OR, D. & JONES, S. B. 2005. On the effective measurement frequency of time domain reflectometry in dispersive and nonconductive dielectric materials. *Water Resources Research,* 41.

ROTH, K., SCHULIN, R., FLUHLER, H. & ATTINGER, W. 1990. Calibration of time domain reflectometry for water content measurement using a composite dielectric approach. *Water Resources Research,* 26**,** 2267-2273.

SAARENKETO, T. 1998. Electrical properties of water in clay and silty soils. *Journal of Applied Geophysics,* 40**,** 73-88.

SAARENKETO, T. 2006. *Electrical properties of road materials and subgrade soils and the use of Ground Penetrating Radar in traffic infrastructure surveys.* Doctor of Philosophy, University of Oulu.

SAARENKETO, T. 2009. Chapter 13 - NDT Transportation. *In:* HARRY, M. J. (ed.) *Ground Penetrating Radar Theory and Applications.* Amsterdam: Elsevier.

SAARENKETO, T. & SCULLION, T. 2000. Road evaluation with ground penetrating radar. *Journal of Applied Geophysics,* 43**,** 119-138.

SAARENKETO, T. & VESA, H. 2000. Use of GPR technique in surveying gravel road wearing course. *In:* NOON, D. A., STICKLEY, G. F. & LONGSTAFF, D. (eds.) *8th International conference on Ground Penetrating Radar (GPR-2000).* Gold Coast, Australia: SPIE.

SACHS, J. 2004. M-sequence radar. *In:* DANIELS, D. J. (ed.) *Ground Penetrating Radar.* 2nd ed. London, UK: Institution of Electrical Engineers (IEE).

SAEVARSDOTTIR, T. & ERLINGSSON, S. 2013. Effect of moisture content on pavement behaviour in a heavy vehicle simulator test. *Road Materials and Pavement Design,* 14**,** 274-286.

SALOUR, F. & ERLINGSSON, S. 2013. Moisture-sensitive and stress-dependent behavior of unbound pavement materials from in situ Falling Weight Deflectometer tests. *Transportation Research Record: Journal of the Transportation Research Board,* 2335**,** 121-129.

SCHEUERMANN, A., HUEBNER, C., SCHLAEGER, S., WAGNER, N., BECKER, R. & BIEBERSTEIN, A. 2009. Spatial time domain reflectometry and its application for the measurement of water content distributions along flat ribbon cables in a full-scale levee model. *Water Resources Research,* 45.

SCULLION, T., LAU, C. L. & CHEN, Y. 1992. *Implementation of the Texas Ground Penetrating Radar system*. Report no. FHWA/TX-92/1233-1. Texas Transportation Institute, Texas A&M University, College Station, USA.

SCULLION, T. & SAARENKETO, T. 2000. Integrating ground penetrating radar and falling weight deflectometer technologies in pavement evaluation. *In:* TAYABJI, S. D. & LUKANEN, E. O. (eds.) *Nondestructive Testing of Pavements and Backcalculation of Moduli (Third Volume).* West Conshohocken, USA: American Society for Testing and Materials (ASTM).

SEBESTA, S., OH, J., LEE, S. I., SANCHEZ, M. & TAYLOR, R. 2013. *Initial review of rapid moisture measurement for roadway base and subgrade*. Report no. FHWA/TX-13/0-6676-1. Texas A&M Transportation Institute, College Station, USA.

SHANG, J. & UMANA, J. 1999. Dielectric constant and relaxation time of asphalt pavement materials. *Journal of Infrastructure Systems,* 5**,** 135-142.

SHANG, J., UMANA, J., BARTLETT, F. & ROSSITER, J. 1999. Measurement of complex permittivity of asphalt pavement materials. *Journal of Transportation Engineering,* 125**,** 347.

SOUTSOS, M. N., BUNGEY, J. H., MILLARD, S. G., SHAW, M. R. & PATTERSON, A. 2001. Dielectric properties of concrete and their influence on radar testing. *ND&E International,* 34**,** 419-425.

SPERL, C., STANJEK, H. & BERKTOLD, A. 1997. On-site measurement of the spatial distribution of soil water content with ground-penetrating radar. *In:* GOTTLEIB, J., HOTZL, H., HUCK, K. & NIESSNER, R. (eds.) *Field Screening Europe: Proceedings of the first international conference on strategies and techniques for the investigations and monitoring of contaminated sites.* Kluwer Academic Publishers.

STEELMAN, C. M. & ENDRES, A. L. 2012. Assessing vertical soil moisture dynamics using multi-frequency GPR common-midpoint soundings. *Journal of Hydrology,* 436–437**,** 51-66.

STICKLEY, G. F., NOON, D. A., CHERNIAKOV, M. & LONGSTAFF, I. D. 2000. Gated stepped-frequency ground penetrating radar. *Journal of Applied Geophysics,* 43**,** 259-269.

STORK, C. 1992. Reflection tomography in the postmigrated domain. *Geophysics,* 57**,** 680-692.

TAAMNEH, M. & LIANG, R. Y. 2010. Long-Term Field Monitoring of Moisture Variations under Asphalt Pavement with Different Drainable Base Materials. *GeoShanghai International Conference.* Shanghai: American Society of Civil Engineers.

TARANTINO, A., RIDLEY, A. M. & TOLL, D. G. 2008. Field Measurement of suction, water content, and water permeability. *Geotechnical and Geological Engineering,* 26**,** 751-782.

THE INTERNATIONAL BANK FOR RECONSTRUCTION AND DEVELOPMENT & QUEENSLAND RECONSTRUCTION AUTHORITY 2011. *Queensland recovery and reconstruction in the aftermath of the 2010/2011 flood events and cyclone Yasi*. Report no. 63393. The World Bank Group, Washington DC.

THE MATHWORKS INC. 2015. MATLAB.

THOM, N. 2008. Unbound material. *Principles of pavement engineering.* London: Thomas Telford.

THOMAS, A. M., CHAPMAN, D. N., ROGERS, C. D. F., METJE, N., ATKINS, P. R. & LIM, H. M. 2008. Broadband apparent permittivity measurement in dispersive soils using quarter-wavelength analysis. *Soil Science Society of America Journal,* 72**,** 1401.

TOPP, G. C., DAVIS, J. L. & ANNAN, A. P. 1980. Electromagnetic determination of soil water content: Measurements in coaxial transmission lines. *Water Resources Research,* 16**,** 574-582.

TOY, C. W., STEELMAN, C. M. & ENDRES, A. L. 2010. Comparing electromagnetic induction and ground penetrating radar techniques for estimating soil moisture content. *13th International conference on Ground Penetrating Radar (GPR-2010).* Lecce, Italy: IEEE.

TRABELSI, S., KRASZEWSKI, A. W. & NELSON, S. O. 1997. Microwave dielectric properties of shelled yellow-dent field corn. *Journal of Microwave Power and Electromagnetic Energy,* 32**,** 188-194.

TRABELSI, S., KRASZEWSKI, A. W. & NELSON, S. O. 2000. Phase-shift ambiguity in microwave dielectric properties measurements. *IEEE Transactions on Instrumentation and Measurement,* 49**,** 56-60.

TRABELSI, S. & NELSON, S. 2006. Microwave sensing technique for nondestructive determination of bulk density and moisture content in unshelled and shelled peanuts. *Transactions of the ASABE,* 49**,** 1563-1568.

TRABELSI, S. & NELSON, S. O. 2003. Free-space measurement of dielectric properties of cereal grain and oilseed at microwave frequencies. *Measurement Science and Technology,* 14**,** 589-600.

TRABELSI, S. & NELSON, S. O. 2010. Microwave moisture meter for granular and particulate materials. *Instrumentation and Measurement Technology Conference (I2MTC).* Austin: IEEE.

TRABELSI, S., NELSON, S. O. & LEWIS, M. 2008. Practical microwave meter for sensing moisture and density of granular materials. *IEEE International Instrumentation and Measurement Technology Conference.* Victoria, Canada IEEE.

ULABY, F. T., MICHIELSSEN, E. & RAVAIOLI, U. 2010. *Fundamentals of Applied Electromagnetics,* New Jersey, Prentice Hall.

VAN DER AA, J. P. C. M. & BOER, G. 1997. Automatic moisture content measuring and monitoring system based on time domain reflectometry used in road structures. *NDT&E International,* 30**,** 239-242.

VEREECKEN, H., HUISMAN, J. A., BOGENA, H., VANDERBORGHT, J., VRUGT, J. A. & HOPMANS, J. W. 2008. On the value of soil moisture measurements in vadose zone hydrology: A review. *Water Resources Research,* 44**,** 1-21.

VILLAIN, G., DÉROBERT, X., SBARTAÏ, Z. M. & BALAYSSAC, J. 2010. Evaluation of concrete water content and other durability indicators by electromagnetic measurements. *13th International conference on Ground Penetrating Radar (GPR-2010).* Lecce, Italy: IEEE.

VUONG, B. 2007. Measuring, predicting and specifying moisture in granular pavements with thin bituminous surfacings. *Road Materials and Pavement Design,* 8**,** 695-718.

VUONG, B., JAMESON, G., SHARP, K. & FIELDING, B. 2008. *Guide to Pavement Technology Part 4A: Granular Base and Subbase Materials,* Sydney, Austroads.

VUONG, B. T. & HAZELL, D. 2003. Development of performance-based specifications for unbound granular materials: Issues and recommendations. *Road & Transport Research,* 12**,** 13-25.

WAGNER, N., SCHWING, M. & SCHEUERMANN, A. 2014. Numerical 3-D FEM and experimental analysis of the open-ended coaxial line technique for microwave dielectric spectroscopy on soil. *IEEE Transactions on Geoscience and Remote Sensing,* 52**,** 880-893.

WALUBITA, L. F., SCULLION, T., LEIDY, J. & LIU, W. 2009. Non-destructive testing technologies: Application of the Ground Penetrating Radar (GPR) to perpetual pavements. *Road Materials and Pavement Design,* 10**,** 259-286.

WHALLEY, W. R. 1993. Considerations on the use of time-domain reflectometry (TDR) for measuring soil water content. *Journal of Soil Science,* 44**,** 1-9.

WIX, R., MURNANE, C. & MOFFATT, M. 2016. Experience Gained Investigating, Acquiring and Operating the First Traffic Speed Deflectometer in Australia. *Transportation Research Procedia,* 14**,** 3060-3069.

WOLLSCHLÄGER, U., GERHARDS, H., YU, Q. & ROTH, K. 2010. Multi-channel ground-penetrating radar to explore spatial variations in thaw depth and moisture content in the active layer of a permafrost site. *The Cryosphere,* 4**,** 269-283.

WRIGHT, A., BENBOW, E., SPIELHOFER, R., SJÖGREN, L., HILDEBRAND, G., KOKOT, D., THOMAS, M. & RABE, R. 2016. Hi-SPEQ – Developing the Technical and Quality Requirements for High-speed Condition Surveys of Road Networks. *Transportation Research Procedia,* 14**,** 2956-2965.

WRIGHT, W. C., YODER, R. E., RAINWATER, N. R. & DRUMM, E. C. 2001. Calibration of five-segment Time Domain Reflectometry probes for water content measurement in high density materials. *Geotechnical Testing Journal (GTJODJ),* 24**,** 172-184.

YANG, S. 2014. *Health monitoring of pavement systems using smart sensing technologies.* Master of Science, Iowa State University.

YI, L., TAKAHASHI, K. & SATO, M. Estimation of vertical velocity profile by multistatic GPR Yakumo. International Geoscience and Remote Sensing Symposium (IGARSS), 26-31 July 2015 2015 Milan. IEEE, 1060-1063.

ZHANG, Z., WU, Z., MARTINEZ, M. & GASPARD, K. 2008. Pavement structures damage caused by Hurricane Katrina flooding. *Journal of Geotechnical and Geoenvironmental Engineering,* 134**,** 633-644.

ZHAO, S. & AL-QADI, I. L. 2016. Development of an analytic approach utilizing the extended common midpoint method to estimate asphalt pavement thickness with 3-D ground-penetrating radar. *NDT&E International,* 78**,** 29-36.

ZOFKA, A., SUDYKA, J., MALISZEWSKI, M., HARASIM, P. & SYBILSKI, D. 2014. Alternative approach for interpreting Traffic Speed Deflectometer results. *Transportation Research Record: Journal of the Transportation Research Board,* 2457**,** 12-18.

Appendix A – Incorporated Papers

This page left intentionally blank

Paper I

Muller, W.B., Scheuermann, A. and Reeves, B., Quantitative moisture measurement of road pavements using 3D noise-modulated GPR, Proceedings of the 14th International Conference on Ground Penetrating Radar (GPR) 2012, Shanghai. IEEE, 517-523, June 2012

This page left intentionally blank

Quantitative moisture measurement of road pavements using 3D Noise-Modulated GPR

Wayne Muller [1,2], Alexander Scheuermann [2] & Bryan Reeves [3]

1. *Department of Transport and Main Roads, Queensland*
2. *The University of Queensland, School of Civil Engineering*
3. *Radar Portal System Pty. Ltd.*

Abstract— Within Queensland, Australia around 90% of state controlled roads are constructed from unbound granular materials with thin bituminous surfacings. These pavements are significantly influenced by moisture. However currently there is no rapid, quantitative method of assessing in-place pavement moisture suitable for use at large scales. This makes it difficult for road engineers to diagnose and treat moisture ingress mechanisms in failing pavements and to properly assess and protect flood weakened roads from heavy vehicle damage.

This research focuses on quantitative moisture measurement of unbound granular road pavements using rapid 3D multi-offset ground penetrating radar (GPR) techniques. The work will use an update of an existing 3D noise-modulated GPR (NM-GPR) system to collect multiple wide angle reflection and refraction (WARR) profiles across the road lane, while moving along the road at highway speeds. The intention is to use geophysical methods on this data to determine pavement layer permittivity values and from this estimate in-place pavement moisture.

While the NM-GPR update is being finalised, preliminary research has commenced. Synthetic data have been produced to model the expected multi-offset data from the new system. These data have been used to test methods of identifying and tracking subsurface layers and the application of geophysical methods to determine pavement layer permittivity values. Preliminary laboratory investigations of moist pavement materials have also commenced using a vector network analyser (VNA) and a phase-shift measurement technique. This has been done in order to develop the necessary moisture-permittivity relations to calibrate the moisture predictions from the GPR permittivity measurements.

This paper describes the current state of research, preliminary simulations and laboratory testing undertaken toward the goal of developing a robust, high-speed method of quantifying in-place road pavement moisture.

Keywords-GPR; multi-offset ground penetrating radar; road pavement moisture; noise-modulated GPR.

1 INTRODUCTION & NEED FOR THIS WORK

The state-controlled road network (SCRN) is Queensland's largest and most valuable built asset, with a replacement value of around $25 billion [1]. It comprises around 20% of the total length of Queensland roads but carries around 80% of total traffic volume. Engineers managing this network face a range of challenges including aging infrastructure, an increasing freight task and the frequent risk of damage from extreme weather events. Flooding and moisture ingress are of particular interest because of the make-up of the network. Around 90% of the network consists of unbound granular pavements [2], the performance of which is particularly sensitive to the influence of moisture [3-7]. Moisture ingress into these pavements leads to increased internal water pressure or decreased matric suction, reducing the effective stress, strength and elastic and plastic stiffness of the pavement and subgrade [8].

While the influence of moisture on these pavements is well recognised, it is currently difficult to measure *in-situ* pavement moisture at larger scales. Existing approaches involving physical sampling are too slow, destructive and impractical at larger scales. Alternatives such as time domain reflectometry (TDR), while suitable for continuous monitoring of individual locations [e.g. 9, 10, 11], are currently too difficult and expensive to achieve high spatial sampling detail.

A rapid, non-contact and quantitative method of determining *in-situ* pavement moisture is therefore required. Such a method would have many potential uses. For example, to gauge the risk of pavement damage and the optimum timing in allowing heavy vehicles back on the road after flooding; to better diagnose, understand and treat the mechanisms of moisture-related road failures; to locate and treat areas of excessive degree of saturation (DOS) in new pavements, avoiding early pavement failures. This paper provides an overview of current

efforts by the Queensland Department of Transport and Main Roads (TMR) to develop such a method.

2 MOISTURE MEASUREMENT USING GPR

2.1 OVERVIEW

The proposed approach involves the use of Ground Penetrating Radar (GPR). To date many researchers have used GPR techniques to identify areas of increased moisture within road pavements [e.g. 12, 13-15]. However, only a few have used quantitative methods to determine the actual amount of water present [e.g. 16, 17, 18]. By contrast, the use of GPR for quantitative moisture measurement in soils is well recognized [19], with numerous examples in the literature [e.g. 20, 21-28].

A key issue limiting the use of these methods for roads is the lack of a suitable investigation method for use at highway speeds. The surface reflection coefficient method, while widely used to determine pavement surface permittivity, is not well suited for pavement moisture quantification due to its inability to address vertical intra-layer attenuation variations [29] and tendency to compound errors when extending the technique beyond the uppermost layer. Other existing approaches are also unsuitable. For example permittivity determination based on comparing pavement layer depths and reflection times is often unsuitable as layer depths are in most cases not accurately known and because coring or trenching to determine this information is slow, disruptive, expensive and destructive. Traditional multi-offset methods, requiring physical separation of antennas, are also impractical for high-speed operating environments.

2.2 MULTI-OFFSET NOISE MODULATED GPR TECHNOLOGY

Recently a new type of noise-modulated ground penetrating radar (NM-GPR) has been developed in Australia [30, 31] – see Fig. 1 An update of this technology is currently being completed with the ability to collect multi-offset data using eight partially overlapping WARR groups covering a width of approximately 2.5 metres. Using geophysical methods it will be

possible to determine the average electromagnetic (EM) wave velocities within individual pavement layers and the corresponding relative permittivity values. These in turn can potentially be used to estimate *in-situ* moisture conditions.

Figure 1. Roadscout 2 system incorporating a highway-speed 24 channel NM-GPR system and ground coupled antennas.

This paper describes preliminary work to date simulating the response of the new NM-GPR equipment; developing the analysis approaches to extract the EM wave velocities and relative permittivity values from the NM-GPR data and laboratory test methods being developed to relate permittivity measurements to *in-situ* moisture parameters.

3 SYNTHETIC MULTI-OFFSET DATA ANALYSIS

Synthetic data were produced to model the new NM-GPR hardware using GPRMax software [32]. As the output from the NM-GPR hardware is essentially equivalent to a time-domain impulse GPR system [33] this modelling approach was considered appropriate. 2D models have been used for most of the work to date due to their relative simplicity and reduced simulation time. Subsequent assessment and processing of the synthetic data were undertaken using Matlab software [34].

The antenna arrays of the new system consist of a row of 8 transmitters (Tx) longitudinally offset by approximately 200mm from a row of receivers (Rx), spanning across the pavement lane width. Each transmitter pairs with a number of antennas within the receiver array.

Omitting overlapping pairs, the end result is a combination of 51 GPR profiles with a lateral spacing between these profiles of around 45mm. To model the configuration in 2D, considering the longitudinal offset between the antenna arrays, it was necessary to place the receivers within the model at the actual 3D radial distances for each Tx-Rx pair. An amount of random noise was also added, to better emulate real data.

As the new NM-GPR system will collect vast quantities of multi-offset data it would be impractical to manually identify each pavement interface in each WARR group for velocity determination. Consequently semi-automated methods of layer tracking and analysis have been developed based on cross-correlation and local maxima / minima detection. In most cases road pavements are constructed in horizontal layers of relatively consistent depth both along the road and across the lane width. As the new NM-GPR configuration will produce closely spaced longitudinal and transverse measurements it thus becomes possible to track a pavement interface identified at one location both along and across the road.

The examples given in Figs. 2 – 4 illustrate tracking of key pavement features within the synthetic WARR data used to extract pavement layer velocity and permittivity information. In these examples four partially overlapping WARR groups are shown, representing half of the width of the proposed NM-GPR hardware update. The pavement model for these figures comprises three pavement layers that are (from the top) 150mm, 200mm and 100mm thick. The static relative permittivity of each of these synthetic layers is 5.0, 7.0 and 8.0, respectively and the conductivity for all layers is 0.005 Siemens/metre.

Fig. 2 shows an example of the raw synthetic data with tracked features. Here the groundwave reflection has been automatically detected and tracked across all WARR groups. The groundwave velocity has been determined based on the slope of this interface relative to the radial Tx-Rx offsets – i.e. Fig. 2(b). Where possible the first lobe of the Ricker wavelet was selected for tracking, to better estimate the position of true time zero and pavement interfaces [35] and to reduce the influence of dispersion effects [17]. The relative permittivity corresponding with the groundwave velocity has been estimated using the simplified velocity-permittivity relationship [33].

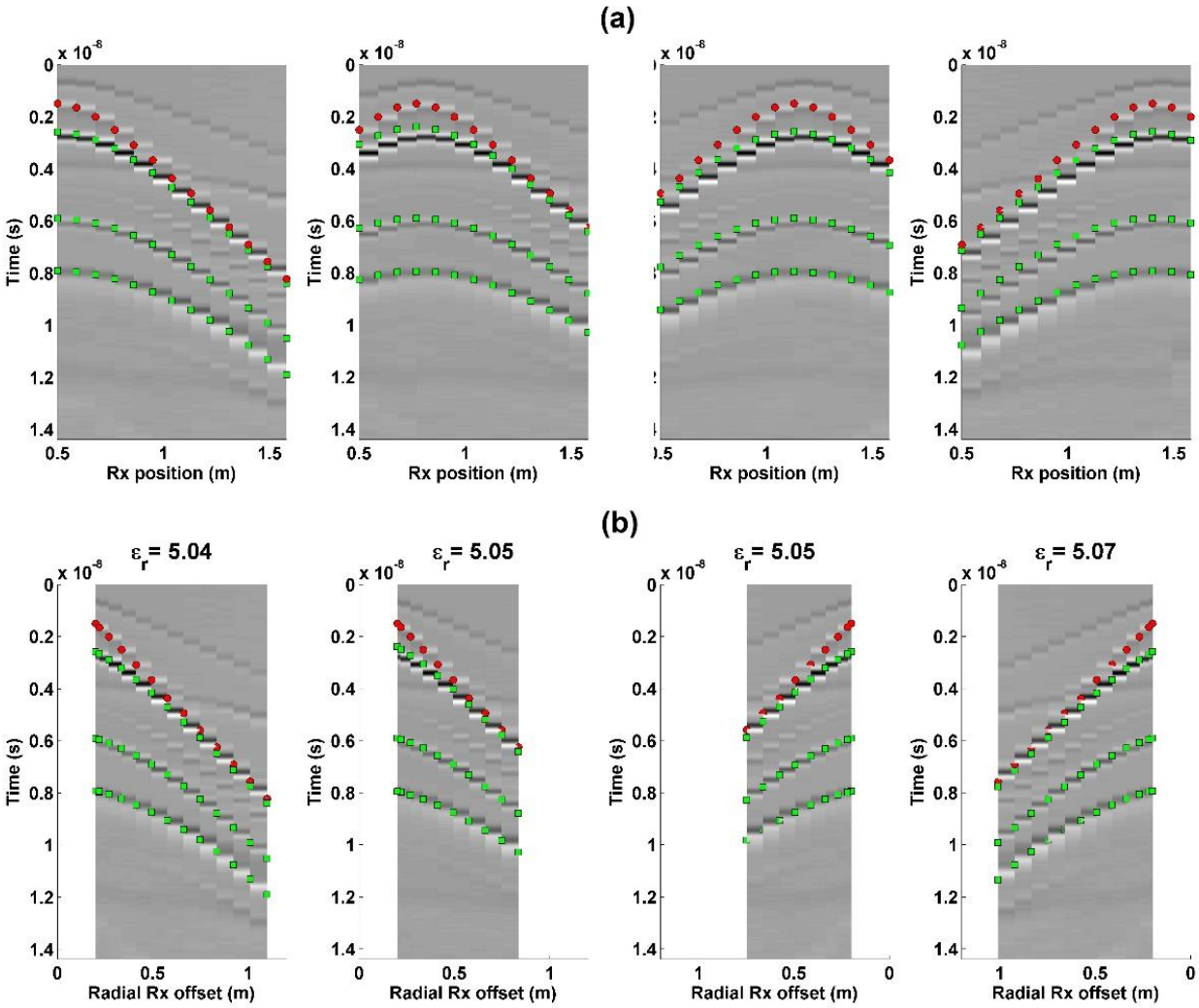

Figure 2. Tracked groundwave & layer reflectors in synthetic data for four adjacent WARR groups plotted against (a) even antenna spactings and (b) radial Tx-Rx distances. Real relative permittivity (ε_r) values determined from the groundwave slope are shown. Modelled value is ε_r =5.0 for the top layer.

Using the groundwave velocities, an initial normal moveout (NMO) correction [36] was undertaken on each WARR group. Fig. 3 shows a subset of this NMO corrected data showing only the receivers closest to each individual transmitter placed side by side. This produces an approximate cross-sectional view across the pavement. A single point on each of the pavement layers in this cross sectional view has then been selected by the user and then automatically tracked across all GPR channels in both the NMO corrected (Figs. 3-4) and non-corrected data (Fig. 2). The Dix Equation [36] has then been used to produce an initial estimate the EM wave

velocity and permittivity values for each individual pavement layer – Fig 4. This provides a starting point for the predicted layer velocity values.

As the WARR datasets partially overlap, each WARR group is effectively 'seeing' a portion of the same pavement interface also seen by its neighbours. Thus when the data for each WARR group is NMO corrected and overlaid, it must match the NMO corrected data from the adjacent groups. Matching NMO corrected pavement interfaces thus provides a method for fine-tuning the EM wave velocities for each individual WARR group and each pavement layer. That is, the model starts with an estimate of permittivity based on the groundwave velocity. Layers are then identified and tracked in the cross-sectional view. Initial layer velocities are estimated using the Dix equation, and then these layer velocities are incrementally adjusted, working from the uppermost pavement layer down, until the tracked layers in the NMO corrected data are consistent across all adjacent WARR groups.

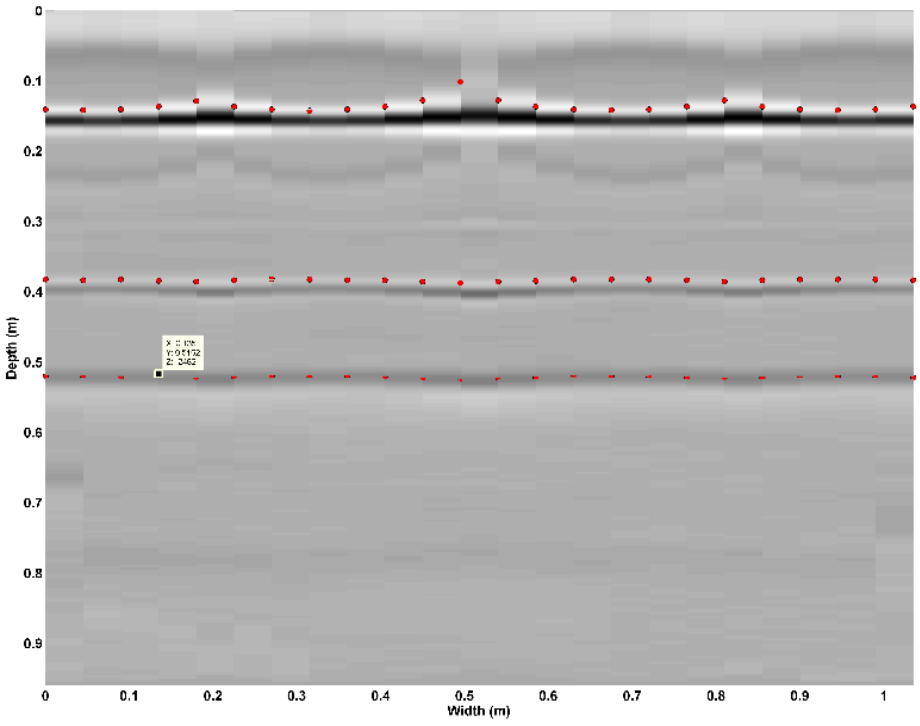

Figure 3. Subset of a preliminary NMO correction of data based on automatically determined groundwave velocity. Three layer interfaces have been tracked based on an initial pick points selected by the user.

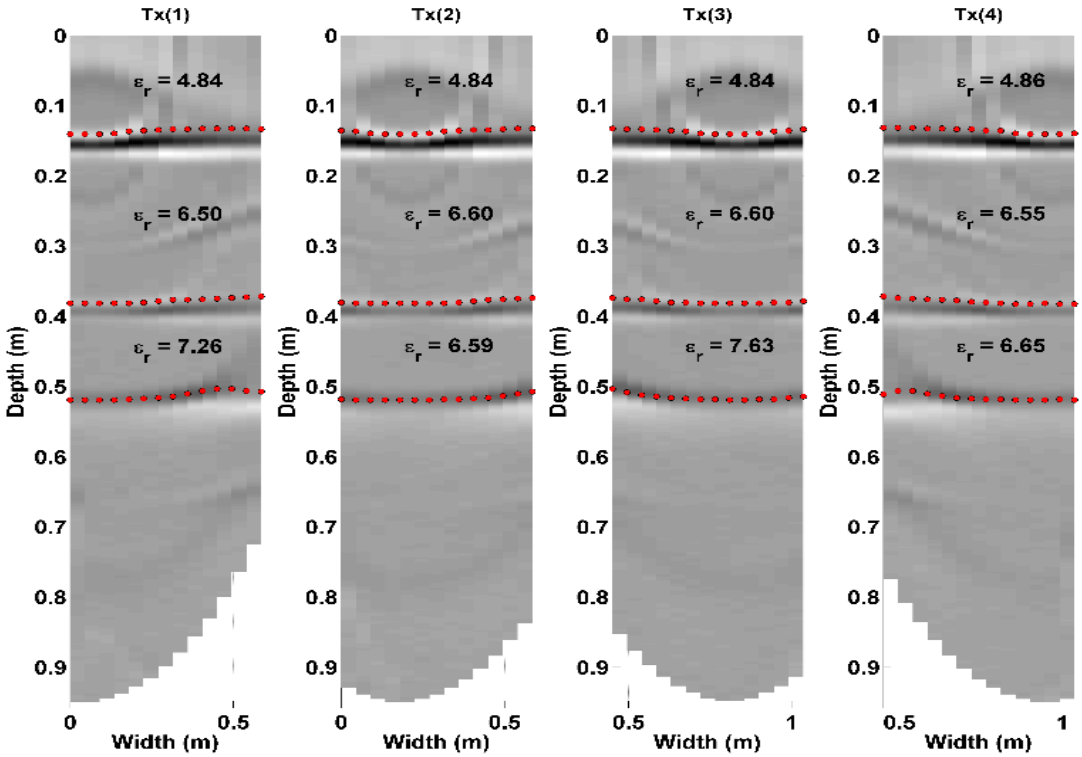

Figure 4. WARR data corrected using interval velocities determined using the Dix Equation on tracked layers.

Key advantages of the proposed approach are that it allows EM wave velocities to be determined for numerous points across the road, and for individual pavement layers; it can also potentially account for non-horizontal pavement interfaces, velocity variations across the road and inter-layer refraction. It also provides two methods of determining the wave velocity in the uppermost portion of pavement (i.e. groundwave and WARR reflections), thus potentially enabling detection of vertical permittivity variations (e.g. a drying pavement).

As multi-offset techniques can only determine EM wave velocities down to the lowest consistent reflector, it will not be possible to use the proposed method beyond that interface. However it may still be possible to estimate the permittivity of the subsequent layer based on its reflectivity, using a similar approach to that used to extend the reflection coefficient method beyond the uppermost layer [14, 29]. Though such an approach becomes complicated as simplifying assumptions, such as normal incidence, do not hold.

Looking at the synthetic data, significant signal distortion can be seen in the uppermost pavement interface in Fig. 4 at locations away from the transmitter. This is a result of re-sampling NM-GPR data within the diminishing time gap between the groundwave and shallow pavement reflection arrivals. This effect is worst for shallow pavement layers, reducing with increasing depth from the surface. Development of these multi-offset analysis methods is continuing.

4 MOISTURE-PERMITTIVITY RELATIONS

To enable field predictions of moisture based on GPR measurements, moisture-permittivity relations are required. Ideally frequency-dependent measurements of pavement permittivity would be used, to better account for the varying influence of water at different frequencies.

However, most existing laboratory methods are not well suited to accommodating the coarse aggregate fraction of unbound granular pavement materials. Specifically, most two-port coaxial cells are too small to suit the typical maximum aggregate dimensions (20mm), with some custom-made exceptions [e.g. 37]; existing commercial open-ended dielectric probes are too small to sample a representative volume of pavement [e.g. 38]; a few one-port coaxial cells have been custom-developed which appear suitable [e.g. 39, 40], though these would be difficult to replicate or access for the current work. Alternatives such as the Percometer [e.g. 41, 42, 43] measure at a fixed frequency at the low end of GPR frequencies and sample only a small pavement volume. Resonance methods [e.g. 44], provide accurate results but only at a limited number of fixed frequencies. TDR probes provide an alternative [4, 10], though most approaches do not provide frequency-dependent information.

A suitable frequency-dependent permittivity measurement approach was identified from agricultural applications [45]. The approach involves measuring the relative phase-shift and signal attenuation due to the insertion of a dielectric sample of known thickness between two antennas. These properties are determined by measuring scattering characteristics (S-parameters) using a Vector Network Analyser (VNA). Assuming the signal is a plane-wave travelling in low-loss conditions, the relative real (ε_r') and imaginary (ε_r'') components of permittivity can be determined via [46]:

$$\varepsilon_r' \approx \left(1 + \frac{\Delta\Phi\lambda_0}{360d}\right)^2 \quad (1)$$

$$\varepsilon_r'' \approx \frac{\Delta A\lambda_0\sqrt{\varepsilon'}}{8.686\pi d} \quad (2)$$

Where: ΔA = attenuation due to dielectric insertion (dB); λ_0 = free space wavelength of EM wave for a given frequency; d = material thickness; and $\Delta\Phi$ = measured phase shift due to dielectric insertion (degrees).

Such an approach is often undertaken using horn antennas. These have the advantage of focussed radiation patterns that meet the plane wave approximation. However, suitable antennas are physically large and relatively expensive to achieve the lower frequencies of interest to GPR. As a result different antenna types were trialled in the current work.

4.1 PRELIMINARY LABORATORY TESTING

Preliminary testing was undertaken on samples of typical new Queensland base course materials. Initially a pair of unshielded loop antennas was trialled. Later a pair of simple, shielded bow-tie dipole antennas was used. These were placed above and below a pavement sample container, constructed from 17 millimetre form-ply, separated top and bottom by 60mm of nylon sheets to reduce coupling variability. A reference measurement of the S_{21} amplitude and phase and S_{11} amplitude was collected through the empty sample container. The pavement material was then placed and compacted in the sample container in two layers and the top screeded to match the top of the box. The filled sample container was then re-inserted into the test apparatus and the updated S_{21} amplitude and phase and S_{11} amplitude were measured.

Measurements of pavement density, relative compaction and moisture content were also determined on the sample after VNA testing, using standard laboratory methods. Water was then added to the unused pavement sample and the testing process repeated at several different moisture levels. The pavement sample used for the presented data was a standard Type 2.1 material, predominately crushed basalt base course material, produced by Holcim Quarry, in Toowoomba, Queensland. The pavement samples were tested at five separate

moisture levels. Figs. 5 – 7 show the test apparatus; measured phase shift and permittivity values; and a plot of measured volumetric moisture versus the real relative permittivity, compared with moisture-permittivity relations from the literature determined on fine-grained materials [47, 48] and unbound granular pavement materials [10] using TDR.

In addition to the S-parameter measurements, the average EM wave velocity was determined by measuring the two-way travel time through the sample using a commercial impulse GPR system. Here the antenna was placed on top of the sample and a metal reflector was moved up to and away from the bottom face of the sample container, producing a clear response in the GPR data. The material testing results and GPR measurements of EM wave velocity and real relative permittivity are summarised in Table I.

TABLE I. Sample material properties: Revised approach

Description	**Moisture**		**%**	**DOS**	**GPR**	
	By mass	***By volume***	**compaction**	**%**	***EM velocity (m/ns)***	ε'_r
Sample 1	3.3%	7.2%	91.5	28	0.096	9.8
Sample 2	4.4%	8.8%	85.1	29	0.096	9.8
Sample 3	5.3%	11.6%	92.5	48	0.082	13.3
Sample 4	5.4%	12.6%	98.9	66	0.079	14.4
Sample 5	7.9%	18.6%	99.7	101	0.073	16.9

Overall these preliminary results appear promising and the measured results appear relatively consistent with the relationships provided in the literature for unbound granular road materials [i.e. 10]. However, further testing using this approach and comparisons with other more established methods is proposed to validate the proposed approach.

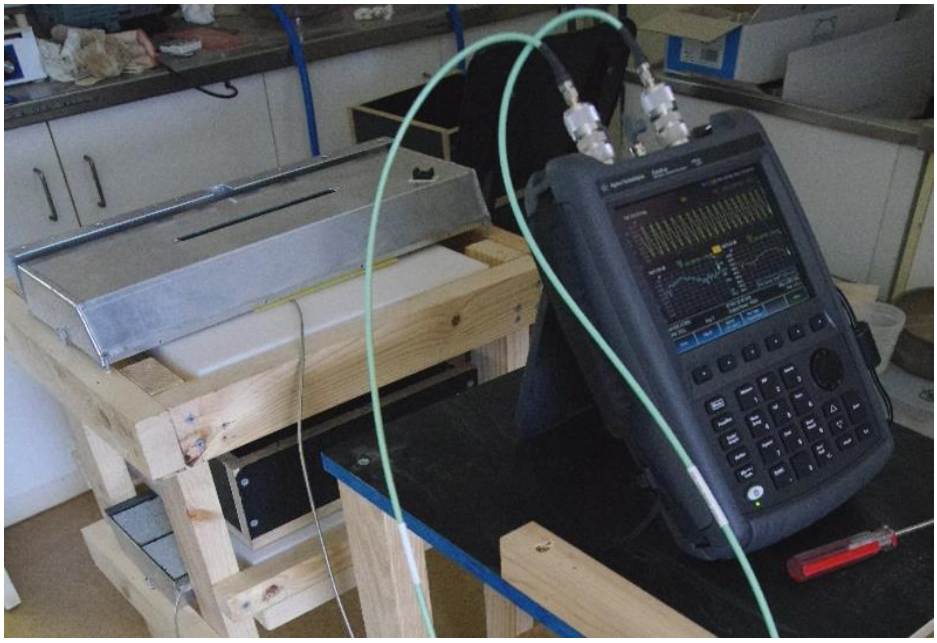

Figure 5. Measurement apparatus with sample box inserted.

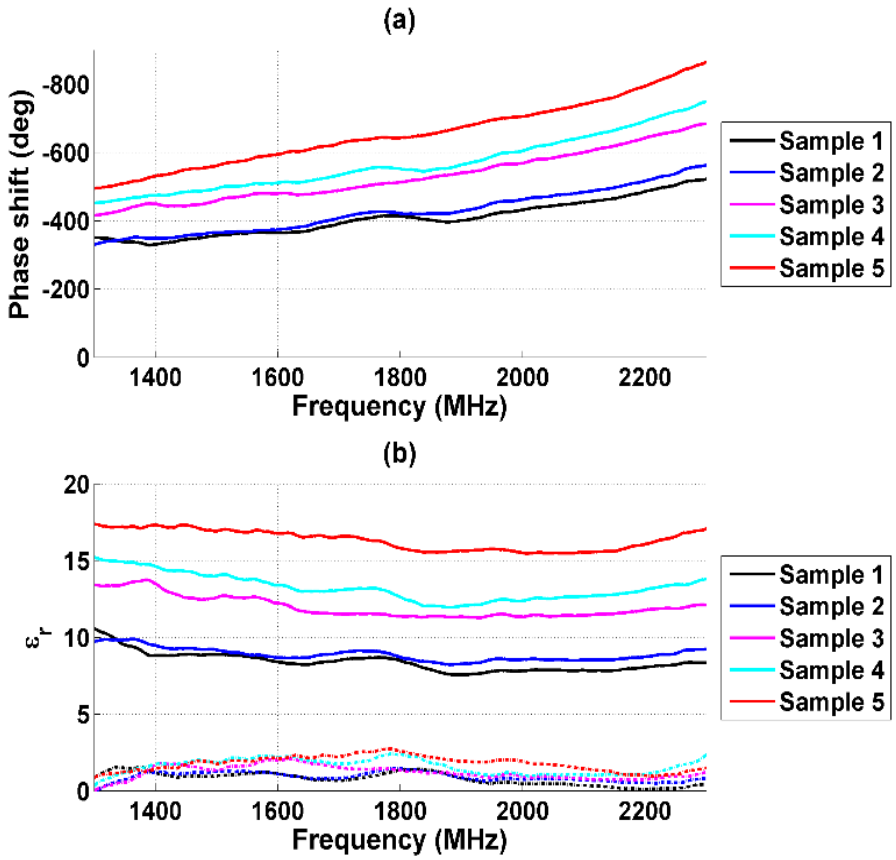

Figure 6. (a) Measured phase shift versus frequeny for each sample; and (b) Corresponding real (ε', solid lines) and imaginary (ε'', dashed lines) relative permittivity values.

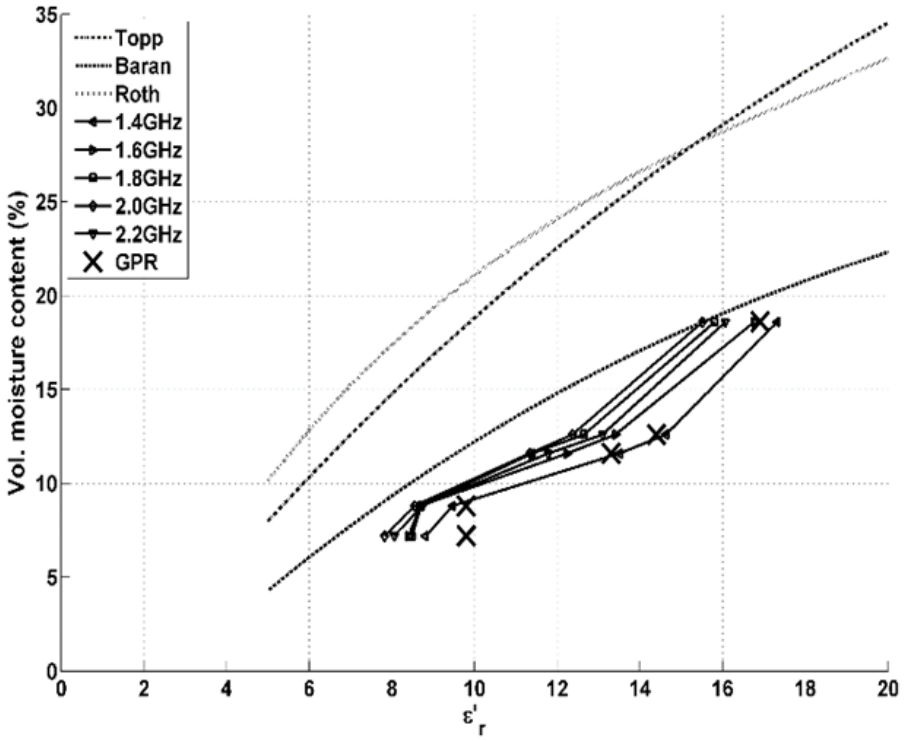

Figure 7. Plot of real relative permittivity (ε') determined from phase-shift measurements and GPR wave velocities versus volumetric moisture content of the test samples. Moisture-permittivity relationships proposed by Topp, Davis & Annan [47], Roth et al. [48] and Baran [10] are shown for comparision.

5 CONCLUSIONS

An overview of current research has been presented, aimed at using multi-offset data from a new type of highway-speed 3D noise modulated ground penetrating radar (NM-GPR) to quantitatively determine *in-situ* moisture conditions within unbound granular road pavements.

Work to date has focused on modelling the expected response from the updated NM-GPR hardware, which consists of eight partially-overlapping wide angle reflection and refraction (WARR) groups, and developing methods of analysing these data. To this end automated methods of tracking key pavement features within the WARR data, such as the groundwave and pavement layer interface reflections, have been developed and demonstrated. The shape of the tracked features has then been used to determine the velocity of the propagating electromagnetic waves within individual pavement layers, using geophysical and other

methods. A novel approach to calibrating electromagnetic wave velocities and pavement permittivity values has been proposed based on matching tracked pavement interfaces in the overlapping portions of adjacent WARR groups, using normal move-out (NMO) corrections.

To enable realistic field predictions of pavement moisture based on the NM-GPR data, frequency-dependent permittivity characterisation of typical unbound granular pavements has commenced using a modified phase-shift measurement technique. Preliminary measurements based on this approach have been given, showing the method produces results similar to that in the literature. Further laboratory testing and comparisons with other more widely accepted permittivity measurement methods is proposed to validate the proposed approach. Research into these topics is continuing.

6 REFERENCES

1. Department of Main Roads, *Roads Connecting Queenslanders: A strategic long-term direction for the Queensland road system and Main Roads*. 2002, Brisbane, Queensland: Queensland Department of Main Roads.
2. Queensland Department of Transport and Main Roads, *Extract of pavement types of the Queensland state-controlled roads from the ARMIS database*. 2011: Brisbane, Queensland.
3. de Carteret, R. and L. Compor, *Guide to Pavement Technology Part 10: Subsurface Drainage*. Guide to Pavement Technology. 2009, Sydney, Australia: Austroads Inc.
4. Ekblad, J., *Influence of water on coarse granular road material properties*, in *Department of Civil and Architectural Engineering*. 2007, KTH Royal Institute of Technology: Stockholm.
5. Jameson, G., *Guide to Pavement Technology Part 2: Pavement Structural Design*. Guide to Pavement Technology. 2010, Sydney, Australia: Austroads Inc.
6. Richter, C.A., *Seasonal variations in the moduli of unbound pavement layers*. 2002, University of Maryland, College Park: Maryland. p. 256.
7. Vuong, B., et al., *Guide to Pavement Technology Part 4: Pavement materials*. Austroads Guide to Pavement Technology. 2007, Sydney, Australia: Austroads Inc.

8. Charlier, R., et al., *Water influence on bearing capacity and pavement performance: Field observations*, in *Water in road structures: Movement, drainage and effects*, A. Dawson, Editor. 2009, Springer Science+Business Media B.V.: Nottingham. p. 175-192.
9. Look, B.G., I.N. Reeves, and D.J. Williams, *Field experiences using time domain reflectometry for monitoring moisture changes in road emankments and pavements*, in *Time domain reflectometry in environmental, infrastructure and mining applications*. 1994: Evanston, Illinois.
10. Baran, E., *Use of time domain reflectometry for monitoring moisture changes in crushed rock pavements*, in *Symposium and workshop on time domain reflectometry in environmental, infrastructure and mining applications*. 1994, United States Bureau of Mines: Evanston, USA. p. 349-356.
11. O'May, D.V., *A study of pavement performance on the Gatton Bypass Duplication*, in *Faculty of Engineering and Surveying*. 2007, University of Southern Queensland: Toowoomba, Australia.
12. Diefenderfer, B.K., D.W. Mokarem, and S.R. Sharp, *Use of nondestructive evaluation to detect moisture in flexible pavements*. 2006, Virginia Transportation Research Council: Charlottesville, USA.
13. Maser, K.R. and T. Scullion, *Influence of asphalt layering and suface treatments on asphalt and base layer thickness computations using radar*. 1992, Infrasense, Cambridge, MA; Texas Transportation Institute.
14. Scullion, T., C.L. Lau, and Y. Chen, *Implementation of the Texas Ground Penetrating Radar system*. 1992, Texas Transportation Institute, Texas A&M University: College Station, USA.
15. Maser, K.R. and J. Puccinelli, *Ground Penetrating Radar (GPR) Analysis: Phase 1 (prepared for the Montana Department of Transportation)*. 2009, Infrasense, Inc.: Arlington, MA, USA.
16. Emilsson, J., P. Englund, and J. Friborg, *Simple method for estimation of water content of roadbeds using multi-offset GPR*, in *9th International conference on Ground Penetrating Radar (GPR-2002)*, S. Koppenjan and H. Lee, Editors. 2002, SPIE: Santa Barbara, USA. p. 422-426.

17. Grote, K., et al., *Evaluation of infiltration in layered pavements using surface GPR reflection techniques.* Journal of Applied Geophysics, 2005. **57**(2): p. 129-153.
18. Li, C., L. Miao, and J. Yue, *Research on detection to moisture content of flexible pavement by GPR*, in *GeoShanghai International Conference*. 2010, ASCE: Shanghai. p. 420-426.
19. Slater, L. and X. Comas, *The contribution of Ground Penetrating Radar to water resouce research*, in *Ground Penetrating Radar: Theory and Applications*, H.M. Jol, Editor. 2009, Elsevier Science: Oxford, UK. p. 203-246.
20. Charlton, M., *Small-scale soil-moisture variability estimated using ground penetrating radar*, in *8th International conference on Ground Penetrating Radar (GPR-2000)*, D.A. Noon, G.F. Stickley, and D. Longstaff, Editors. 2000, SPIE: Gold Coast, Australia. p. 798-804.
21. Charlton, M., *Characterization of ground-penetrating radar (GPR) response in a variety of Earth materials under different moisture conditions*, in *Subsurface and Surface Sensing Technologies and Applications III*, C. Nguyen, Editor. 2001, SPIE: San Diego, USA. p. 288-299.
22. Charlton, M., *Ground penetrating radar techniques for the determination of subsurface moisture variability*. 2002, King's College London, UK: London.
23. Huisman, J.A., et al., *Soil water content measurements at different scales: Accuracy of time domain reflectometry and ground-penetrating radar.* Journal of Hydrology, 2001. **245**(1-4): p. 48-58.
24. Huisman, J.A., et al., *Mapping spatial variation in surface soil water content: Comparison of ground-penetrating radar and time domain reflectometry.* Journal of Hydrology, 2002. **269**(3-4): p. 194-207.
25. Huisman, J.A. and W. Bouten, *Mapping surface soil water content with the ground wave of ground-penetrating radar*, in *9th international conference on Ground Penetrating Radar (GPR-2002)*, S. Koppenjan and H. Lee, Editors. 2002, SPIE: Santa Barbara, USA p. 162-169.
26. Huisman, J.A. and W. Bouten, *Accuracy and reproducibility of mapping surface soil water content with the ground wave of ground-penetrating radar.* Journal of Environmental & Engineering Geophysics, 2003. **8**(2): p. 67-75.

27. Weihermuller, L., et al., *Mapping the spatial variation of soil water content at the field scale with different ground penetrating radar techniques.* Journal of Hydrology, 2007. **340**(3-4): p. 205-216.
28. Huisman, J.A., et al., *Measuring soil water content with Ground Penetrating Radar: A review.* Vadose Zone Journal, 2003. **2**(4): p. 476-491.
29. Saarenketo, T., *Electrical properties of road materials and subgrade soils and the use of Ground Penetrating Radar in traffic infrastructure surveys*, in *Faculty of Science, Department of Geosciences*. 2006, University of Oulu: Oulu, Finland.
30. Reeves, B., *Automatic road surface assessment and high speed 3D GPR technology*, in *NDE/NDT for Highways and Bridges, Structural Materials Technology (SMT)*. 2010, The American Society for Nondestructive Testing: New York City. p. 326-333.
31. Muller, W.B. and B. Reeves, *Application of a traffic-speed road scanning system including a new type of 3D GPR*, in *NDE/NDT for Highways and Bridges, Structural Materials Technology (SMT)*. 2010, The American Society for Nondestructive Testing: New York City, NY, USA. p. 538-545.
32. Giannopoulos, A., *Modelling Ground Penetrating Radar by GPRMax.* Construction and Building Materials, 2005. **19**(10): p. 755-762.
33. Daniels, D.J., ed. *Ground penetrating radar*. 2nd ed. IEE Radar, Sonar, Navigation and Avionics Series 15. Vol. 15. 2004, Institution of Electrical Engineers (IEE): London.
34. The Mathworks Inc., *MATLAB*. 2012, The Mathworks Inc.,.
35. Yelf, R.J. and D. Yelf, *Where is true time zero?* Electromagnetic Phenomena, 2006. **7**(18): p. 158-163.
36. Reynolds, J.M., *An introduction to applied and environmental geophysics*. 1997, Chichester: John Wiley & Sons Ltd.
37. Shang, J., et al., *Measurement of complex permittivity of asphalt pavement materials.* Journal of Transportation Engineering, 1999. **125**: p. 347.
38. Agilent Technologies Inc., *Agilent 85070E Dielectric Probe Kit, 200 MHz to 50 GHz: Technical Overview*. 2011: USA.
39. Huang, Y., *Design, calibration and data interpretation for a one-port large coaxial dielectric measurement cell.* Measurement Science and Technology, 2001. **12**: p. 111–115.

40. Adous, M., P. Quéffélec, and L. Laguerre, *Coaxial/cylindrical transition line for broadband permittivity measurement of civil engineering materials.* Measurement Science and Technology, 2006. **17**(8): p. 2241-2246.

41. Berthelot, C., et al., *Ground-penetrating radar evaluation of moisture and frost across typical Saskatchewan road soils.* Advances in Civil Engineering, 2010. **2010**.

42. Loizos, A. and C. Plati, *Accuracy of pavement thicknesses estimation using different ground penetrating radar analysis approaches.* NDT&E International, 2007. **40**(2): p. 147-157.

43. Saarenketo, T., *Tube suction test - Results of round robin tests on unbound aggregates*. 2000, Finish National Road Administration.

44. Fauchard, C., et al., *GPR performances for thickness calibration on road test sites.* NDT&E International, 2003. **36**(2): p. 67-75.

45. Nelson, S.O., *Dielectric properties measurement techniques and applications.* Transactions of the ASAE-American Society of Agricultural Engineers, 1999. **42**(2): p. 523-530.

46. Trabelsi, S., A.W. Kraszewski, and S.O. Nelson, *Phase-shift ambiguity in microwave dielectric properties measurements.* IEEE Transactions on Instrumentation and Measurement, 2000. **49**(1): p. 56-60.

47. Topp, G.C., J.L. Davis, and A.P. Annan, *Electromagnetic determination of soil water content: Measurements in coaxial transmission lines.* Water Resources Research, 1980. **16**(3): p. 574-582.

48. Roth, K., et al., *Calibration of time domain reflectometry for water content measurement using a composite dielectric approach.* Water Resources Research, 1990. **26**(10): p. 2267-2273.

Paper II

Muller, W.B., Self-correcting pavement layer depth estimates using 3D multi-offset ground penetrating radar (GPR), Proceedings of the 15th International conference on Ground Penetrating Radar (GPR-2014), Brussels. IEEE, 887-892

This page left intentionally blank

Self-correcting pavement layer depth estimates using 3D multi-offset Ground Penetrating Radar (GPR)

Wayne Muller[1,2,3]

1. ARRB Group Ltd.
2. Department of Transport and Main Roads, Queensland
3. The University of Queensland, School of Civil Engineering

Brisbane, Australia

Abstract— An update on the development of a self-correcting method of calibrating pavement layer depths is presented. The approach is applied to multi-offset simulations of a forthcoming 3D noise-modulated ground penetrating radar (NM-GPR) system. The expected response of a series of wide angle reflection and refraction (WARR) datasets produced by this equipment is modelled for typical road pavement configurations using the finite difference time domain (FDTD) approach.

As an initial step, conventional geophysical methods and layer interface tracking algorithms are used to determine approximate layer depths and bulk permittivity values from the WARR data. One of two self-correcting analysis methods is then used to refine the layer depth predictions. The first method, *interface matching*, involves adjusting permittivity values within a 2D ray-path model until the corrected depth of the tracked interfaces is consistent between adjacent WARR groups. The second method, *ray-path modelling*, involves adjusting assumed interface depths, gradients and permittivity values within a 3D ray-path model until predicted two-way travel times match that of the tracked layer interfaces. Both methods proceed iteratively, working layer-by-layer from the top and account for inter-layer refraction in the calculations. Potential advantages of these methods include continuous non-destructive calibration of pavement layer depths and more representative estimates of bulk layer properties, particularly for lossy materials and in situations where moisture, material or compaction gradients may be present.

Keywords—multi-offset ground penetrating radar, permittivity calibration, road pavements.

1 INTRODUCTION

Accurate pavement layer depth information is important for various pavement management applications [1–2]. However, in many instances layer depths are unknown or construction records are unreliable, requiring field investigations to confirm the true conditions. Various authors have described the benefits of using ground penetrating radar (GPR) to determine layer depths of existing roads for inventory or segmentation purposes, project or network level assessments or for use in structural assessments combined with deflection measurement devices such as the falling weight deflectometer (FWD) [3–10].

However, there are several issues that have limited the wider use of GPR for pavement investigations, particularly when combined with deflection measurements. One issue is the mismatch in data collection speed between fast GPR and slow methods such as FWD [11]. Recent developments in rapid continuous deflection measurement devices, specifically the traffic speed deflectometer (TSD) [12-13], show potential to overcome this speed limitation while also producing deflection results similar to those from FWD [14]. Furthermore, preliminary investigations indicate TSD results complement and correlate well with GPR measurements enabling far more rapid pavement investigations [15]. Another issue affecting the GPR itself is the need for a fast and accurate method to calibrate layer depth predictions for changes in the bulk relative permittivity (ε_r) of pavement layers. While several calibration methods exist they are slow and destructive, or alternatively lack accuracy in lossy and more variable pavement conditions.

The current work aims to address this latter issue by developing a robust layer depth calibration approach using multi-offset GPR data. The work will use data collected at highway speeds using a forthcoming update of 3D noise-modulated ground penetrating radar (NM-GPR) technology [16]. An additional goal of the work is to enable quantitative estimates of in situ moisture levels within unbound granular pavements [17]. To that end a free-space laboratory characterisation technique has been investigated, including simulations and validation of the results against other characterisation methods [17−18].

2 CALIBRATION APPROACHES

There are several approaches for GPR pavement layer depth calibration. A common approach involves adjusting assumed bulk permittivity values and the corresponding depth of layer interface predictions within a GPR radargram until they match the findings of physical sampling from cores or trenches. While simple and providing 'ground-truth' comparisons, this approach is also slow, costly, is disruptive and damages the pavement. Consequently it often becomes impractical for large-scale investigations.

A popular alternative is the surface reflection coefficient method. This approach involves using an air-coupled antenna to compare the magnitude of the surface reflection to the reflection from a reference calibration plate placed on the road surface. From this comparison an estimate of near-surface permittivity is determined, and a similar approach can be applied to subsequent layers [1], [4], [6], [19–21]. While fast, simple and non-destructive the underlying assumptions of layer homogeneity and the omission [6], [20] or assumption of constant signal attenuation [2] can lead to errors, particularly for more variable and lossy pavement materials. Such conditions can be expected in older, more degraded pavements or where moisture or compaction gradients are present. Another approach is to use full waveform inversion techniques to determine layer depths and pavement dielectric properties [22−24]. While this approach offers flexibility to model a range of material attributes and can use off-the-shelf equipment, the modelling process is also somewhat complicated; calculation intensive and procedures are not yet sufficiently streamlined for field use.

An alternative approach involves the use of multi-offset methods. Here geophysical methods are used to determine wave velocities within individual layers based on the change in arrival time of the groundwave and reflection arrivals at varying transmitter-receiver spacings [25]. Common midpoint (CMP) and wide angle reflection and refraction (WARR) are two commonly used multi-offset antenna configurations. However, to date the use of multi-offset methods has been somewhat limited for road investigations, though with some notable examples in the literature [2], [26−29]. Perhaps the most sophisticated use to date involved use of a 3D GPR system with air-launched antennas to rapidly collect CMP data [30]. Semblance and the Dix equation were then used to determine wave velocities for layer depth calibrations.

However, the use of air-launched antennas for such applications leads to significant refraction and range resolution issues compared to ground-coupled configurations [31].

There are several potential advantages of using multi-offset methods for pavement investigations. For one they enable layer depth calibrations based solely on the GPR data itself, largely avoiding the need for physical sampling and risk of misaligning GPR data with physical samples. As such they could potentially be advantageous for large-scale investigations where physical sampling is cost prohibitive and impractical. If using ground-coupled arrays, multi-offset methods also provide two approaches to determining electromagnetic (EM) wave velocity – based on layer reflections and groundwave arrivals. These in turn could potentially be compared to investigate near surface material gradients. Furthermore, unlike surface-reflection-based methods, multi-offset reflections have passed through entire pavement layer depths on their way back to the GPR receiver. Thus intra-layer variations, for example moisture or compaction gradients, will proportionally influence the measured response. Consequently multi-offset methods should provide more representative estimates of bulk layer properties. However, disadvantages of these methods include increased data quantity, complexity and also many GPR practitioners are unfamiliar with this data type. Furthermore, the methods outlined here also require specialised equipment for data collection. Nonetheless multi-offset data collected at highway speeds using the next generation of 3D GPR equipment provides many potential advantages for pavement investigations.

3 CALIBRATION CONCEPT

The current work uses simulations of the expected response of the forthcoming 3D NM-GPR system update described previously [15], [32–33]. Fig. 1 shows the updated NM-GPR equipment, prior to completion.

Fig. 1. Updated 3D NM-GPR system.

The antenna configuration of the new system consists of a row of 8 transmitters (Tx) and a row of 20 receivers (Rx). These are housed within four adjacent ground-coupled pods, each of which contains 2 transmitters and 5 receivers. By pairing different transmitters and receivers a series of virtual antennas is achieved across the lane width arranged into eight partially-overlapping WARR groups (see Fig. 2). When operating at 100 km/h all 8 WARR groups complete their measurements every 60 mm along the road (adjustable), providing multi-offset measurements across the lane width. To enable calibration of the GPR layer depths two self-correcting analysis methods are being investigated: *Interface matching* and *ray-path modelling*.

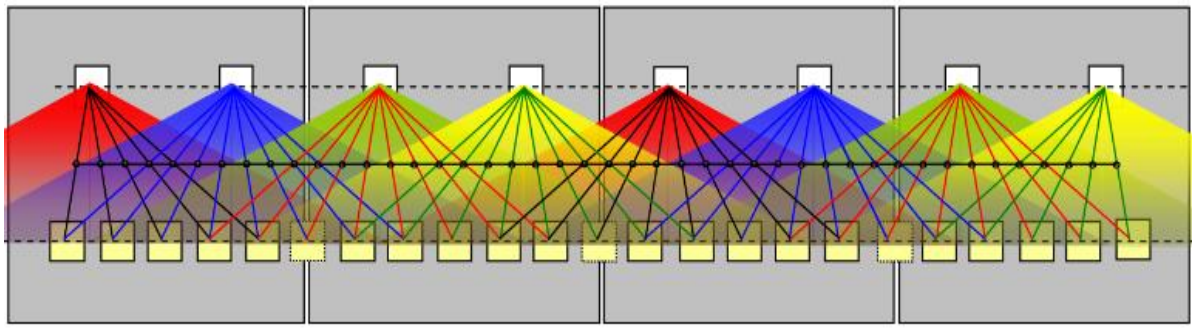

Fig. 2. Illustration of the 3D NM-GPR antenna configuration and combinations used to achieve the eight WARR groups.

3.1 INTEFACE MATCHING (IM)

As the positions of virtual antenna pairs produced by adjacent WARR groups partially overlap, and as road layers are often relatively consistent across their lane width, it follows that after normal moveout (NMO) correction the depth of any continuous interface must be consistent across adjacent WARR groups. This then provides a basis for determining EM wave velocities. That is, to adjust the assumed layer velocities until the calculated depth of NMO-corrected layer interfaces within the NM-GPR data are consistent between adjacent WARR groups.

3.2 RAY-PATH MODELLING (RM)

This approach involves determining the two-way travel time for each pavement layer and antenna pair within each WARR group. Initial estimates of interface depth, angle and layer permittivity for each layer are adjusted within a 3D ray-path model until the predicted reflection times for all antenna pairs of the modelled layer and WARR group best match that observed within the field WARR measurements. The use of a 3D ray-path is intended to provide more accurate ray-path and travel time predictions and greater flexibility to deal with more complex pavement configurations, for example those with sloping layers.

4 APPROACH AND RESULTS

To model the expected NM-GPR response for typical pavement configurations, GPRMax software [34], which uses the finite difference time domain (FDTD) approach, was used in combination with MATLAB software [35]. This approach was used to quickly generate GPRMax input files for each of the eight WARR groups and to instigate their simulations. This enabled various combinations of layer depths and permittivity to be quickly and easily trialled. For the initial phase of modelling, 2D simulations with homogeneous horizontal layers were used. To account for the longitudinal offset between the transmitter and receiver arrays, receivers were placed within the 2D models at their radial offsets (Fig. 3).

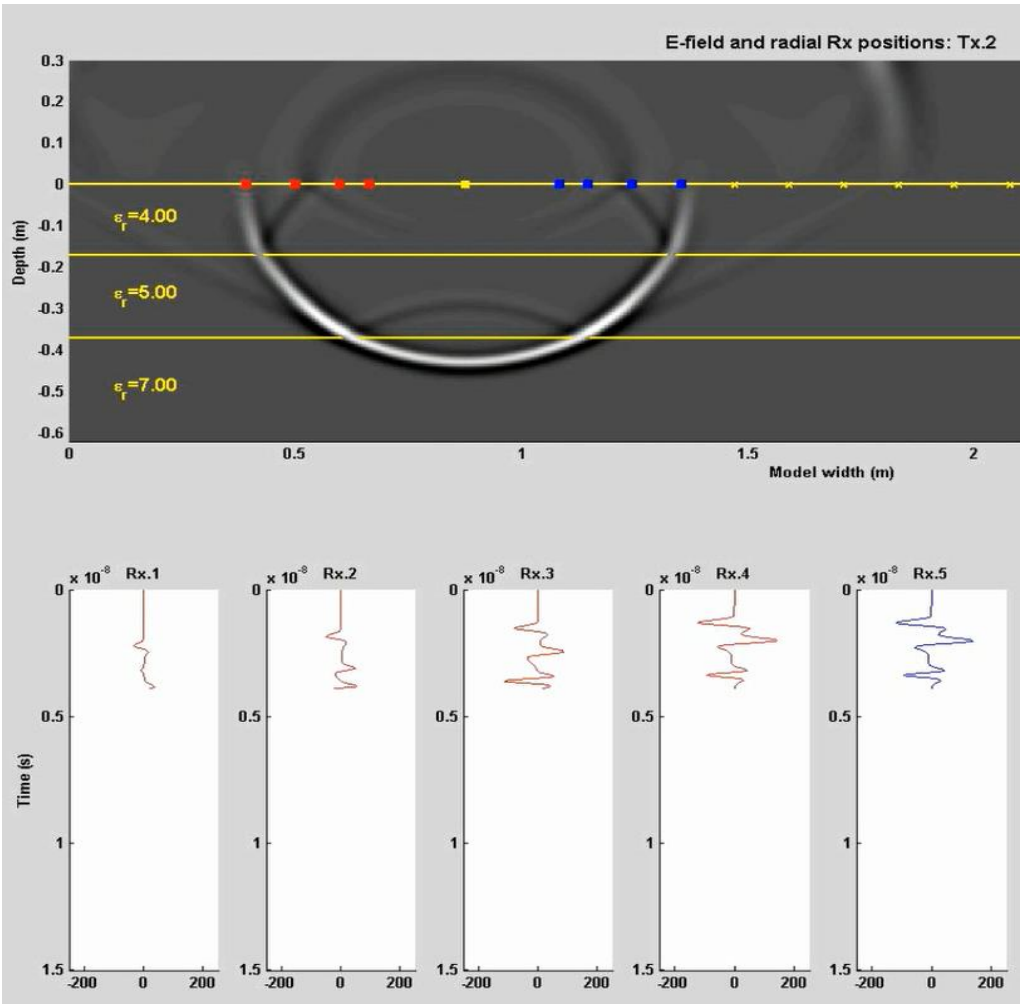

Fig. 3. (Top) 2D GPRMax model of wave propagation within pavement layers; and (bottom) corresponding signal intensity measured by the recievers.

Later, 3D GPRMax models were used to more accurately model sloping layer interfaces. However, due to memory limitations the 3D models needed to be kept relatively coarse compared to the 2D models (5 mm v. 2 mm Yee cells). This resulted to notable steps within the sloping interfaces, which in turn had an influence on the GPR response and analysis results.

Prior to applying the IM and RM methods, the general approach outlined in [17] was used. This included adding noise to the simulations to better model real GPR data. An automated tracking algorithm was then used to track groundwave arrivals across the WARR groups, and from this its velocity was determined. An initial NMO correction of the data was then undertaken using the groundwave velocity to produce an approximate pavement cross-section (Fig. 4). Next the operator selects a point on each layer interface of interest, which is in turn

tracked across the cross-section (Fig. 4) and full WARR datasets (Fig. 5). Next, conventional geophysical methods were used to determine interval velocities for each layer and WARR group based on the time of the tracked layer interfaces. These then form the starting point for further refinement of layer depth and permittivity estimates using the IM and RM methods.

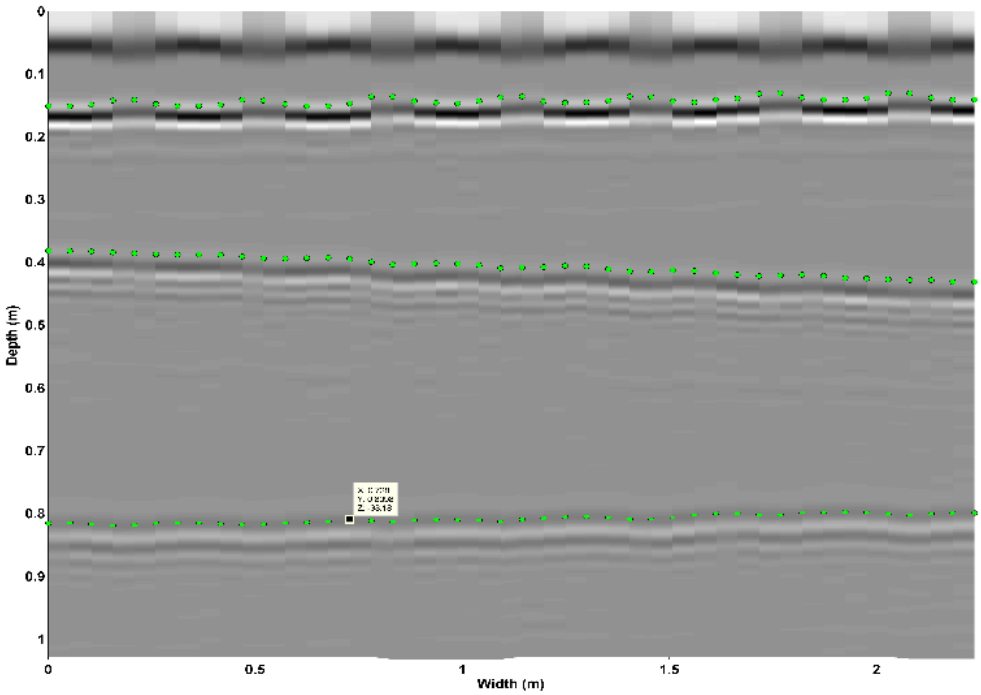

Fig. 4. NMO-corrected cross-section based on groundwave velocity with tracked interfaces shown.

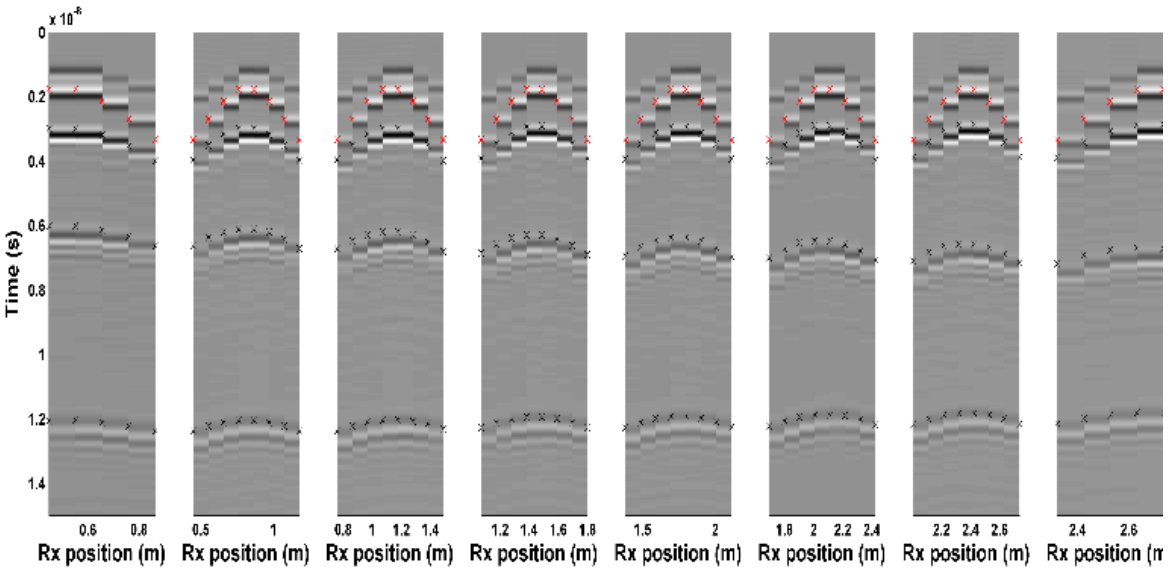

Fig. 5. Tracked layer interfaces of all 8 NM-GPR WARR groups.

4.1 INTERFACE MATCHING

The IM method commences by using a simplified 2D ray-path model to determine the depth of the uppermost tracked pavement interface. To achieve this, the depth of this layer at each tracked point, antenna pair and WARR group is calculated based on its reflection time. Horizontal homogeneous layers and the bulk relative permittivity or the corresponding wave velocity are assumed. Once completed, a line of best fit is determined through the point from each WARR group closest to the transmitter. As the NMO-corrected depths in these locations are least affected by the choice of trial velocity, this line provides a relatively stable reference. Either a straight line or curve can be used, depending on the required flexibility.

Next, the error between the line of best fit and the predicted layer depths is determined for each WARR group. The assumed permittivity for each WARR group is then adjusted after which the layer depths and line of best fit are recalculated. Permittivity adjustments are then continually made within each WARR group until the error is minimised. The permittivity for this completed layer is then fixed for each WARR group and the process is repeated for subsequent layers. For the lower layers, inter-layer refraction is also considered when calculating layer depths, using the determined and trial permittivity values to determine the refracted ray-path. Fig. 6 shows the predicted layer depths from an IM analysis applied to tracked layer positions originally determined within a 2D GPRMax simulation. Fig. 7 shows IM analysis applied to layer tracks within a 3D GPRMax model.

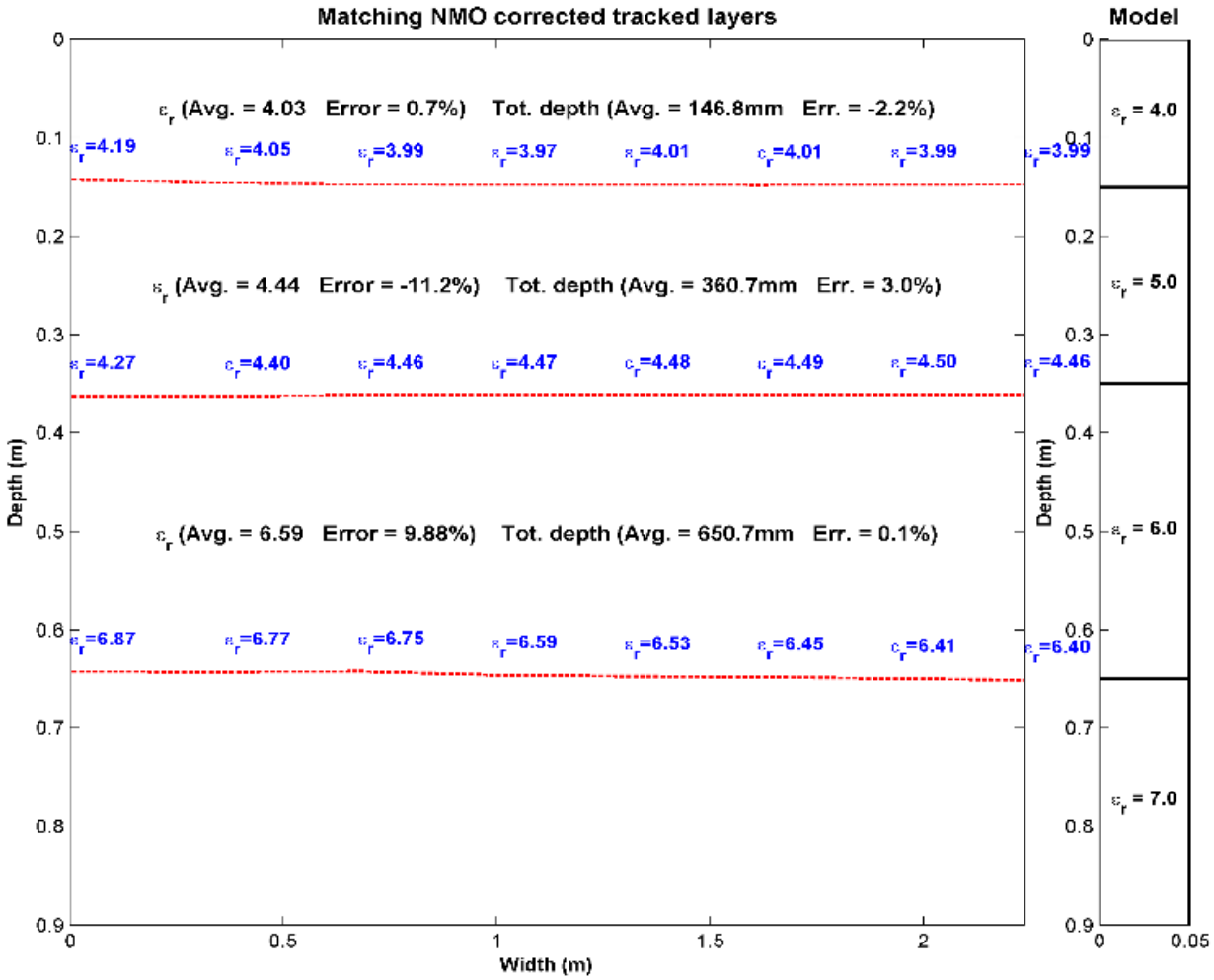

Fig. 6. Completed IM analysis (left) compared to the original horizontally layered model (right).

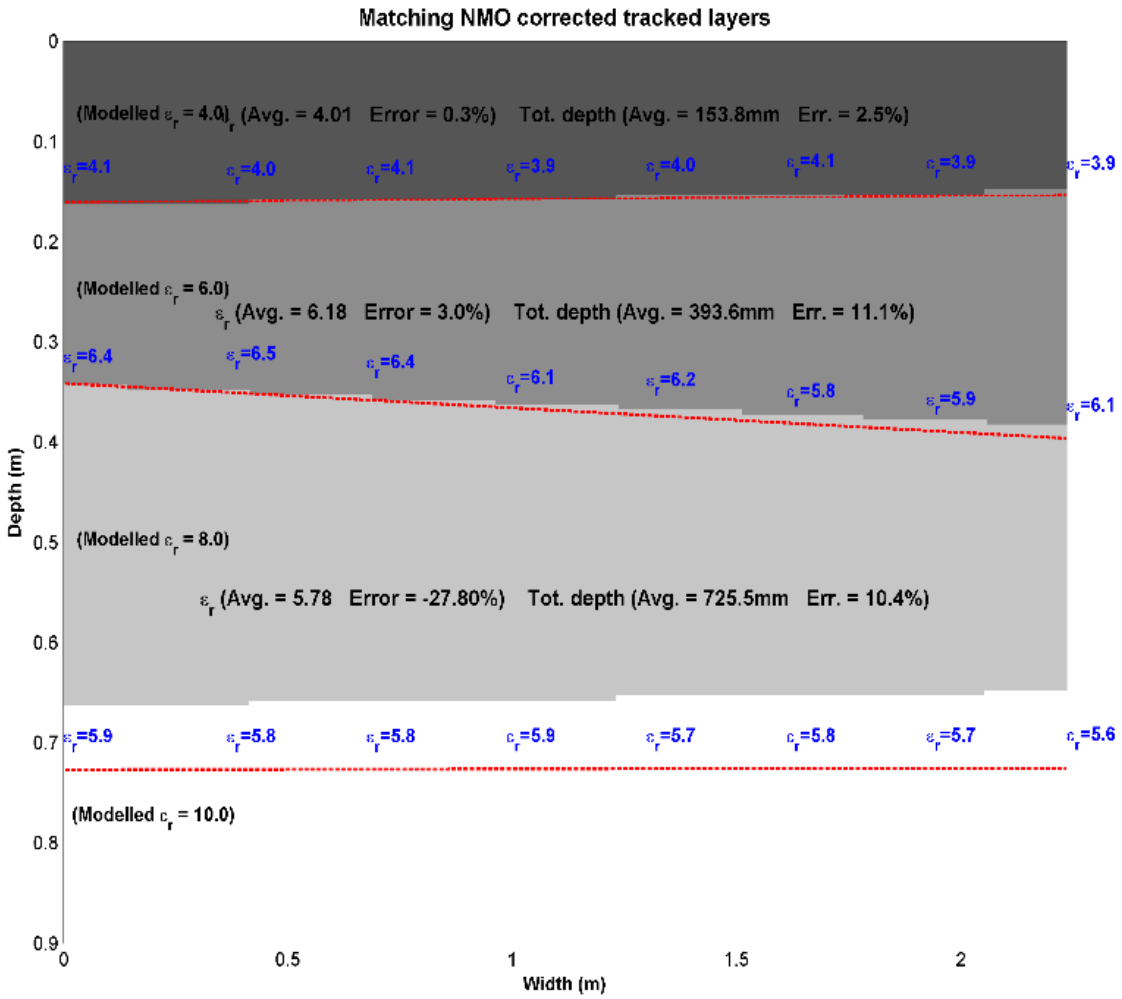

Fig. 7. GPRMax 3D model (solid colours) compared to IM predictions of bulk permittivity and interface layer depths (lines)

4.2 Ray-path Modelling

This approach determines the two-way travel time using a 3D ray-path model. The procedure commences using the estimated interface depths and layer permittivity using conventional geophysical methods. The 3D ray-paths and corresponding two-way travel times are then determined for each antenna pair within the first WARR group for the first pavement interface. The predicted times are then compared with the time of tracked layers within the GPR data. The assumed interface depth, transverse interface angle and layer permittivity for the WARR group are then adjusted and the ray-path and travel time are recalculated. The process continues for the current layer until the best match between predicted and tracked

layer interface reflection times is achieved. The process continues for each subsequent layer within the current WARR group, or alternatively is repeated for the current layer across all WARR groups. Like the IM approach, inter-layer refractions of the ray-path are determined using trial layer properties. However, as the method considers non-horizontal interfaces in its calculations, it should provide more accurate ray-path and reflection-time predictions.

An example of the RM approach applied on a 3D GPRMax modelled pavement is shown in Fig. 8. As the RM approach treats all WARR groups separately and does not match adjacent interfaces it is more flexible, thus potentially more able to consider lateral variations within the GPR response such as sloping layers. However, this flexibility can also be a disadvantage, resulting in greater instability in the predictions across the road width (Fig. 8).

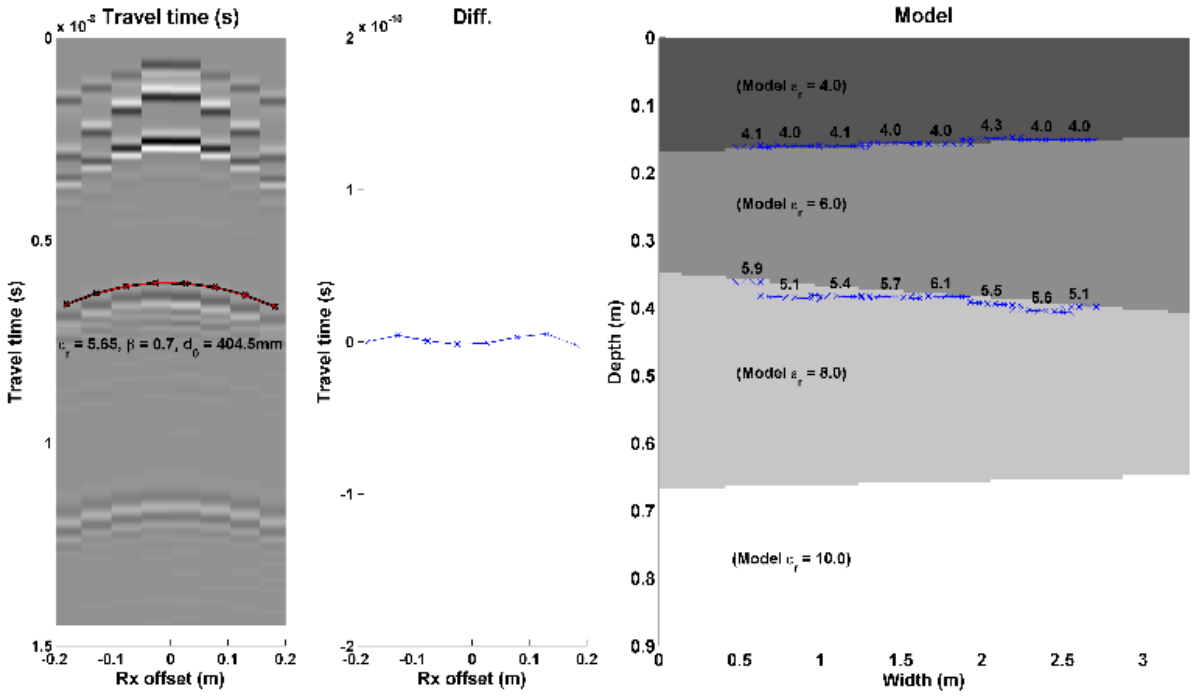

Fig. 8. Left: WARR data with tracked and modelled interfaces; Centre: Time difference between tracked and modelled interfaces; Right: Modelled geometry compared to RM-determined layer depths and ε_r values.

5 DISCUSSION

Overall, both the IM and RM methods produced relatively accurate results for shallow layers, with accuracies decreasing with depth. The IM approach has produced relatively accurate analysis in Fig. 6 and Fig. 7, particularly for the uppermost layers where layer depths are shallow relative to the antenna separations. When applied to the sloping interfaces, as shown in Fig. 7, the IM method results in a small discrepancy in the determined interface angles. However, considering this approach assumes a 2D model and horizontal layers this result is relatively good. For layers at greater depths the results of the IM method diverge from those of the model (Fig. 7). However, it should be noted that the conventional geophysical results also substantially deviated from the model for these deeper layers and produced more variable depth predictions. Regarding the RM approach, the layer depth and permittivity predictions matched the model relatively closely in the uppermost layer of the example shown in Fig. 8. A small error in permittivity for the uppermost layer is noted at one location (i.e. the $\varepsilon_r = 4.3$ value), however this coincides with a step in the 3D model and is likely to be due to this feature. As the depth of layer interfaces is not constrained by the results of adjacent WARR groups, layer predictions using the RM approach are more variable, particularly for the deeper layers. Owing to their approach, both the IM and RM methods are sensitive to calculation errors in the preceding layers. Consequently the accuracy of predictions is expected to decrease with depth of features and number of layers. Furthermore the flattening of hyperbolic reflectors at greater depths, particularly when using narrow receiver spreads, also limits the sensitivity of this approach. Thus a potential method to improve the results would be to program an occasional WARR or CMP fold using a single transmitter and the full set of receivers, say once every 50 profiles, to maximise fold spread. As the updated NM-GPR is fully programmable, such an approach should be possible if the standard configuration proves inadequate during field use.

Both the IM and RM approaches provide certain advantages and limitations in practice. In theory RM should produce superior results due to more accurate 3D ray-path modelling. However, in practice its increased flexibility also increases instability in the data analysis. As the lateral gradient of most pavement layer interfaces is typically mild, reductions in analysis stability may well outweigh any theoretical advantages in flexibility or accuracy. In any case

the final analysis method will most likely incorporate aspects of both IM and RM methods to ensure the best balance of stability and accuracy for layer permittivity and interface depth calibrations.

6 CONCLUSIONS

An update regarding the development of a self-correcting approach for calibrating the depth of road pavement layers using 3D multi-offset ground penetrating radar (GPR) has been presented. The approach commences by using a combination of conventional geophysical methods and layer tracking algorithms to estimate layer depths and bulk permittivity values. Afterwards, one of two self-correcting analysis methods, *interface matching (IM)* or *ray-path modelling (RM)*, is used to fine-tune the results. Examples of applying these methods to 2D and 3D finite difference time domain (FDTD) models for typical pavement configurations have been presented. Overall, both methods provided good estimates of layer permittivity and depth for the uppermost pavement layer, though the accuracy of these methods decreases for subsequent layers and increasing interface depth. Advantages of the IM approach include increased stability, consistent layer depth predictions and reasonable results on mildly sloping pavement layers. By contrast the RM method enables greater flexibility, though at the cost of greater prediction instability. The accuracy of both methods is influenced by the aggregation of errors in the preceding layers and measurement insensitivity for lower layers.

Despite these issues, the combination of multi-offset data collected using 3D noise modulated GPR (NM-GPR) and the proposed analysis techniques is expected to bring many practical benefits compared to conventional methods. This is particularly the case for larger scale uses where physical sampling becomes impractical and for more variable pavement conditions where existing non-destructive calibration methods falter. Development of these techniques is continuing and field trials to assess the accuracy and reliability of the proposed methods will soon commence.

7 ACKNOWLEDGMENT

The author expresses his sincere thanks to Dr Bryan Reeves and Dr-Ing. Alexander Scheuermann for their guidance and assistance. The author also acknowledges and supports the ongoing activities of COST Technical Committee TU1208 'Civil Engineering Applications of Ground Penetrating Radar'.

8 REFERENCES

[1] K. R. Maser, "Condition Assessment of Transportation Infrastructure Using Ground-Penetrating Radar," Journal of Infrastructure Systems, vol. 2, pp. 94-101, 1996.

[2] I. L. Al-Qadi, S. Lahouar and A. Loulizi, "GPR: From the state-of-the-art to the state-of-the-practice" in Non-Destructive Testing in Civil Engineering (NDT-CE 2003), Berlin, Germany, 2003.

[3] T. Scullion and T. Saarenketo, "Integrating Ground Penetrating Radar and Falling Weight Deflectometer technologies in pavement evaluation," ASTM Special Technical Publication, pp. 23-37, 2000.

[4] C. Plati and A. Loizos, "Using ground-penetrating radar for assessing the structural needs of asphalt pavements," Nondestructive Testing and Evaluation, vol. 27, pp. 273-284, 2012.

[5] D. H. Chen and T. Scullion, "Using nondestructive testing technologies to assist in selecting the optimal pavement rehabilitation strategy," Journal of Testing and Evaluation, vol. 35, pp. 211-219, 2007.

[6] T. Saarenketo, "Electrical properties of road materials and subgrade soils and the use of Ground Penetrating Radar in traffic infrastructure surveys," PhD thesis, Faculty of Science, Department of Geosciences, University of Oulu, Finland, 2006.

[7] C. Berthelot, D. Podborochynski, A. Anthony and B. Marjerison, "Mechanistic-based nondestructive structural asset management testing to optimize low-volume road structural upgrades," Transportation Research Record: Journal of the Transportation Research Board, vol. 2205, pp. 173-180, 2011.

[8] A. S. Noureldin, K. Zhu, S. Li and D. Harris, "Network pavement evaluation with Falling-Weight Deflectometer and Ground-Penetrating Radar," Transportation Research Record: Journal of the Transportation Research Board, vol. 1860, pp. 90-99, 2003.

[9] E. Kohler, N. Santero and J. Harvey, "Pilot project for fixed segmentation of the pavement network," University of Californa, Pavement Research Center, USA UCPRC–RR-2005-11, 2006.

[10] T. Saarenketo and T. Scullion, "Road evaluation with Ground Penetrating Radar," Journal of Applied Geophysics, vol. 43, pp. 119-138, 2000.

[11] A. B. Goktepe, E. Agar and A. H. Lav, "Advances in backcalculating the mechanical properties of flexible pavements," Advances in Engineering Software, vol. 37, pp. 421-431, 2006.

[12] G. R. Rada, J. F. Daleiden and H. T. Yu, "Moving pavement deflection testing measurements," presented at the CONINFRA 2010 - 4º Transportation Infrastructure Conference, São Paulo, Brasil, 2010.

[13] G. Flintsch, S. Katicha, J. Bryce, B. Ferne, S. Neil and B Diefenderfer, "Assessment of Continuous Pavement Deflection Measuring Technologies", SHRP Report S2-R06F-RW-1, Transportation Research Board, Washington DC, USA, 2013.

[14] W. B. Muller and J. Roberts, "Revised approach to assessing Traffic Speed Deflectometer (TSD) data and field validation of deflection bowl predictions," International Journal of Pavement Engineering, vol. 14, pp. 388-402, 1 April 2013.

[15] W. Muller and B. Reeves, "Comparing Traffic Speed Deflectometer and Noise-Modulated Ground Penetrating Radar data for rapid road pavement investigations," in 14th International Conference on Ground Penetrating Radar (GPR-2012), Shanghai, China, 2012, pp. 502-509.

[16] B. Reeves and W. Muller, "Traffic-speed 3-D Noise Modulated Ground Penetrating Radar (NM-GPR)," in 14th International conference on Ground Penetrating Radar (GPR-2012), Shanghai, China, 2012, pp. 165-171.

[17] W. B. Muller, A. Scheuermann and B. Reeves, "Quantitative moisture measurement of road pavements using 3D GPR," in 14th International Conference on Ground Penetrating Radar (GPR-2012), Shanghai, China, 2012, pp. 517-523.

[18] W. Muller and X. Dérobert, "A comparison of phase-shift and one-port coaxial cell permittivity measurements for GPR applications," in 7th International Workshop on Advanced Ground Penetrating Radar, IWAGPR 2013, Nantes, France., 2013.

[19] K. R. Maser, H. T.J., R. Roberts and J. Popovics, "Technology for quality assurance of new pavement thickness," in Non-Destructive Testing in Civil Engineering (NDT-CE 2003), Berlin, Germany, 2003.

[20] T. Scullion, C. L. Lau and Y. Chen, "Implementation of the Texas Ground Penetrating Radar system," Texas Transportation Institute, Texas A&M University, College Station, Texas Research Report 1233-1, 1992.

[21] C. Plati and A. Loizos, "Estimation of in-situ density and moisture content in HMA pavements based on GPR trace reflection amplitude using different frequencies," Journal of Applied Geophysics, 2013.

[22] J. Minet, C. Patriarca, E. C. Slob, M. Vanclooster and S. Lambot, "Characterization of layered media using full-waveform inversion of proximal GPR data," presented at the URSI International Sympsium on Electromagnetic Theory, 2010.

[23] Y. Cao, J. Labuz and B. Guzina, "Evaluation of pavement system based on Ground-Penetrating Radar full-waveform simulation," Transportation Reserach Record: Journal of the Transportation Research Board, pp. 71-78, 2011.

[24] M. R. Mahmoudzadeh, J. B. Got and S. Lambot, "Road inspection using full-waveform inversion of GPR data," presented at the 7th International Workshop on Advanced Ground Penetrating Radar (IWA-GPR2013), Nantes, France, 2013.

[25] J. M. Reynolds, An introduction to applied and environmental geophysics: John Wiley & Sons, Chichester, England, UK., 1997.

[26] J. Emilsson, P. Englund and J. Friborg, "Simple method for estimation of water content of roadbeds using multi-offset GPR," in Ninth International Conference on Ground Penetrating Radar, Santa Barbara, California, 2002, pp. 422-426.

[27] K. Grote, S. Hubbard, J. Harvey and Y. Rubin, "Evaluation of infiltration in layered pavements using surface GPR reflection techniques," Journal of Applied Geophysics, vol. 57, pp. 129-153, 2005.

[28] C. Fauchard, X. Dérobert, J. Cariou and P. Côte, "GPR performances for thickness calibration on road test sites," NDT & E International, vol. 36, pp. 67-75, 2003.

[29] H. Liu and M. Sato, "Robust estimation of dielectric constant by GPR using an antenna array," in Geoscience and Remote Sensing Symposium (IGARSS), Vancouver, Canada, 2011, pp. 178-181.

[30] M. L. Scott, N. Gagarin, J. R. Mekemson and S. R. Chintakunta, "Development of rapid, continuous calibration techniques and implementation as a prototype system for civil engineering matieral evaluation," in AIP Conf. Proc., 2011, pp. 1597-1604.

[31] J. L. Davis, J. R. Rossiter, D. E. Mesher and C. B. Dawley, "Quantitative measurement of pavement structures using radar," in Proceedings of the Fifth International Conference on Ground Penetrating Radar, Kitchener, Ontario, Canada, 1994, pp. 319-334.

[32] W. B. Muller and B. Reeves, "Application of a traffic-speed road scanning system including a new type of 3D GPR," in NDE/NDT for Highways and Bridges, Structural Materials Technology (SMT-2010), New York City, NY, USA, 2010, pp. 538-545.

[33] W. B. Muller, "A network-level road investigation trial using Australian-made traffic-speed 3D Ground Penetrating Radar (GPR) technology," 25th ARRB Conference, Perth, Western Australia, 2012.

[34] A. Giannopoulos, "Modelling ground penetrating radar by GPRMax," Construction and Building Materials, vol. 19, pp. 755-762, 2005.

[35] The Mathworks Inc., "MATLAB," V7 ed:, 2012.

Paper III

Muller, W.B. and Dérobert, X. A comparison of phase-shift and one-port coaxial cell permittivity measurements for GPR applications, 7th International Workshop of Advanced GPR (IWAGPR-2013), Nantes. IEEE, 1-6, July 2013

This page left intentionally blank

A comparison of phase-shift and one-port coaxial cell permittivity measurements for GPR applications

Wayne Muller[1,2] & Xavier Dérobert[3]

1. Department of Transport and Main Roads, Brisbane, Australia
2. The University of Queensland, School of Civil Engineering, Brisbane, Australia
3. LUNAM University, IFSTTAR, MACS Department, Bouguenais, France

***Abstract*—**The coarse and loose nature of unbound granular road materials presents a number of challenges for conventional permittivity characterisation approaches. An alternative that appears better suited to these materials involves measuring the phase-shift at discrete frequencies through a sample of known thickness. To validate this approach against more established methods, a comparison is required on materials that can be easily measured using either method. To this end phase-shift measurements were undertaken on a range of solid dielectric slabs including various types of stone, plastic and an artificial material. Permittivity predictions from this method were then compared to results from a one-port coaxial cell. As an additional comparison, and to better understand the results, the phase-shift test setup was also modelled using GPRMax software. To improve the predictions, reverberations within the test apparatus were minimized by isolating the direct wave using time-domain Blackman windowing. However, the narrow window necessary for this particular test setup also degraded the ability to detect frequency-dependent permittivity changes.

Overall the phase-shift approach produced real relative permittivity predictions similar to that from the one-port coaxial cell. Despite limitations in the current approach, the results validate the phase-shift approach as a simple and rapid method of characterizing the permittivity of larger dielectric material samples of constant thickness.

Keywords-permittivity characterisation, ground penetrating radar, phase-shift, coaxial cell, dielectric characterisation.

1 INTRODUCTION

Moisture is well known to affect the strength and mechanical performance of unbound granular pavement materials. Within Australia these materials are commonly used for road construction, comprising approximately 90% of the total length of Queensland state-controlled roads. However it is currently difficult to assess or monitor in-situ pavement moisture at medium or larger scales. This is because conventional physical sampling approaches become impractical and other options such as time domain reflectometry (TDR), while useful for monitoring a handful of fixed locations, become expensive for large-scale use. This in turn makes it difficult for engineers to make informed pavement management decisions. For example, when trying to determine the extent of pavement moisture infiltration in the wake of flooding or when trying to detect and treat moisture related problems early, before they become more serious.

Recently a rapid, quantitative moisture estimation approach has been proposed for road pavements [1] based on an updated 3D noise-modulated ground penetrating radar (NM-GPR) technology [2]. The approach involves estimating pavement layer permittivities by tracking and then matching normal moveout (NMO) corrected pavement interfaces across a series of adjacent, partially overlapping wide angle reflection and refraction (WARR) groups. Moisture-permittivity relationships, for example the variant of the Topp equation [3] proposed by Baran [4], are then be used to estimate in-situ pavement moisture based on the NM-GPR permittivity predictions. Work to date has included simulating the expected 3D NM-GPR response for typical pavement configurations; developing algorithms to track interfaces and determine layer permittivities using synthetic data and undertaking permittivity characterisation of moist unbound granular pavement samples [1].

2 PERMITTIVITY MEASUREMENT OPTIONS

To generate the necessary moisture-permittivity relationships, laboratory testing of typical pavement materials at a range of moisture levels is required. Approaches used by previous researchers to characterise the frequency-dependent permittivity of concrete and asphalt have included using small [5] and large open-ended dielectric probes [6]; custom one-port [7, 8] and two-port coaxial cells [9-13]; waveguides [14] and surface reflection techniques [15].

Other researchers have used fixed frequency methods, including resonant methods [16] or capacitance-based open-ended probes [17-19], though this latter approach typically measures at frequencies below the range of interest for pavement GPR.

However, the coarse aggregate fraction and loose nature of unbound granular materials presents a number of practical challenges for these methods. Unlike bound materials such as concrete or asphalt, unbound material samples cannot be easily cut or polished to achieve regular, smooth surfaces for good apparatus contact. Many of these methods only measure small sample volumes, making it difficult to characterise a representative sample. While several large custom coaxial cells have been developed to accommodate larger sampling volumes [9-13], the literature also attests to the considerable time and effort required for cell development and calibration, reducing their appeal. In addition, there is the challenge of achieving adequate sample compaction to replicate realistic field conditions without damaging or distorting the test apparatus.

Other more simplified characterisation approaches have also been demonstrated, for example the use of TDR probes [4, 20] or GPR [1, 21] to measure the two-way travel time along a probe or through a sample of known thickness, respectively. Alternatively several GPR techniques also enable permittivity determination. These vary in complexity and include the surface reflection coefficient method [22, 23], multi-offset methods [16, 21], techniques using embedded reflectors [24] and full waveform inversion [25, 26]. While each has benefits and limitations, the simpler time-domain methods usually involve a degree of judgement in picking key reflection events and cannot be used for frequency-dependent characterisation, which may be useful for more sophisticated models.

Due to limitations of existing methods, previous work [1] focussed on trialling a phase-shift approach [27, 28] to characterise samples of moist unbound granular pavement materials compacted within a rectangular plywood container. The approach involved using a Vector Network Analyzer (VNA) connected to bowtie antennas placed either side of the sample to pass sinusoidal electromagnetic signals through the material at various frequencies. Transmission (S_{21}) scattering parameters were measured and compared to similar measurements through the empty sample container. From this the real (ε_r') and imaginary (ε_r'') components of relative permittivity can be determined via [28]:

$$\varepsilon_r' \approx \left(1 + \frac{\Delta\Phi\lambda_0}{360d}\right)^2 \qquad (1)$$

$$\varepsilon_r'' \approx \frac{\Delta A\lambda_0\sqrt{\varepsilon'}}{8.686\pi d} \qquad (2)$$

Where ΔA = attenuation due to dielectric insertion (dB); λ_0 = free space wavelength of EM wave for a given frequency; d = material thickness; and $\Delta\Phi$ = measured phase shift due to dielectric insertion (degrees).

3 APPARATUS AND METHODOLOGY

A recent visit by the first author to the *Institut Français des Sciences et Technologies des Transports, de l'Aménagement et des Réseaux* (IFSTTAR, France) provided an opportunity to compare permittivity predictions based on the phase-shift approach to measurements using the one-port coaxial cell apparatus developed by Adous Quéffélec & Laguerre [8]. This cell had previously been used by researchers at IFSTTAR to characterise cylindrical samples cut from several solid dielectric civil engineering material samples [29, 30]. The current work involved testing larger, rectangular samples of the same homogeneous materials using the phase-shift approach and then comparing the results to the coaxial cell results, considered as references.

The test apparatus for this work used the same bowtie antennas and VNA used for the preliminary work in Australia. To minimise equipment transportation costs, materials readily available at IFSTTAR were used to configure a modified test apparatus – see Fig. 1. Sheets of 40mm thick polyvinyl chloride (PVC) were placed between the antennas and the material sample to reduce coupling changes during sample insertion. A gap of 111mm was maintained between the PVC sheets to enable material insertion without disturbing the test apparatus. The axis of the bowtie antennas was orientated horizontally, parallel with the floor, with a 345mm thick layer of microwave adsorbing foam placed behind each to reduce spurious reflections. The test setup was positioned on top of a 40mm slab of PVC which was placed on a reinforced concrete floor. This was done to reduce the influence of any reinforcement within the floor and to allow easer sliding insertion of the test materials. The centre of the bowtie antennas were positioned approximately 178mm above the PVC sheet placed on the floor. The

VNA measurements consisted of averaging five measurements collected at each of 1001 evenly spaced frequencies, ranging between 7.984MHz and 4.0GHz. The lower frequency limit of 7.984MHz was chosen as it enabled an integer of frequency steps down to DC to be achieved.

The materials used for this test were a range of plastics, rock types and also a man-made dielectric mixture designated 'K16' – see Fig. 2. The size of the samples was approximately 300mm x 300mm square. The sample thickness varied between 39.1mm to 100.5mm. S_{21} measurements were collected using an Agilent FieldFox VNA (Model N9923A). MATLAB [31] code was written to analyse these data. The analysis consisted of converting the raw S_{21} measurements into the time domain using Fourier techniques and applying a Blackman window centred on the largest time-domain peak, assumed to be the arrival of the direct wave. Different window widths were trialled, though a relatively narrow window was eventually chosen to better isolate the direct wave from spurious reflections within the test apparatus. The widowed signal was then transformed back into the frequency domain and un-wrapped over the frequency range which the results were considered most reliable (800MHz – 1.7GHz). The phase-shift was then determined at each frequency step relative to a similarly windowed response collected when the sample was absent, noting the potential for ambiguity [28]. The real relative permittivity was then calculated based on the measured phase-shift and the known material thickness.

The influence of sample edges on the transmission signal was investigated by undertaking S_{21} measurements while incrementally inserting the material into the apparatus in 50mm steps. To aid insertion, samples were placed on top of a 25mm thick piece of plywood and then incrementally slid into the test apparatus. The measured response at each location was transformed into a time domain signal and combined as a B-scan plot. This was done in order to observe the positions at which the sample edge affected the transmitted signal and thus determine the extent of edge effects.

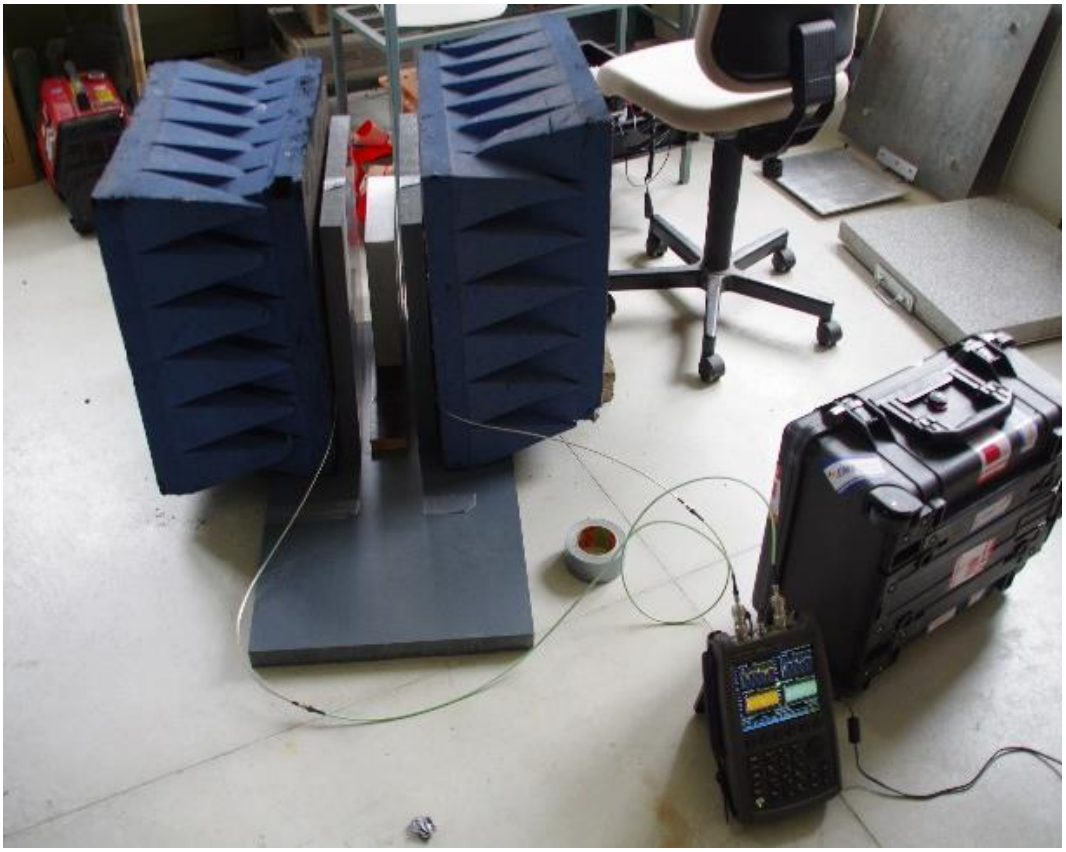

Figure 1. Modified phase-shift test apparatus.

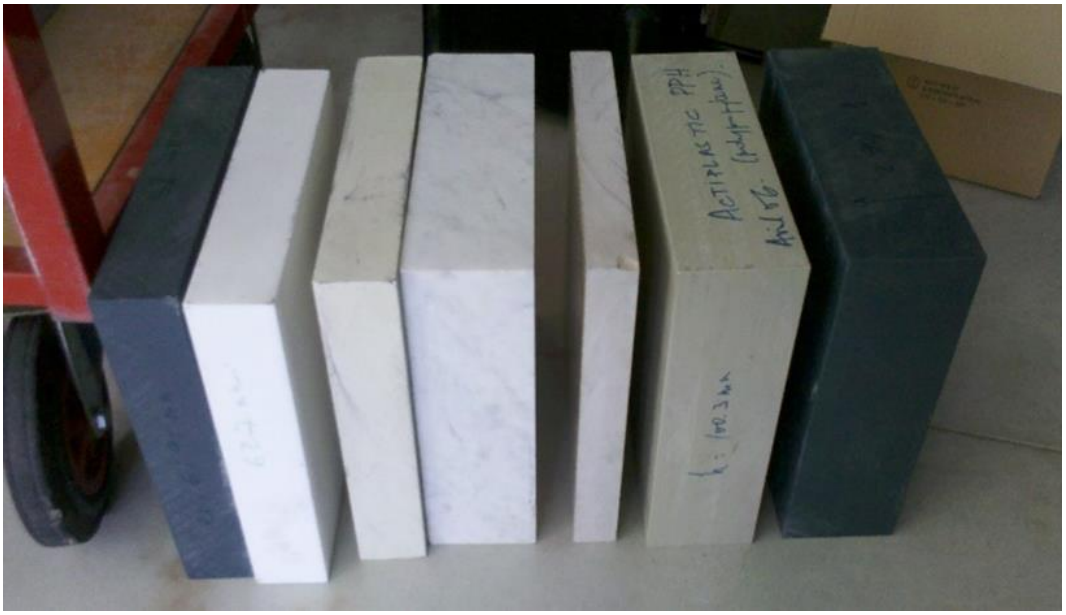

Figure 2. Samples tested using the phase-shift approach: (L-R): PVC, PTFE (Teflon), 'K16', Marble, Limestone, Polypropylene, PVC (thicker sample).

As the response measured by the VNA at each sample position is analogous to a stepped frequency GPR system operating in transmission mode, thus it is possible to model the response of the phase-shift apparatus using GPR simulation software. To this end multiple 2D models were simulated using GPRMax software [32] for each of the different material types and positions. These were then compared to the measurements made by the VNA. Snapshots of the electric field intensities at discrete times were also animated to better understand the wave propagation occurring within the model and test apparatus.

4 RESULTS & ANALYSIS

An example of raw and windowed S_{21} data for the Marble sample is shown in Fig. 3. The real relative permittivities from the phase-shift, coaxial cell and theoretical values over the measured frequency range are given in Fig. 4. In this figure the frequency range of coaxial-cell results has been limited to the range judged most reliable for each material type. Details of the material thicknesses average permittivity values are also summarised in Table 1.

TABLE I. Material details and mean measured relative permittivity values

Material type	**Sample thickness (mm)**	**Phase-shift ε_r'**	**Coaxial-cell or theoretical ε_r'**	**Diff. (%)**
PVC	61.95	2.7	2.9	-6.9
PTFE	62.7	2.1	2.1[a]	0
K16	60.0	16.2	16.8	-3.0
Marble	100.5	8.5	8.0[a]	+6.3
Limestone	39.1	8.8	8.1	+9.9
Polypropylene	100.3	2.3	2.2[a]	+4.5

a. Assumed theoretical value

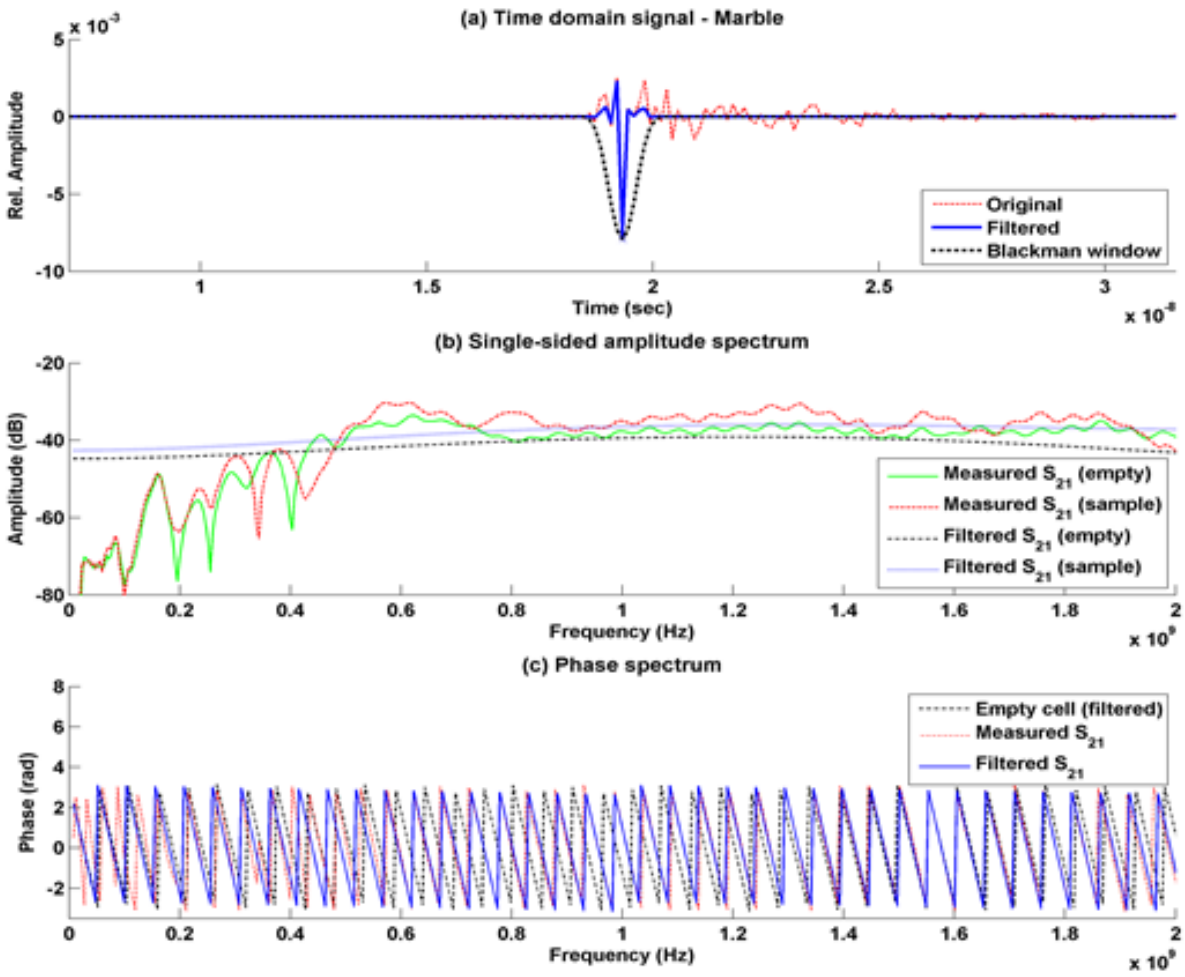

Figure 3. Measured phase-shift data for Marble: (a) Time domain signals and Blackman window envelope; (b) S_{21} amplitude; (c) S_{21} phase.

Overall there was a reasonably good agreement between the phase-shift and coaxial cell predictions of real permittivity, with a discrepancy of less than 10% compared to the coaxial cell for all samples. The greatest discrepancy was observed for the limestone sample, which was also the thinnest sample. This result is understandable considering (1) as any phase measurement errors or errors in apparent material thickness, for example due to the sample not being aligned perpendicular to the path between antennas, would be exaggerated for thinner samples. In addition, looking at the unfiltered VNA measurements Fig. 5(e) (top), unlike the other samples the limestone sample response appears to vary with the degree of insertion. The reason for this is unclear, but may be due to a combination of stronger internal reflections because of this materials higher permittivity contrast to the surrounding air and reduced

effectiveness of the Blackman window to reduce the influence of edge and other reflections from the direct wave for thinner samples.

Regarding the coaxial cell results shown in Fig. 4, a slight increase can be seen in the high frequency permittivity predictions for the limestone and the K16 materials. This corresponds to a numerical shift in the inversion for the coaxial cell approach and is not the true characteristic of the materials. For these materials the valid coaxial-cell results are below approximately 600 MHz for the limestone and 300 MHz for the K16 material. For the marble, polypropylene and PTFE samples, cell measurements were not undertaken and so comparisons in Table 1 and Fig. 4 are based on assumed values for these materials from the literature. While a relative permittivity of 8.0 has been assumed for marble, variations from 8 to 10 have also been reported [33].

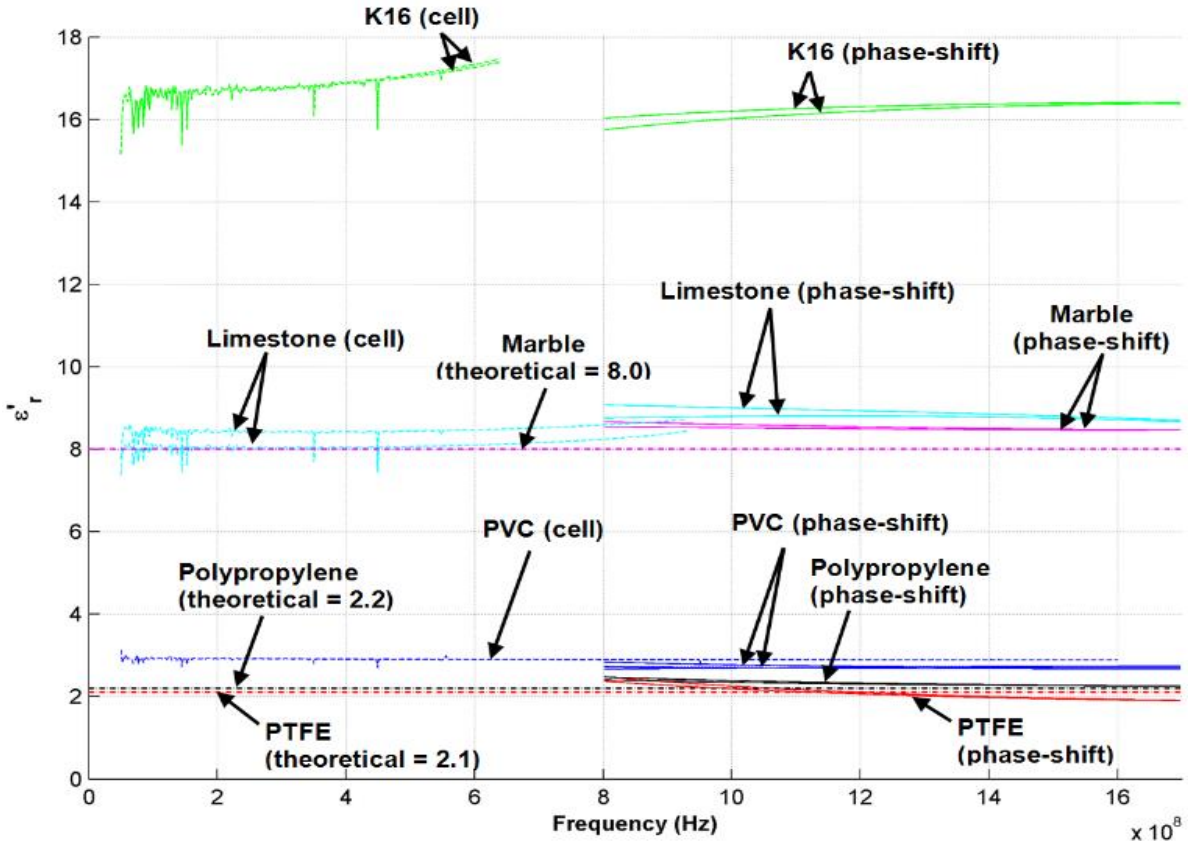

Figure 4. Phase-shift and coaxial cell measurements and theoretical values of real relative permittivity (ε'_r) for the sample materials.

As illustrated in Fig. 3, the narrow Blackman window that was used significantly smoothed the amplitude and phase response of the S_{21} data over the measured frequency range. This in turn also smooths the calculations of real permittivity and thus reduces the ability to detect frequency-dependent variations. Other issues were also noted with the approach. For one, the signal attenuation within these materials was low and did not achieve the recommended 10dB loss to avoid multiple reflections [28]. In some cases the magnitude of the transmitted signal was noted to be greater with the dielectric present, most likely due to reduced permittivity contrasts across the PVC-air-sample boundaries. As the calculation of imaginary permittivity (ε_r'') in (2) is based on measuring an increase in signal attenuation during sample insertion, such observations indicate that the imaginary permittivity calculations were unreliable and so have not been reported. Coupling variability during material insertion may have also had some influence on the signal attenuation, despite the inclusion of the PVC spacers. Slight indications of this can be seen in Fig. 3(b) as shifts in lower-frequency resonant nulls for the unfiltered response compared to the empty apparatus. However such coupling effects should only affect the imaginary permittivity calculation. Other possible influences include signal reflections within the coaxial cables attaching the VNA to the antennas and also the potential for reflections from reinforcement within the underlying concrete floor.

The measurements and simulations used to investigate edge effects are presented in Figs. 5 – 7. The top row of Fig 5 shows raw time domain VNA S_{21} measurements whereas the bottom row shows the corresponding simulations. The time zero of the VNA measurements was adjusted to allow better comparison with the simulation. Overall, there was a good match between the simulated and measured results, though unsurprisingly the VNA measurements using rudimentary bowtie antennas and short cables exhibited additional reverberations. Both the VNA measurements and simulations show an abrupt change in the response as the edge of the samples reached the direct path between antenna feed points, but then showed a relatively consistent response when inserted beyond this point.

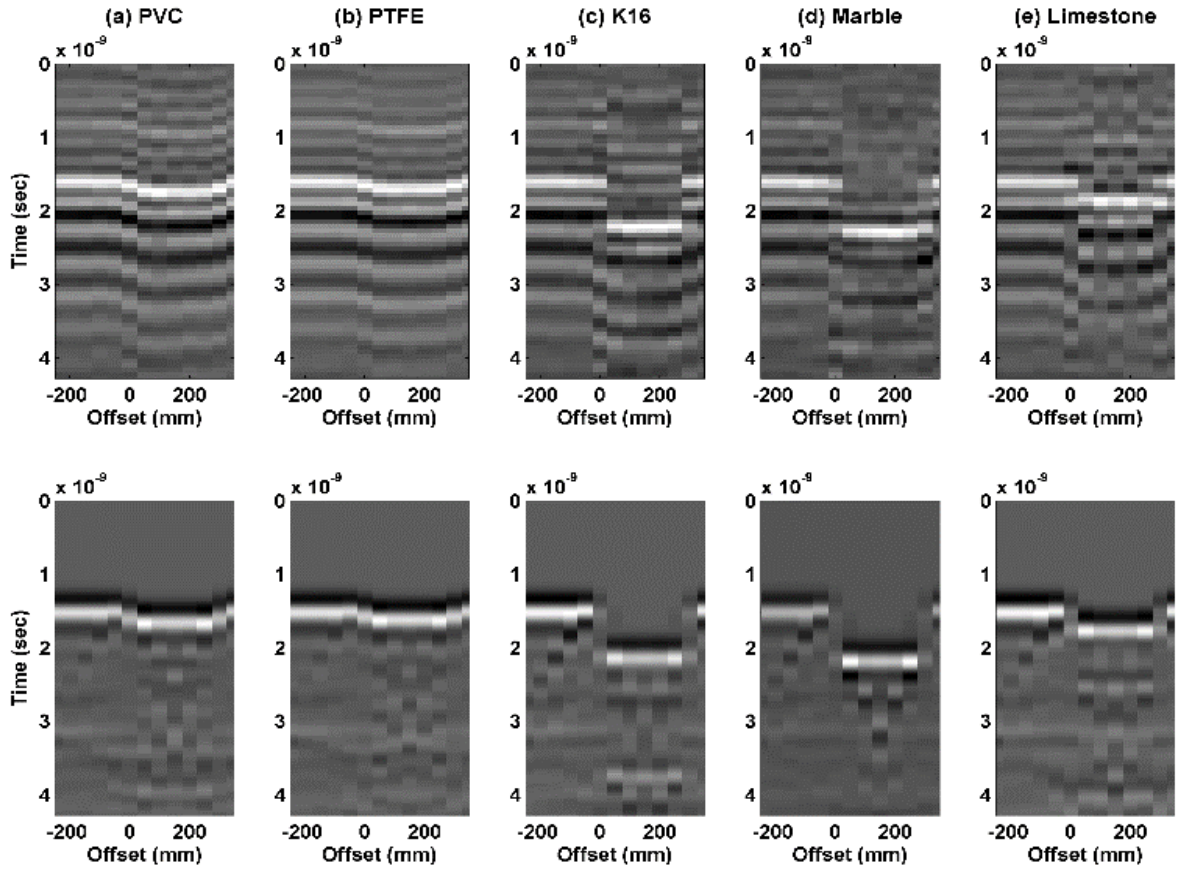

Figure 5. Unfiltered time-domain S_{21} measurements during incremental insertion of samples (top) and corresponding simulations (bottom

To consider what is happening in terms of wave propagation within the test apparatus, Figs. 6 – 7 present two simulated examples. These show snapshots of the electric field strength at discrete times for a centrally positioned limestone sample and an asymmetrically positioned K16 sample, respectively. In Fig. 6, reflections arriving at the receiving antenna reflected from the top and edges of the limestone and from the edges of the PVC spacers are separated in time from the direct wave by just enough to enable effective windowing. In Fig. 7 the side reflection from the K16 is essentially inseparable from the direct wave when arriving at the receiver, though it is relatively weak compared to the direct wave. Also the asymmetric positioning and increased permittivity contrast of the sample compared to the surrounding air has resulted in strong spurious reflections within the sample material, complicating the later response.

Figures 5 – 7 illustrate the value of simulations to better understand wave propagation within the test apparatus and the sources of unwanted reflections. These techniques also enable different combinations of sample size, thickness, antenna spacing, spacer materials, and so forth, to be considered prior to laboratory testing. It is hoped that these methods can be used to improve the phase-shift measurement approach, optimise sample dimensions and minimise the occurrence and influence of reflections on the measurement results for future work.

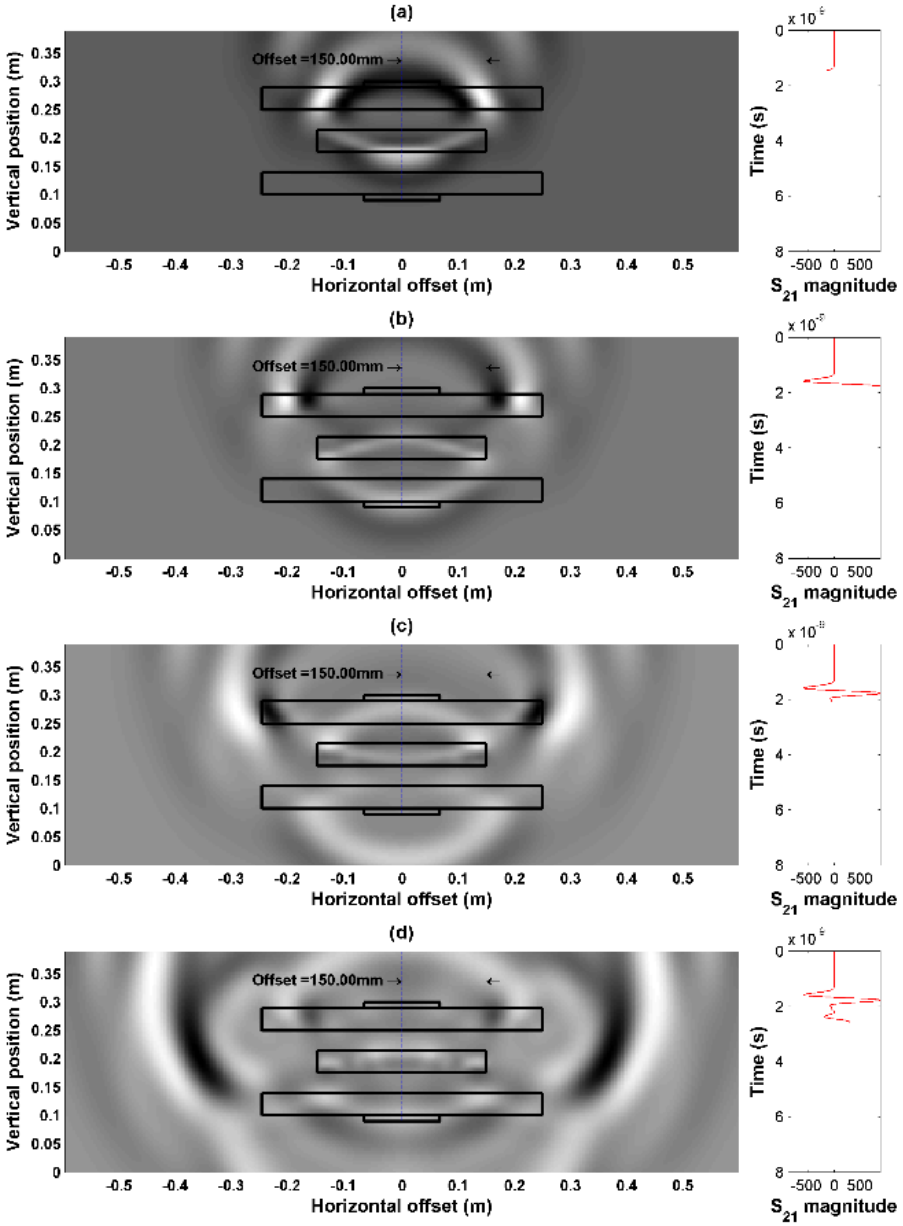

Figure 6. Simulated magnitude of the electric field for the Limestone sample at discrete times (left) and corresponding S_{21} magnitude (right).

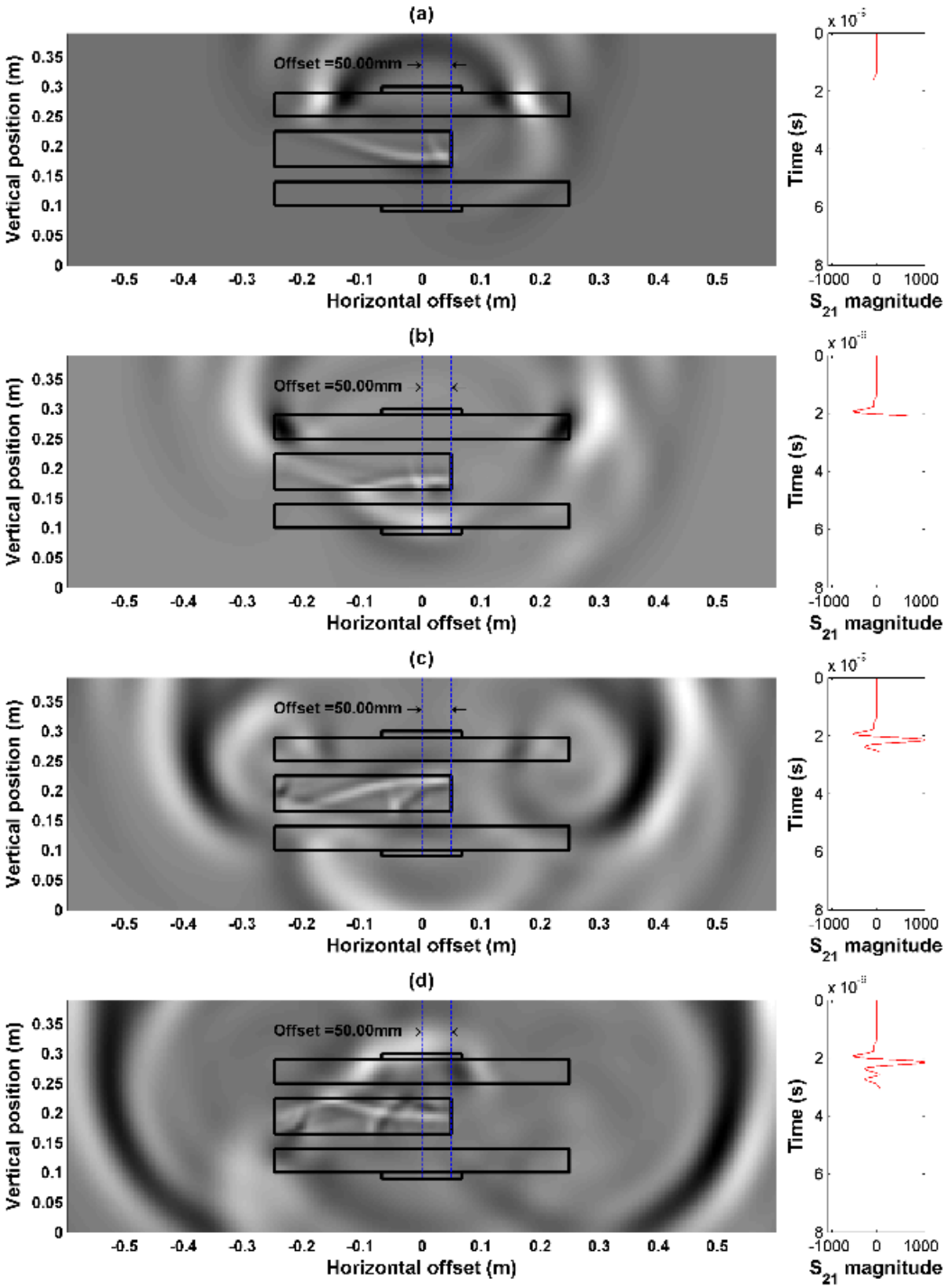

Figure 7. Simulated magnitude of the electric field for the Limestone sample at discrete times (left) and corresponding S_{21} magnitude (right).

5 CONCLUSIONS

Measurements of relative permittivity were undertaken on several solid dielectric materials using a phase-shift transmission approach and were compared to previous coaxial cell measurements, considered as references. Simulations of the phase-shift approach were also undertaken as an additional comparison and to better understand the measurement results.

Overall the methods produced similar estimates of real relative permittivity for the materials tested. While some measurements presented slight shifts in predicted permittivities, the phase shift transmission approach appears complementary to the coaxial cell technique at higher frequencies. However a number of issues were noted with the approach in its current form, including the trade-off between reducing spurious reverberations and frequency-dependent measurement fidelity. Imaginary permittivity values were not reported, as the attenuation measurement was found to be unreliable for the low loss materials tested. The influence of edge effects was generally low, particularly for centrally positioned samples once time-domain windowing of the direct wave was undertaken. Other potential issues such as misalignment of test samples, coupling variability during sample insertion, thin samples and reflections within the VNA cables were also briefly discussed.

While further refinement of the test apparatus and approach is required, the results of this investigation validate the phase-shift approach as a relatively quick and simple method of material dielectric characterisation at frequencies of interest for GPR applications. The advantages of this approach become clear when considering larger, more representative samples of compacted unbound granular pavement materials, which can be difficult to characterise using conventional methods. Based on the results of this study, further use and development of the phase-shift approach is recommended.

6 ACKNOWLEDGMENT

The authors wish to express their sincere thanks to all the very helpful and welcoming colleagues at IFSTTAR and also to Dr Bryan Reeves from Radar Portal Systems Pty Ltd and Dr.-Ing. Alexander Scheuermann from the University of Queensland for their many helpful

suggestions. This study was funded by the University of Queensland under the Graduate Student International Travel Award (GSITA).

7 REFERENCES

[1] W. B. Muller, A. Scheuermann and B. Reeves, "Quantitative moisture measurement of road pavements using 3D GPR," in 14th International Conference on Ground Penetrating Radar (GPR-2012), Shanghai, China, 2012, pp. 517-523.

[2] B. Reeves and W. Muller, "Traffic-speed 3-D Noise Modulated Ground Penetrating Radar (NM-GPR)," in 14th International conference on Ground Penetrating Radar (GPR-2012), Shanghai, China, 2012, pp. 165-171.

[3] G. C. Topp, J. L. Davis and A. P. Annan, "Electromagnetic determination of soil water content: measurements in coaxial transmission lines," Water Resources Research, vol. 16, pp. 574-582, 1980.

[4] E. Baran, "Use of time domain reflectometry for monitoring moisture changes in crushed rock pavements," in Symposium and workshop on time domain reflectometry in environmental, infrastructure and mining applications, Northwestern University, Evanston, Illinois, USA, 1994, pp. 349-356.

[5] C.-M. Chang, J.-S. Chen and T.-B. Wu, "Dielectric Modeling of Asphalt Mixtures and Relationship with Density," Journal of Transportation Engineering, vol. 137, pp. 104-111, 2011.

[6] B. Filali, F. Boone, J. Rhazi and G. Ballivy, "Design and calibration of a large open-ended coaxial probe for the measurement of the dielectric properties of concrete," IEE Transactions on Microwave Theory and Techniques, vol. 56, pp. 2322-2328, 2008.

[7] Y. Huang, "Design, calibration and data interpretation for a one-port large coaxial dielectric measurement cell," Measurement Science and Technology, vol. 12, pp. 111–115, 2001.

[8] M. Adous, P. Quéffélec and L. Laguerre, "Coaxial/cylindrical transition line for broadband permittivity measurement of civil engineering materials," Measurement Science and Technology, vol. 17, pp. 2241-2246, 2006.

[9] J. Shang, J. Umana, F. Bartlett and J. Rossiter, "Measurement of complex permittivity of asphalt pavement materials," Journal of Transportation Engineering, vol. 125, p. 347, 1999.

[10] J. Shang and J. Umana, "Dielectric constant and relaxation time of asphalt pavement materials," Journal of Infrastructure Systems, vol. 5, pp. 135-142, 1999.

[11] A. Robert, "Dielectric permittivity of concrete between 50 MHz and 1 GHz and GPR measurements for building materials evaluation," Journal of Applied Geophysics, vol. 40, pp. 89-94, 1998.

[12] M. N. Soutsos, J. H. Bungey, S. G. Millard, M. R. Shaw and A. Patterson, "Dielectric properties of concrete and their influence on radar testing," ND&E International, vol. 34, pp. 419-425, 2001.

[13] S. G. Millard, et al., "Coaxial transmission lines: Development of test procedures for concrete," Journal of Materials in Civil Engineering, vol. 13, pp. 202-208, 2001.

[14] E. J. Jaselskis, J. Grigas and A. Brilingas, "Dielectric properties of asphalt pavement," Journal of Materials in Civil Engineering, vol. 15, pp. 427-434, 2003.

[15] J. Davis, Y. Huang, S. G. Millard and J. H. Bungey, "Determination of dielectric properties of insitu concrete at radar frequencies," presented at the International Symposium on Non-Destructive Testing in Civil Engineering 2003, Berlin, Germany, 2003.

[16] C. Fauchard, X. Dérobert, J. Cariou and P. Côte, "GPR performances for thickness calibration on road test sites," NDT & E International, vol. 36, pp. 67-75, 2003.

[17] T. Saarenketo, "Tube suction test - Results of round robin tests on unbound aggregates," Finish National Road Administration, 2000.

[18] C. Berthelot, D. Podborochynski, T. Saarenketo, B. Marjerison and C. Prang, "Ground-penetrating radar evaluation of moisture and frost across typical Saskatchewan road soils," Advances in Civil Engineering, 2010.

[19] A. Loizos and C. Plati, "Accuracy of pavement thicknesses estimation using different ground penetrating radar analysis approaches," NDT & E International, vol. 40, pp. 147-157, 2007.

[20] J. Ekblad, "Influence of water on coarse granular road material properties," Doctor of Philosophy, Department of Civil and Architectural Engineering, KTH Royal Institute of Technology, Stockholm, Sweden, Stockholm, 2007.

[21] K. Grote, S. Hubbard, J. Harvey and Y. Rubin, "Evaluation of infiltration in layered pavements using surface GPR reflection techniques," Journal of applied geophysics, vol. 57, pp. 129-153, 2005.

[22] I. L. Al-Qadi, Z. Leng, S. Lahouar and J. Baek, "In-place hot-mix asphalt density estimation using ground-penetrating radar," Transportation research record, vol. 2152, pp. 19-27, 2010.

[23] T. Saarenketo and T. Scullion, "Road evaluation with ground penetrating radar," Journal of applied geophysics, vol. 43, pp. 119-138, 2000.

[24] I. L. Al-Qadi, S. Lahouar and A. Loulizi, "In situ measurements of hot-mix asphalt dielectric properties," NDT & E International, vol. 34, pp. 427-434, 2001.

[25] A. Kalogeropoulos, J. van der Kruk and J. Hugenschmidt, "Monitoring the evolution of water and chloride in concrete using GPR full-waveform inversion," presented at the 6th International Workshop on Advanced Ground Penetrating Radar (IWAGPR-2011), Aachen, Germany, 2011.

[26] Y. Cao, J. Labuz and B. Guzina, "Evaluation of pavement system based on Ground-Penetrating Radar full-waveform simulation," Transportation Reserach Record: Journal of the Transportation Research Board, pp. 71-78, 2011.

[27] S. O. Nelson, "Dielectric properties measurement techniques and applications," Transactions of the ASAE-American Society of Agricultural Engineers, vol. 42, pp. 523-530, 1999.

[28] S. Trabelsi, A. W. Kraszewski and S. O. Nelson, "Phase-shift ambiguity in microwave dielectric properties measurements," IEEE Transactions on Instrumentation and Measurement, vol. 49, pp. 56-60, 2000.

[29] X. Dérobert, G. Villain, R. Cortas and J. L. Chazelas, "EM charazerisation of hydraulic concretes in the GPR frequency-and using a quadratic experimental design," in 7th International Symposium of Non-Destructive Testing in Civil Engineering (NDTCE'09), Nantes, France, 2009, pp. 177-182.

[30] A. Ihamouten, K. Chahine, V. Balazart, G. Villain and X. Dérobert, "On variants of the frequency power law for the electromagnetic characterisation of hydraulic concrete," IEEE Transactions on Instrumentation and Measurement, vol. 60, pp. 3658-3668, 2011.

[31] The Mathworks Inc., "MATLAB," V7 ed: The Mathworks Inc.,, 2012.

[32] A. Giannopoulos, "Modelling ground penetrating radar by GPRMax," Construction and Building Materials, vol. 19, pp. 755-762, 2005.

[33] S. Liu, J. Wu, L. Zhang and H. Dong, "Wide-band rock and ore samples complex permittivity measurement," in Behaviour of Electromagnetic Waves in Different Media and Structures, A. Aldagli, Ed., ed: InTech, 2011, pp. 101-120.

Paper IV

Muller W.B. and Scheuermann A., Optimising a modified free-space permittivity characterisation method for civil engineering applications, Journal of Geophysics and Engineering 13(2):S9-S18, April 2016

This page left intentionally blank

Optimising a modified free-space permittivity characterisation method for civil engineering applications

Wayne Muller[a,b,c] and Alexander Scheuermann[c]

[a]Department of Transport and Main Roads, Brisbane, QLD 4006

[b]ARRB Group Ltd., Brisbane, QLD 4010;

[c]School of Civil Engineering, The University of Queensland, Brisbane, QLD 4072, Australia

Corresponding author: Wayne Muller,

Tel.:+61 7 32603510; E-mail address: wayne.b.muller@tmr.qld.gov.au

This is an author-created, un-copyedited version of an article accepted for publication in the Journal of Geophysics and Engineering. The publisher is not responsible for any errors or omissions in this version of the manuscript or any version derived from it. The Version of Record is available online at http://dx.doi.org/10.1088/1742-2132/13/2/S9.

Abstract – Measuring the electrical permittivity of civil engineering materials is important for a range of ground penetrating radar (GPR) and pavement moisture measurement applications. Compacted unbound granular (UBG) pavement materials present a number of preparation and measurement challenges using conventional characterisation techniques. As an alternative to these methods, a modified free-space (MFS) characterisation approach has previously been investigated. This paper describes recent work to optimise and validate the MFS technique. The research included Finite Difference Time Domain (FDTD) modelling to better understand the nature of wave propagation within material samples and the test apparatus. This research led to improvements in the test approach and optimisation of sample sizes. The influence of antenna spacing and sample thickness on the permittivity results was investigated by a series of experiments separating antennas and measuring samples of nylon and water. Permittivity measurements of samples of nylon and water approximately 100 mm and 170 mm thick were also compared, showing consistent results. These measurements also agreed well with surface probe measurements of the nylon sample and literature values for water. The results indicate permittivity estimates of acceptable accuracy can be obtained using the proposed approach, apparatus and sample sizes.

Keywords – Permittivity characterisation; unbound granular road pavements; GPR.

1.0 INTRODUCTION

UBG pavements are widely used within Australia as economical road construction materials. The structural performance of these materials is highly moisture sensitive and so methods of monitoring pavement moisture are useful for a range of pavement engineering applications. The permittivity of these materials is strongly influenced by, and can be related to, the volumetric moisture content. An approach using multi-offset noise-modulated ground penetrating radar (NM-GPR) is currently being developed to quantify moisture within UBG pavements by measuring the permittivity of pavement layers (Muller et al., 2012, Muller, 2014). To enable moisture estimates from these measurements, moisture-permittivity relations need to be developed and calibrated by measuring the bulk permittivity of UBG samples prepared to mimic a range of field moisture and density conditions in the laboratory. Existing characterisation methods, however, have difficulty accommodating these unbonded coarse-grained materials; only measure small material volumes; use delicate apparatus that may be damaged during sample compaction or lack measurement precision. A more precise and practical approach better suited to measuring larger, more representative samples of compacted UBG materials is therefore required.

2.0 METHODS

2.1 Free-space characterisation

There are several approaches to free-space permittivity characterisation of materials. One method involves measuring the variation in phase and amplitude of electromagnetic (EM) signals passing between a fixed pair of antennas when a known thickness of a sample material placed in between. These measurements are normally collected using a vector network analyser (VNA) attached to the antennas, which collects measurements before and after the sample is inserted. Assuming far-field conditions for low-loss materials the frequency-dependent real and imaginary components of complex relative permittivity, herein referred to as real permittivity (ε'_r) and imaginary permittivity (ε''_r), can be determined via (Trabelsi et al., 2000):

$$\varepsilon'_r \approx \left(1 + \frac{\Delta\Phi\lambda_0}{360d}\right)^2 \qquad (1)$$

$$\varepsilon''_r \approx \frac{\Delta A\lambda_0\sqrt{\varepsilon'_r}}{8.686\pi d} \qquad (2)$$

where A = attenuation due to sample insertion (dB); λ_0 = free space wavelength for a given frequency; d = material thickness; and $\Delta\Phi$ = measured phase-shift (degrees). The measured phase-shift occurs due to slowing of the EM wave within the sample compared to the initial measurement through air. For non-magnetic and low loss ($\varepsilon'_r >> \varepsilon''_r$) materials the phase velocity (v) of propagating EM waves is related to the real permittivity via:

$$v = \frac{c}{\sqrt{\varepsilon'_r}} \tag{3}$$

where c is the speed of light in a vacuum.

Free-space techniques have been used to a limited extent for the characterisation of civil engineering materials. Examples in the literature have involved more complicated analysis methods, measured relatively thin samples or measured at frequencies well above that used for pavement GPR (e.g. Büyüköztürk et al., 2006, Panzner et al., 2010, Jamil et al., 2013, Pellinen et al., 2015). Such measurements are normally undertaken using horn antennas with relatively large samples; or using focussed antennas or high measurement frequencies to achieve far-field focussing and minimise the effects of material boundaries (Chen et al., 2004, Kaatze and Hübner, 2010). The need for specialist focussing antennas or a controlled measurement environment, however, limits the practicality of these methods for routine use in a soil laboratory. Furthermore, high frequency measurements require relatively expensive VNA equipment and may limit the thickness of samples due to focussing considerations and losses due to signal attenuation and scattering.

MFS is an adaptation of the free-space approach that uses a compact arrangement comprising of a pair of antennas and material coupling similar to that used in a typical ground-coupled GPR system. The approach was initially trialled on moist compacted samples of UBG materials and compared to GPR permittivity measurements (Muller et al., 2012). It was later compared to results from a large one-port coaxial cell for a range of dielectric materials (Muller and Dérobert, 2013) and to TDR and GPR measurements for UBG material samples prepared to a range of moisture content and density conditions (Muller et al., 2015), overall showing good agreement with these other techniques. MFS is intended as a means of calibrating GPR estimates of layer depth and moisture content. The similarity of the MFS and GPR equipment provides the potential advantage that any permittivity measurement errors due to material

properties (for example, when measuring lossy materials) should equally affect both methods and so should not affect the accuracy of field estimates. Moreover, as the VNA equipment can be used as a GPR (e.g. Kong et al., 2012), reflected signals viewed in the time-domain can be directly compared to GPR measurements and the change in arrival times of direct and reflected signals can be used as an additional means of calculating the sample permittivity. The ability to measure through material samples enables characterisation of larger, more representative sample volumes compared to typical surface probes or small coaxial cells. The use of a removable dielectric container enables easier compaction of loose UBG materials to better replicate field conditions without the risk of damaging delicate or expensive test apparatus. Furthermore the measurement of phase-shift is more precise compared to conventional time-domain techniques such as time-domain reflectometry (TDR) or GPR measurements through a sample of known thickness.

There are, however, a number of limitations of the MFS approach. For one, it is not possible to reliably measure the imaginary permittivity due to changes in antenna performance with coupling (Muller and Dérobert, 2013). Although the effect of sample edges was previously investigated and found to be minor (Muller and Dérobert, 2013), reflections within the sample or apparatus remain a potential concern. Furthermore, due to the relatively close antenna separation, near-field effects have potential to influence the measurements.

2.2 Approach

The aim of this paper is to better understand and optimise the MFS test configuration, to investigate concerns regarding near-field effects and to further assess the measurement accuracy of the MFS approach. To this end numerical techniques are used to model wave propagation within the sample and apparatus to enable better understanding and optimisation of the test procedure and the size of material samples. The influence of near-field effects is investigated in a series of laboratory experiments that involve assessing the linearity of phase with increasing antenna separation and assessing the accuracy of real permittivity measurements for known materials (water, air) and for an independently characterised material (nylon).

2.3 Equipment

A FieldFox N9923A portable VNA was used for the investigation. It was configured to measure at 1001 frequency steps over the range 7.984 MHz to 4.0 GHz using the VNA's high power setting and taking the average of five frequency sweeps per measurement. The VNA's inbuilt 'QuickCal' calibration procedure was used prior to these measurements. VNA measurements, called scattering parameters (S-Parameters), are denoted S_{xy}, where x and y denote the receiving and transmitting ports of the VNA, respectively. While Eqn. 1 only requires the phase change of the transmitted signal to determine ε', the magnitude and phase of both transmitted (S_{21}) and reflected (S_{11}) signals were collected to enable additional time-domain analysis and signal filtering options.

The antennas used for the S-parameter measurements were a custom pair of shielded ground-coupled bow-tie dipole antennas. These passive antennas incorporate a balun at the antenna feed point to improve signal transmission. In terms of radiation pattern, numerical modelling of shielded dipole antennas in free-space indicates a downward lobe directly beneath the antenna (Diamanti and Annan, 2013). Bow-tie antennas produce a narrower beam pattern compared to small dipoles (Millard et al., 2002). The antenna performance changes with the proximity to, and properties of, the ground and other nearby materials (Diamanti and Annan, 2013, Millard et al., 2002). Beam patterns measured in air narrow significantly when in contact with the dielectric material (Millard et al., 2002) and become narrower and more directional with increasing permittivity (Diamanti and Annan, 2013). The vast majority of energy emitted by these antennas is pulled into the ground, which has little to do with the antenna shielding (Diamanti and Annan, 2013).

3.0 RESULTS AND DISCUSSION

3.1 Numerical Modeling

To better understand wave propagation within the test apparatus 2-dimensional FDTD modelling was undertaken (Fig. 1). Sample boxes with internal dimension of 300 x 300 x 100 mm containing material samples with real permittivity values of 5 – 15 were modelled using GPRMax 2D software (Giannopoulos, 2005). The excitation used for these models was a simple 1.5 GHz point source Ricker wavelet located at the position of the feed-point of the

transmitting antenna. The directionality of the bow-tie antenna and effects of shielding were not considered in this modelling.

This FDTD modelling was useful as it revealed several key points. The first was that the existing sample box aspect ratio of 3:1 was a good choice as spurious reflections from box sides and the double bounce arrived at a similar time, indicated with an arrow in Fig. 1(a). That is, this aspect ratio enables the direct wave to be maximally separated from these unwanted reflections, which in turn makes it easier to isolate the direct wave or remove the unwanted effects – for example, by using time-domain windowing as per Muller and Dérobert (2013). A second observation was the detrimental effect the sides of the empty ply box had when collecting the reference signal. That is, when the box is empty, the signal reflecting from the sides of the box arrives soon after the direct wave resulting in a poor reference signal (Fig 1(b)). Subsequent modelling of a ply sheet as the reference instead of an empty box showed a significant reduction of such unwanted reflections (Fig. 1(c)).

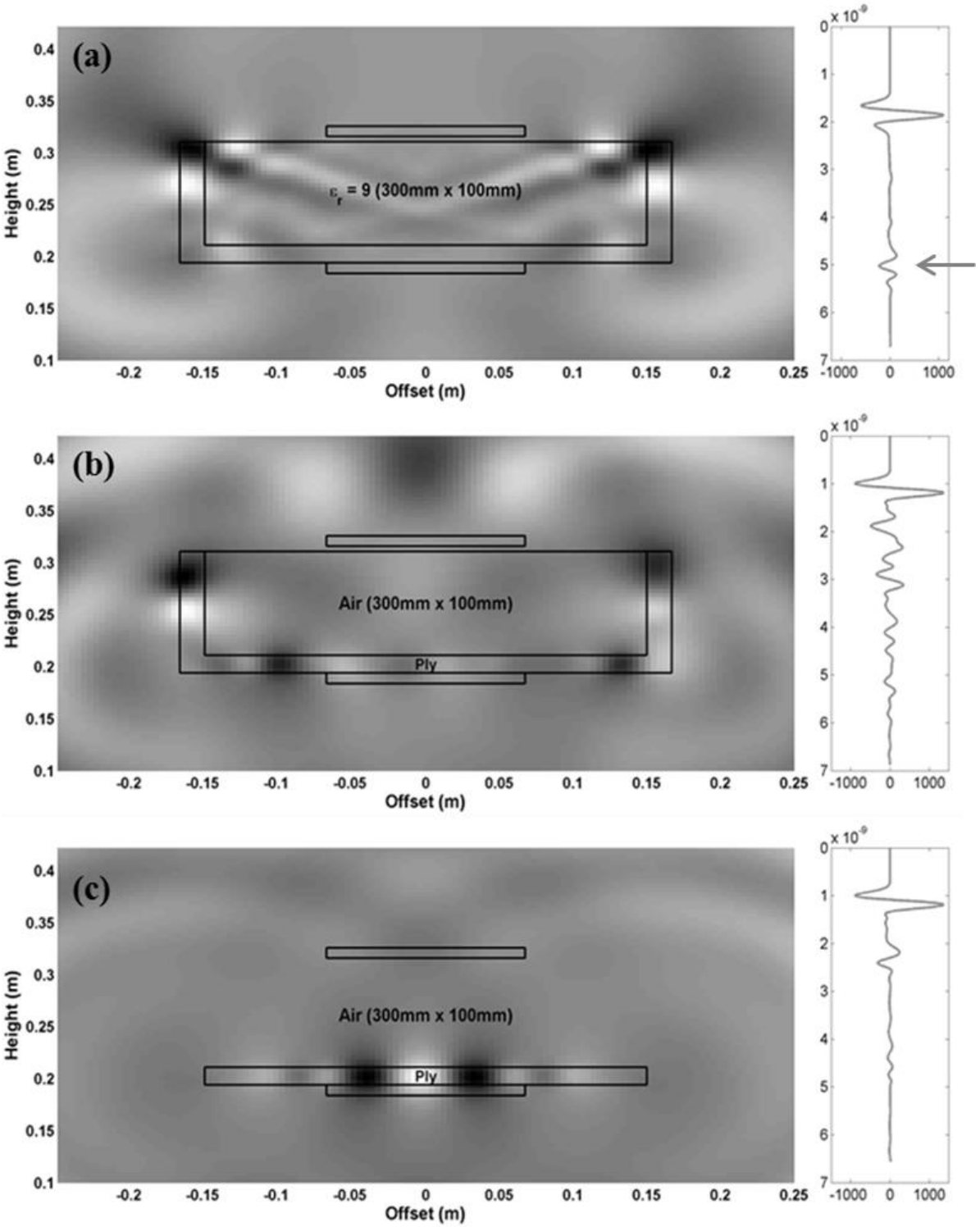

Fig. 1. Numerical model showing instantaneous electric-field strength (left) and transmitted signal strength measured by the receiving antenna (right): (a) Within a ply box with ε'_r = 9 sample material, (b) Within an empty ply box, and (c) With only a ply sheet present.

As the calculation of real permittivity depends on sample thickness, slight variations in the depth of prepared samples will affect the results. Using thicker samples would reduce the relative effect of such variations, however maintaining the 3 : 1 sample aspect ratio would significantly increase the mass, making manual handling impractical. To understand the consequences on the VNA measurements of using deeper sample boxes with an altered aspect ratio, 2D FDTD modelling was undertaken for boxes of internal dimensions 170 x 250 x 250 mm. This change corresponds to a slight increase in mass from approximately 23 kg to 26 kg. However, as observed in Fig. 2 a disadvantage of the change is that the side reflections arrive much closer in time and begin to impinge on the arrival of the direct wave signal, as indicated with an arrow.

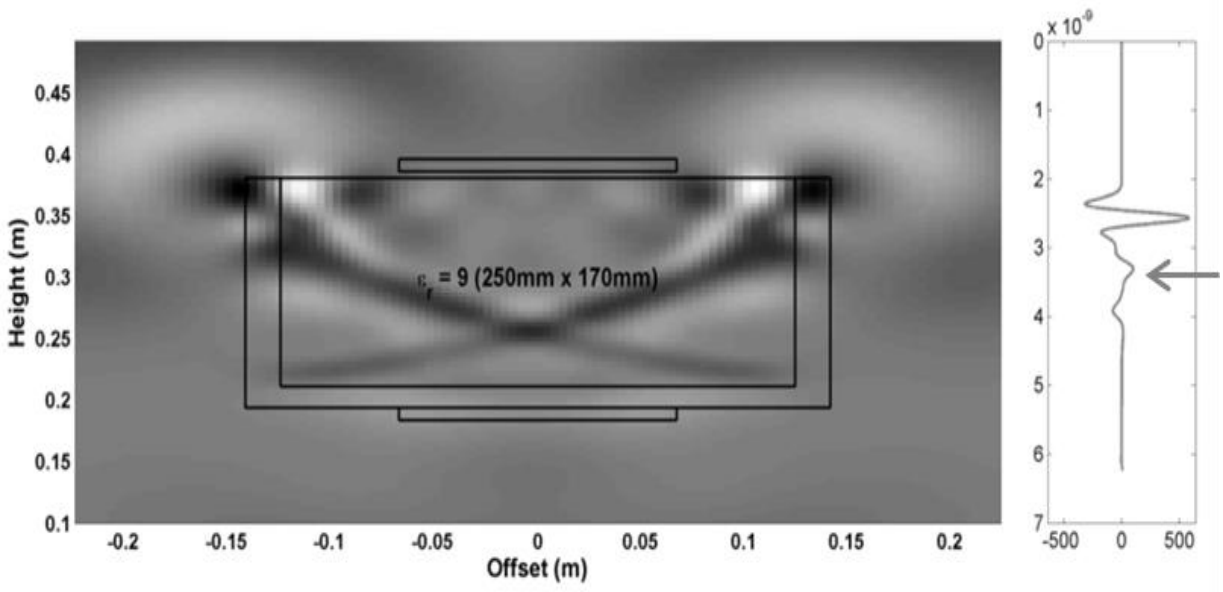

Fig. 2: 2D FDTD numerical modelling of a 170 x 250 mm sample box filled with a ε'_r = 9 UBG material.

3.2 Investigation of near-field effects

Eqn. 1 assumes plane waves. These occur in the far-field region of the antenna (Millard et al., 2002). There are different methods of estimating the distance to the transition between near-field and far-field regions, including those described by Johnson et al. (1973) and Millard et al. (2002). Numerical modelling indicates that this transition may in fact be much further away than predicted by conventional methods of estimating the distance to the far-field region (Diamanti and Annan, 2013). However the boundaries between the near-field and far-field regions are not well defined and the suitability of the means of estimation depends on the intended application (Johnson et al., 1973). Using any of these estimation methods, it is

unlikely that far-field conditions are being unambiguously met using the current MFS test configuration. Previous investigations, however, produced permittivity estimates that match relatively well with measurements using other techniques (Muller et al., 2012; Muller and Dérobert, 2013; Muller et al., 2015), indicating the influence of near-field effects may be relatively limited for the test configurations used to date. To further investigate and better understand the influence of these effects on the MFS measurements, a series of experiments was undertaken.

Experiment 1

The first experiment was a simple test to determine the linearity of phase measurements in air using the MFS antennas. The experiment involved collecting VNA S_{21} phase measurements while separating the antennas in 100 mm increments from zero to one metre apart. The phase-shift between a reference measurement at zero offset and each subsequent antenna position was used to calculate the real permittivity of air ($\varepsilon'_r \approx 1$) using Eqn. 4, a modification of Eqn. 1 that accounts for the varying antenna separation. The real permittivity values were then recalculated taking the measurements at 100 mm, 200 mm and 300 mm as the reference. The calculated values are shown in Fig. 3. While care was taken during the measurements, the results can only be considered approximate as the antennas were manually separated and the offset was determined using a simple tape measure.

$$\varepsilon'_r \approx \left(\frac{\Delta\Phi\lambda_0}{360d} \right)^2 \qquad (4)$$

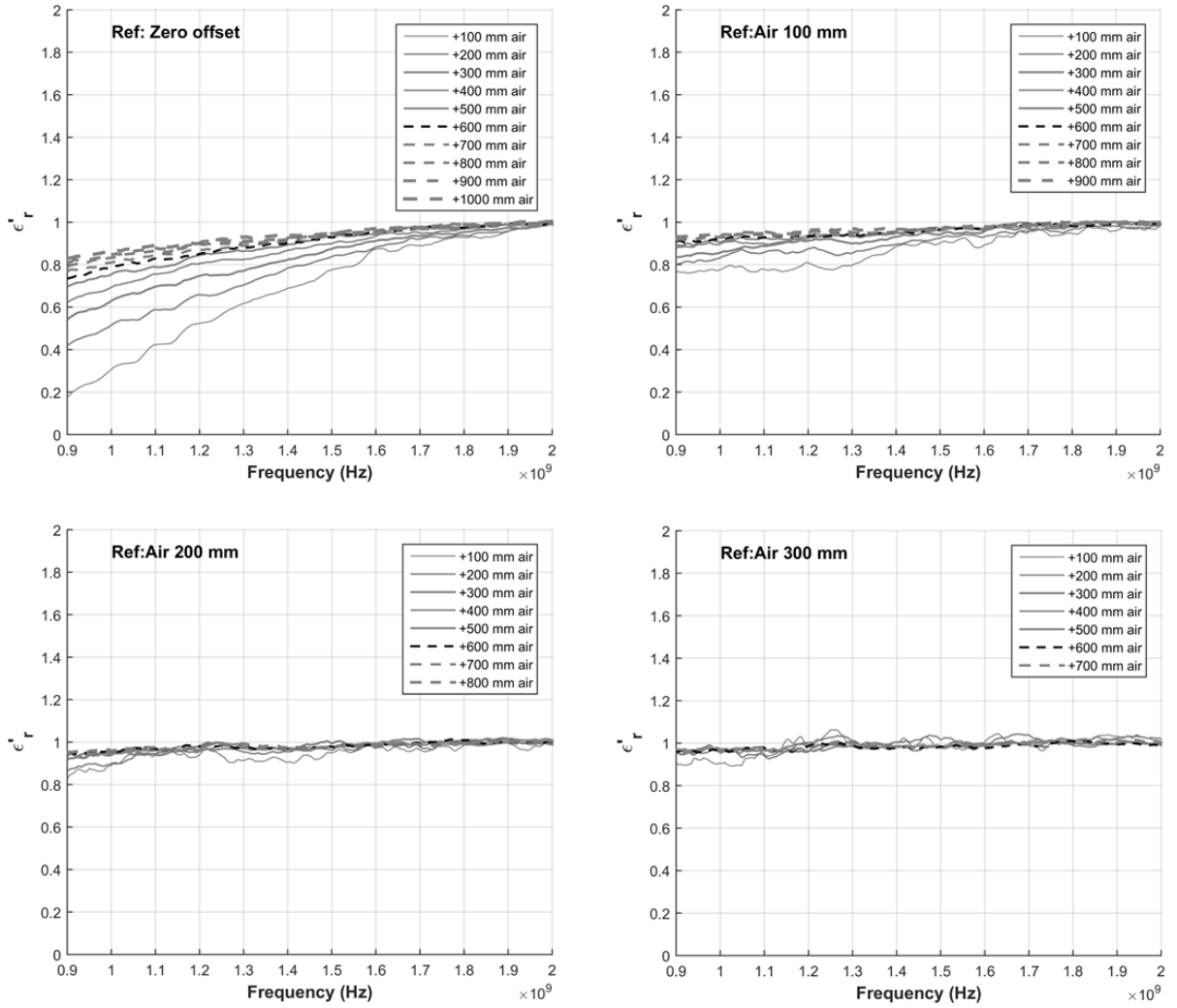

Fig. 3: Real permittivity calculated for air using different antenna reference offsets.

The results in Fig. 3 indicate there is a significant error in the real permittivity calculation using the zero spacing measurement as the reference, most likely due to the influence of near-field effects. These errors decrease when measurements at 100 mm and 200 mm were used as the reference, however there was little difference when increasing from 200 mm to 300 mm. This indicates the phase-change with increasing distance is relatively linear at 200 mm, though may be acceptable at some point between 100 mm and 200 mm. However, as sample boxes of size 300 x 300 x 100 mm already weigh more than 23 kg when filled with compacted UBG materials, maintaining the same 3 : 1 aspect ratio while increasing the depth to 200 mm would make manual handling impossible (~187 kg).

Experiment 2

The next experiment involved initially fixing the pair of antennas at an offset of 125 mm. A reference transmission (S_{21}) measurement was then collected through a 400 x 400 x 18 mm ply sheet placed on top of the lower receiving antenna. As shown in Fig. 4, a series of 350 x 350 mm nylon sheets were then incrementally placed on top of the ply sheet and between the antennas. After each sheet was added the phase of the transmitted signal passing between the antennas was measured and the phase-shift relative to the initial calibration was determined. The antenna spacing was then increased to 190 mm and an updated reference measurement was collected through the ply sheet. Nylon sheets 170 mm thick were then placed on top of the ply sheet. The phase measurement of the transmitted signal was collected and the phase-shift was determined compared to the updated calibration measurement. The real permittivity was then determined for each sample thickness and antenna separation, without time-domain windowing (Fig. 5). The results were then compared to an independent measurement of one of the nylon sheets using the dielectric probe described by Wagner et al. (2014) and an Agilent E5061B-3L5 network analyser.

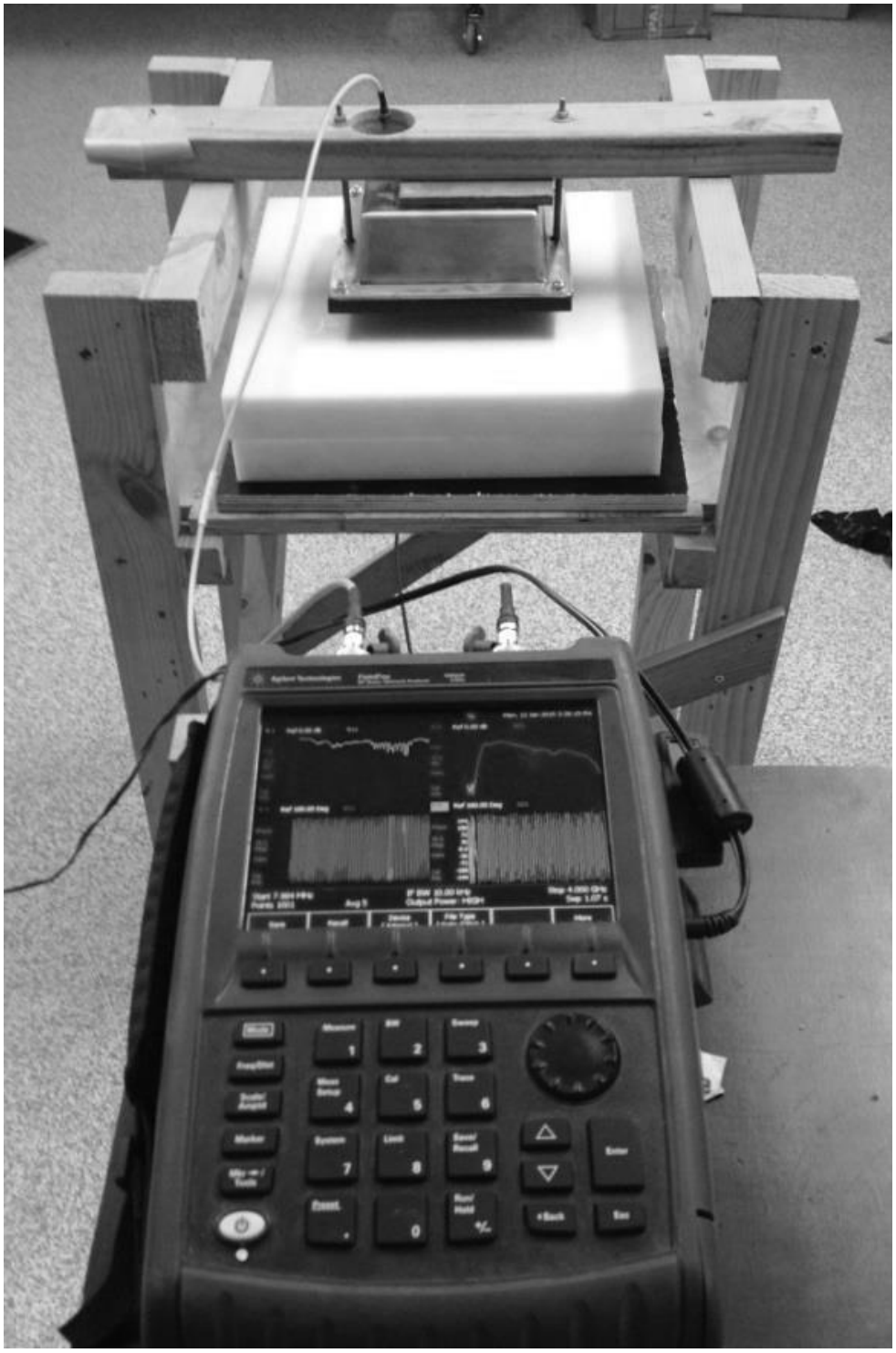

Fig. 4: VNA measurements with fixed antenna separation through samples of nylon and a ply sheet.

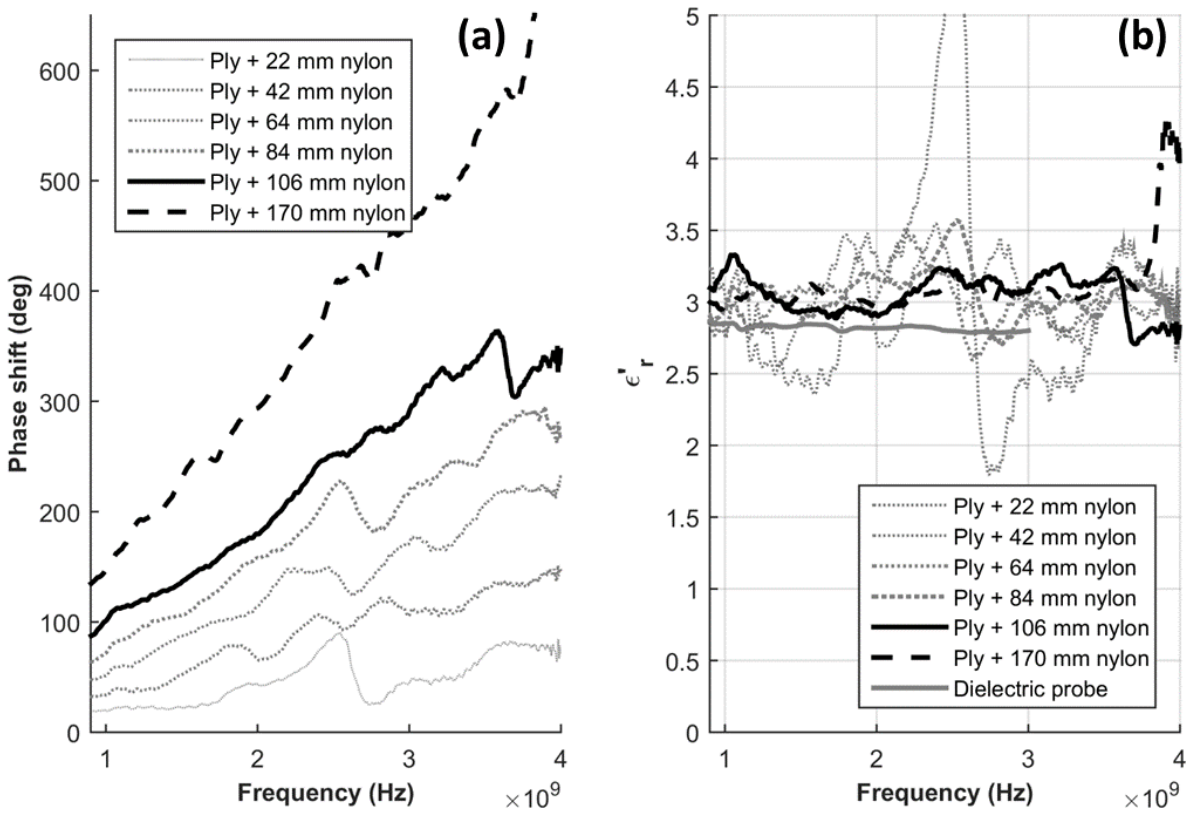

Fig. 5: Effect of increasing the thickness of nylon on (a) phase-shift linearity and (b) real permittivity calculations.

As shown in Fig. 5, the phase-shift linearity and consistency of real permittivity predictions improve with increasing sample thickness. When the sample thickness has reached 106 mm the measurements are becoming relatively consistent over the range 1.2 to 3.5 GHz and are similar to the measurement through the 170 mm thick nylon sample. These results, which averaged ε'_r = 3.00 for the 106 mm thick nylon sample and 3.04 for the 170 mm sample over the frequency range 900 MHz to 3.5 GHz compare relatively well with the dielectric probe results which reported a flat response that averaged ε'_r = 2.82 and ε''_r = 0.07 over the range 900 MHz to 3.0 GHz. This corresponds to a difference of 6 to 8% between the methods; but the probe produced more consistent results over this range. Another aspect to note in the MFS data is the spike in the phase plots and corresponding real permittivity results at around 2.6 – 2.8 GHz. This feature corresponds to the first frequency null of the antenna, clearly visible in the S_{21} amplitude results. Consequently, for these antennas it is recommended to limit the measurement frequency range to between 900 MHz to 2 GHz to avoid potential phase measurement errors in the vicinity of the null.

Experiment 3

One issue with this experiment is that because the antennas were fixed while the sample thickness was increased the antenna coupling will have varied. The approach also introduces a notable asymmetry in the measurement setup. When measuring UBG samples a small asymmetry is also present due to the floor of the sample box. To investigate these effects, an experiment was undertaken that again measured the phase-shift through an increasing thickness of nylon sheets, but this time the upper antenna was moved to maintain consistent sample coupling and a symmetric test configuration. The upper antenna was fixed at a separation that enabled the nylon to be inserted with a small gap of approximately 5 mm. Prior to inserting the nylon a reference measurement was collected. The nylon was then slid in between the antennas and a second measurement was made. The antenna separation was increased to accommodate the next thickness of nylon and the measurements were repeated. This process continued until a total nylon thickness of 170 mm was measured. In the next part of the experiment the measurements were repeated, but this time the ply sheet used in the previous experiment was inserted for each reference measurement and was placed under the nylon sheets for each sample measurement. Real permittivity values calculated over the frequency range 900 MHz to 2.0 GHz using these measurements are shown in Fig. 6.

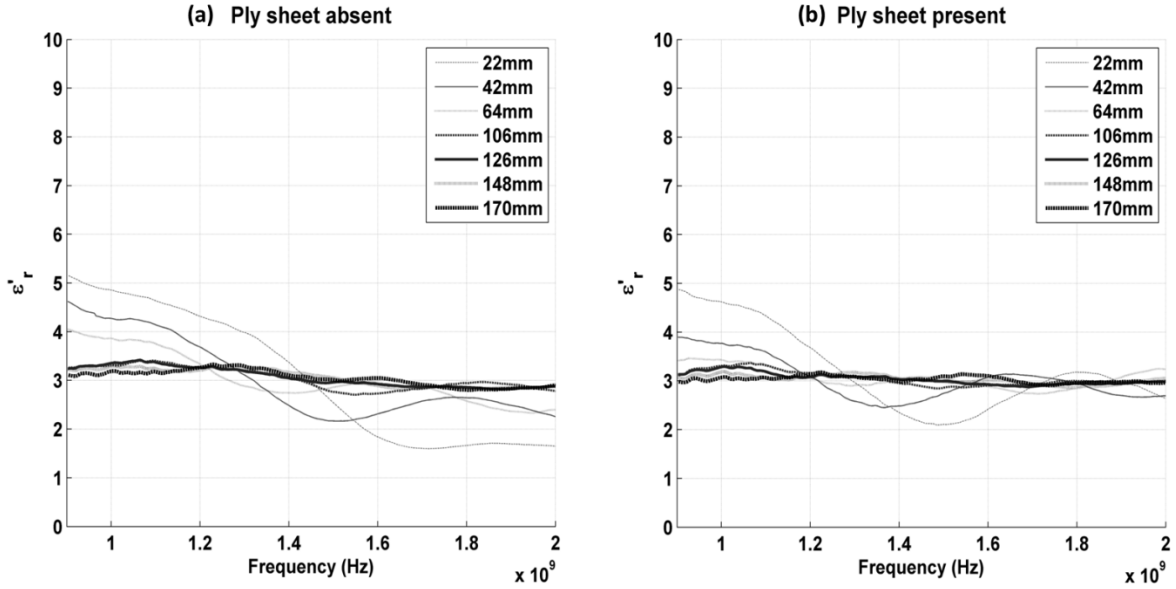

Fig. 6: Real permittivity measured for an increasing thickness of nylon sheets (a) using a symmetric test configuration; and (b) the same measurements including a ply sheet placed against the lower antenna.

As observed in Fig. 6 (a), the stability of measurements over this frequency range improves with the increasing sample thickness. When the sample thickness has reached 106 mm is it is relatively stable and consistent with measurements of thicker samples. Comparing Fig 6 (a) and Fig 6 (b), for samples 106 mm thick and greater the ply sheet appears to have only a small effect on the calculated permittivity values.

Experiment 4

In the final experiment, permittivity measurements were undertaken using two different thicknesses of nylon, distilled water (via reverse osmosis) and tap water. Both the distilled and tap water samples were at a temperature of 21.3 °C at the time of testing and were poured into the plywood sample boxes normally used for UBG materials (Fig. 7). The sample boxes used for the water measurements had internal dimension of 300 x 300 x 100 mm and 250 x 250 x 170 mm. The corners of the ply boxes were sealed with silicone to prevent leakage. S_{21} measurements were first collected through a ply sheet, 106mm of nylon placed on the ply sheet and the 100 mm sample box filled to the top with water. These initial measurements were collected with a fixed antenna separation of 125 mm. The antenna separation was then increased to 190 mm and the measurements were repeated through the ply sheet, 170 mm of nylon placed on the ply sheet and 170 mm of distilled and tap water placed in the deeper sample box. For each of these measurements the samples was aligned centrally with the antennas and the lower antenna was mounted flush with the surface on which the ply sheet or sample boxes was placed. The upper antenna was aligned with the lower antenna and fixed to achieve the smallest possible air gap above the surface the nylon and water. As a result the measurements included a small asymmetry due to the presence of the ply sheet or base of the sample box. Equivalent time domain signals passing through these samples were later determined from the VNA measurements of amplitude and phase (Fig. 8).

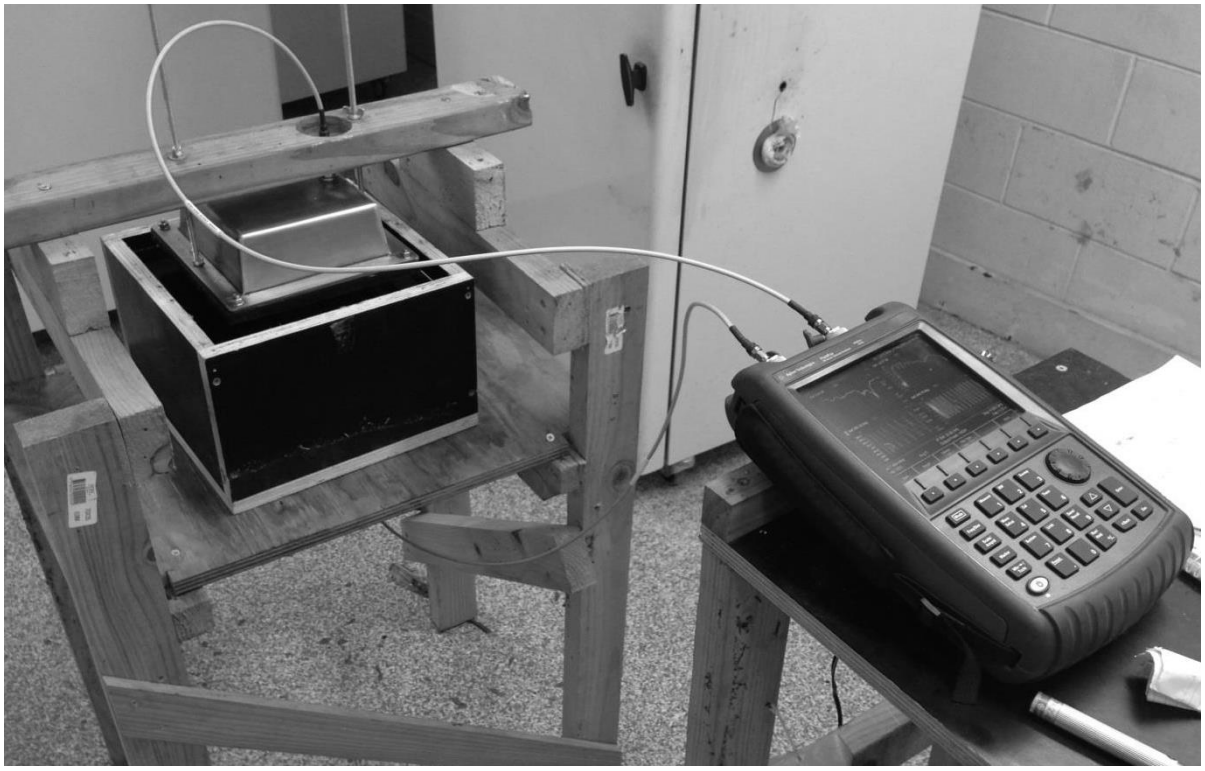

Fig. 7: MFS test configuration used for measuring a 170 mm deep sample of distilled water shown prior to complete filling of the sample box.

The permittivity values determined during this experiment are show in Fig. 9, with measurements undertaken at 125 mm and 190 mm shown as solid and dashed lines, respectively. Time domain windowing has not been applied to these data. The results reveal only a small (1%) difference in the mean permittivity measurement of nylon and water for the different combinations of sample thickness and antenna spacing. A notable oscillation is seen within the 100 mm distilled water permittivity results over the range 900 MHz – 1.5 GHz. A corresponding oscillation is also noted below approximately 1.5 GHz in the amplitude spectrum of the 100 mm distilled water S_{21} measurements, as indicated with the angled arrow in Fig. 8 (b). A similar effect is also seen in the amplitude spectrum of the 170 mm water measurement, though any influence on phase and consequently the permittivity result in Fig. 8, appears minimal. This oscillation may be due to a low frequency resonance within the water sample, as the significant dielectric contrast at the water-plywood and water-air boundaries results in strong reflections. An indication of this is the relative strength of the double bounce of the transmitted signal, the location of which is indicated with a vertical arrow in Fig. 8 (a). The asymmetry of the test setup may also have contributed to the oscillation, however this is

unlikely as the effect was not observed in either the air or nylon measurements which also included a ply sheet.

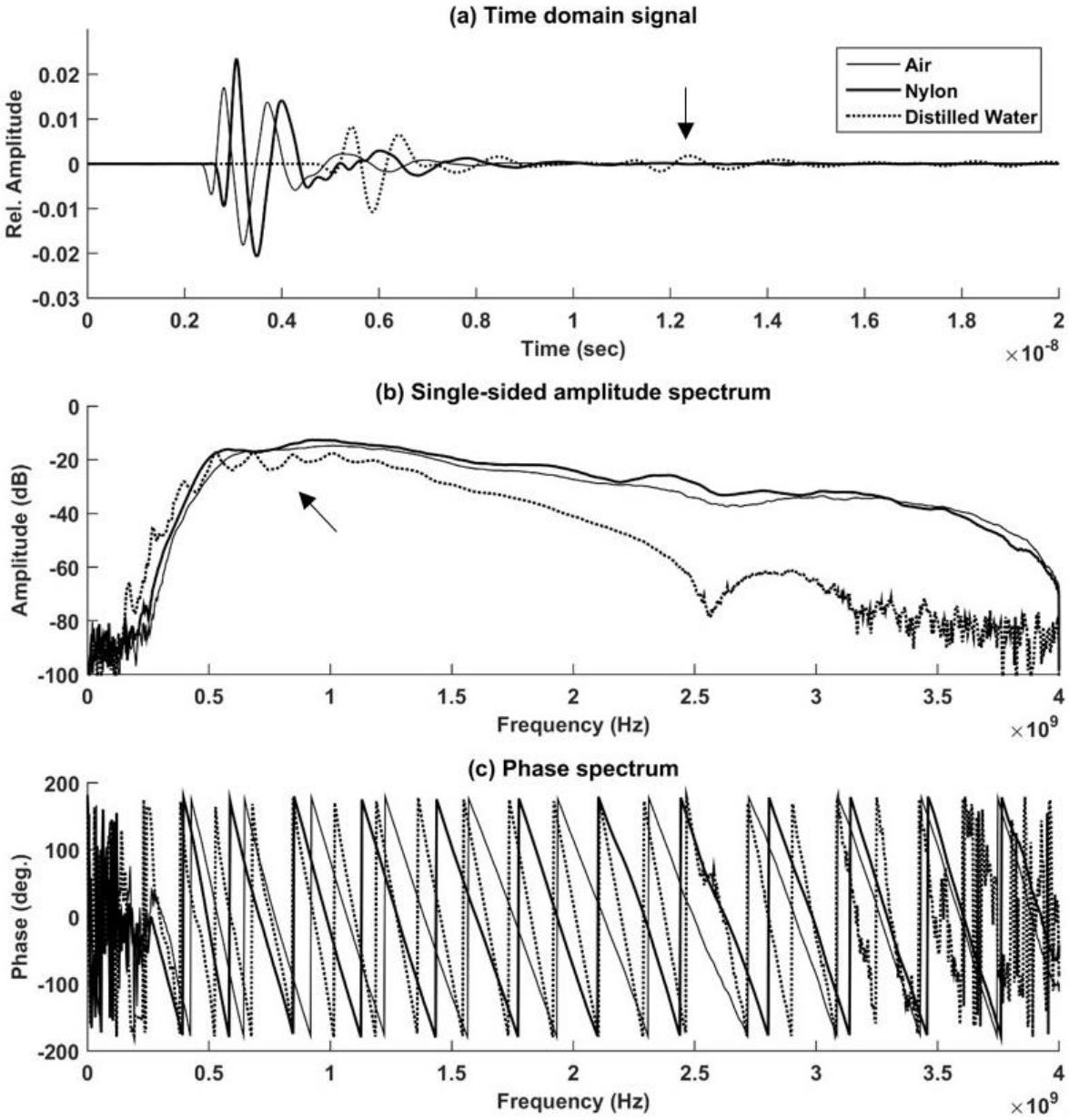

Fig. 8: (a) The time domain signal determined from VNA S_{21} transmission measurements; (b) VNA amplitude measurement; and (c) VNA phase measurement. These measurements were collected through the ply sheet (labelled 'air'), 106 mm of nylon with the ply sheet and a 100 mm depth of distilled water in a 300 x 300 x 100 mm sample box.

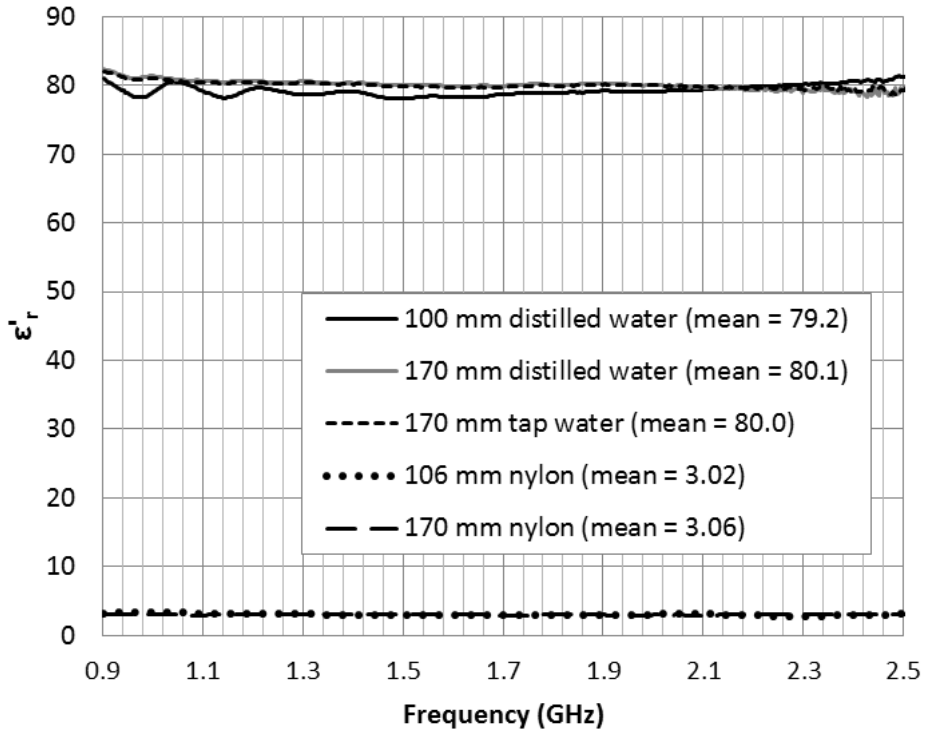

Fig. 9: Real permittivity determined using the MFS approach for nylon and distilled and tap water using different antenna separations and sample thicknesses.

Despite this low frequency irregularity, the overall results for water permittivity are relatively consistent, with average real permittivity values measured through 100 mm and 170 mm sample thicknesses ranging between 79.2 and 80.1. These are within 1% of the value of 79.8 for water at 1.0 GHz interpolated to 21.3 °C based on Buchner et al. (1999). As the permittivity of nylon and water are beyond the expected upper and lower bounds for UBG pavement materials, which are typically in the range 5 – 15, the results indicate that near-field effects are unlikely to have significantly affected the accuracy of real permittivity measurements for the size of samples used to date. As observed in the calculation of permittivity for water, it may be advantageous to use a sample thickness greater than 100 mm to reduce the effect of any unwanted oscillations occurring within the sample or test apparatus. The experiment separating antennas in air indicated that an antenna offset of 100 mm was insufficient as a reliable reference. As the antenna separation used for measuring the 100 mm samples was only 125 mm, it would be preferable to increase this spacing to increase confidence in the validity of the reference phase measurement. Furthermore, the permittivity measurements for water using 170 mm deep sample boxes and the varied aspect ratio produced more consistent results than the 100 mm deep samples, despite the concerns raised from the FDTD modelling that side

reflections may affect the measurements. The influence of side reflections would also have been reduced by narrowing of the antenna beam pattern due to the high permittivity of the water sample.

4.0 CONCLUSIONS

This paper provides an overview of recent studies aimed at optimising and investigating the influence of near-field effects on the MFS permittivity characterisation approach. The work included FDTD modelling to assist understanding of the nature of wave propagation within the test apparatus. This revealed that a sample aspect ratio of approximately 3:1 (width : depth) was preferable to maximise separation of the direct signal from unwanted reflections from the sides of the sample box and the double bounce from the top of the sample. The modelling also revealed it was best to collect the reference signal through a ply sheet rather than an empty box, as spurious reflections from the box sides complicated the reference measurement.

The influence of near-field effects on the measurements was investigated in four experiments. The first indicated that a minimum antenna spacing of between 100 mm and 200 mm in air was required to achieve a linear-phase reference measurement using the custom antennas. The second showed the consistency of permittivity results for nylon improved with increasing sample thickness, though there was little improvement for samples thicker than 106 mm. The third investigated the influence of sample thickness and symmetry of the test configuration, finding the measurements were relatively stable for samples of 106 mm or greater and that the presence of the ply sheet had little effect on permittivity results calculated for these thicker samples. In the final experiment measurements of samples of nylon, distilled water and tap water approximately 100 mm and 170 mm thick were compared, revealing similar results. The average real relative permittivity result for nylon over the frequency range 900 MHz – 3.5 GHz was within 6-8% of an independent measurement using a broadband dielectric probe over the range 900 MHz – 3.0 GHz. The result for distilled water also agreed well with the literature (within 1%), though a notable oscillation was observed most likely due to internal reflections within the sample.

As the samples of nylon and water are beyond the likely upper and lower bounds of permittivity for UBG pavement materials, the investigation indicates measurements through a sample thickness of at least 100 mm using the current MFS apparatus are unlikely to be significantly affected by near-field effects. However, despite concerns raised from FDTD modelling, it appears that the deeper 170 x 250 x 250 mm sample boxes may be preferable to enable greater

antenna separation and achieve more consistent and accurate permittivity measurements. Furthermore, narrowing of the antenna beam pattern due to coupling with the material sample, particularly for high permittivity materials, may help improve the results by reducing the strength of reflections from the sample edges.

5.0 ACKNOWLEDGEMENTS

This work was funded under NACOE research project P12 'Field-validation of Noise Modulated Ground Penetrating Radar' by the Queensland Department of Transport and Main Roads. The authors express their sincere thanks to Dr Bryan Reeves for assistance during this work and also to Moritz Schwing and Zhen Chen from UQ for undertaking the independent nylon permittivity measurements. This contribution supports the work of COST Action TU1208 'Civil Engineering applications of Ground Penetrating Radar'. The presented research is supported by a Queensland Science Fellowship awarded to A. Scheuermann.

6.0 REFERENCES

BUCHNER, R., BARTHEL, J. & STAUBER, J. 1999. The dielectric relaxation of water between 0° C and 35° C. *Chemical Physics Letters,* 306**,** 57-63.

BÜYÜKÖZTÜRK, O., YU, T. & ORTEGA, J. 2006. A methodology for determining complex permittivity of construction materials based on transmission-only coherent, wide-bandwidth free-space measurements. *Cement and Concrete Composites,* 28**,** 349-359.

CHEN, L. F., ONG, C. K., NEO, C. P., VARADAN, V. V. & VARADAN, V. K. 2004. *Microwave electronics: Measurement and materials characterization,* John Wiley & Sons, Ltd., Chichester, West Sussex, England.

DIAMANTI, N. & ANNAN, A. P. 2013. Characterizing the energy distribution around GPR antennas. *Journal of Applied Geophysics,* 99**,** 83-90.

GIANNOPOULOS, A. 2005. Modelling ground penetrating radar by GPRMax. *Construction and Building Materials,* 19**,** 755-762.

JAMIL, M., HASSAN, M. K., AL-MATTARNEH, H. M. A. & ZAIN, M. F. M. 2013. Concrete dielectric properties investigation using microwave nondestructive techniques. *Materials and Structures,* 46**,** 77-87.

JOHNSON, R. C., ECKER, H. A. & HOLLIS, J. S. 1973. Determination of far-field antenna patterns from near-field measurements. *Proceedings of the IEEE,* 61**,** 1668-1694.

KAATZE, U. & HÜBNER, C. 2010. Electromagnetic techniques for moisture content determination of materials. *Measurement Science and Technology,* 21**,** 1-26.

KONG, F. N., BHASIN, R. K., WANG, L. Z. & ZHANG, Y. G. Development of handheld GPR using FieldFox network analyzer and its application in detecting structure of Qian Tang river Dike, Hang Zhou, China. 14th International Conference on Ground Penetrating Radar (GPR-2012), 4-8 June 2012 Shanghai, China. IEEE, 146-151.

MILLARD, S. G., SHAARI, A. & BUNGEY, J. H. 2002. Field pattern characteristics of GPR antennas. *NDT & E International,* 35**,** 473-482.

MULLER, W. Self-correcting pavement layer depth estimates using 3D multi-offset ground penetrating radar (GPR). 15th International Conference on Ground Penetrating Radar (GPR-2014), June 30 - July 4 2014 Brussels, Belgium. IEEE, 887-892.

MULLER, W. & DÉROBERT, X. A comparison of phase-shift and one-port coaxial cell permittivity measurements for GPR applications. 7th International workshop on advanced ground penetrating radar (IWAGPR-2013), 2-5 July 2013, 1-6.

MULLER, W. B., BHUYAN, H. & SCHEUERMANN, A. 2015. A comparison of modified free-space (MFS), GPR and TDR techniques for permittivity characterisation of unbound granular pavement materials. *In:* WIGGENHAUSER, H. (ed.) International Symposium Non-Destructive Testing in Civil Engineering (NDT-CE), 15-17 September 2015 Berlin, Germany, BAM/TU Berlin, 421-424.

MULLER, W. B., SCHEUERMANN, A. & REEVES, B. Quantitative moisture measurement of road pavements using 3D GPR. 14th International Conference on Ground Penetrating Radar (GPR-2012), 2012 Shanghai, China. IEEE, 517-523.

PANZNER, B., JOSTINGMEIER, A. & ABBAS, O. 2010. Estimation of soil electromagnetic parameters using frequency domain techniques. 13th International Conference on Ground Penetrating Radar (GPR-2010), 2010 Lecce, Italy: IEEE.

PELLINEN, T., HUUSKONEN-SNICKER, E., ESKELINEN, P. & OLMOS MARTINEZ, P. 2015. Representative volume element of asphalt pavement for electromagnetic measurements. *Journal of Traffic and Transportation Engineering (English Edition),* 2**,** 30-39.

TRABELSI, S., KRASZEWSKI, A. W. & NELSON, S. O. 2000. Phase-shift ambiguity in microwave dielectric properties measurements. *IEEE Transactions on Instrumentation and Measurement,* 49**,** 56-60.

WAGNER, N., SCHWING, M. & SCHEUERMANN, A. 2014. Numerical 3-D FEM and experimental analysis of the open-ended coaxial line technique for microwave dielectric spectroscopy on soil. *IEEE Transactions on Geoscience and Remote Sensing,* 52**,** 880-893.

Paper V

Muller, W.B., Permittivity characterisation of unbound granular pavement materials using a modified free-space approach. Transportation Research Record: Journal of the Transportation Research Board, 2578, 93–101, Washington, D.C., 2016.

This page left intentionally blank

Permittivity characterisation of unbound granular pavement materials using a modified free-space approach

Wayne Muller[1, 2, 3]

1. Department of Transport and Main Roads, Herston, Australia
Tel: +61732603510; Fax: +61738624699; Email: wayne.b.muller@tmr.qld.gov.au
2. School of Civil Engineering, The University of Queensland, St. Lucia, Australia
3. ARRB Group Ltd, 123 Sandgate Road, Albion, Australia

Abstract— Moisture has a considerable influence on the structural performance of unbound granular (UBG) pavements. Multi-offset ground penetrating radar (GPR) has potential to quantify moisture within these materials by measuring the permittivity of pavement layers. To enable moisture estimates from these field measurements, relations between permittivity and volumetric moisture are required. This paper describes the use of a modified free-space (MFS) laboratory approach to measure the permittivity of compacted UBG material samples and to develop these relations. Material samples were compacted within form-ply boxes targeting a range of density and moisture conditions. A vector network analyser (VNA) was used to measure the phase shift between a fixed pair of ground-coupled dipole antennas due to sample insertion, compared to an initial ply sheet reference measurement. Frequency-dependent permittivity values for the samples were then determined over the range 1.0 to 2.0 GHz based on these measurements. Mean values over this range were then related to the volumetric moisture content of the samples. An indicative moisture-permittivity relation was proposed based on MFS measurements of samples from several quarries. Overall, the permittivity results using the MFS approach showed reasonably good agreement for samples at higher moisture contents compared to the literature relations based on time domain reflectometry (TDR). However, for drier samples, the MFS permittivity values were higher than the literature predictions. Possible reasons for these differences are discussed and an overview of the advantages and limitations of using the technique for characterising unbound granular materials is also given.

Keywords: Permittivity characterisation; ground penetrating radar; pavement moisture measurement; unbound granular pavements.

1 INTRODUCTION

Unbound granular (UBG) materials are widely used for road construction within Australia. The structural performance of these materials is highly moisture sensitive (1; 2). While construction and maintenance strategies aim to limit moisture ingress (3; 4), at times it is unavoidable – with water entering via surface cracking, poor adjacent drainage and other mechanisms. After heavy rain or flooding, it can be difficult to determine the location and extent to which moisture has entered and may be affecting the pavement. This in turn affects the ability of engineers to assess and manage these potentially vulnerable road assets and to determine the risk and optimum timing when allowing heavy vehicles back on the road. Thus, methods of measuring the amount and distribution of moisture within the pavement and its effect on the structural response are of interest.

Conventional moisture measurement approaches, for example, physical sampling or installed sensors such as time domain reflectometry (TDR) probes (5–7), provide only spot measures and therefore become impractical for detailed large-scale investigations. The falling weight deflectometer (FWD) has also been used to detect changes in structural response due to moisture changes (8), seasonal variations (9), and to detect flood damage (10); however, it is relatively slow for large-scale investigations. The traffic speed deflectometer (TSD) provides a much faster alternative, capable of collecting surface deflection results comparable to a FWD for flexible pavements (11). Annual large-scale TSD investigations are now undertaken within Queensland, New South Wales and New Zealand, providing a basis for monitoring changes in structural response over time. However, methods of quantifying the amount of moisture within pavement layers are required in combination to determine the relative influence of moisture on the structural response and to better understand moisture distribution and infiltration mechanisms.

2 BACKGROUND

2.1 MOISTURE MEASUREMENT USING GPR

Ground penetrating radar (GPR) provides an alternative approach to measuring moisture within soil and pavements (*12–15*). Multi-offset GPR is a subset of these techniques that involves emitting electromagnetic (EM) signals into the pavement and measuring the change in arrival times of the resulting groundwaves and reflections from layer interfaces at varying antenna offsets. The GPR antennas are typically arranged in either a common midpoint (CMP) or wide angle reflection and refraction (WARR) configuration. These can be implemented at highway speeds by using different antenna pairings within a three-dimensional (3D) GPR array. Geophysical methods can then be used to determine the velocity of EM waves within individual pavement layers from the measured multi-offset response (*16*). From the wave velocity, the relative permittivity (ε_r) of the soil or pavement material can be calculated, which in turn is strongly influenced by the volumetric moisture content (*12; 17*). Moisture-permittivity relations such as the one for soil by Topp et al. (*18*), variants tailored to UBG materials (*19; 20*), or volumetric mixing models such as CRIM (*21*) can then be used to estimate the corresponding in situ volumetric moisture content.

While relative permittivity, also called the 'dielectric constant', is often simplified as a real number, it is more generally a complex and frequency-dependent parameter. The real (ε'_r) and imaginary (ε''_r) components of permittivity are related to the phase velocity (v) of propagating EM waves via:

$$v = \frac{c}{\sqrt{\varepsilon'_r \mu_r \frac{1+\sqrt{1+\tan^2\delta}}{2}}} \quad (1)$$

where

$\tan \delta = \varepsilon''_r / \varepsilon'_r$;

c = velocity of light in a vacuum; and

μ_r = relative magnetic permeability.

Here permittivity and permeability are reported relative to the intrinsic values of free-space, and thus are dimensionless ratios. In practical terms, the real component of permittivity is a measure of energy storage within the material in the form of charge polarisation, whereas the imaginary component is a measure of energy loss (*22*). In most practical cases for roads, the materials being investigated are non-magnetic ($\mu_r = 1$) and low loss ($\varepsilon'_r >> \varepsilon''_r$), enabling the imaginary component to be ignored in the estimation of phase velocity, resulting in the simplified relation:

$$v \approx \frac{c}{\sqrt{\varepsilon'_r}} \tag{2}$$

While many researchers have applied multi-offset techniques for soil moisture quantification, for example (*12; 23–24*), only a few have applied these techniques for moisture measurement for roads (*25*). However, several have used these techniques for mapping asphalt density variations (*26*) and for pavement thickness applications (*27–29*). Recent research within Australia aims to apply these techniques to a new type of 3D noise-modulated GPR (NM-GPR) (*30*). An advantage of this equipment is the ability to collect multi-offset datasets across the road lane while travelling at highway speeds. To prepare for this new equipment, self-correcting algorithms were developed using simulations of the expected multi-offset NM-GPR response to automatically determine pavement layer depths and permittivity values (*31–32*). The NM-GPR equipment has since been completed with preliminary field comparisons undertaken alongside the TSD, demonstrating the benefits of using these methods in combination for road investigations (*33*). Field testing of the multi-offset capabilities of the NM-GPR equipment and adaptation of the analysis algorithms to real field data has also commenced. Refinement of these techniques is continuing with the aim of field validating layer depth and moisture predictions in the near future.

3 METHODOLOGY

3.1 MODIFIED FREE-SPACE (MFS) APPROACH

To enable field estimates of moisture from multi-offset NM-GPR measurements of EM wave velocity and pavement layer permittivity, moisture-permittivity relations for these materials are required. These can be determined in the laboratory by characterising the permittivity of samples prepared to field conditions at a range of moisture contents. As permittivity is frequency-dependent, it is preferable to characterise over the same frequency range as the NM-GPR. Furthermore, as UBG materials are a conglomerate of aggregates, water and air, the sample should be sufficiently large to enable representative measurements and be compacted to mimic field density conditions.

Due to limitations with existing methods, an alternative characterisation approach using a modified free-space (MFS) technique was previously investigated (*31*), validated (*34*) and further optimised (*35*). The approach involves measuring the magnitude and phase of sinusoidal EM signals passing between a fixed pair of antennas conducted initially without, and then later with, a sample of known thickness placed in between. As these signals usually attenuate and also slow within the material sample compared to the initial measurement with the sample absent, a relative change in the magnitude and phase of the transmitted signal occurs. Assuming far-field conditions and plane waves, the real (ε'_r) component of relative permittivity can be determined from the measured phase change via (*36*):

$$\varepsilon'_r \approx \left(1+\frac{\Delta\Phi\lambda_0}{360d}\right)^2 \quad (3)$$

where

λ_0 = free-space wavelength for a given frequency;

$\Delta\Phi$ = measured phase shift (degrees); and

d = material thickness.

These measurements can be collected over a wide range of frequencies using a vector network analyser (VNA). The MFS approach uses a portable VNA connected to relatively simple and compact shielded ground-coupled bow tie antennas, similar to those used in the NM-GPR system. As the antennas limit the operational bandwidth of both devices, the MFS measurements occur over the same frequency range as the NM-GPR. Sample edges, thickness, aspect ratio, antenna spacing and other aspects can also influence the results and have previously been investigated and optimised (*34*–*35*). The antennas are vertically aligned to measure through a boxed material sample. To remove the influence of the floor of the sample box, the initial reference measurement is collected through a ply sheet, representing the base of the box. A ply sheet is used instead of an empty box to avoid reflections from the sides of the box (*35*). Figure 1 illustrates the antenna arrangement during ply sheet calibration and sample measurement, and also shows an image of the VNA connected to the antennas during measurement of a boxed material sample.

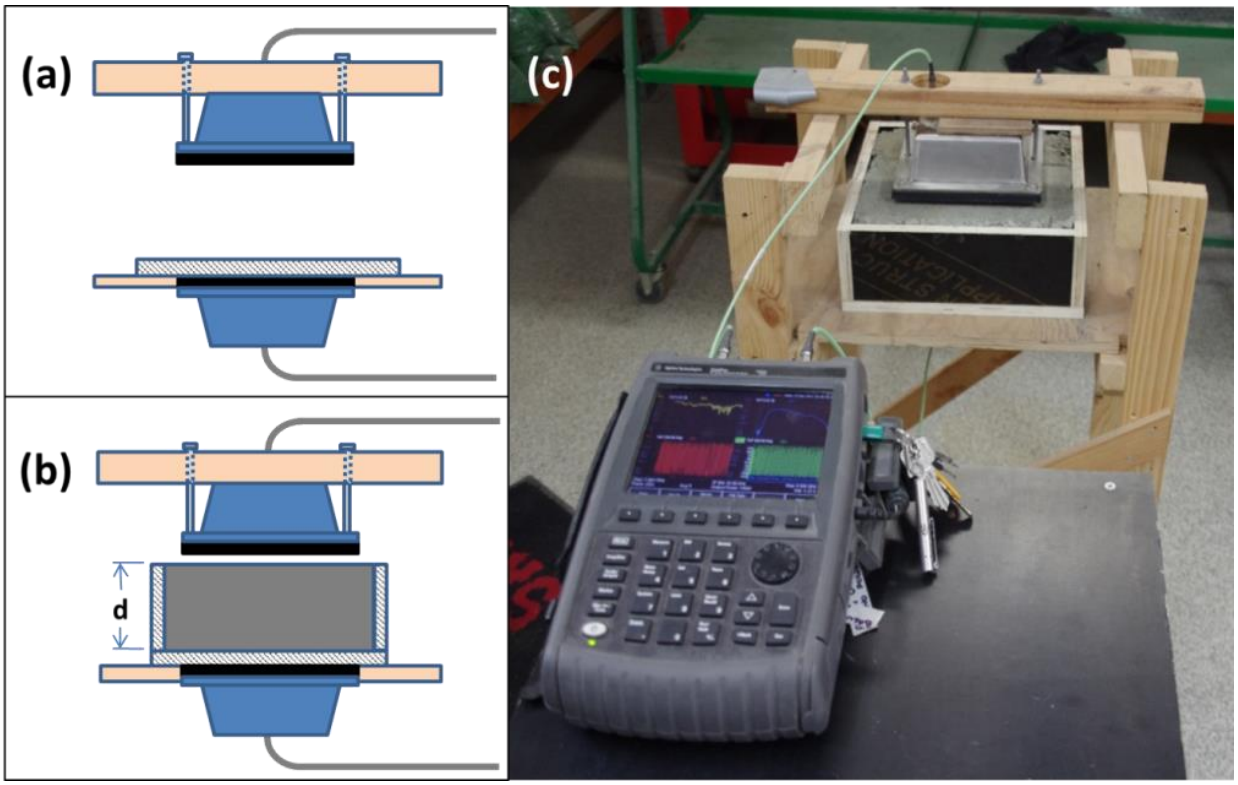

Figure 1: Illustrations of the MFS antenna configuration: (a) during ply sheet calibration, (b) during UBG sample characterisation; and (c) an image of the test apparatus

3.2 MATERIAL DETAILS AND PREPARATION

Samples of typical Type 2.1 UBG base course materials were obtained from four South East Queensland quarries. A summary of conventional laboratory test results for these materials and their particle size distributions are given in Table 1.

TABLE 1: UBG material details

Name	Quarry 1	Quarry 2	Quarry 3	Quarry 4
Material type	Meta-greywacke	Basalt	Metamorphosed basalt (Greenstone)	Metamorphic (Hornfels)
Moisture-density relations				
OMC (%)	7.9	7.2	6.9	7.9
MDD (t/m^3)	2.174	2.173	2.442	2.211
APD (t/m^3)	2.688	2.853	2.987	2.698
Atterberg limits				
LS (%)	2.6	1.8	2.2	5.0
LL (%)	19.2	20	19.6	22.6
PI (%)	2.6	1.8	3.6	5.0
WPI (%)	53	25	63	94
WLS (%)	53	25	39	94
Particle size distribution (% passing, by mass)				
26.5 mm	100	100	100	100
19 mm	96	97	98	99
9.5 mm	73	74	68	76
4.75 mm	58	58	54	64
2.36 mm	44	42	41	50
425 µm	20	14	18	19
75 µm	8.7	7	9	9.4

Note: OMC = optimum moisture content; MDD = maximum dry density to Q142; APD = apparent particle density to Q109; LS = linear shrinkage to Q106; LL= liquid limit to Q104D, PI = plasticity index; WPI = weighted plasticity index; WLS = weighted linear shrinkage, and particle size distribution of aggregate to Q103B. All testing is in accordance with the TMR Materials Testing Manual (*37*).

Samples from Quarries 1–3 were collected from leftover material from recent Department of Transport and Main Roads (TMR) projects. The material from Quarry 4 was sampled from a current construction project. The delivered bulk material was first fractionated sieved to determine the particle size distribution, and then proportionally recombined to achieve samples large enough to fill the sample boxes. Each sample was then mixed with sufficient water to reach its target moisture content and left overnight in sealed plastic containers. The following day the samples were removed from the containers and the moisture content of each sample was determined. Each sample was then compacted within a form-ply box for testing. For rounds 1 to 5, ply boxes with internal dimensions of 100 x 300 x 300 mm were used. For the sixth round of testing, deeper boxes with internal dimensions of 170 x 250 x 250 mm were also used. The ply sheet used for the reference measurement was 400 x 400 x 18 mm in size and was made from the same material and kept in the same ambient conditions as the sample boxes.

The UBG materials were compacted in 50 mm deep layers within the sample boxes. The compaction effort was adjusted to the predefined target density for each sample, considering its moisture content and workability. For all rounds of testing, samples were prepared with fixed density and varying gravimetric moisture targets. In the final two rounds, additional samples targeting fixed gravimetric moisture and varying density values were also prepared. A range of target moisture contents were chosen to represent potential variation in the field. It typically ranged from the driest condition that could realistically be compacted within the boxes, to a target value above the optimum moisture content (OMC). The target density was usually set at a value below 100% of the maximum dry density (MDD) to enable the targets to be achieved without excessive effort for the driest samples. Once prepared, the sample boxes were covered with a thin plastic sheet to limit moisture loss prior to MFS testing.

3.3 VNA MEASUREMENTS

An Agilent FieldFox VNA (model N9923A) was used for the MFS measurements. The VNA ‘S-parameter’ measurements were recorded in terms of magnitude (decibels) and phase (degrees) at a series of discrete frequencies, denoted S_{xy}, where x and y are the receiving and sending ports of the VNA, respectively. The upper and lower antennas were attached to ports

1 and 2 of the VNA. Signals passing through the sample (S_{21}) and the portion reflected back to the upper antenna (S_{11}) were recorded for the ply sheet reference and each boxed sample. Afterwards, the ply sheet reference measurement was repeated, both as a precaution and a double check to ensure the antennas did not move during the measurements. These measurements were collected at 1001 frequency steps from 7.894 MHz to 4.0 GHz, taking an average of five sweeps. The high-power signal setting of the VNA was used and data smoothing was disabled. While only the phase component of the S_{21} signal is required for Equation 3, both magnitude and phase of S_{21} and S_{11} signals were collected to enable additional time domain analysis options.

The measurements were later transferred to a computer for analysis. This involved unwrapping the S_{21} phase measurements and determining the phase shift at each measured frequency. The phase shift measurements were then used along with Equation 3 to calculate the real relative permittivity over the stable measurement range, determined to be 1.0 GHz to 2.0 GHz. The S_{21} measurements were also converted into an equivalent time domain signal using a discrete inverse fast-Fourier approach. This enabled the shape and arrival time of the direct wave passing through the ply sheet and boxed UBG samples to be observed. The measured change in arrival times enabled the wave velocity through each sample to be determined along with the corresponding apparent permittivity, which was used as a check on the phase shift permittivity calculation.

4 RESULTS AND DISCUSSION

4.1 LABORATORY MEASUREMENTS AND ANALYSIS

Six rounds of testing were undertaken using the MFS approach. This occurred between June 2013 and March 2015 at the TMR Material Testing Laboratory in Herston, Queensland, Australia. After completing the MFS testing, the gravimetric moisture, proportion of OMC, volumetric moisture (θ_v), dry density, and proportion of the MDD of the samples were determined using conventional laboratory test methods. These results are summarised in Table 2. While incremental improvements in the MFS test procedure and analysis methods were introduced over the period of testing, the same general approach was used throughout.

The MFS measurements were usually undertaken within two hours of the completion of sample compaction.

TABLE 2: Material testing results

Sample description	Moisture			Density	
	% by mass	% of OMC	% by volume (θ_v)	Dry density (kg/m^3)	% of MDD
Round 1 - 4 June 2013 - Quarry 1 materials					
Sample 1a (target: OMC - 3%, 97% of MDD)	5.1	64	10.7	2106	96.9
Sample 2a (target: OMC, 97% of MDD)	7.6	96	16.0	2114	97.3
Sample 3a (target:OMC+2.6%, 97% of MDD)	10.1	128	21.3	2113	97.2
Round 2 - 9 July 2013 - Quarry 1 materials					
Sample 1 (target: 2.4% M/C, 97% of MDD)	2.4	30	5.1	2107	96.9
Sample 2 (target: 4.0% M/C, 97% of MDD)	4.2	53	8.8	2104	96.8
Sample 3 (target: 5.5% M/C, 97% of MDD)	5.3	67	11.2	2113	97.2
Sample 4 (target: 7.1% M/C, 97% of MDD)	7.0	89	14.8	2108	97.0
Sample 5 (target: 8.7% M/C, 97% of MDD)	8.8	111	18.5	2099	96.6
Round 3 - 16 September 2013 - Quarry 1 & 3 materials					
Sample 1A - Quarry 3 (target: 6.9% M/C)	6.7	97	15.3	2290	93.8
Sample 1B - Quarry 3 (target: 6.9% M/C)	6.5	94	14.8	2285	93.6
Sample 2A - Quarry 1 (target: 7.9% M/C)	7.7	98	16.0	2064	95.0
Sample 2B - Quarry 1 (target: 7.9% M/C)	7.6	97	16.4	2140	98.5
Round 4 - 12 March 2014 - Quarry 2 materials					
Sample 1 (target: 2.4% M/C, 95% of MDD)	2.2	31	4.3	1977*	91.0*
Sample 2 (target: 4.0% M/C, 95% of MDD)	3.8	53	7.8	2057*	94.7*
Sample 3 (target: 5.5% M/C, 95% of MDD)	5.2	72	10.4	2005*	92.3*
Sample 4 (target: 7.1% M/C, 95% of MDD)	6.5	90	13.4	2057*	94.7*
Sample 5 (target: 8.7% M/C, 95% of MDD)	7.9	110	16.3	2058*	94.7*
Round 5 - 16 December 2014 - Quarry 1 materials					
Sample 1A (target: 2.4% M/C, 90% MDD)	2.8	40	6.1	2194	89.8
Sample 2A (target: 4.0% M/C, 90% MDD)	4.1	59	9.0	2197	90.0
Sample 3A (target: 5.5% M/C, 90% MDD)	5.5	79	12.0	2198	90.0
Sample 4A (target: 7.1% M/C, 90% MDD)	7.2	104	15.8	2192	89.8
Sample 1B (target: 6.0% M/C, 85% MDD)	6.1	89	12.7	2077	85.0
Sample 2B (target: 6.0% M/C, 90% MDD)	6.1	89	13.5	2194	89.8
Sample 3B (target: 6.0% M/C, 95% MDD)	6.1	89	14.2	2318	94.9
Sample 4B (target: 6.0% M/C, 100% MDD)	6.1	89	15.0	2441	99.9
Sample 5B (target: 6.0% M/C, 105% MDD)	6.1	89	15.7	2562	104.9
Round 6 - 30 March 2015 - Quarry 4 materials					
Sample 1A (target: 2.7% MC, 95% MDD)	2.9	37	5.8	2007	90.8
Sample 2A (target: 4.0% MC, 95% MDD)	4.0	51	8.4	2101	95.0
Sample 3A (target: 5.3% MC, 95% MDD)	5.7	72	11.9	2090	94.5
Sample 4A (target: 6.6% MC, 95% MDD)	7.1	90	14.9	2093	94.7
Sample 5A (target: 7.9% MC, 95% MDD)	8.0	101	16.8	2098	94.9
Sample 1B (target: 7.9% M/C, 85% MDD)	8.2	104	15.4	1875	84.8
Sample 2B (target: 7.9% M/C, 90% MDD)	8.2	103	16.2	1987	89.9
Sample 3B (target: 7.9% M/C, 95% MDD)	8.1	103	17.0	2099	94.9
Sample 4B (target: 7.9% M/C, 100% MDD)	7.9	100	17.5	2204	99.7

*Estimated based on an assumed empty sample box mass.

An example of the VNA S_{21} frequency-domain measurements for UBG samples and the corresponding time domain signals are shown in Figure 2. This figure shows the moisture content of samples increasing from Sample 1 (driest) to 5 (wettest). Unlike previous investigations (*34*), good separation between the direct wave and unwanted reflections was achieved, avoiding the need for time domain windowing of the direct wave arrival.

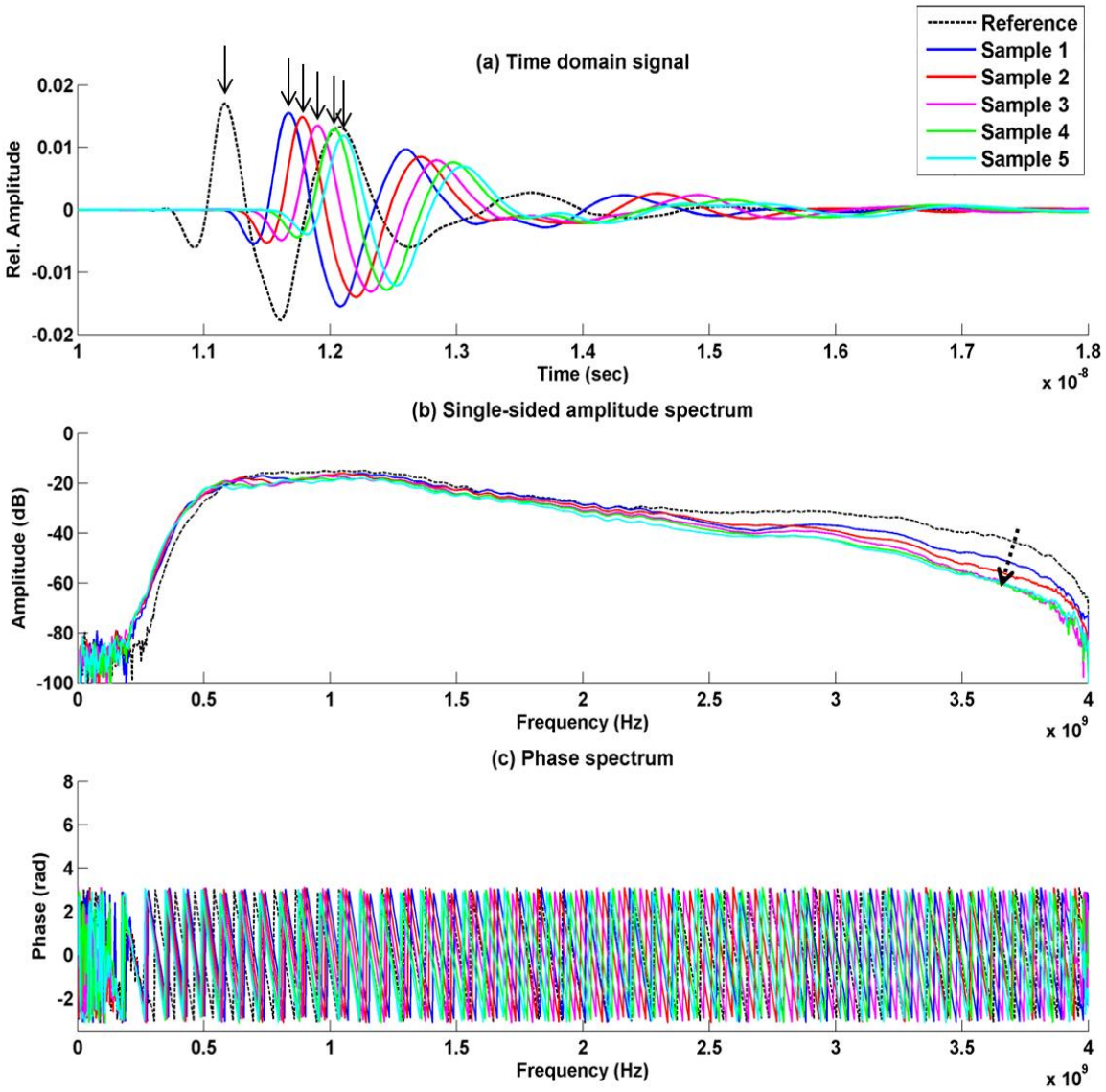

Figure 2: (a) Time domain signals generated from S_{21} VNA measurements of: (b) amplitude and (c) phase of signals passing through UBG material sample during Round 4 of MFS testing

The vertical arrows shown in Figure 2(a) indicate the arrival of the direct wave transmitted through the ply sheet (left-most arrow) and material samples, arriving progressively later in time with increasing moisture content. As observed in the amplitude spectrum in Figure 2(b), a loss in the high-frequency content of the direct signal occurred with increasing sample moisture, indicated by the dashed arrow. As shown in Figure 2(b), the bow tie antenna transmits over a relatively wide range of frequencies, with the strength of the transmitted signal dropping off below approximately 500 MHz. A slight dip in the amplitude spectrum is seen at approximately 2.7 GHz, corresponding to the first frequency null of this antenna. The null frequency varies with coupling conditions and the permittivity of material under test. While the strength of the amplitude spectrum indicates that it should be possible to measure over a very wide frequency range, in practice, the phase was found to be most stable near the central frequency of the antenna over the range 1.0 to 2.0 GHz.

To address the potential issue of phase shift ambiguity (*37*), permittivity values were calculated several times, each time adding increments of 360 degrees to the measured phase shift. As permittivity values vary slowly with frequency, and as the addition of incorrect increments of 360 degree phase results in notably sloping plots, the correct phase shift adjustment was identified as the one producing a flattest permittivity gradient over the stable measurement range. An example of the resulting frequency-dependent real relative permittivity measurements is illustrated in Figure 3. A clear change in sample permittivity can be seen with each increase of sample moisture. These particular results were collected during round 2 of testing, in which the sample measurements were collected three times – once using the original passive antennas (PHP) and the other two times using an amplified version of the antennas using the low (ALP) and high (AHP) power settings of the VNA. The amplified versions are the same as that used in the NM-GPR system. The comparison was undertaken to ensure similar permittivity results would be obtained using either antenna type and also to determine if there was an advantage in using active antennas. As changing between low and high power settings in the VNA made no difference and changing between active and passive antennas made only a small difference, it was decided to continue using passive antennas for the remainder of testing.

A plot of the mean relative permittivity values over the range 1.0 to 2.0 GHz for each sample and the corresponding volumetric moisture content (θ_V) determined for each sample is shown in Figure 4. The following relation and an unconstrained third-order polynomial fit of the MFS measurements and several relations from the literature are also shown for comparison:

$$\theta_V = 0.000006\varepsilon_r'^3 - 0.000556\varepsilon_r'^2 + 0.02538\varepsilon_r' - 0.08758 \quad (4)$$

This relation is intended as an approximation based on the material types and conditions used in this study. It should be noted that the number of measurements collected per quarry varies, which may have skewed the relation. For more accurate estimates, and where practical to do so, it is recommended to develop site-specific relations using the same material types and proportions, grading, density and temperature conditions within the pavement of interest.

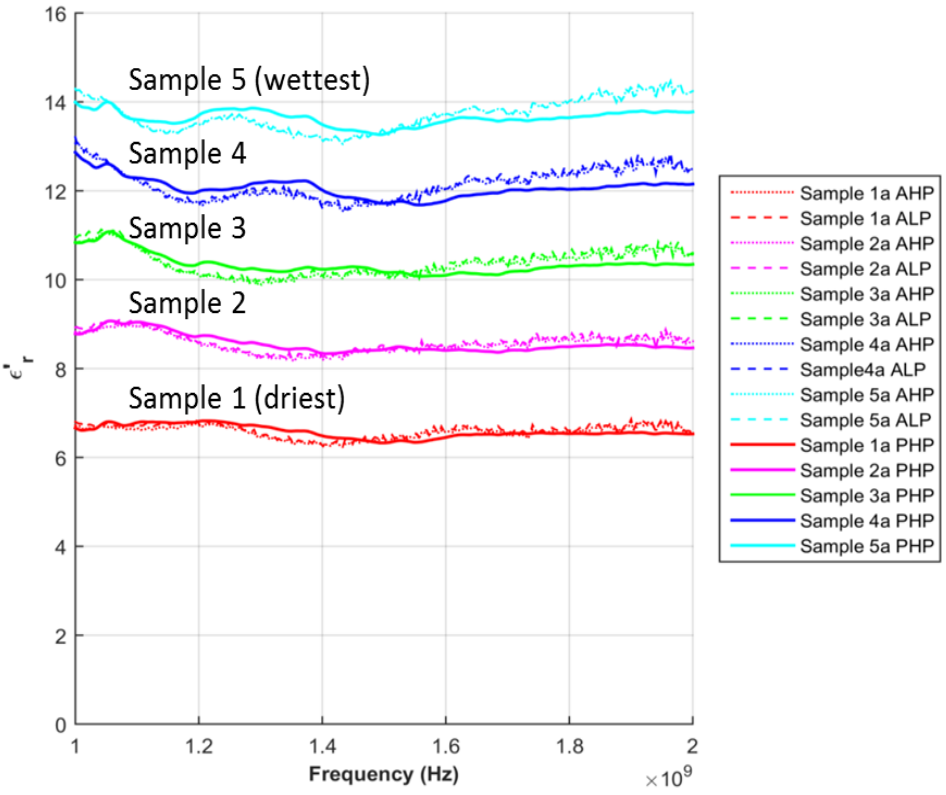

Figure 3: Frequency-dependent real permittivity (ε'_r) measurements collected during round 2 of testing using active antennas with the VNA's high-power setting (AHP), active antennas with low power (ALP) and passive antennas with high power (PHP)

Comparing the MFS results to the literature relations illustrated in Figure 4, for samples with higher moisture contents, there appears to be relatively good agreement to TDR-determined relations for crushed rock pavement materials proposed by Baran (*19*) and Ekblad and Isacsson (*20*). However, for drier samples, the MFS results produced somewhat higher permittivity values for the given volumetric moisture contents compared to those literature relations. As annular air gaps adjacent to TDR prongs result in an underestimate of moisture content (*38*), a possible explanation for the observed difference is that if air gaps or pockets are forming adjacent to the embedded TDR sensors this may have led to an underestimate of permittivity within drier and more difficult to compact samples. On the other hand the variation may be due to differences in type, grading or other aspects of the sample materials. Looking at the MFS results for Quarry 1 samples in Figure 4, which were prepared and tested on four occasions over 18 months, these follow a relatively consistent moisture-permittivity response. This indicates the observed differences are unlikely to be due to an erroneous setting or mistake during one round of MFS testing, but rather some difference in the material properties of the samples being measured or alternatively some systematic difference in the measurement or analysis methods.

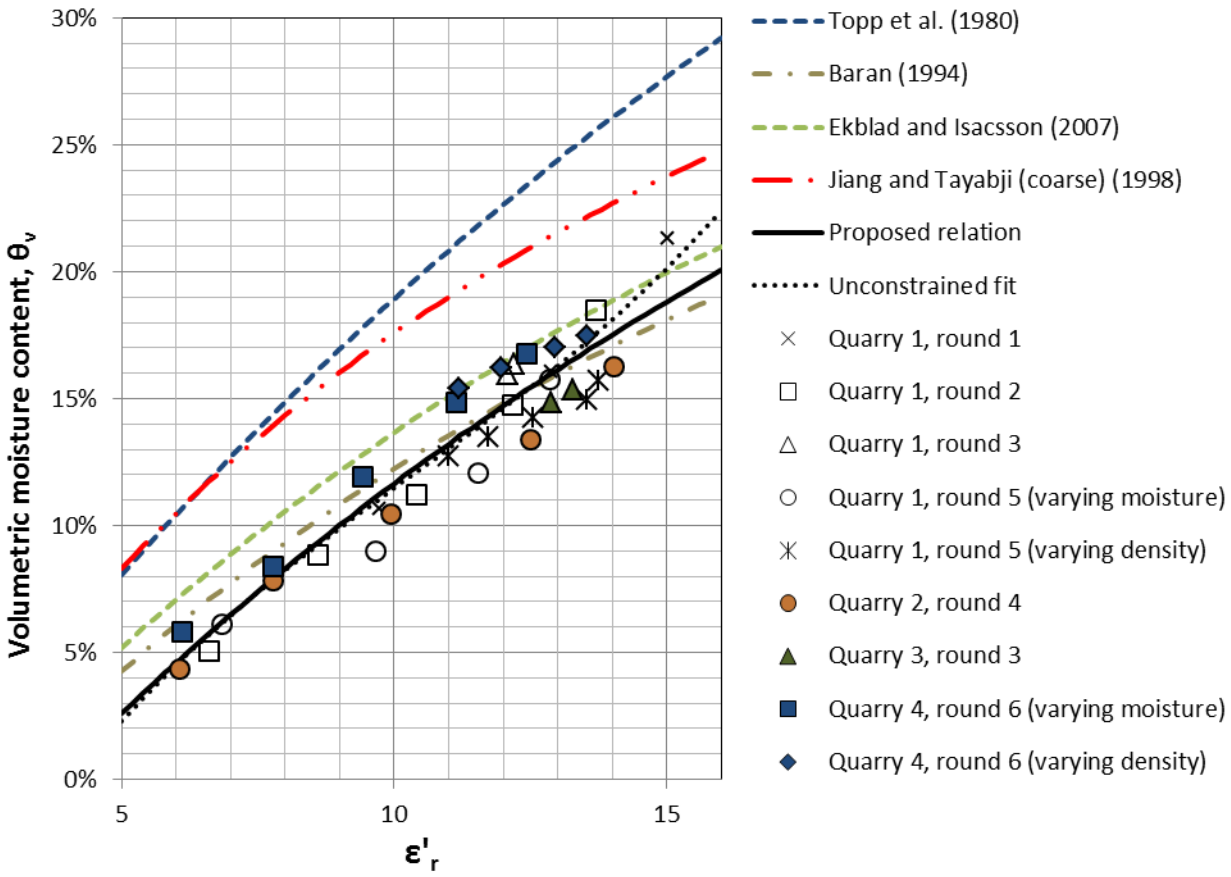

Figure 4: Results from MFS testing compared to published moisture-permittivity relations

4.2 Advantages and limitations of the approach

Considering laboratory practicalities, the MFS approach provides a number of advantages for characterising UBG materials. The test is relatively quick, taking approximately two minutes per VNA measurement; though the time and effort to compact material samples is significantly greater at approximately 20 to 30 minutes per sample. Conventional permittivity characterisation apparatus such as coaxial cells and surface probes, are usually small to maximise their frequency response. However, this in turn limits their sampling volume, and in the case of coaxial cells, presents challenges in accommodating coarse aggregates. Unlike methods that are sensitive to localised material variations, the MFS measurement occurs through a relatively large and well-defined sample thickness, in turn giving greater confidence when characterising bulk electrical properties of conglomerate materials. The use of simple and low-cost sample boxes enables unbonded materials to be contained and vigorously compacted to mimic realistic field conditions without the risk of damaging or distorting

delicate or expensive apparatus and use of ground-coupled antennas similar to the NM-GPR, ensures characterisation is undertaken over the relevant frequency range. Finally, the measurement of phase is relatively precise, avoiding the somewhat subjective process of reliably picking reflection features within TDR signals.

However, there are also a number of potential issues and sources of error that need to be observed when using the MFS approach. As noted in previous investigations (*7; 19; 20*), various aspects of the test setup including sample dimensions, aspect ratio and antenna spacing, affect the measurements. Poorly optimised test apparatus can result in unwanted reflections or resonances that may lead to errors in the phase measurement and permittivity results. An issue with the current apparatus is water absorption into the form-ply boxes. The original intention was to monitor changes in bulk permittivity over time for sealed and also drying samples. However, during early testing, discrepancies were noted between the low change in boxed sample mass over time and the much larger moisture loss determined using gravimetric analysis of the samples. It was concluded that moisture was being absorbed from the sample materials into the form-ply boxes. A notable smell of bacteria was also observed when removing the plastic covers, the growth of which may also have also contributed to the discrepancy. The use of sample boxes with additional waterproofing layers, or those made from plastic or other less permeable dielectric materials may be considered in the future to address these issues.

5 CONCLUSIONS

This paper presents test results using a modified free-space (MFS) approach to characterise the bulk real relative permittivity of compacted UBG pavement materials. The aim of the work was to develop a practical laboratory test method to determine moisture-permittivity relations for compacted UBG pavement materials. These relations will in turn be used to estimate pavement moisture from multi-offset NM-GPR field measurements of pavement permittivity.

The MFS approach was used to measure UBG material samples with varying moisture contents. Materials from four quarries were characterised and the results were used to determine an indicative moisture-permittivity relation. Comparing these results to the literature, at higher moisture contents, the MFS permittivity measurements were close to relations in the literature for similar materials determined using TDR. However, for drier samples, the MFS permittivity values were slightly higher than predictions using the literature relations, which may relate to the sensitivity of TDR to adjacent air gaps within these drier and more difficult to compact samples. A summary of benefits and limitations of the MFS approach has also been given. The benefits include the ability to measure larger and more representative sample volumes of UBG materials and relative measurement precision.

6 ACKNOWLEDGEMENTS

This work was funded under the National Asset Centre of Excellence (NACOE) research project P12 'Field-validation of Noise Modulated Ground Penetrating Radar' by the Queensland Department of Transport and Main Roads (TMR). The author wishes to express his sincere thanks to Dr Bryan Reeves and Dr-Ing. Alexander Scheuermann for their guidance and suggestions, as well as to Jason Maudsley for his efforts in UBG sample preparation. This paper contributes to the work of COST Action TU1208 'Civil Engineering Applications of Ground Penetrating Radar'.

7 REFERENCES

1. Charlier, R., P. Hornych, M. Sršen, Å. Hermansson, G. Bjarnason, S. Erlingsson, and P. Pavšič. Water Influence on Bearing Capacity and Pavement Performance: Field Observations. In *Water in Road Structures: Movement, Drainage and Effects*, Springer Science & Business Media B.V., Nottingham, UK, 2009, pp. 175-192.
2. Saevarsdottir, T., and S. Erlingsson. Effect of Moisture Content on Pavement Behaviour in a Heavy Vehicle Simulator Test. *Road Materials and Pavement Design,* Vol. 14, No. sup.1, 2013, pp. 274-286.
3. Jameson, G. *Guide to Pavement Technology: Part 2: Pavement Structural Design*. Publication AGPT02-10, Austroads, Sydney, Australia, 2010.
4. Vuong, B., G. Jameson, K. Sharp, and B. Fielding. *Guide to Pavement Technology: Part 4A:*

Granular Base and Subbase Materials. Publication AGPT04A-08, Austroads, Sydney, Australia, 2008.

5. Look, B. G., I. N. Reeves, and D. J. Williams. Field Experiences Using Time Domain Reflectometry for Monitoring Moisture Changes in Road Embankments and Pavements. In *Time Domain Reflectometry in Environmental, Infrastructure and Mining Applications*, Evanston, Illinois, 1994.
6. Diefenderfer, B. K. Moisture Content Determination and Temperature Profile Modelling of Flexible Pavement Structures. PhD diss., Civil Engineering, Virginia Polytechnic Institute and State University, Blacksburg, VA, 2002. p. 313.
7. Hore-Lacy, W., D. Bodin, and A. Scheuermann. Time Domain Reflectometry (TDR) Based Moisture Monitoring System For Unbound Granular Pavements. In *ARRB Conference, 26th, Sydney, New South Wales, Australia, 2014*, ARRB Group, Vermont South, Victoria, Australia, 2014.
8. Salour, F., and S. Erlingsson. Moisture-Sensitive and Stress-Dependent Behavior of Unbound Pavement Materials from In Situ Falling Weight Deflectometer Tests. In *Transportation Research Record: Journal of the Transportation Research Board,* No. 2335, Transportation Research Board of the National Academies, Washington, D.C., 2013, pp. 121-129.
9. Richter, C. A. Seasonal Variations in the Moduli of Unbound Pavement Layers. Publication FHWA-HRT-04-079, Federal Highways Administration, Turner-Fairbank Highway Research Center, McLean, Virginia, USA, 2006.
10. Zhang, Z., Z. Wu, M. Martinez, and K. Gaspard. Pavement Structures Damage Caused by Hurricane Katrina Flooding. *Journal of Geotechnical and Geoenvironmental Engineering,* Vol. 134, No. 5, 2008, pp. 633-644.
11. Muller, W. B., and J. Roberts. Revised Approach to Assessing Traffic Speed Deflectometer (TSD) Data and Field Validation of Deflection Bowl Predictions. *International Journal of Pavement Engineering,* Vol. 14, No. 4, 2013, pp. 388-402.
12. Huisman, J. A., S. S. Hubbard, J. D. Redman, and A. P. Annan. Measuring Soil Water Content with Ground Penetrating Radar: A Review. *Vadose Zone Journal,* Vol. 2, No. 4, 2003, pp. 476-491.
13. Grote, K., S. Hubbard, J. Harvey, and Y. Rubin. Evaluation of Infiltration in Layered Pavements Using Surface GPR Reflection Techniques. *Journal of Applied Geophysics,* Vol. 57, No. 2, 2005, pp. 129-153.
14. Benedetto, A., and S. Pensa. Indirect Diagnosis of Pavement Structural Damages Using Surface GPR Reflection Techniques. *Journal Of Applied Geophysics,* Vol. 62, No. 2, 2007, pp. 107-123.
15. Plati, C., and A. Loizos. Estimation Of In-Situ Density and Moisture Content in HMA Pavements Based on GPR Trace Reflection Amplitude Using Different Frequencies. *Journal*

Of Applied Geophysics, Vol. 97, October, 2013, pp. 3-10.

16. Reynolds, J. M. *An Introduction to Applied and Environmental Geophysics*. John Wiley & Sons, Chichester, England, UK., 1997.
17. Kaatze, U., and C. Electromagnetic Techniques for Moisture Content Determination of Materials. *Measurement Science and Technology,* Vol. 21, No. 8, 2010, pp. 1-26.
18. Topp, G. C., J. L. Davis, and A. P. Annan. Electromagnetic Determination of Soil Water Content: Measurements in Coaxial Transmission Lines. *Water Resources Research,* Vol. 16, No. 3, 1980, pp. 574-582.
19. Baran, E. Use of Time Domain Reflectometry For Monitoring Moisture Changes in Crushed Rock Pavements. In *Symposium and Workshop On Time Domain Reflectometry in Environmental, Infrastructure and Mining Applications*, United States Bureau of Mines, Northwestern University, Evanston, Illinois, USA, 1994, pp. 349-356.
20. Ekblad, J., and U. Isacsson. Time-Domain Reflectometry Measurements and Soil-Water Characteristic Curves of Coarse Granular Materials Used in Road Pavements. *Canadian Geotechnical Journal,* Vol. 44, No. 7, 2007, pp. 858-872.
21. Liu, L., and T. Guo. Determining the Condition of Hot Mix Asphalt Specimens in Dry, Water-Saturated, and Frozen Conditions Using GPR. *Journal of Environmental & Engineering Geophysics,* Vol. 8, No. 2, 2003, pp. 46-52.
22. Cassidy, N. J. Electrical and Magnetic Properties of Rocks, Soils and Fluids. In *Ground Penetrating Radar: Theory and Applications*, Elsevier Science, Amsterdam, 2009, pp. 41-72.
23. Greaves, R. J., D. P. Lesmes, J. M. Lee, and M. N. Toksöz. Velocity Variations and Water Content Estimated from Multi-Offset, Ground-Penetrating Radar. *Geophysics,* Vol. 61, No. 3, 1996, pp. 683-695.
24. Steelman, C. M., and A. L. Endres. Assessing Vertical Soil Moisture Dynamics Using Multi-Frequency GPR Common-Midpoint Soundings. *Journal of Hydrology,* Vol. 436–437, 2012, pp. 51-66.
25. Emilsson, J., P. Englund, and J. Friborg. Simple Method for Estimation of Water Content of Roadbeds Using Multi-Offset GPR. In *Ninth International Conference on Ground Penetrating Radar*, SPIE Proceedings Vol. 4758, SPIE, Santa Barbara, California, 2002, pp. 422-426.
26. Leng, Z., and I. L. Al-Qadi. An Innovative Method for Measuring Pavement Dielectric Constant Using the Extended CMP Method with Two Air-Coupled GPR Systems. *NDT & E International,* Vol. 66, September, 2014, pp. 90-98.
27. Maser, K. R., T. J. Holland, R. Roberts, and J. Popovics. Technology for Quality Assurance of New Pavement Thickness. In *International Symposium on Non-Destructive Testing in Civil Engineering, Berlin, Germany, 2003*. DGZfP (German Society for Non-Destructive Testing), Berlin, Germany, 2003.

28. Edwards, L., and Mason, Q.. Evaluation of Nondestructive Methods for Determining Pavement Thickness. Publication ERDC/GSL TR-11-4. US Army Corp of Engineers, Engineer Research and Development Center, 2011.

29. Al-Qadi, I. L., S. Lahouar, and A. Loulizi. GPR: From the State-of-the-Art to the State-of-the-Practice. In *International Symposium on Non-Destructive Testing in Civil Engineering, Berlin, Germany, 2003*. DGZfP (German Society for Non-Destructive Testing), Berlin, Germany, 2003.

30. Reeves, B. Noise Modulated GPR: Second Generation Technology. In *GPR 2014: 15th International Conference on Ground Penetrating Radar*, *Brussels, Belgium*. IEEE, 2014, pp. 708-713.

31. Muller, W. B., A. Scheuermann, and B. Reeves. Quantitative Moisture Measurement of Road Pavements Using 3D GPR. In *GPR-2012:14th International Conference on Ground Penetrating Radar Shanghai, China*. IEEE, 2012, pp. 517-523.

32. Muller, W. Self-Correcting Pavement Layer Depth Estimates Using 3D Multi-Offset Ground Penetrating Radar (GPR). In *GPR 2014: 15th International Conference on Ground Penetrating Radar*, *Brussels, Belgium*. IEEE, 2014, pp. 887-892.

33. Muller, W. B. A Comparison of TSD, FWD and GPR Field Measurements. In *International Symposium Non-Destructive Testing in Civil Engineering (NDT-CE 2015), Berlin, Germany, 2015*. DGZfP (German Society for Non-Destructive Testing), Berlin, Germany, 2015.

34. Muller, W., and X. Derobert. A Comparison of Phase-Shift and One-Port Coaxial Cell Permittivity Measurements for GPR Applications. In *7th International Workshop on Advanced Ground Penetrating Radar,* Nantes, France, (*IWAGPR-2013)*. IEEE, 2013, pp. 1-6.

35. Muller, W. B. Optimising a Modified Free-Space Permittivity Characterisation Method for Civil Engineering Applications. *Journal of Geophysics and Engineering,* Submitted for publication.

36. Trabelsi, S., A. W. Kraszewski, and S. O. Nelson. Phase-Shift Ambiguity in Microwave Dielectric Properties Measurements. *IEEE Transactions on Instrumentation and Measurement,* Vol. 49, No. 1, 2000, pp. 56-60.

37. Department of Transport and Main Roads. *Material Testing Manual.* 4th Edition, TMR, Brisbane, Queensland, Australia, 2014.

38. Whalley, W. R. Considerations on the use of Time-Domain Reflectometry (TDR) for Measuring Soil Water Content. *Journal of Soil Science,* Vol. 44, No. 1, 1993, pp. 1-9.

Paper VI

Muller W.B., Bhuyan H. and Scheuermann A., A comparison of modified free-space (MFS), GPR and TDR techniques for permittivity characterisation of unbound granular pavement materials. Near Surface Geophysics, 14(6), 537-550, December 2016.

This page left intentionally blank

A comparison of modified free-space (MFS), GPR and TDR techniques for permittivity characterisation of unbound granular pavement materials

Wayne B. Muller[*1,2,3], Habibullah Bhuyan[2] and Alexander Scheuermann[2]

1. Department of Transport and Main Roads, 35 Butterfield Street, Herston, Queensland, Australia 4006

2. School of Civil Engineering, The University of Queensland, Queensland, Australia 4072

3. ARRB Group Ltd., 123 Sandgate Road, Albion, Queensland, Australia, 4010

* Corresponding author. Email wayne.b.muller@tmr.qld.gov.au

Abstract – This paper reports on a laboratory experiment comparing permittivity measurements using a modified-free space (MFS) approach to results using common-offset ground penetrating radar (GPR) and time-domain reflectometry (TDR) on moist and compacted samples of unbound granular (UBG) road pavement materials. In the first part of the experiment, UBG samples from the same source were prepared to varying moisture contents and a fixed target density. Separate samples were prepared for MFS and TDR testing, all of which were also measured using GPR. In the second part of the experiment, samples were mixed to a consistent gravimetric moisture content and varying densities before undertaking the MFS, TDR and GPR measurements. A reasonably good agreement was found between MFS and GPR measurements, which also compared well with literature relations for crushed rock pavement materials. The TDR results were relatively consistent with those literature relations, though appeared to deviate from the GPR and trend of MFS results for lower density and drier samples.

Keywords: Permittivity; ground penetrating radar; moisture.

1. Introduction

The moisture content of unbound granular (UBG) pavement materials has a significant influence on their structural performance (Charlier, et al. 2009, Saevarsdottir and Erlingsson 2013). Non-destructive techniques for measuring moisture within these materials are therefore of interest for a variety of pavement investigation and monitoring applications.

High-frequency electromagnetic (EM) techniques are the most promising category of water content sensors as they measure the same soil water content proxy, the dielectric permittivity, at a range of spatial scales (Huisman, et al. 2003). One EM method, time-domain reflectometry

(TDR), has been used by many authors to monitor moisture within granular pavements and underlying subgrade materials (Baran 1994, Diefenderfer, et al. 2000, Ekblad and Isacsson 2007, Jiang and Tayabji 1998, Liang, et al. 2006, Rainwater, et al. 1999, Richter 2006). The conventional approach involves relating the average or 'apparent' relative permittivity of the pavement material, determined from the two-way travel time of an EM signal travelling along an embedded TDR probe, to its volumetric moisture content. The sample dry density, electrical conductivity, temperature and dielectric dispersion of the materials and the length and resistance of the TDR cable also affect these measurements (Chung and Lin 2009, Logsdon 2000, Tarantino, et al. 2008). While TDR is useful for monitoring a modest number of locations, the need for embedded probes limits its practicality for large-scale pavement monitoring.

Another high-frequency EM technique, ground penetrating radar (GPR), is a more mobile alternative. Huisman et al. (2003) identified four methodologies using GPR to determine soil moisture content based on either measuring the velocity of reflected waves, the groundwave, waves transmitted between boreholes or by measuring the surface reflection coefficient. These measurements are used to determine the sample apparent permittivity, which like TDR is related to the volumetric moisture content. Changes in the sample mineralogy, density, temperature and other attributes can therefore also be expected to influence the measurements. If the depths of layers are reliably known, the wave velocity can be determined using a conventional fixed or 'common-offset' GPR antenna to measure the two-way travel time of reflected waves. For many existing roads, however, layer depth information is unreliable or unavailable. Where layer depths are unknown, multi-offset GPR acquisition geometries can be used to determine soil water content (Huisman, Hubbard, Redman and Annan 2003). This is achieved by using geophysical analysis methods to determine the depth of layers and the velocity of EM waves within those layers. Due to safety and practical considerations, for road investigations these measurements ideally should be collected at traffic speeds. An approach currently being investigated involves using a multi-channel noise-modulated GPR (NM-GPR) system (Reeves 2014) to collect multi-offset data while moving along the road at up to 100 km/hr. The multi-offset measurements are collected by combining the response of a number of antenna pairs at different offsets within a 3D ground-coupled array. To prepare for this new equipment and enable efficient data analysis, numerical modelling was undertaken simulating the expected response from typical pavement structures on which self-correcting geophysical

methods were then developed and applied to automate determination of pavement layer depths and EM wave velocities (Muller 2014). To enable in situ pavement moisture estimates from field measurements, laboratory investigations are required to relate the velocity of EM waves within these materials and the corresponding apparent permittivity to the in situ volumetric moisture content.

To calibrate these moisture-permittivity relations, a number of approaches are available to either measure the velocity of EM waves within material samples or to measure their permittivity. One approach involves using common-offset GPR to determine the two-way travel time through a known depth of laboratory prepared (Liu and Guo 2003) or field-cored samples (Evans, et al. 2008), though coring is usually unsuitable for coarse-grained unbound materials. These techniques can be used if the layer depths are reliably known or alternatively multi-offset techniques can be used (Grote, et al. 2005, Plooy, et al. 2013). TDR probes can be embedded within representative samples to measure the two-way travel time along the probe (Baran 1994, Diefenderfer, Al-Qadi and Loulizi 2000, Ekblad and Isacsson 2007). Alternatively the permittivity of samples can be determined using one-port (Huang 2001) or two-port coaxial cells (Chazelas, et al. 2007, Millard, et al. 2001, Shang and Umana 1999), surface probes (Berthelot, et al. 2010, Chang, et al. 2011, Loizos and Plati 2007, Saarenketo 1998), resonant cavities (Fauchard, et al. 2003), waveguides (Panzner, et al. 2010), surface reflection measurements (Panzner, Jostingmeier and Abbas 2010) or free-space reflection (Al-Qadi 1992, Al-Qadi, et al. 1991) or transmission techniques (Pellinen, et al. 2015).

Many of these techniques require specialised equipment that may be difficult to access or complicated and time-consuming to develop. There are also a number of practical issues and uncertainties when applying these methods to compacted, coarse-grained and un-bonded pavement materials. These include difficulties inserting representative samples within the test apparatus or preparing suitably smooth measurement surfaces; small or uncertain sampling volumes and the risk of potentially damaging the test apparatus during sample compaction. In some cases the measurement frequency range of these methods differ from that of the GPR equipment it is intended to calibrate. For dispersive materials this may lead to uncertainty when comparing results from devices operating at different measurement frequencies. In addition, sample attributes that may influence ground-coupled GPR equipment may not affect these other techniques in the same manner or to the same extent.

Considering these issues and available techniques, a modified free-space (MFS) approach was initially investigated as a potential method of measuring moist and compacted UBG samples for the purpose of calibrating GPR field measurements (Muller, et al. 2012). Various aspects of the approach including its accuracy compared to conventional apparatus and the influence of sample edges (Muller and Dérobert 2013), the influence of sample aspect ratio, antenna spacing and beam pattern (Muller and Scheuermann 2016) have previously been investigated or discussed. While the approach has been used to measure the permittivity of moisture-varying UBG samples from several quarry sources (Muller 2016), the influence of sample attributes such as density had not been investigated. As the approach is intended as a means of calibrating GPR measurements, it is important to understand how these variations affect MFS and GPR measurements. Furthermore, as field estimates of moisture determined using multi-offset NM-GPR will be calibrated using MFS and compared with TDR measurements, it is also important to understand how the response of these methods vary with moisture and density changes.

As an initial step, the aim of the current study is to investigate the influence of the volumetric moisture content and dry density of compacted UBG samples on permittivity measurements determined using the MFS approach, embedded TDR probes and two-way travel time measurements using a conventional common-offset GPR. For simplicity the same pavement material has been used for all measurements and the sample temperature has been kept at a constant temperature of approximately 22°C.

2. Methodology

2.1 MFS background and equipment

The real component of the relative permittivity (ε'_r) of a material sample can be estimated using a vector network analyser (VNA) to measure the phase-shift occurring between a fixed pair of antennas due to insertion of a known sample thickness. Assuming far-field conditions (Trabelsi, et al. 2000):

$$\varepsilon'_r \approx \left(1 + \frac{\Delta\Phi\lambda_0}{360d}\right)^2 \qquad (1)$$

where λ_0 = free space wavelength for a given frequency; $\Delta\Phi$ = measured phase shift (degrees); d = sample thickness.

Equation 1 is derived by accounting for the change in wavelength occurring between fixed antennas at a given frequency due to slowing of the EM waves within the known sample depth, compared to unimpeded travel through free space. The approach therefore measures the 'apparent permittivity' based on the mean EM wave velocity through the sample thickness, similar to TDR measurements along an embedded probe or GPR measurements through a known sample depth. For simplicity the term 'permittivity' (ε_r) is used herein in place of relative 'apparent permittivity' regarding results using these methods.

For the investigation ground-coupled bow-tie antennas similar to those found in the NM-GPR system were used for the MFS measurements. The outer dimensions of the bow-tie element were 80 x 35 mm. These are the same physical size as the antenna used in the NM-GPR and exhibit a similar response (Muller 2016), however the version used in the NM-GPR are active whereas those used in this study are passive, with only a balun at the antenna feed point. The antennas were resistively loaded with microwave absorbing foam placed within the shielded antenna enclosure and a 10 mm thick sheet of nylon fixed on the face of the enclosure. They were aligned vertically within a wooden frame at a fixed offset so the test sample could be slid in-between with a small air-gap at the top – Figure 1 (a). A previous study (Muller and Scheuermann 2016) investigated the influence of antenna separation and sample thickness on the MFS results, finding relatively stable performance when using samples at least 100 mm thick. Comparisons using active and passive versions of the antennas on the same UBG samples prepared to a range of moisture contents showed relatively consistent permittivity results (Muller 2016), demonstrating the repeatability of the measurements.

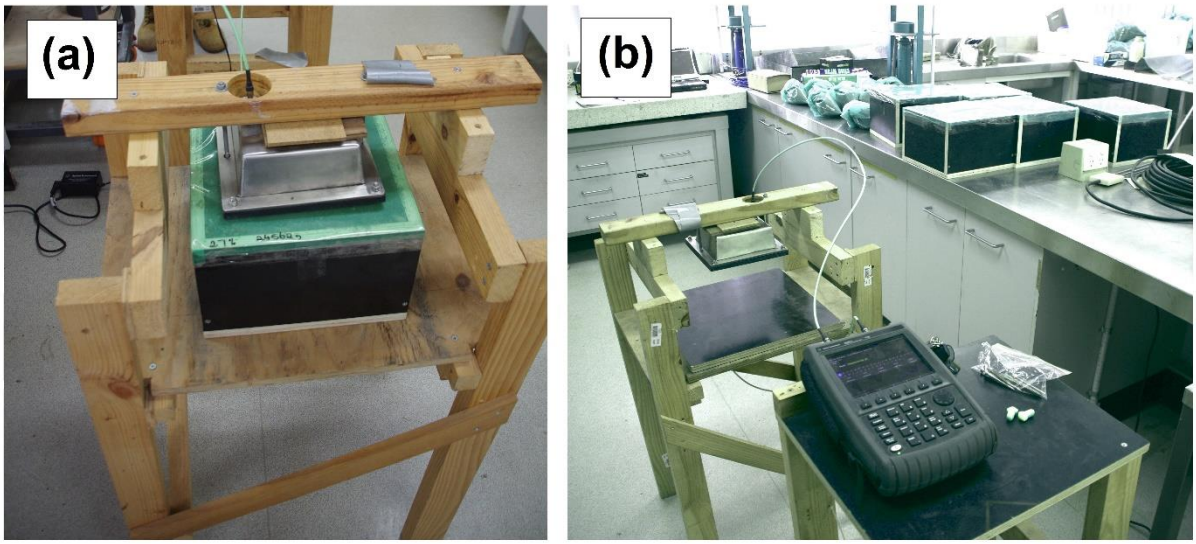

Figure 1: MFS test set-up measuring (a) a prepared UBG sample, and (b) the ply sheet reference measurement.

The VNA used for the investigation was an Agilent FieldFox portable VNA, model N9923A. Ports 1 and 2 were attached to the upper and lower antennas, respectively. The amplitude and phase of signals transmitted between the antennas (S_{21}) and reflected back to the uppermost antenna (S_{11}) were recorded at 1001 frequency steps up to 4.0 GHz, taking the average of five frequency sweeps. The VNA's high power setting was used and data smoothing was disabled. Prior to measuring the UBG samples a reference measurement was collected through a sheet of form-ply. This was done to account for the effect of the sample box base on the measurements, essentially removing its influence when measuring the boxed samples. A ply sheet was used rather than an empty box to avoid unwanted reflections from the sides. The ply sheet was of the same material used for the sample-boxes and kept in the same ambient conditions prior to testing. A photograph of the MFS test apparatus during ply calibration is shown in Figure 1 (b).

As an additional comparison, the S_{21} and S_{11} magnitude and phase measurements were converted into their time-domain equivalent and the arrival times of direct and reflected signals were used to determine travel time through the sample and its permittivity. The 'time-zero' for these measurements was determined from the ply sheet calibration measurement, by subtracting the travel time through the sample depth in air from the measured time-domain arrival.

2.2 TDR measurements

The TDR sample box was constructed of 14 mm thick polyvinyl chloride (PVC) with internal dimensions of 557 x 155 x 159 mm (length x width x height). The box was placed within a steel frame during sample compaction to prevent bursting, but was removed from the frame prior to testing. A number of steel screws were added in the corners to reinforce the box, though these are not expected to influence the measurements. The UBG material was compacted within the TDR sample box in three horizontal layers. The top and bottom UBG layers were approximately 45 mm thick with a 60 mm layer in between, producing a total sample depth of between 150 to 153 mm. The TDR sensor used for this investigation was a CS610-L probe manufactured by Campbell Scientific. The rod length for this three-prong probe was 300 mm with a rod diameter of 4.8 mm and spacing between outer rods of 45 mm. The probe was installed at the upper interface of these layers – Figure 2. The TDR probe was connected via a 25 metre long Belden 9914 RG8 coaxial cable to a Campbell Scientific TDR100 control unit that was used to make the measurements. A time window of 19.9 ns was recorded in the vicinity of the sensor and the measurements were stacked 10 times to produce each result. The collected data were then analysed using a custom Matlab script to pick the times corresponding to the start and end of the probe from which the wave velocity and permittivity were determined. During the data analysis a running average 20 samples long was applied to reduce the influence of noise.

Figure 2: Positioning the TDR rod probe sensor within the UBG material sample.

2.3 GPR measurements

The GPR system used for the investigation was a Geophysical Survey Systems Inc. (GSSI) SIR-3000 control unit connected to a 1.5 GHz ground-coupled antenna (model 5100B). The GPR measurements on the MFS samples were undertaken in two steps. First, the boxed samples were aligned on a steel table top in order of increasing moisture content for samples M1 to M5 and increasing density for samples D1 to D4. A stack of nylon sheets was placed on top of a ply sheet alongside the driest and lowest density samples, respectively. The samples were scanned using the GPR (Figure 3) and the change in two-way travel time to the bench-top was observed. Next, each individual sample was suspended with only one edge of the box on the table and the GPR antenna was placed on top. A metal plate was repeatedly moved up to and away from the centre of the box soffit to ensure this point could be correctly identified within the GPR response.

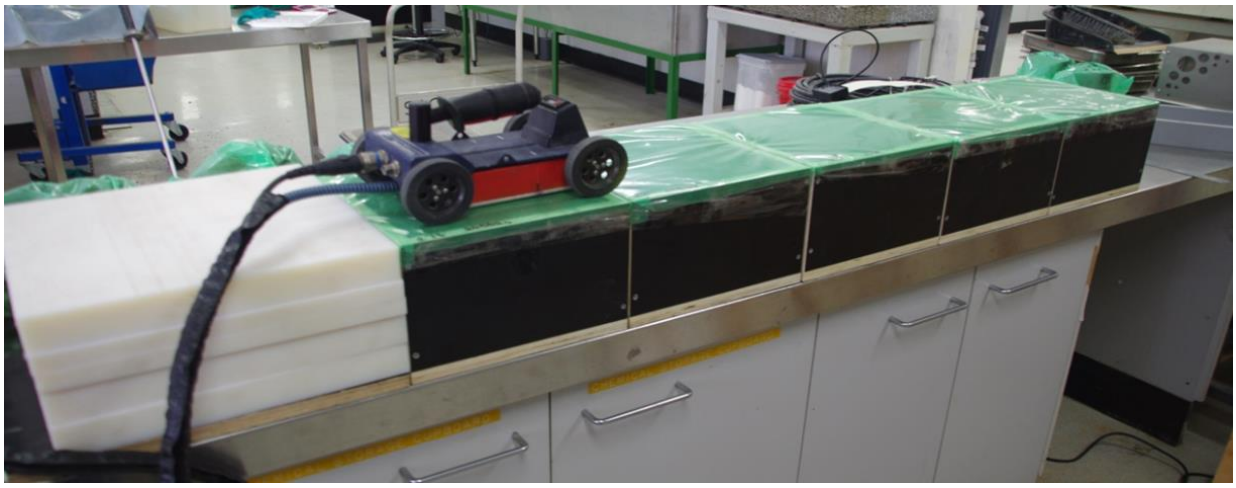

Figure 3: Collecting impulse GPR measurements of nylon and moisture-varying UBG samples M1 to M5.

For the TDR samples, after sample compaction and removal of the PVC box from the steel frame, dielectric spacers were placed under each end of the box so it was suspended above the table. The GPR antenna was placed centrally on top of the sample and the metal plate was repeatedly moved up to the box soffit while recording the response. To ensure any influence of the TDR probes on the GPR measurements was minimal, a second reading was collected with the GPR antenna rotated through 90 degrees as a check and precaution.

The permittivity of MFS and TDR samples was determined from the GPR measurements using a ray-path approach. It involved calculating the refracted ray-path and corresponding travel time of EM waves passing from transmitter to receiver through the sample and box floor. The assumed sample permittivity was incrementally adjusted until the difference in groundwave and reflected wave arrivals matched that measured on each of the MFS and TDR samples using GPR. Figure 4 illustrates an example of the ray-path geometries and permittivity values determined for samples M1 to M5 using this approach.

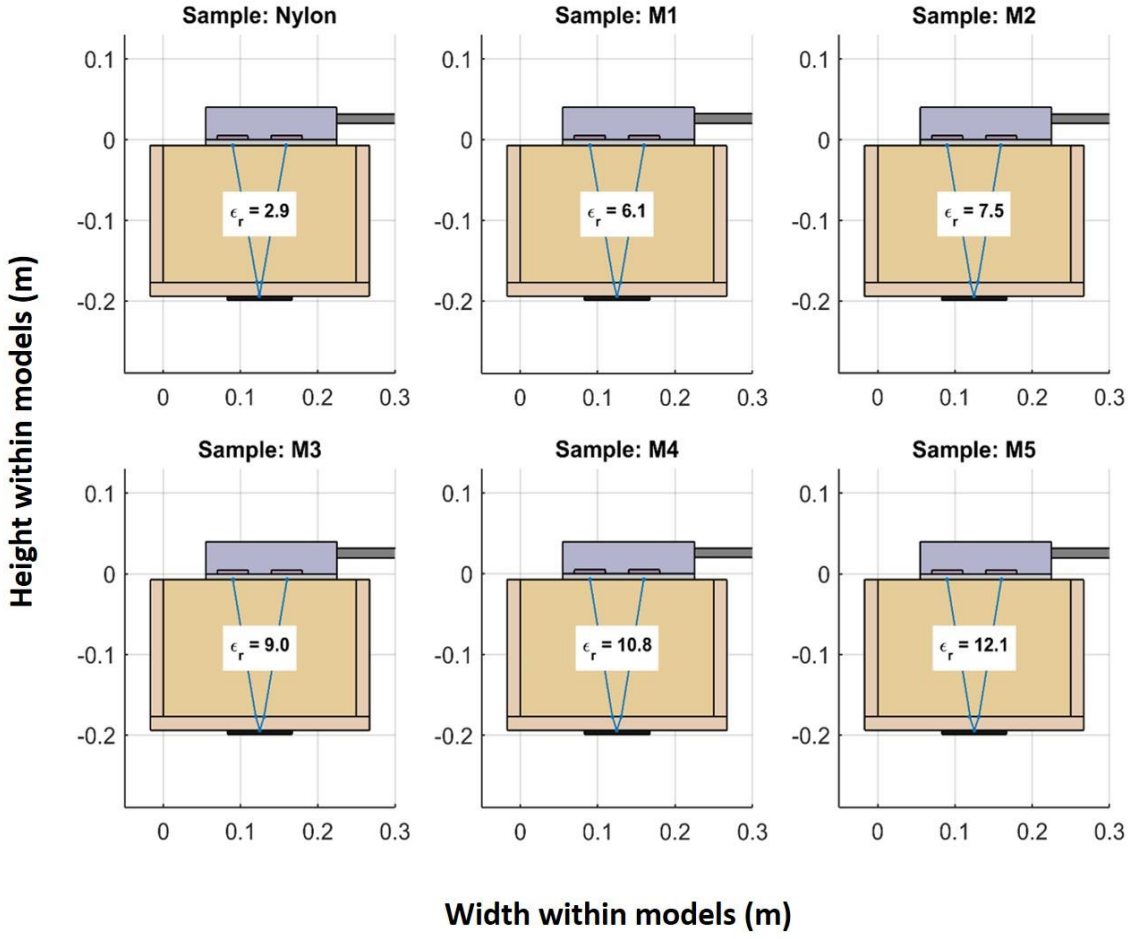

Figure 4: Refracted ray-paths determined in calculating the permittivity of nylon and samples from GPR measurements of samples M1 to M5.

For these calculations it was assumed that the common-offset GPR antenna spacing was 70 mm; the near-surface permittivity was equal to the mean of the sample and the antenna skid and that the permittivity of the antenna skid and the PVC and form-ply sample box materials was $\varepsilon_r = 3.0$.

2.4 Materials

The UBG material used for this investigation was a type 2.1 base-course material manufactured at a quarry in South-East Queensland to the 'C' grading classification in accordance with the MRTS05 'Unbound Pavements' specification (Department of Transport and Main Roads 2015). The material was supplied as part of a recent construction project from a registered quarry and was manufactured using a fine grained contact metamorphic source rock of hornfels origin. Available petrographic analytical reports revealed that this is a pasammo-pelitic rock. That is, the rock was metamorphosed from sedimentary rocks composed of clay and mud-rich minerals. Its primary minerology consisted of 32 to 58% feldspar, 4 to 19% microcrystalline feldspar, 6 to 13% quartz, 3 to 6% epidote and 1 to 4% calcite. The material also has an approximate volume of 26% soft, weak or deleterious minerals including 15 to 21% biotite mica, 3 to 6% serisite, 1 to 4% limonite, 1 to 4% chlorite and trace amounts of pyrite.

The sample was fractionated to determine the particle size distribution, illustrated in Figure 5 with the Department's grading limits also shown.

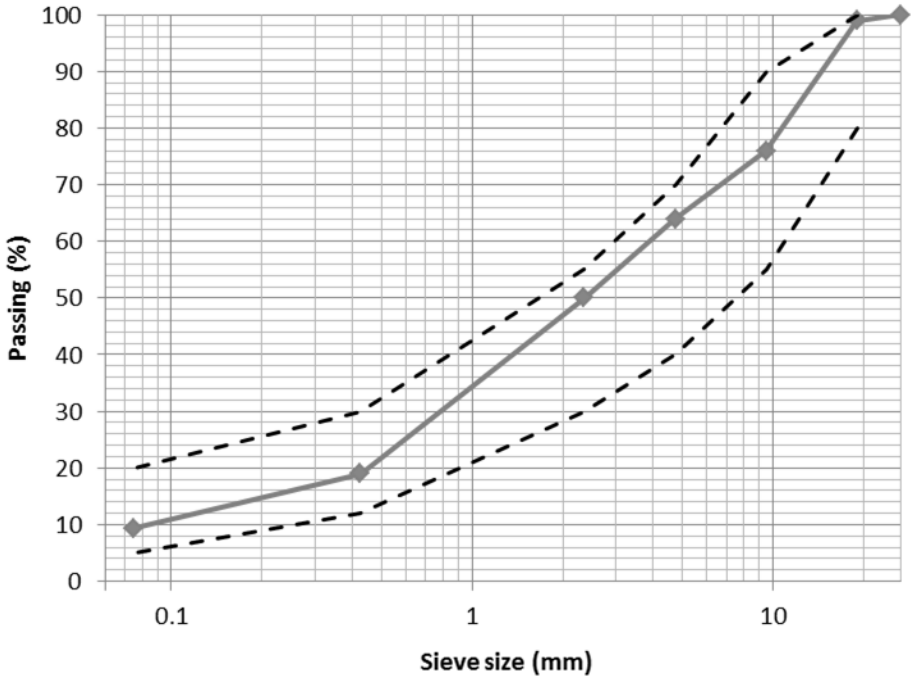

Figure 5: Particle size distribution of the measured UBG material and specification limits.

The moisture-density relationship and Atterberg limits were determined in accordance with the Department's *Material Testing Manual* (2014). The optimum moisture content (OMC) of the material was 7.9% with a maximum dry density (MDD) of 2211 kg/m^3. The coarse fraction of the material, recently crushed during the manufacturing process, had an apparent particle density (APD) of 2698 kg/m^3. The liquid limit of the sample was 22.6%, with a plasticity index of 5.0%. A linear shrinkage value of 5.0% was recorded for the sample, which is above the specification limit of 3.5% and may indicate an increased proportion of weathered materials within the fine fraction. Clay-rich phyllosilicates, including clay and mica-rich materials, liberated during the mechanical crushing process are present in the fine-fraction and so have potential to significantly influence permittivity response. For example, Saarenketo (1998) observed clear variations in the permittivity response of clays as the amount of water increased and became less tightly bound to aggregate boundaries.

2.5 Sample and measurement preparation

Prior to filling the sample boxes, the gravimetric moisture content of the UBG material was determined. It was then subdivided into portions large enough to fill each sample box. Prior to filling the boxes the samples were weighed and reverse-osmosis water was added and mixed through to reach the desired target moisture content. The material was then compacted in the sample box in layers approximately 50 mm thick and a small amount was set aside for gravimetric moisture content assessment.

In the first part of the experiment, the 'moisture-varying' samples M1 to M5 were prepared for MFS testing targeting a density of 95% of the MDD and gravimetric moisture contents of 2.7, 4.0, 5.3, 6.6 and 7.9%, respectively. These values were chosen to cover a wide range of field moisture conditions. The ply boxes used for these samples had internal dimensions of 170 x 250 x 250 mm, which differed from previous investigations (Muller, Scheuermann and Reeves 2012). The change was based on recent laboratory investigations that indicated these deeper boxes may be preferable for more consistent and accurate permittivity measurements (Muller and Scheuermann 2016). Once prepared the MFS samples were sealed with a plastic sheet to limit evaporation and were tested approximately half an hour to an hour later. TDR samples TM2 to TM5 were prepared targeting the same moisture and density values as for samples M2 to M5, using the one sample box for all measurements. A TDR sample was not produced to

match sample M1 due to concerns that the PVC box may not withstand the required compaction for this very dry material.

In the second part of the experiment the UBG material was prepared targeting the OMC gravimetric moisture content of 7.9%. A sample was collected for gravimetric assessment and 'density-varying' MFS samples D1 to D4 were compacted in the sample boxes targeting dry densities of 85, 90, 95 and 100% of the MDD, respectively. As there was too few of the deeper boxes, the older box size of 100 x 300 x 300 mm was used for this part of the experiment. TDR samples TD1 to TD4 were prepared targeting the same dry densities as MFS samples D1 to D4. As the one sample box was used for all TDR measurements a delay occurred between the addition of moisture and testing of the final sample. To account for the loss of moisture due to evaporation over this time, samples were collected during preparation of the first and last samples for gravimetric assessment.

In addition to measuring the UBG material samples, samples of nylon were also measured using the MFS and GPR methods. As the permittivity of the nylon was known from previous testing (ε_r = 3.0) (Muller and Scheuermann 2016), these measurements were used as an additional check on the MFS and GPR results. In the first part of the trial, nylon sheets totalling 170 mm thick were measured, matching the internal depth of the sample boxes. In the second part there was a slight mismatch between the internal box depth (100 mm) and the available thickness of nylon sheets (106 mm), requiring an adjustment in the calculations.

The moisture and dry density achieved for the UBG samples are summarised in Table 1. While the density achieved within samples M2 to M5 and D1 to D4 were close to their targets, the density of the TDR samples were a little lower, averaging 2.3% lower for moisture-varying samples and 3.5% for density-varying samples compared to the MDD. MFS sample M1 was also notably lower than its target density due to the difficulty compacting such a dry sample. As two different box depths were used for the MFS samples it was necessary to either change the antenna spacing when changing between box depths or keep the antenna spacing fixed while having an air gap above the shallower boxes or add a dielectric spacer to minimise the gap. The original intention was to monitor variations in permittivity over several days as the samples dried in a temperature and humidity controlled room. With this in mind, for measurement consistency it was decided to add a 64 mm thick nylon spacer beneath the shallower MFS sample box to avoid moving the antennas.

Table 1: Summary of MFS, GPR and TDR permittivity results

Fixed target density, varying moisture									
Sample ID	**M1**	**M2**	**M3**	**M4**	**M5**	**TM2**	**TM3**	**TM4**	**TM5**
Moisture content									
- Target (%)	2.7	4.0	5.3	6.6	7.9	4.0	5.3	6.6	7.9
- Achieved (%)	2.9	4.0	5.7	7.1	8.0	4.4	5.1	6.5	7.9
θv (achieved, %)	5.8	8.4	11.9	14.9	16.8	9.2	10.7	13.7	16.4
Dry density									
- Achieved (kg/m^3)	2007	2101	2090	2093	2098	2042	2057	2067	2031
- % of MDD	90.8	95.0	94.5	94.7	94.9	92.4	93.0	93.5	91.9
Method	***Calculated ε_r***								
GPR	6.1	7.5	9.0	10.8	12.1	6.8	8.7	10.0	11.1
S_{21} phase shift	6.1	7.8	9.4	11.1	12.4	-	-	-	-
S_{11} time-domain	6.2	8.0	9.6	11.2	12.7	-	-	-	-
S_{21} time-domain	5.9	7.6	9.4	11.0	12.5	-	-	-	-
TDR (peaks)	-	-	-	-	-	6.6	8.0	9.9	12.1
TDR (tangents)	-	-	-	-	-	5.9	7.4	9.4	11.3
TDR (head-corrected)	-	-	-	-	-	6.7	7.8	9.6	11.5
Fixed gravimetric moisture, varying target density									
Sample ID	**D1**	**D2**	**D3**	**D4**		**TD1**	**TD2**	**TD3**	**TD4**
Moisture content									
- Target (%)	7.9	7.9	7.9	7.9		7.9	7.9	7.9	7.9
- Achieved (%)	8.2	8.2	8.1	7.9		8.1	7.9	7.8	7.6
θv (achieved, %)	15.4	16.2	16.2	17.5		14.6	15.3	15.7	16.0
Dry density									
- Achieved (kg/m^3)	1875	1987	2099	2204		1806	1932	2027	2109
- % of MDD	84.8	89.9	94.9	99.7		81.7	87.4	91.7	95.4
Method	***Calculated ε_r***								
GPR	10.6	10.9	11.9	12.7		-	11.2	11.5	11.6
S_{21} phase shift	11.2	12.0	13.0	13.5		-	-	-	-
S_{11} time-domain	-	-	-	-		-	-	-	-
S_{21} time-domain	10.8	11.7	12.5	12.8		-	-	-	-
TDR (peaks)	-	-	-	-		8.3	9.6	10.0	12.3
TDR (tangents)	-	-	-	-		8.0	9.1	9.8	12.3
TDR (head-corrected)	-	-	-	-		7.9	9.3	10.1	11.8

A discrepancy was later identified between the change in box mass and sample moisture content indicating moisture was being lost from the sample, either due to absorption into the form-ply box, bacteria growth within the sample, or both (Muller 2016). As moisture absorption into the box floor would affect the validity of the ply calibration and accuracy of the sample permittivity measurements, only the initial measurements have been reported. To limit these issues in future, use of less absorbent sample box materials or addition of waterproofing layers has been recommended (Muller 2016).

3. Results

3.1 MFS measurements

A plot of the frequency-domain measurements and the corresponding time-domain signals determined from MFS S_{21} measurements are shown in Figure 6, with the time-domain arrivals indicated with crosses.

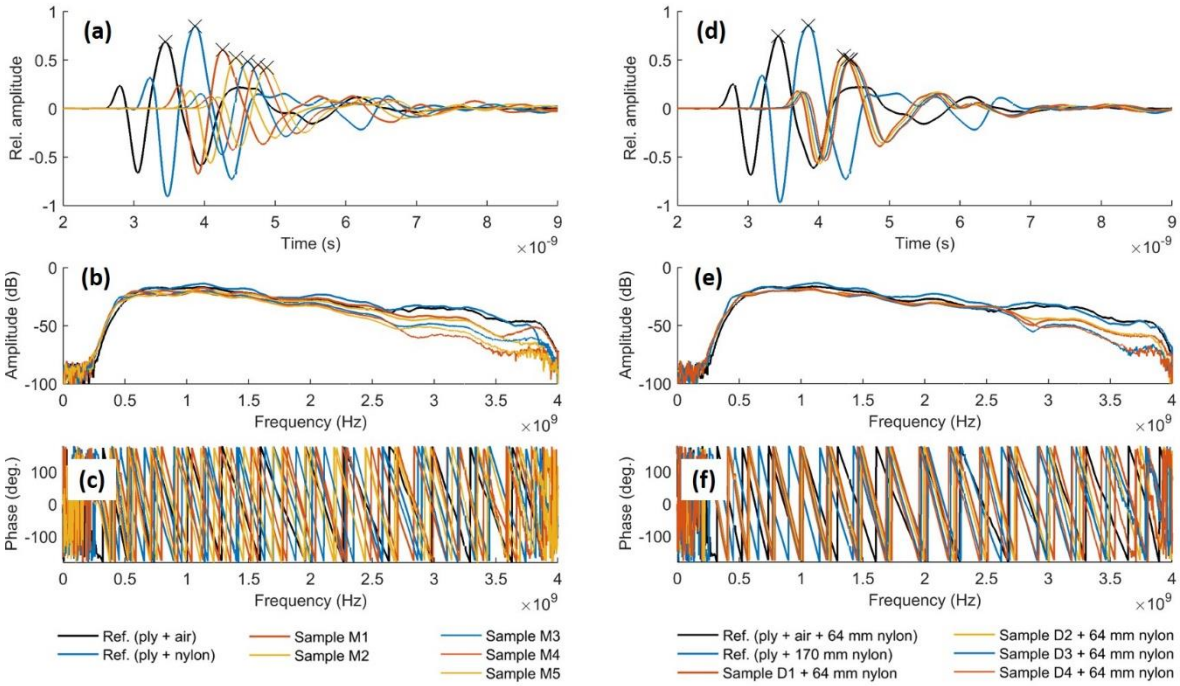

Figure 6: MFS S21 measurements collected on the ply sheet, nylon and moisture-varying samples M1 to M5 shown in the (a) time-domain and as measured by the VNA as (b) amplitude and (c) phase measurements. The MFS S21 measurements shown in the (d) time domain and as (e) amplitude and (f) phase measurements are also shown for the ply

sheet calibration, nylon and density-varying samples D1 to D4, with a 64 mm nylon spacer placed underneath.

The ε_r values calculated from the S_{21} phase measurements using Equation 1 from 1.0 to 2.0 GHz are illustrated in Figure 7. For samples M1 to M5, shown in Figure 7 (a), the results are relatively consistent over this frequency range, showing clear steps in permittivity with each increase in sample moisture content. In comparison samples D1 to D4 show a much smaller increase in the average permittivity with each increase in density, though it is noted that these samples also increase slightly in volumetric moisture content. These measurements, shown in Figure 7 (b), are also more variable over the measured frequency range. This variability is most likely due to the inclusion of the nylon spacer, causing unwanted internal reflections and affecting the phase-measurements.

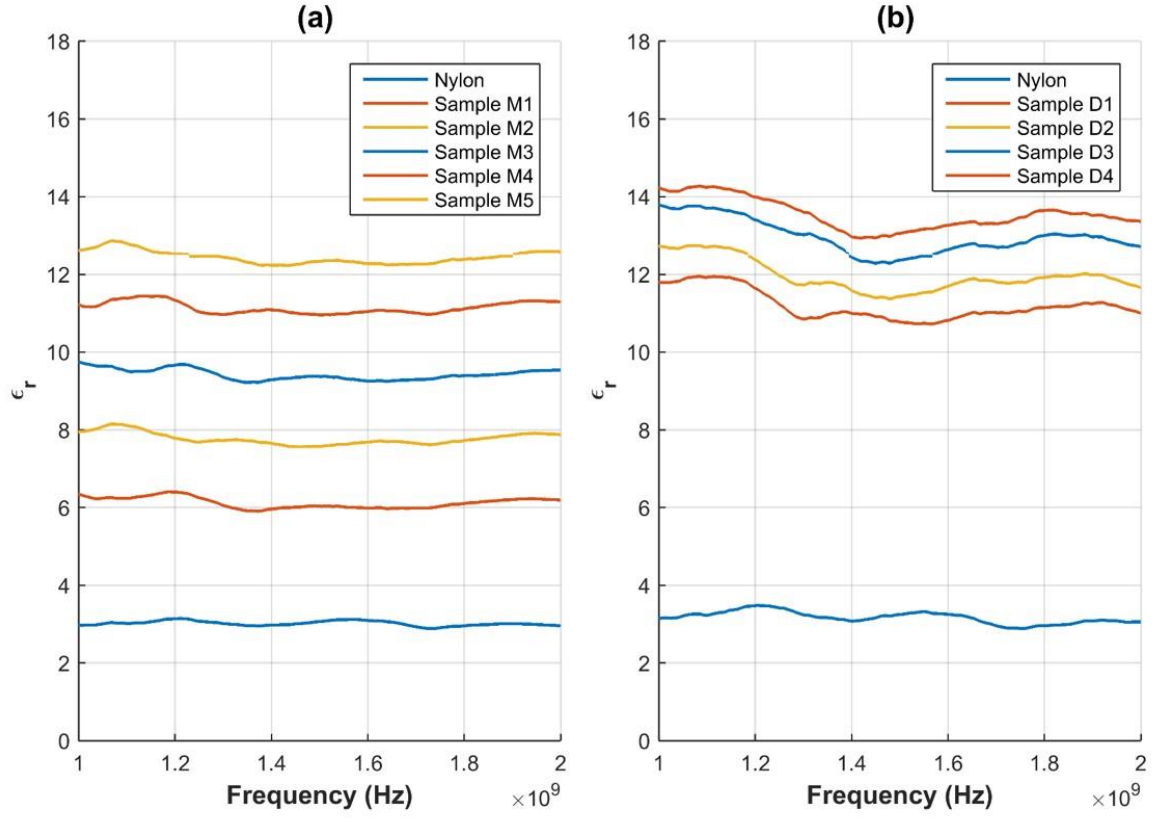

Figure 6: MFS S_{21} frequency-dependent permittivity measurements for (a) nylon and samples M1 to M5, and (b) nylon and samples D1 to D4.

The S_{21} time-domain signals shown in Figure 6 (a) and (b) are also illustrated using a B-scan format in Figure 8 (c) and (f). These are shown alongside the S_{11} time-domain signals recorded by the VNA (Figure 8 (b) and (e)) and the signal recorded by the GPR (Figure 8 (a) and (d)). MFS permittivity measurements based on S_{21} phase-shift, S_{11} two-way travel and S_{21} one-way travel through the MFS samples are included in Table 1.

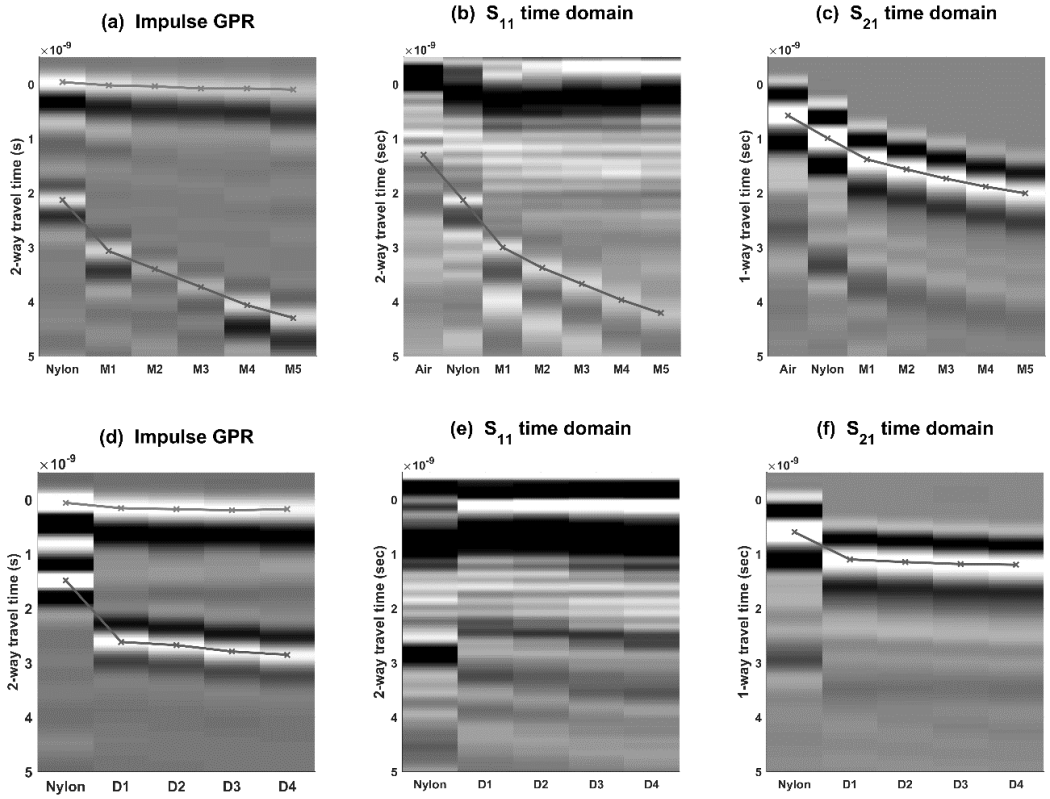

Figure 7: Visual comparison of measurements through air, nylon and moisture-varying samples M1 to M5 using (a) GPR, (b) the reflected MFS S_{11} signal and (c) the transmitted MFS S_{21} signal and for density-varying samples D1 to D4 using (d) GPR, (e) MFS S_{11} and the (f) MFS S_{21} measurements.

3.2 GPR measurements

The GPR measurements collected on MFS and TDR samples are illustrated in Figure 8 (a) and (d) and in Figure 9. The time-domain reflections from the TDR box soffit are indicated in Figure 9 (c) and (d). The reflections from the soffit of sample M1 to M5 (Figure 9 (a)) were not as clearly distinguishable compared to samples D1 to D4 (Figure 9 (b)) due to the combination of changes in sample depth, aspect ratio and strong reflections from the box sides.

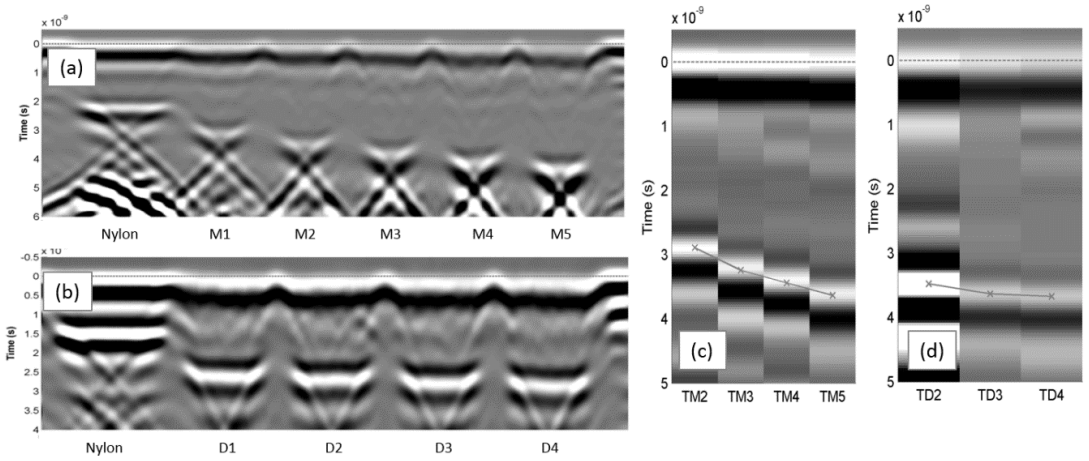

Figure 8: GPR measurements collected on samples of (a) nylon and moisture-varying MFS samples M1 to M5, (b) nylon and density-varying samples D1 to D4, and on (c) moisture-varying TDR samples TM2 to TM5 and (d) density-varying samples TD2 to TD4.

The GPR response collected individually on samples M1 to M5, however, was somewhat clearer and so these measurements were used to produce Figure 8 (a). This was done by taking the average of around 10 measurements when the steel plate was placed up against the soffits of the nylon sample and each sample box, which were then displayed side-by-side to produce the image. Figure 8 (d) was produced in a similar way for samples D1 to D4, though using the measurement at the centre of the nylon sample and each box in Figure 9 (a). The visual comparison of GPR measurements (Figure 8 (a)) and MFS S_{11} measurements (Figure 8 (b)) for nylon and samples M1 to M5 illustrate a similar response, though the GPR measurements are clearer. Likewise, the GPR (Figure 8 (d)) and MFS S_{11} (Figure 8 (e)) measurements for nylon and samples D1 to D4 appear similar, though the GPR is much clearer. The superior response from the GPR antenna is perhaps unsurprising considering this is a refined commercial product. Nonetheless the comparison is important as the similarity provides confidence that the time-domain conversion of the VNA measurements was undertaken correctly. The groundwave and reflected wave arrivals within each GPR scan are also indicated in Figures 8 (a) and (d), and it is observed that the groundwave arrives progressively later in time with increasing sample permittivity illustrating the influence of the ground coupling on the measurement.

Permittivity values calculated from the GPR measurements of UBG samples and using the ray-path approach are summarised in Table 1. They are also illustrated in comparison to MFS and TDR measurements in Figure 10.

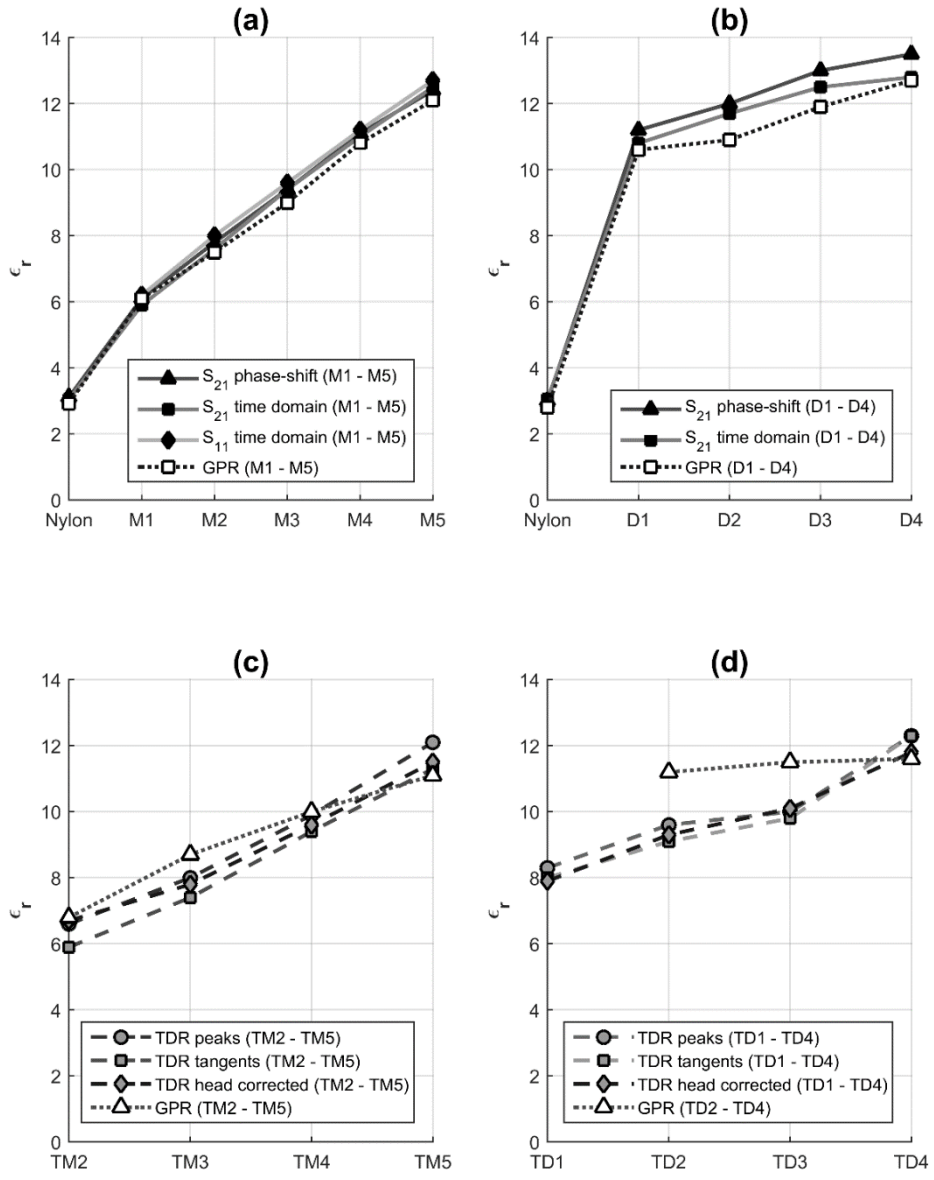

Figure 9: Permittivity measurements collected using GPR and MFS for (a) nylon and samples M1 to M5, (b) nylon and samples D1 to D4; and using GPR and TDR for samples (c) TM2 to TM5, and (d) TD1 to TD4.

3.3 TDR measurements

The TDR measurements were analysed using several different approaches. Initially the method of peaks and the method of tangents (Jiang and Tayabji 1998, Jiang and Tayabji 1999,

Klemunes 1998) were applied to the measurements using a custom Matlab script. The application of these methods to the TDR measurements for samples TM2 to TM5 and TD1 to TD4 are illustrated in Figure 11. The corresponding permittivity results are included in Table 1.

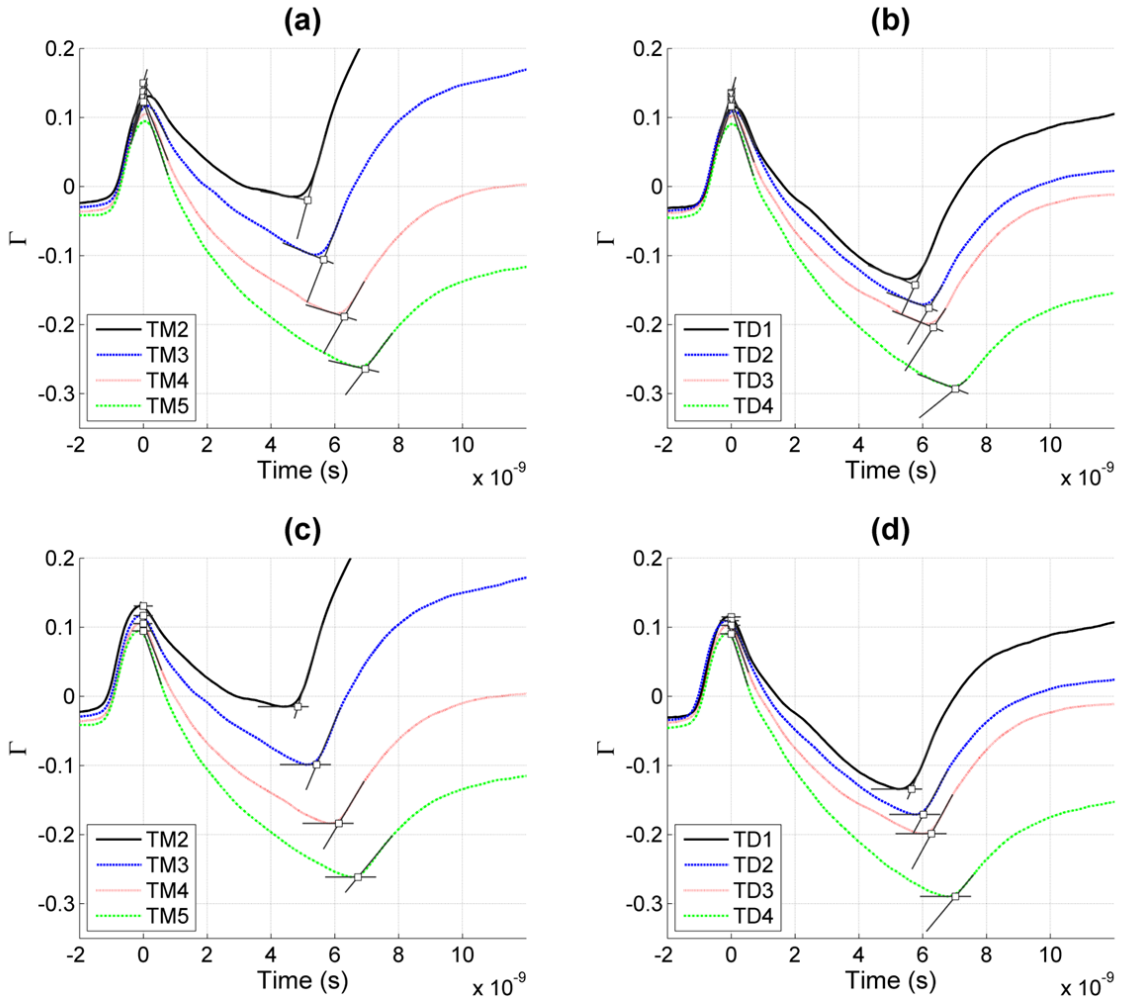

Figure 10: TDR measurements along with the interpreted start and end times for samples using the method of peaks for (a) samples TM2 to TM5 and (b) TD1 to TD4; and using the method of tangents for these same samples, (c) and (d), respectively.

It is observed that the method of tangents produced lower permittivity values compared to the method of peaks, both of which were lower than GPR for drier and lower density samples. A potential issue with these methods, however, is that they do not consider the influence of the travel time within the probe head. To investigate this aspect, an equipment-specific calibration was undertaken. The approach described by Heimovaara (1993) was used to determine the

travel time using the same TDR equipment for a number of liquid samples. An example of this approach applied to a TDR measurement is shown in Figure 12.

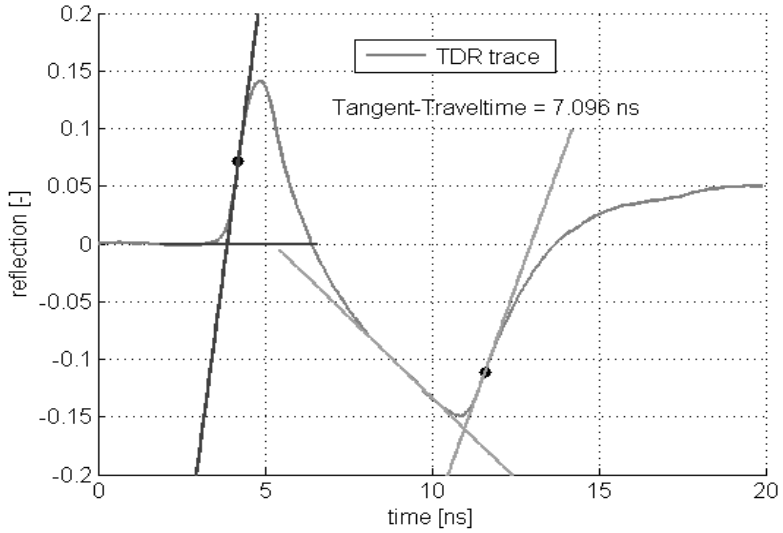

Figure 11: Example of TDR signal analysis using the approach by Heimovaara (1993) to determine the two-way TDR travel time prior to head-correction.

Samples of mineral turpentine, ethanol and distilled water were tested using TDR and this approach. Afterwards the samples were tested using a VNA and an open-ended coaxial line probe (Wagner, et al. 2014). A linear regression was determined between the TDR measurements of two-way travel time and the square root of the mean value of permittivity from 100 MHz to 1.5 GHz for mineral turpentine and distilled water. This regression was used to determine the travel time in the TDR sensor head. The measurement for ethanol was not used for the calibration due to its variability over that frequency range. A sensor head travel time correction of 0.90 ns was determined and was subtracted from the measured two-way travel time determined for the UBG samples using the Heimovaara (1993) approach. These 'head-corrected' permittivity values are reported in Table 1 and were roughly midway between the results determined using the method of peaks and method of tangents.

3.4 Permittivity results and comparisons

The permittivity of each sample compared to θ_v and to dry density as a percentage of the MDD are illustrated in Figure 13. Relations proposed for crushed rock pavement materials by Baran

(1994), Ekblad and Isacsson (2007), for soil by Topp et al. and by Jiang and Tayabji (1998) for coarse grained soils have been included for comparison in Figure 13 (a) and (b).

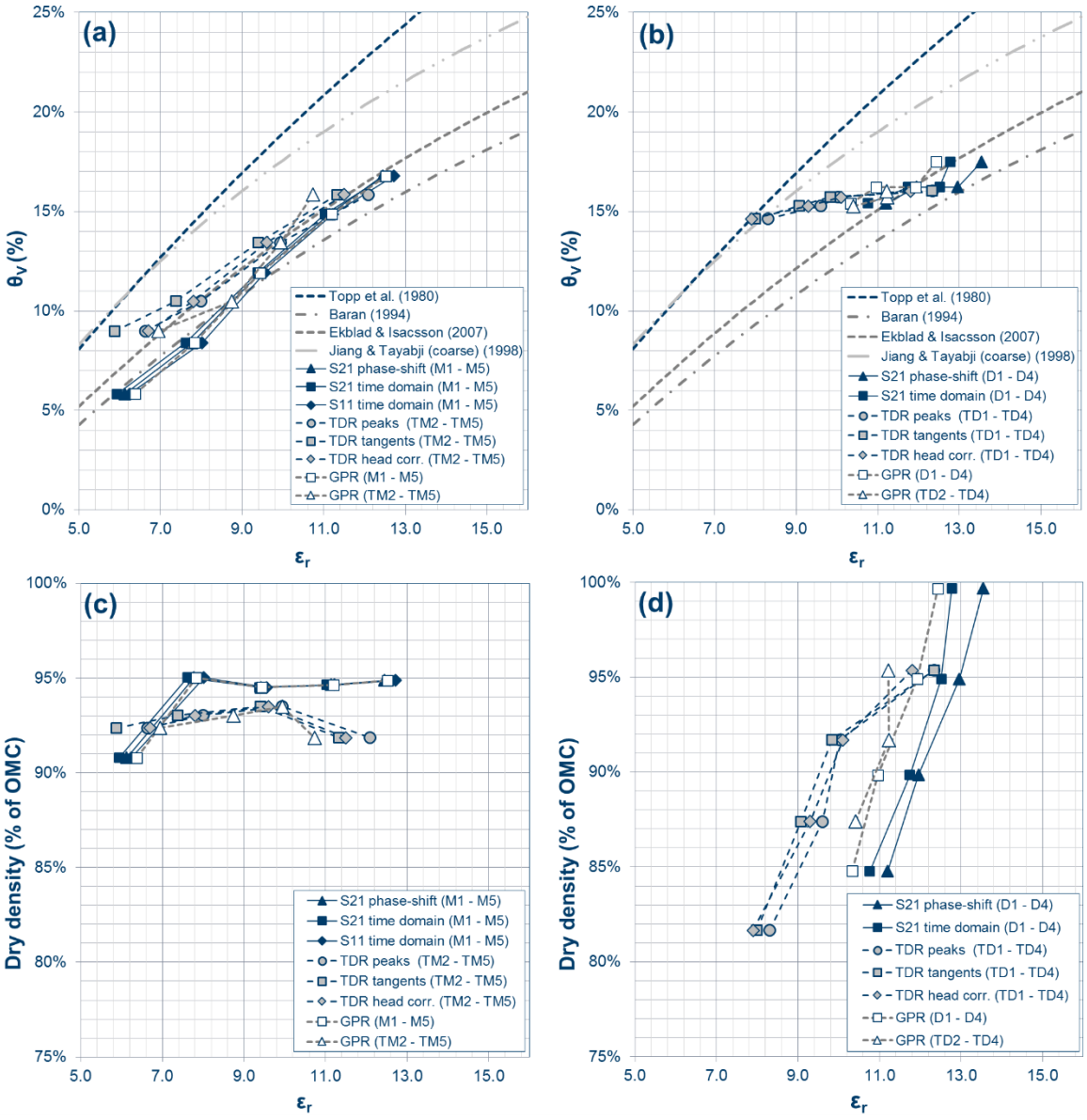

Figure 12: (a) The volumetric moisture content (θ_V) and (c) density of samples compared to permittivity for moisture-varying samples M1 to M5 and TM2 to TM5; and for density-varying samples D1 to D4 and TD1 to TD4, (b) and (d), respectively.

4. Discussion

4.1 Comparing MFS and GPR results

Overall the results illustrated in Figures 10 (a) and 12 (a) and (c) indicate good agreement between MFS and GPR measurements for samples M1 to M5. For the density-varying samples D1 to D4 the GPR results were similar to the MFS results for samples D1 and D4, though slightly lower for samples D2 and D3. These differences may be due to inaccuracies in the assumed material properties of the antenna skid and box materials and simplifications in the ray-path analysis. Such errors will have a greater influence on thinner samples and so may explain why the differences between MFS and GPR were greater for the shallower sample boxes. A possible indication of these issues can be seen in the GPR permittivity measurements of the nylon samples, which calculated $\varepsilon_r = 2.9$ for the thicker 170 mm sample but only $\varepsilon_r = 2.7$ for the 106 mm sample. A difference in the MFS S_{21} phase-shift and MFS S_{21} time-domain permittivity measurements was reported for samples D1 to D4 and can be seen in Figure 10 (b). This is most likely due to the greater variability of MFS results with frequency due to inclusion of the nylon spacers. Specifically, there is a notable increase in permittivity from 1.0 to 1.3 GHz for samples D1 to D4 shown in Figure 7(b). This 'bump' in the results will have increased the mean permittivity result for the phase-shift measurements but is unlikely to have had a great influence on the time-domain measurements. While the inclusion of nylon spacers was intended to improve measurement stability, it appears they have caused more problems than they solved and so are not recommended for future investigations. A consistent sample box size, preferably the deeper 250 x 250 x 170 mm boxes, is recommended to avoid other potential differences when comparing measurements.

4.2 Comparing TDR with GPR and MFS results

Looking at the TDR samples illustrated in Figure 10 (c), for moisture-varying samples TM2 to TM5 there was a relatively good agreement between the TDR and GPR permittivity measurements. For the density-varying TDR samples shown in Figure 10 (d), however, there is a notable difference compared to GPR measurements on the same samples and the overall trend of results. Specifically, the TDR permittivity results were lower compared to GPR for the lower density samples TD2 and TD3, but similar for the highest density sample TD4. For samples TD2 to TD4 the GPR permittivity values varied by only 0.4 compared to between 2.5

and 3.2 for TDR, depending on the analysis method. Unfortunately due to an error in equipment settings no GPR result was available for sample TD1 to complete this comparison.

4.3 Comparison to literature relations and analysis

Comparing to moisture-permittivity relations in the literature, as illustrated in Figure 13 (a) there appears to be reasonable agreement between the various methods on the moisture-varying samples compared to relations determined using TDR for compacted crushed rock road materials by Baran (1994) and by Ekblad and Isacsson (2007). For the drier samples the TDR permittivity results appear to trend towards lower permittivity values. In general the density of TDR samples was a little lower compared to the MFS samples, which may have contributed to this trend. On the other hand, the MFS and GPR measurements for sample M1 seemed to follow a similar trend to that of samples M2 to M5, even though its density was lower than for the TDR samples. Baran (1994) observed a variation in the moisture-permittivity relations with sample density, observing that the Topp equation was only valid for loosely compacted crushed rock.

For the density-varying samples illustrated in Figure 13 (b) and (d), a more pronounced difference can be seen between TDR and the other measurements. For the lower-density samples TD2 to TD3 the TDR reported lower permittivity values compared to GPR measurements on the same samples, though the higher density sample TD4 was similar. The lower-density TDR results also appear shifted to the left in Figure 13 (d) compared to the trend of MFS and GPR measurements for samples D1 to D4. Furthermore, the similarity in the trend of GPR results for samples D1 to D4 and TD2 to TD4 indicates that the variations are more likely due to differences in equipment operation or data analysis rather than material properties.

4.4 Analysis

There are a range of possible reasons for the observed differences between TDR and the MFS and GPR results. Perhaps the simplest explanation is that voids or gaps have formed near the TDR probes. Annular air gaps adjacent to the TDR probes can result in a significant underestimate of permittivity (Whalley 1993). Thus, while care was taken during probe installation to avoid these issues, they would be more likely to occur in lower density or dry samples that are more difficult to compact. In contrast the GPR and MFS approaches measure through the entire sample depth and so would be less susceptible to localised density variations.

Another potential issue is material dispersion, or in other words the variation in real permittivity as a function of frequency (Robinson, et al. 2005). The MFS phase-shift measurements occur over a well-defined frequency range of 1.0 to 2.0 GHz. The frequency range of the time-domain MFS measurements ranges from approximately 400 MHz to 4.0 GHz, as illustrated in Figures 6 (b) and (e). The impulse GPR antenna, rated as a 1.5 GHz model, is expected to exhibit a similar frequency response to the time-domain MFS measurements. The effective frequency of the TDR measurements was estimated using the same approach used by Robinson et al. (2005). For the moisture-varying and density-varying samples the effective frequency was essentially constant, ranging between approximately 80 MHz and 105 MHz. These frequencies are lower compared to the MFS and GPR measurements and so may be a potential source of the observed differences. That is, if changes in the sample permittivity or the influence of conductivity with frequency has had a varying effect on the different measurement methods. For example, numerical simulations indicate the apparent permittivity determined using TDR will be influenced by variations in the cable length and the sample electrical conductivity when measuring dispersive materials (Chung and Lin 2009). For GPR, however, the influence of conductivity is often considered insignificant at radar frequencies (Cassidy 2009).

Another potential source of difference is in the influence of the TDR sensor head. While a calibration process was undertaken to determine the head-corrected permittivity results, only two liquids were used for the calibration which may not have been adequate. This approach also assumes that the travel time is constant within the head, which may not be the case if the EM fields extend beyond the sensor head and are influenced by the surrounding dielectric. The influence of the TDR sensor head can therefore not be discounted as a potential cause of the observed differences. In addition to these issues, there were a number of limitations in the experimental approach that need to be considered. For one, only a relatively small number of samples were investigated. The results may also have been influenced by inconsistences due to differing box depths, inclusion of nylon spacers and slight variations in the volumetric moisture content for the density-varying samples. A more extensive comparison of TDR, GPR and MFS measurements, with changes to address these issues, is recommended to confirm the trends and differences observed in this study.

4.5 MFS advantages and disadvantages

In any case, the main purpose of this investigation was not to focus on differences with TDR per se. Rather, the aim was to see if variations in sample moisture and density influenced the MFS results in a similar manner to GPR, and to investigate its suitability as a permittivity calibration approach. As illustrated in Figures 10 and 13, overall the MFS approach produced permittivity results that compared relatively well with common-offset GPR measurements of moisture-varying and density-varying UBG samples. An advantage of the MFS approach compared to TDR and GPR is the increased precision of frequency-domain measurements. Provided the issue of phase-shift ambiguity (Trabelsi, Kraszewski and Nelson 2000) is addressed, the phase-shift measurements are precise and avoid the need to subjectively choose peaks or other features within the time-domain signal. In addition, the transmitted and reflected signals recorded by the VNA can also be used to generate time-domain signals that can be used as a secondary check on the sample permittivity, but can also be used to identify unwanted reflections or other features in the measured response. The measurements are quick and can be collected through relatively thick material samples, providing potential for more representative measurements of bulk material properties and avoiding the installation sensitivity of TDR probes. Using antennas along a single axis avoids the refraction issues encountered with ground-coupled common-offset GPR measurements, particularly for relatively shallow samples. As the phase-shift measurements are based on transmitted signals they have potential to be used on deeper samples or on lossy materials that may be more difficult to penetrate using GPR. While it is possible to use two conventional common-offset antennas in a transmission or multi-offset configuration (e.g. Klysz 2004), the larger aim of the work is to enable greater use of the new NM-GPR technology. As the approach uses similar antennas, which band-limits the signal, the MFS measurements inherently occur over the same frequency range as the NM-GPR equipment, eliminating this element of uncertainty when comparing results. Furthermore, the MFS equipment can be used for other purposes. For example, the same antennas and VNA can be used to collect multi-offset data on which to test analysis methods as well as testing different antenna types and configurations.

There are, however, a number of disadvantages in using the MFS approach. While data collection is relatively straightforward, it is still necessary to analyse the VNA measurements. This includes steps to unwrap the phase measurements, determine the phase-shift and address the phase-shift ambiguity issue when determining the sample permittivity. As seen in this

study, changes in the test setup (e.g. the addition of nylon spacers) can lead to variations in phase that may go unnoticed during testing and cause issues. However, these problems can be limited by using a consistent apparatus and approach. Compared to the commercial impulse GPR measurements, the quality of the MFS reflected signal was not as refined, though this antenna was fairly rudimentary and could be further improved. Issues with moisture absorption into the sample box are also an issue in the current approach that needs to be addressed. Nonetheless, the MFS approach provides a viable alternative to existing methods for measuring the permittivity of civil engineering materials that appears to agree well with GPR measurements.

5. Conclusions

This paper reports on an experiment comparing permittivity measurements determined using MFS, GPR and TDR techniques on samples of UBG road pavement materials prepared to a range of moisture contents and densities. The results indicate reasonably good agreement between MFS and GPR measurements which also compare well with literature relations for crushed rock pavement materials. The TDR results were relatively consistent with those literature relations, though they appeared to deviate from the GPR and trend of MFS results for lower density and drier samples. A more extensive study comparing MFS, GPR and TDR using a greater number of samples and a wider range of materials is recommended to further investigate the observed trends and differences between these methods.

Acknowledgements

This work was funded under the National Asset Centre of Excellence (NACOE) research project P12 ‘Field-validation of Noise Modulated Ground Penetrating Radar’ by the Queensland Department of Transport and Main Roads (TMR). The authors express their thanks to Dr Bryan Reeves for assistance during this work, Jason Maudsley for efforts in UBG sample preparation, Thierry Bore for collecting the surface probe measurements and Ajith (Diss) Dissanayake for advice regarding the sample petrography. This paper supports and contributes to the work of COST Action TU1208 ‘Civil Engineering applications of Ground Penetrating Radar’. The presented research is supported by a Queensland Science Fellowship awarded to A. Scheuermann.

References

I.L. Al-Qadi 1992. Using Microwave Measurements to Detect Moisture in Asphaltic Concrete. Journal of Testing and Evaluation 20, 43-50.

I.L. Al-Qadi, D.K. Ghodgaonkar, V.K. Varada and V.V. Varadan 1991. Effect of moisture on asphaltic concrete at microwave frequencies. IEEE Transactions on Geoscience and Remote Sensing 29, 710-717.

E. Baran 1994. Use of time domain reflectometry for monitoring moisture changes in crushed rock pavements. Symposium and workshop on time domain reflectometry in environmental, infrastructure and mining applications, Northwestern University, Evanston, Illinois, USA, 349-356.

C. Berthelot, D. Podborochynski, T. Saarenketo, B. Marjerison and C. Prang 2010. Ground-penetrating radar evaluation of moisture and frost across typical Saskatchewan road soils. Advances in Civil Engineering 2010, 1-9.

N.J. Cassidy 2009. Electrical and magnetic properties of rocks, soils and fluids. In: *Ground Penetrating Radar: Theory and applications* (ed. H.M. Jol), 41-72. Elsevier Science.

C.M. Chang, J.S. Chen and T.B. Wu 2011. Dielectric modelling of asphalt mixtures and relationship with density. Journal of transportation engineering 137, 104-111.

R. Charlier, P. Hornych, M. Sršen, Å. Hermansson, G. Bjarnason, S. Erlingsson and P. Pavšič 2009. Water influence on bearing capacity and pavement performance: Field observations. In: *Water in roads* (ed. A. Dawson), 175-192. Springer Science+Business Media B.V.

A.J.L. Chazelas, B.X. Derobert, C.M. Adous, D.G. Villain, E.V. Baltazart, F.L. Laguerre and G.P. Queffelec 2007. EM characterization of bituminous concretes using a quadratic experimental design. 4th International workshop on Advanced Ground Penetrating Radar (IWAGPR-2007) Naples, Italy, 278-283.

C.C. Chung and C.P. Lin 2009. Apparent dielectric constant and effective frequency of TDR measurements: Influencing factors and comparison. Vadose Zone Journal 8, 548-556.

Department of Transport and Main Roads 2014. Material testing manual, 4th edition, Brisbane, Australia.

Department of Transport and Main Roads 2015. MRTS05 Unbound pavements, Technical Specification, Brisbane, Australia.

B. Diefenderfer, I. Al-Qadi and A. Loulizi 2000. Laboratory calibration and in situ measurements of moisture by using time-domain reflectometry probes. Transportation Research Record: Journal of the Transportation Research Board 1699, 142-150.

J. Ekblad and U. Isacsson 2007. Time-domain reflectometry measurements and soil-water characteristic curves of coarse granular materials used in road pavements. Canadian Geotechnical Journal 44, 858-872.

R.D. Evans, M.W. Frost, N. Dixon and M. Stonecliffe-Jones 2008. The response of ground penetrating radar (GPR) to changes in temperature and moisture condition of pavement materials. Advances in Transportation Geotechnics, Nottingham, UK, 713-718.

C. Fauchard, X. Dérobert, J. Cariou and P. Côte 2003. GPR performances for thickness calibration on road test sites. NDT & E International 36, 67-75.

K. Grote, S. Hubbard, J. Harvey and Y. Rubin 2005. Evaluation of infiltration in layered pavements using surface GPR reflection techniques. Journal of Applied Geophysics 57, 129-153.

T.J. Heimovaara 1993. Design of Triple-Wire Time Domain Reflectometry Probes in Practice and Theory. Soil Science Society of America Journal 57, 1410-1417.

Y. Huang 2001. Design, calibration and data interpretation for a one-port large coaxial dielectric measurement cell. Measurement Science and Technology 12, 111–115.

J.A. Huisman, S.S. Hubbard, J.D. Redman and A.P. Annan 2003. Measuring soil water content with Ground Penetrating Radar: A review. Vadose Zone Journal 2, 476-491.

Y.J. Jiang and S.D. Tayabji 1998. Evaluation of in situ moisture content at long-term pavement performance seasonal monitoring program sites. Transportation Research Record: Journal of the Transportation Research Board 1655, 32-40.

Y.J. Jiang and S.D. Tayabji 1999. Analysis of time domain reflectometry data from LTPP seasonal monitoring program test sections - Final report. In: Analysis of time domain reflectometry data from LTPP seasonal monitoring program test sections - Final report. US Department of Transportation, Federal Highway Administration.

J. Klemunes, Jr 1998. Determining soil volumetric moisture content using time domain reflectometry. In: Determining soil volumetric moisture content using time domain reflectometry. Federal Highways Administration (USA).

G. Klysz 2004. Spectral analysis of radar surface waves for non-destructive evaluation of cover concrete. NDT & E International 37, 221-227.

R. Liang, K. Al-Akhras and S. Rabab'ah 2006. Field monitoring of moisture variations under flexible pavement. Transportation Research Record: Journal of the Transportation Research Board 1967, 160-172.

L. Liu and T. Guo 2003. Determining the condition of hot mix asphalt specimens in dry, water-saturated, and frozen conditions using GPR. Journal of Environmental and Engineering Geophysics 8, 46-52.

S.D. Logsdon 2000. Effect of cable length on time domain reflectometry calibration for high surface area soils. Soil Science Society of America Journal 64, 54-61.

A. Loizos and C. Plati 2007. Accuracy of pavement thicknesses estimation using different ground penetrating radar analysis approaches. NDT & E International 40, 147-157.

S.G. Millard, I.L. Al-Qadi, M.R. Shaw, S.M. Riad, A. Shaari and J.H. Bungey 2001. Coaxial transmission lines: Development of test procedures for concrete. Journal of Materials in Civil Engineering 13, 202-208.

W. Muller 2014. Self-correcting pavement layer depth estimates using 3D multi-offset ground penetrating radar (GPR). 15th International Conference on Ground Penetrating Radar (GPR-2014), Brussels, Belgium, 887-892.

W. Muller 2016. Permittivity characterization of unbound granular pavement materials using a modified free-space approach. Paper accepted for publication in: Transportation Research Record: Journal of the Transportation Research Board.

W. Muller and X. Dérobert 2013. A comparison of phase-shift and one-port coaxial cell permittivity measurements for GPR applications. 7th International Workshop on advanced ground penetrating radar (IWAGPR-2013), 1-6.

W. Muller and A. Scheuermann 2016. Optimising a modified free-space permittivity characterisation method for civil engineering applications. Journal of Geophysics and Engineering 13, S9-S18.

W. Muller, A. Scheuermann and B. Reeves 2012. Quantitative moisture measurement of road pavements using 3D GPR. 14th International Conference on Ground Penetrating Radar (GPR-2012), Shanghai, China, 517-523.

B. Panzner, A. Jostingmeier and O. Abbas 2010. Estimation of soil electromagnetic parameters using frequency domain techniques. 13th International Conference on Ground Penetrating Radar (GPR-2010), Lecce, Italy, 1-5.

T. Pellinen, E. Huuskonen-Snicker, P. Eskelinen and P. Olmos Martinez 2015. Representative volume element of asphalt pavement for electromagnetic measurements. Journal of Traffic and Transportation Engineering (English Edition) 2, 30-39.

R. Plooy, G. Villain, S. Palma Lopes, A. Ihamouten, X. Dérobert and B. Thauvin 2013. Electromagnetic non-destructive evaluation techniques for the monitoring of water and

chloride ingress into concrete: a comparative study. Materials and Structures 48, 369-386.

N.R. Rainwater, E.C. Drumm, R.E. Yoder and G.V. Wilson 1999. Comprehensive monitoring systems for measuring subgrade moisture conditions. Journal of Transportation Engineering 125, 439-448.

B. Reeves 2014. Noise modulated GPR: Second generation technology. 15th International Conference on Ground Penetrating Radar (GPR-2014), 708-713.

C.A. Richter 2006. Long-Term Pavement Performance Program: Seasonal Variations in the Moduli of Unbound Pavement Layers. Publication no. FHWA-HRT-04-079. Federal Highways Administration (FHWA), USA.

D.A. Robinson, M.G. Schaap, D. Or and S.B. Jones 2005. On the effective measurement frequency of time domain reflectometry in dispersive and nonconductive dielectric materials. Water Resources Research 41 (2).

T. Saarenketo 1998. Electrical properties of water in clay and silty soils. Journal of applied geophysics 40, 73-88.

T. Saevarsdottir and S. Erlingsson 2013. Effect of moisture content on pavement behaviour in a heavy vehicle simulator test. Road Materials and Pavement Design 14, 274-286.

J. Shang and J. Umana 1999. Dielectric constant and relaxation time of asphalt pavement materials. Journal of Infrastructure Systems 5, 135-142.

A. Tarantino, A.M. Ridley and D.G. Toll 2008. Field Measurement of suction, water content, and water permeability. Geotechnical and Geological Engineering 26, 751-782.

S. Trabelsi, A.W. Kraszewski and S.O. Nelson 2000. Phase-shift ambiguity in microwave dielectric properties measurements. IEEE Transactions on Instrumentation and Measurement 49, 56-60.

N. Wagner, M. Schwing and A. Scheuermann 2014. Numerical 3-D FEM and experimental analysis of the open-ended coaxial line technique for microwave dielectric spectroscopy on soil. Geoscience and Remote Sensing, IEEE Transactions on 52, 880-893.

W.R. Whalley 1993. Considerations on the use of time-domain reflectometry (TDR) for measuring soil water content. Journal of Soil Science 44, 1-9.

Paper VII

Muller, W.B., Semi-automatic determination of layer depth, permittivity and moisture for unbound granular pavements using multi-offset 3D GPR, Submitted 11 August 2016 to the Journal of Applied Geophysics

This page left intentionally blank

Semi-automatic determination of layer depth, permittivity and moisture for unbound granular pavements using multi-offset 3D GPR

Wayne B. Muller[*a,b]

a. Department of Transport and Main Roads, 35 Butterfield Street, Herston, Queensland, Australia 4006

b. School of Civil Engineering, The University of Queensland, Queensland, Australia 4072

* Corresponding author. Email wayne.b.muller@tmr.qld.gov.au

Abstract – A novel semi-automated multi-offset ground penetrating radar (GPR) analysis method has been developed. It was used to predict the depth, permittivity and volumetric moisture content of unbound granular (UBG) pavement layers along a recently-constructed site. The predictions compared well with physical measurements of layer depth and moisture at selected locations, however permittivity predictions were somewhat higher compared to results based on time domain reflectometry (TDR) and common-offset GPR measurements of buried reflectors. The ability to monitor pavement moisture along the site and over time using the approach was demonstrated by comparing multi-offset GPR predictions and also TDR and common-offset GPR measurements collected approximately 11 months apart. The reproducibility of results using the analysis approach was also confirmed by comparing predictions for repeat runs along the site. The key benefits, limitations and a number of potential uses for the approach are also discussed.

Keywords: Multi-offset ground penetrating radar, road pavements, moisture quantification, permittivity, time domain reflectometry.

1 Introduction

Thin bituminous pavements comprising layers of compacted unbound granular (UBG) materials and a sprayed chip seal or thin asphalt surfacing are commonly used within Australia and elsewhere [1, 2]. As moisture significantly influences the performance of these pavements [3], affects the resilient response of unbound aggregates [4] and can lead to premature failure of new UBG pavements [5], techniques for quantifying water within these materials are of interest for a range of road investigation and monitoring uses. Of available soil moisture measurement techniques [6-8], high-frequency electromagnetic (EM) methods are the most

promising category enabling measurements at a range of spatial scales [9]. Time domain reflectometry (TDR) is one such method used by many researchers to monitor temporal variations of pavement and subgrade moisture [10-15], although the need for embedded sensors reduces its practicality for large-scale pavement monitoring. Ground penetrating radar (GPR) has also been used to detect moisture variations within pavements using qualitative analysis methods [16-18]. Quantitative estimates are also possible based on measuring the surface reflection coefficient or the velocity of EM waves reflected from subsurface layer interfaces, propagating as the groundwave or passing between boreholes [9]. The apparent permittivity of pavement layers determined from these measurements [9] can then be related to the volumetric moisture content using the Topp equation [19] or variants calibrated for compacted granular pavement materials [10, 12]. To enable safe and efficient use of these techniques on roads, rapid non-invasive data collection methods are required. The surface reflection coefficient method is one approach offering these advantages, however it is normally used assuming homogenous layers without moisture or defects present [20-22]. While this approach has been used to estimate pavement permittivity and moisture content [23, 24] estimates have also been observed to change with antenna frequency, most likely due moisture inhomogeneity with depth [23].

Another data collection approach is multi-offset GPR, which involves collecting a series of measurements with different offsets between transmitting and receiving antennas. The depth of pavement layers and velocity of EM waves within these materials can then be determined based on the arrival time of reflections returning from layer interfaces measured at these different offsets. While this approach has been widely used for measuring soil moisture [25-30], it has only been used to a limited extent for pavement moisture quantification [31, 32]. The approach has been more widely used for calibrating the depth and permittivity of pavement layers where the response of common-offset ground and air-coupled antennas [20, 21] or air-coupled antenna pairs [33, 34] have been combined or air-coupled three-dimensional (3D) GPR systems have been used [35, 36] to achieve mobile multi-offset measurements at regular spacings along the road. Automated analysis methods have also been developed to determine the depth of a single pavement layer using two-antenna offsets [21] and conventional geophysical techniques such as semblance and the Dix equation [37] or its variants have been used to analyse road data collected with multiple antenna offsets [38, 39]. An advantage of the multi-offset approach compared to surface-reflection methods is that permittivity estimates are

based on the mean travel time through the full depth of pavement layers and therefore account for vertical inhomogeneity [20, 21], although data analysis is usually more complicated. While previous studies have used air-coupled antennas to maximise the speed of data collection this is problematic because refraction at the ground surface limits the sensitivity of velocity calibrations [40] and presents a number of challenges when applying conventional semblance analysis techniques [35]. While ground-coupled measurements are preferable [40], suitable equipment able to collect these data along the road has not been readily available.

In this study a recently-updated 3D noise-modulated GPR (NM-GPR) technology [41] was used to collect multi-offset measurements using ground-coupled antenna arrays. The equipment was configured to collect four adjacent wide angle reflection and refraction (WARR) gathers quasi-continuously while travelling along the road. These measurements partially overlap and so also achieve multi-fold coverage of the subsurface layers. Prior to equipment completion, semi-automated implementations of conventional [42] and two self-correcting geophysical methods [43] were investigated using numerical simulations. A modified free-space (MFS) permittivity characterisation approach was also developed to calibrate petro-physical relations for UBG pavement materials to enable field moisture predictions [42, 44-46]. In this paper an improved semi-automated analysis method is presented. It was used to predict the depth, permittivity and volumetric moisture content of UBG pavement layers along a recently-constructed site on two occasions approximately 11 months apart. Predictions from these visits were compared and results from the later investigation were validated using a combination of physical sampling, embedded sensor and surface measurements. The paper commences with an overview of the site and equipment used for the experiment. It then describes the multi-offset analysis procedure and presents the results of field trials and validations. Potential sources of analysis error, benefits, limitatons and possible uses of the approach are also discussed.

2 Site investigation

2.1. Site and equipment details

The site for these investigations was the Fischer Park truck stop, located adjacent to the Cunningham Highway approximately five kilometres south of Cunningham's Gap in Queensland, Australia. It was constructed between March and June 2015 and consists of two,

and in places three, layers of compacted UBG pavement materials each approximately 150 mm thick. The first half of the site was constructed in two layers, a base layer and sub-base layer. The second half was constructed in three layers – base, upper sub-base and lower sub-base. All of pavement layers were constructed in accordance with MRTS 11.05 Unbound Pavements [47] and all except for the lower sub-base used the same Type 2.1 UBG crushed rock gravel manufactured from a hornfels metamorphic source. This material had previously been characterised as part of a laboratory investigation, details of which can be found elsewhere [48]. The lower sub-base was constructed using a Type 2.5 material which was manufactured using the same source materials but to a lower California Bearing Ratio (CBR) requirement.

The site was instrumented at one location using a number of conventional rod-probe (Campbell Scientific model CS610-L) and ribbon TDR sensors. Only the rod-probe sensors were used in this study. A Campbell Scientific TDR100 was used for the measurements, connected to the probes via approximately 25 metres of RG8 coaxial cable. Three rod-probe sensors were installed at the interface of the lower sub-base and upper sub-base layers and two more were installed at the interface of the base and upper sub-base. A 300 x 900 x 0.5 mm aluminium sheet and a 1 metre long 10 mm dimeter steel rod were placed near the TDR sensors and also at the subgrade interface. The purpose of the plates was to provide distinct reflectors to ensure clear identification of each interface within the GPR response. The purpose of the steel rods was to provide point reflectors to enable permittivity determination for the overlying material based on the hyperbolic shape of the measured response using a conventional common-offset GPR [49]. The shielding within the buried coaxial TDR cables can also be used for this purpose. Figure 1 shows the arrangement of TDR sensors and metal reflectors during installation.

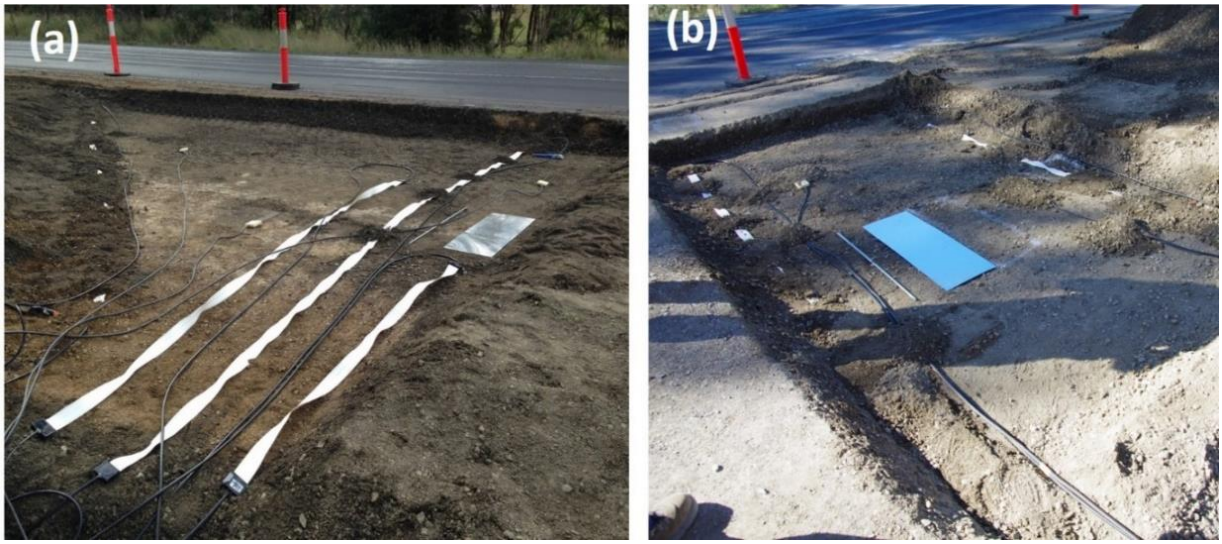

Figure 1: Installation of TDR sensors and reflectors (a) at the interface of upper and lower sub-base and (b) at the interface of upper sub-base and base layers

2.2. GPR equipment

The 3D NM-GPR systems used for the site investigations are shown in Figure 2. These systems use the same control unit but the antennas are housed in different trailer designs. A prototype trailer was used for Site Visit 1, designated T02 (Figure 2 (a)).

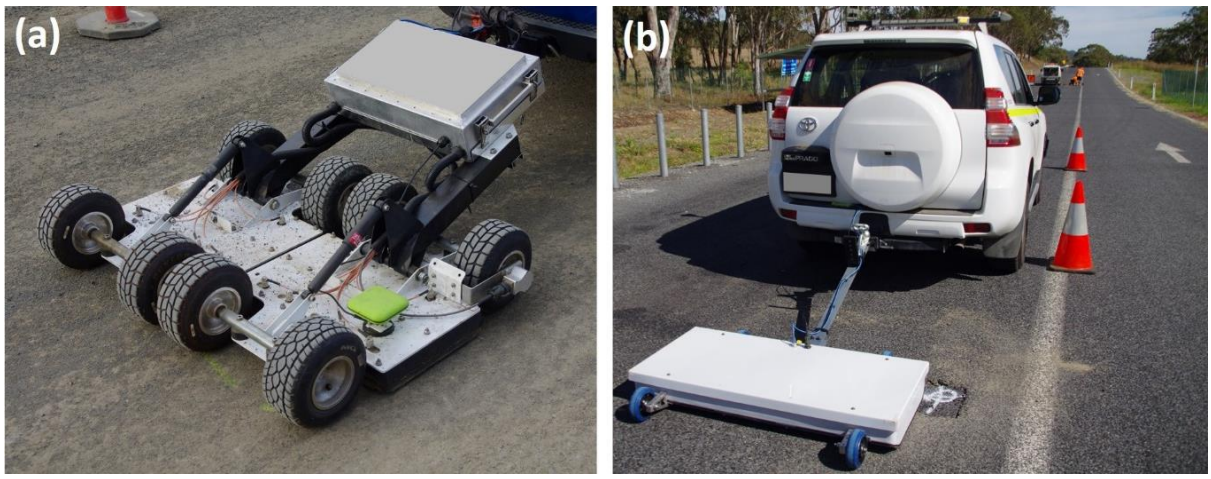

Figure 2: Ground-coupled NM-GPR equipment used during (a) Site Visit 1 and (b) Site Visit 2

The antennas in T02 are arranged as a row of four transmitters ahead of a row of eight receivers spaced evenly across the 1.2 metre wide array (Figure 3). They are housed within two adjacent pods, half the number used in the larger trailer system used previously [50]. Like its larger brother, this equipment can collect ground-coupled measurements at up to 100 kilometres per

hour. For this study the NM-GPR control unit was configured to operate the four transmitters within T02 in sequence while simultaneously recording at the eight receiving antenna positions (Figure 3 (a) to (d)). The resulting response is four partially-overlapping WARR gathers recorded on 32 GPR channels. Alternatively the response can be considered as 14 non-overlapping virtual antenna pairs with their central locations indicated as black dots in Figure 3. A NM-GPR trailer designed for utility investigations was used for Site Visit 2, due to its availability at the time of testing (Figure 2 (b)). That system, designated T03, contains eight transmitters and eight receivers. For this study only four of the transmitters were operated to achieve a configuration similar to that shown in Figure 3. For both investigations an encoder wheel was used to trigger distance-based sampling and GPS coordinates were collected.

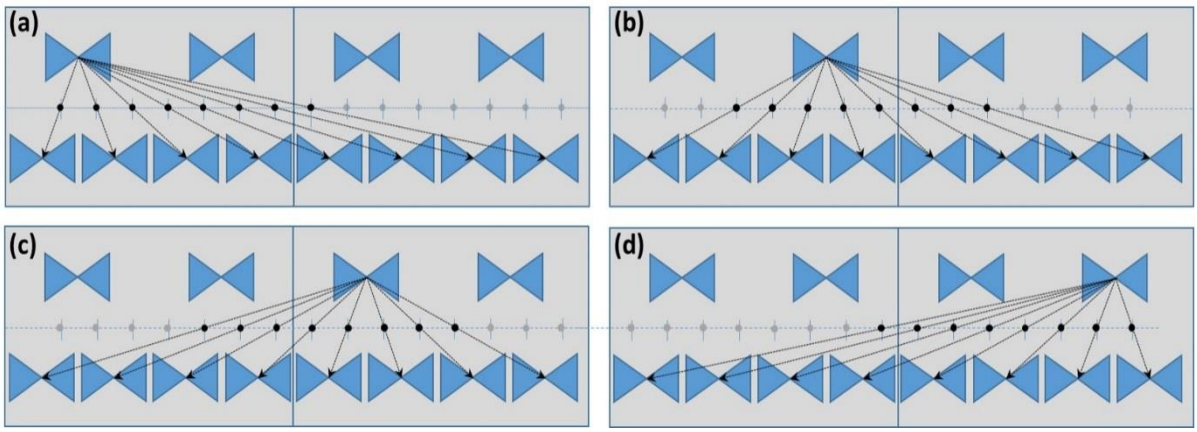

Figure 3: Antenna configuration and transmitter operating sequence

The common-offset impulse GPR system used for this study was a Geophysical Survey Systems Inc. (GSSI) SIR-3000 control unit connected to a 1.5 GHz ground-coupled antenna (model 5100B). The antenna was placed on a thin polyethylene skid with an encoder wheel to trigger distance-based sampling.

3 Analysis approach

The approach developed to analyse the multi-offset data collected during the site investigations is called ray-path modelling – semblance (RM-S). It combines elements of the two previously-developed analysis methods [43], which were implementations of reflection tomography and migration velocity analysis [51], with the semblance technique to create a hybrid approach that is applied in a semi-automated manner. The analysis procedure commences much like a conventional common-offset GPR investigation: A radargram (B-scan) is displayed for a single

pair of antennas within the array; the operator selects the start and end points of a number of layer interface reflections of interest which are automatically tracked along the road using conventional phase-following techniques. Once all interfaces of interest have been selected and tracked the operator instigates the RM-S procedure. After this point the analysis is fully automatic. The algorithm undertakes multi-offset analysis at regular intervals along the length of road with layer tracks. At the first location, the uppermost tracked interface is used as a seed point and the signal peak at this location is followed from one WARR gather to the next, but only for the subset of GPR channels where the receiving antennas are physically closest to each transmitter. It then tests the validity of a number of trial permittivity values for the uppermost layer. This involves optimising the depth and dipping angle using a ray-path (ray-tracing) model using the trial permittivity so the predicted travel times best match the tracked values on a number of adjacent WARR gathers, with the number depending on the analysis variant. The travel times at all other antenna offsets are then determined using these parameters and the corresponding signal strengths within the measured WARR response are determined. This procedure is repeated for all other trial permittivity values and the correct combination of trial permittivity, depth and dipping angle is selected as that producing the strongest mean response of the same polarity as the tracked interface. The algorithm then fixes these parameters for the completed layer within the ray-path model and then analyses the next layer. Once all layers have been competed the algorithm moves on to assess the next location along the road.

The variant of the RM-S approach used in this paper (RM-S1) involved numerically optimising the ray-path model to best match all near-transmitter receivers across the array width. The antenna skid was also included within the ray-path model as part of this analysis, with the skid depth increased slightly to account for the increased travel time through the 10 mm air-gap to the road surface.

4 Data collection and analysis

The NM-GPR measurements for Site Visit 1 were collected on 8 June 2015. TDR and impulse GPR measurements were collected the following day and the site was bitumen sealed two days later. Site Visit 2 occurred on 19 May 2016 and involved the collection of NM-GPR, impulse GPR and TDR measurements and a number of physical samples along the length of the site. No rain occurred during these periods. Figure 4 shows the response recorded using impulse GPR over the location of embedded TDR sensors and metal reflectors during each site visit.

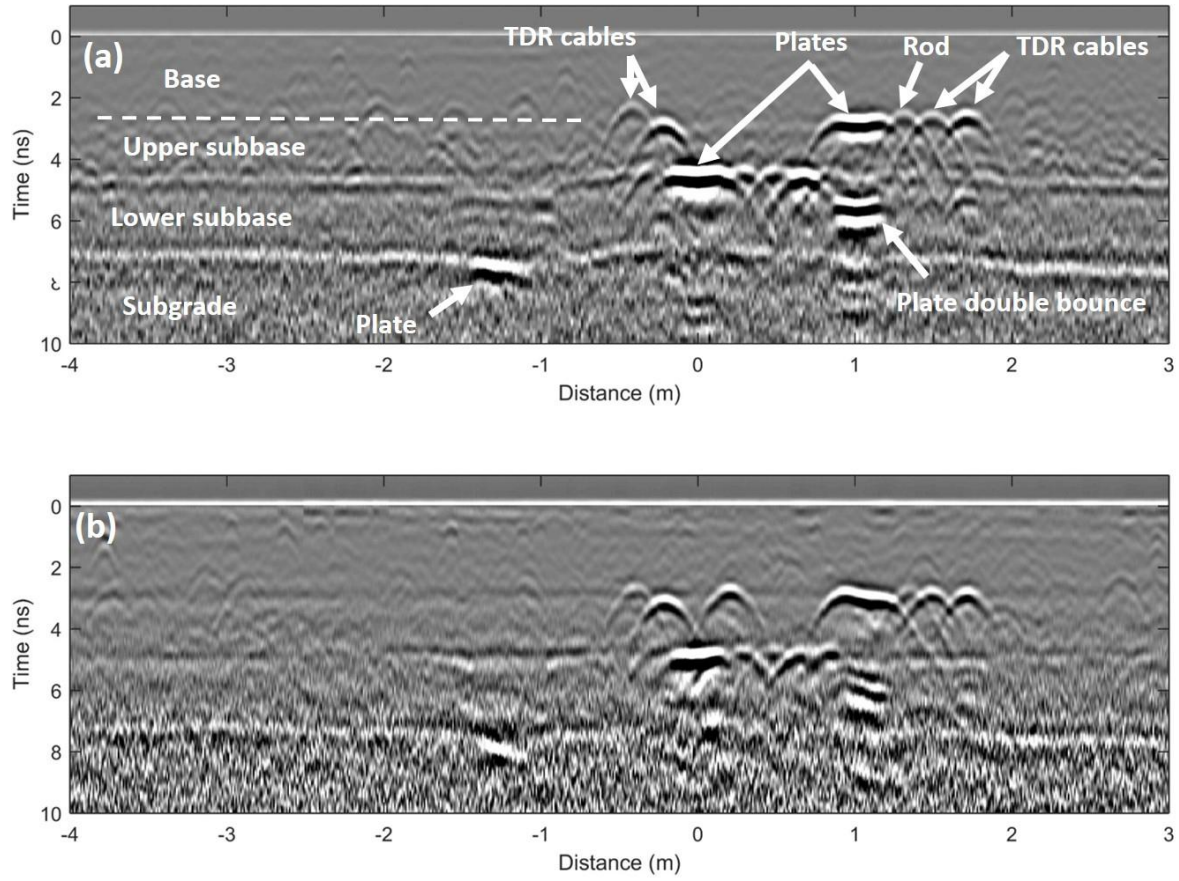

Figure 4: Common-offset GPR radargrams collected over the location of embedded TDR sensors and metal reflectors during (a) Site Visit 1 and (b) Site Visit 2

The NM-GPR and impulse GPR scans collected during each site visit were aligned with each other and were positioned laterally to target the approximate centreline. For Site Visit 1 no surfacing or line markings were present and this position was estimated visually. For Site Visit 2 the alignment of scans and investigation holes was adjusted slightly to avoid damaging the pavement near the wheel-paths of the traffic lane. A later comparison using the GPS coordinates collected during these investigations indicated a lateral offset of up to 2 metres between site visits. The NM-GPR was configured to collect multi-offset gathers at 30 mm intervals along the road during Site Visit 1 and at 15 mm intervals during Site Visit 2. The impulse GPR measured at 10 mm intervals.

Eight (8) sample locations (S1 to S8) were excavated during Site Visit 2 to determine the as-constructed depth of pavement layers and to collect material for moisture content determination. The locations of S1 to S4 were randomly positioned along the first half of the site. The pavement layers in these locations had been essentially knitted-together during

construction and could not be distinguished during sampling. Consequently the material samples for S1 to S4 were collected in 100 mm increments within the pavement and an additional sample was collected in the subgrade. Sample locations S5 to S8 were located in the second half of the site and the material was sampled within individual pavement layers and in the subgrade. Locations S5 and S6 were positioned either side of the TDR installation and were aligned laterally to match the NM-GPR run and the majority of TDR rod-probe sensors. As this was offset from the embedded plates and rods, the shielded TDR cables in this location were instead used for the common-offset GPR assessment of pavement permittivity. The position of S7 was selected randomly and S8 was targeted to the position of a developing pavement failure. The gravimetric moisture content of all samples was determined in the laboratory following test method Q102A *Standard moisture content of soil – oven drying* [52]. The volumetric moisture contents were calculated using these results and the dry density results recorded at the time of construction, which were approximately 2.2 tonnes per cubic metre for pavement layers and 2.0 tonnes per cubic metre for the subgrade.

5 Results and discussion

5.1. Site measurements

Figure 5 presents the response measured on one of the 32 NM-GPR channels during each site visit. It also shows the impulse GPR measurement collected during Site Visit 2 for comparison. These data have been corrected for time zero, background-removed and the distance scale has been zeroed at the approximate location of TDR sensors and metal reflectors. A Butterworth filter was applied to the NM-GPR data collected during Site Visit 1 to reduce the influence of high-frequency noise caused by a hardware issue, which has since been rectified. The comparison indicates that the impulse GPR is operating at a higher central frequency, providing crisp layer reflections but with a reduced penetration depth compared to the NM-GPR. A number of differences can also be seen at the start and end of the NM-GPR runs, most likely due to lateral misalignment between runs but possibly due to changes caused by moisture ingress.

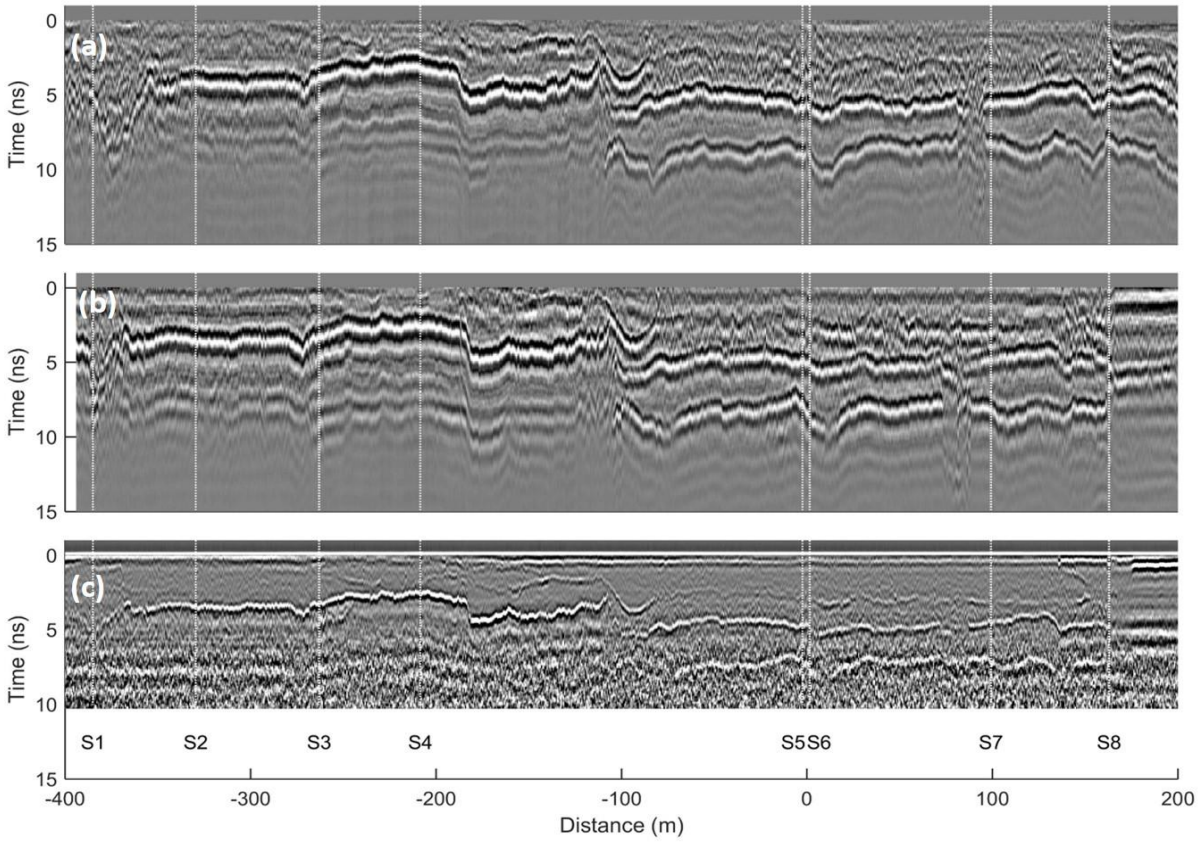

Figure 5: GPR scans along the test site for: (a) Site Visit 1 on 8 June 2015 using the NM-GPR and for Site Visit 2 on 19 May 2016 using the (b) NM-GPR and (c) impulse GPR. The approximate position of sample locations S1 to S8 are also indicated.

Figure 6 shows a screenshot during the RM-S1 analysis. It illustrates the measured multi-offset response (Figure 6 (a)), the optimised ray-path model determined at the current location (Figure 6 (b)) and an illustration and summary of the calculated layer depth, dipping angle, relative permittivity and predicted volumetric moisture content (Figure 6 (c)). The lower panel (Figure 6 (d)) illustrates the volumetric moisture content predictions for locations already analysed along the road. In this example the RM-S analysis was performed at one metre intervals along the road. This spacing can be varied as desired.

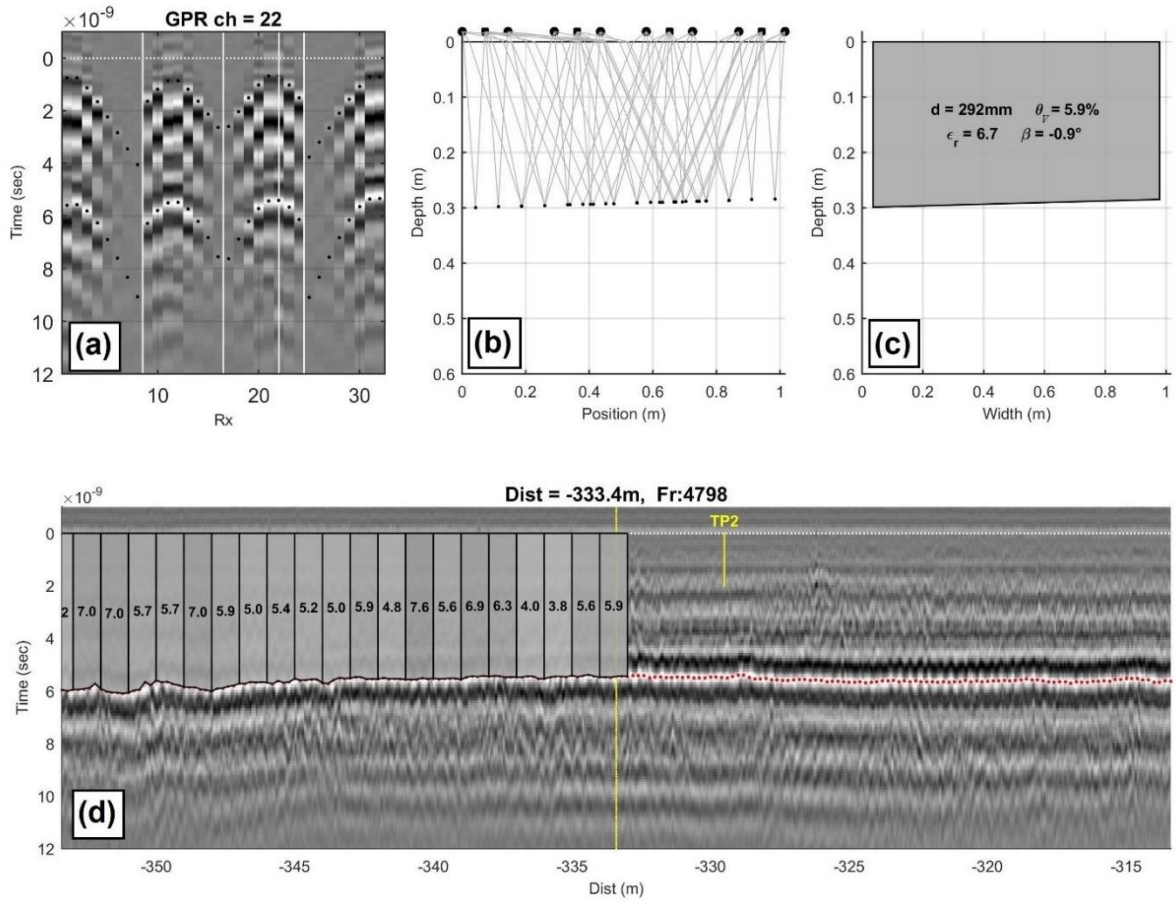

Figure 6: A screen shot during multi-offset analysis using the RM-S1 approach showing the: (a) measured WARR response with the airwave and optimised ray-path travel time predictions overlaid (black dots); (b) calculated ray-path geometries; (c) calculated layer depth *(d)*, volumetric moisture content *(θ_V)*, relative permittivity *(ε_r)* and dipping angle *(β)* at the current location; and (d) predicted volumetric moisture contents for analysed locations overlaid over a radargram of the selected channel with interface tracks also shown (red dots).

5.2. Layer depths, permittivity and moisture

Figure 7 presents the mean layer depth predictions determined using the RM-S1 approach for Site Visits 1 and 2. The findings of physical sampling are also shown for comparison and are summarised in Table 1. RM-S1 predictions that achieved a weak semblance result with the measured WARR response have been omitted. The interfaces have been numbered with depth and the permittivity and moisture predictions in Figures 8 and 9 also correspond to these interfaces.

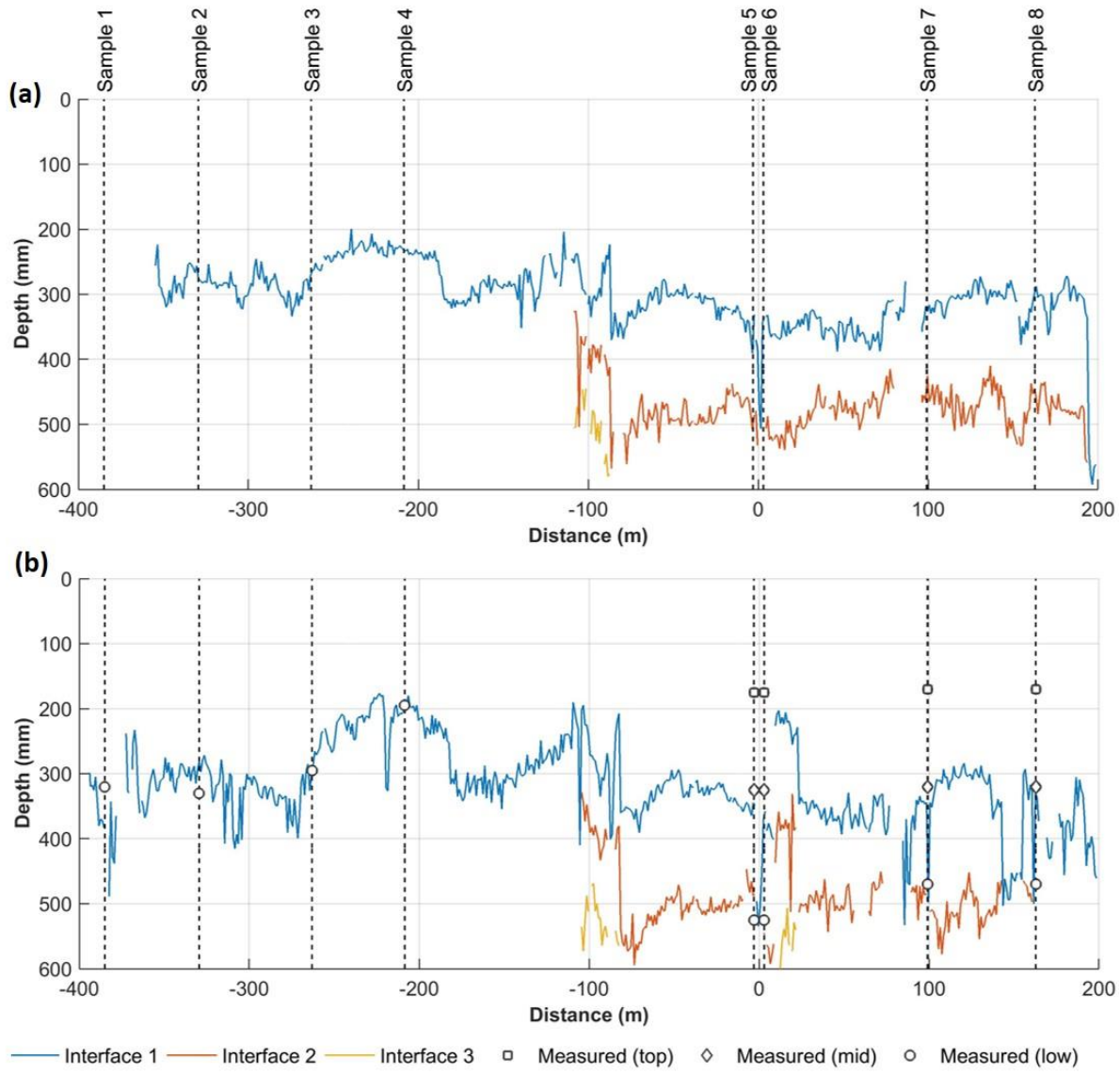

Figure 7: Layer depth predictions using the RM-S1 approach for (a) Site Visit 1 and (b) Site Visit 2.

Table 1: Depth to layer interfaces determined via physical sampling

Sample location	Interface depth			
	Surfacing (mm)	Base / Upper Sub-base (mm)	Upper Sub-base/ Lower Sub-base (mm)	Subgrade (mm)
S1	20	-	-	320
S2	20	-	-	330
S3	20	-	-	295
S4	20	-	-	195
S5	25	175	325	525
S6	25	175	325	525
S7	20	170	320	470
S8	20	170	320	-

Figure 8 presents the RM-S1 relative permittivity predictions for Site Visits 1 and 2 and shows the TDR and common-offset GPR measurements of pavement permittivity for comparison. The TDR measurements were analysed using the method of peaks [48]. The corresponding volumetric moisture content (θ_V) predictions presented in Figure 9 were calculated using the petro-physical relation developed previously [46]. The moisture content results determined via physical sampling are also shown for comparison in Figure 9 and are summarised in Table 2.

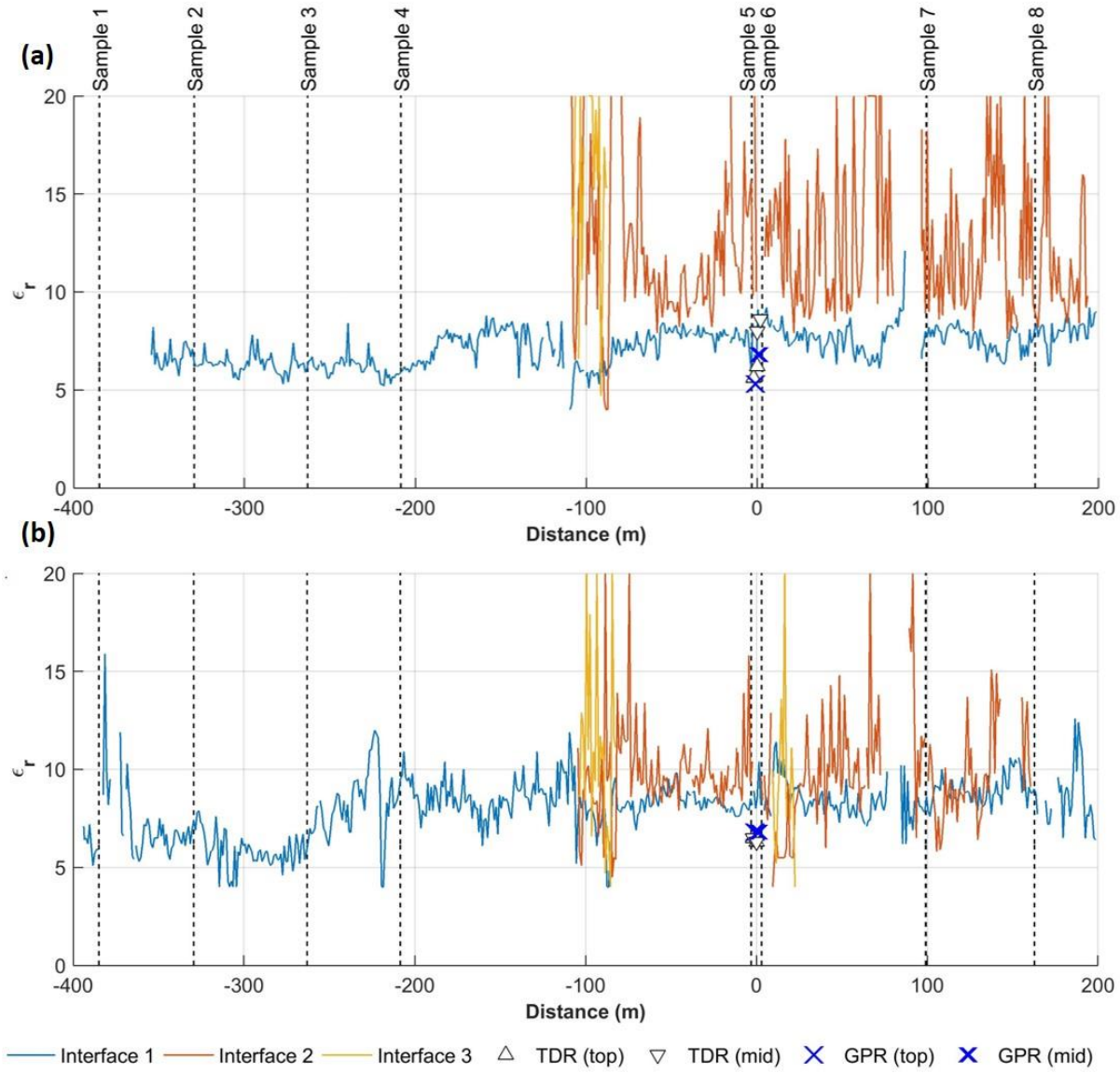

Figure 8: Layer permittivity values determined using the RM-S1 approach during (a) Site Visit 1 and (b) Site Visit 2.

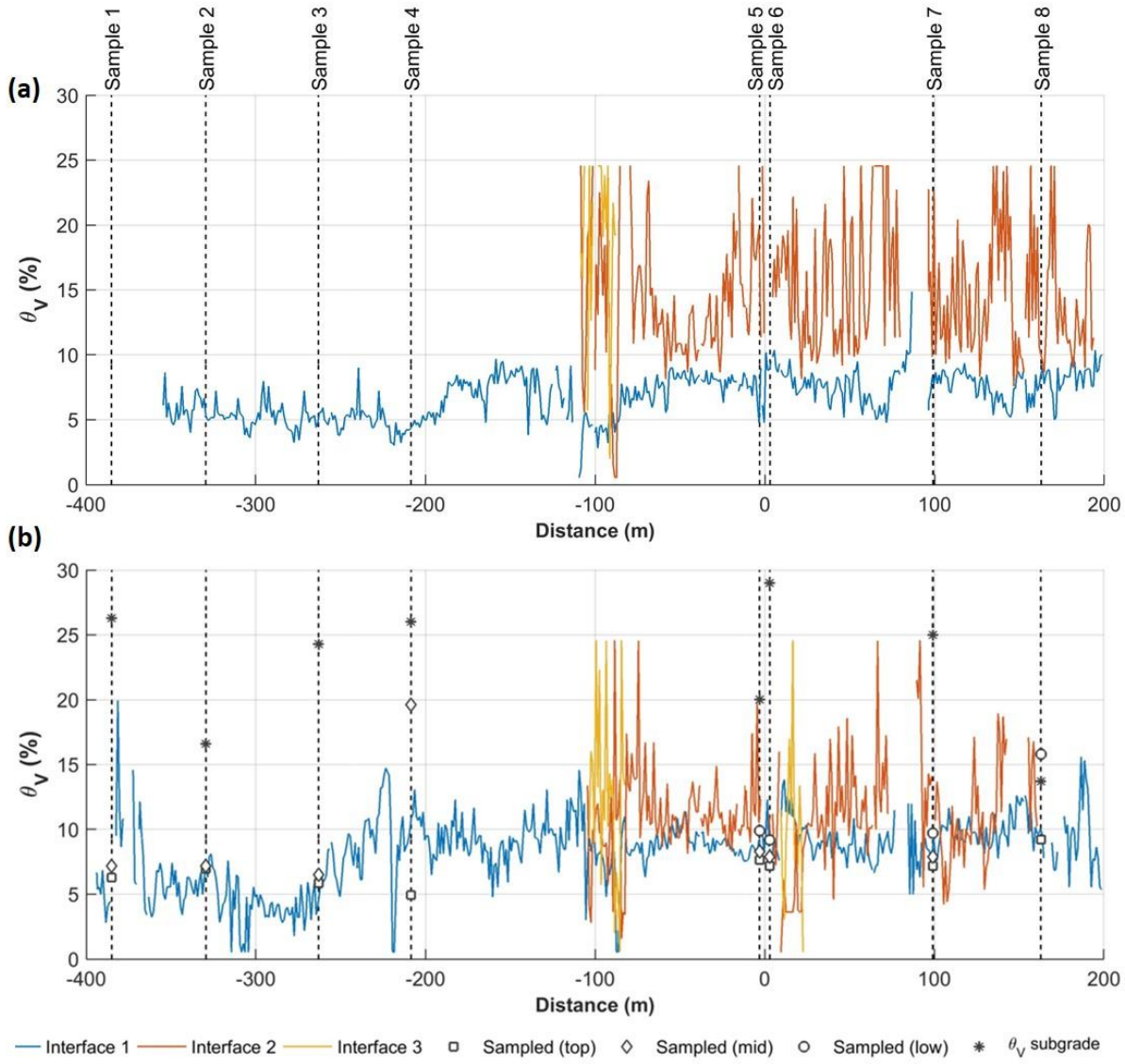

Figure 9: Volumetric moisture content predictions determined from permittivity results during (a) Site Visit 1 and (b) Site Visit 2.

Table 2: Volumetric moisture contents determined via physical sampling

Sample location	Volumetric moisture content (θ_V) (%)			
	Upper layer	Middle layer	Lower layer	Subgrade
	Sampled in 100 mm increments			
S1	6.3	7.2	7.7	29.2
S2	7.0	7.2	10.6	16.6
S3	5.9	6.5	10.6	24.3
S4	5.0	19.6	-	26.0
	Sampled in layers			
S5	7.7	8.3	9.9	20.0
S6	7.2	7.9	9.2	29.0
S7	7.2	7.9	9.7	25.0
S8	9.2	10.1	15.8	13.7

Overall the RM-S1 approach produced layer depth predictions that were relatively consistent with the physical sampling findings. There was some variability in places, most likely due to a combination of lateral misalignment between the runs sampling, lateral layer dip (as the mean layer depth is being reported), inaccuracies in selecting time zero in the multi-offset analysis, improper data fits by the analysis algorithms or simplifications within the ray-path modelling analysis that led to prediction errors. The most notable depth discrepancy was for sample location S1. Examination of the NM-GPR measurements revealed it was located in a change of construction with tapers in layer thicknesses both along and across the road, explaining why the algorithm struggled in this location.

There was also a good overall correlation between the RM-S1 volumetric moisture content predictions and the physical sampling results. In two locations, S4 and S8, sampling revealed a notable increase in moisture with pavement depth. For S4 a relatively low moisture content was measured in the top 100 mm of the pavement (θ_V = 5.0%) and a much higher moisture content was found in the bottom 75 mm (θ_V = 19.6%). In this location the RM-S1 approach predicted a mean value of approximately 12 % through the full pavement depth, which is consistent with the physical sampling findings. For S8 physical sampling identified an elevated

moisture content that increased from base (θ_V = 9.2 %) to upper sub-base (θ_V = 10.1 %) and lower sub-base (θ_V = 15.8 %) layers. It also uncovered that the subgrade in this location was not natural material but rather was an imported gravel over a culvert. As a result a dry density of 2.2 tonnes per cubic metre was used when calculating the volumetric moisture content in this location (θ_V = 13.7 %). As seen in Figure 5 the layer interface reflections in Site Visit 2 change significantly near S8 (Figure 5 (b) and (c)) compared to Site Visit 1 (Figure 5 (a)) with the subgrade interface disappearing, presumably due to the poor dielectric contrast of gravel-on-gravel. As a result it was not possible to predict the moisture content through the full pavement depth at S8 using RM-S1. Nonetheless the upper layer prediction at this location matched the physical sampling findings and moisture predictions down to subgrade on approach to S8 were consistent with the physical sampling findings.

5.3. Moisture monitoring along the site and over time

Comparisons of the RM-S1 permittivity and moisture predictions along the site, over time and compared to TDR and common-offset GPR measurements reveal a number of interesting trends. The mean permittivity down to Interface 1 determined using the RM-S1 approach started off relatively consistent along the site during Site Visit 1, as would be expected immediately after pavement construction (Figure 8 (a)). By the time of Site Visit 2 approximately 11 months later the permittivity down to this interface, and by inference the volumetric moisture content of the layer above, had increased slightly in most locations and to a greater extent in others resulting in a variable pavement moisture distribution along the site (Figure 8 (b)). The permittivity differential between upper and lower layers based on the RM-S1 analysis reduced over this period, as the moisture equalised between upper and lower layers. The TDR and common-offset GPR measurements also showed a similar trend over this period. During Site Visit 1 the permittivity results were higher based on deeper TDR sensors and deeper GPR point reflectors compared to upper sensors or reflectors (Figure 8 (a)). By the time of Site Visit 2 the permittivity at these deeper installations had decreased and those at the upper installations had increased slightly, becoming more similar over this period (Figure 8 (b)). However, while the TDR and common-offset GPR measurements showed a similar trend over time compared to RM-S, they also reported consistently lower permittivity results.

5.4. Reproducibility of results

To assess reproducibility of results, RM-S1 approach was applied to a second NM-GPR scan collected during Site Visit 2 and its predictions were compared to the first run (Figure 11). The comparison shows that the layer depth and moisture predictions were relatively consistent between repeat runs, however the moisture content predictions were more variable in places for the second and third layers. There also appears to be a longitudinal offset between the datasets in a number of locations. This was due to the temporarily-installed encoder on T03 slipping against the wheel on which it was mounted during the survey.

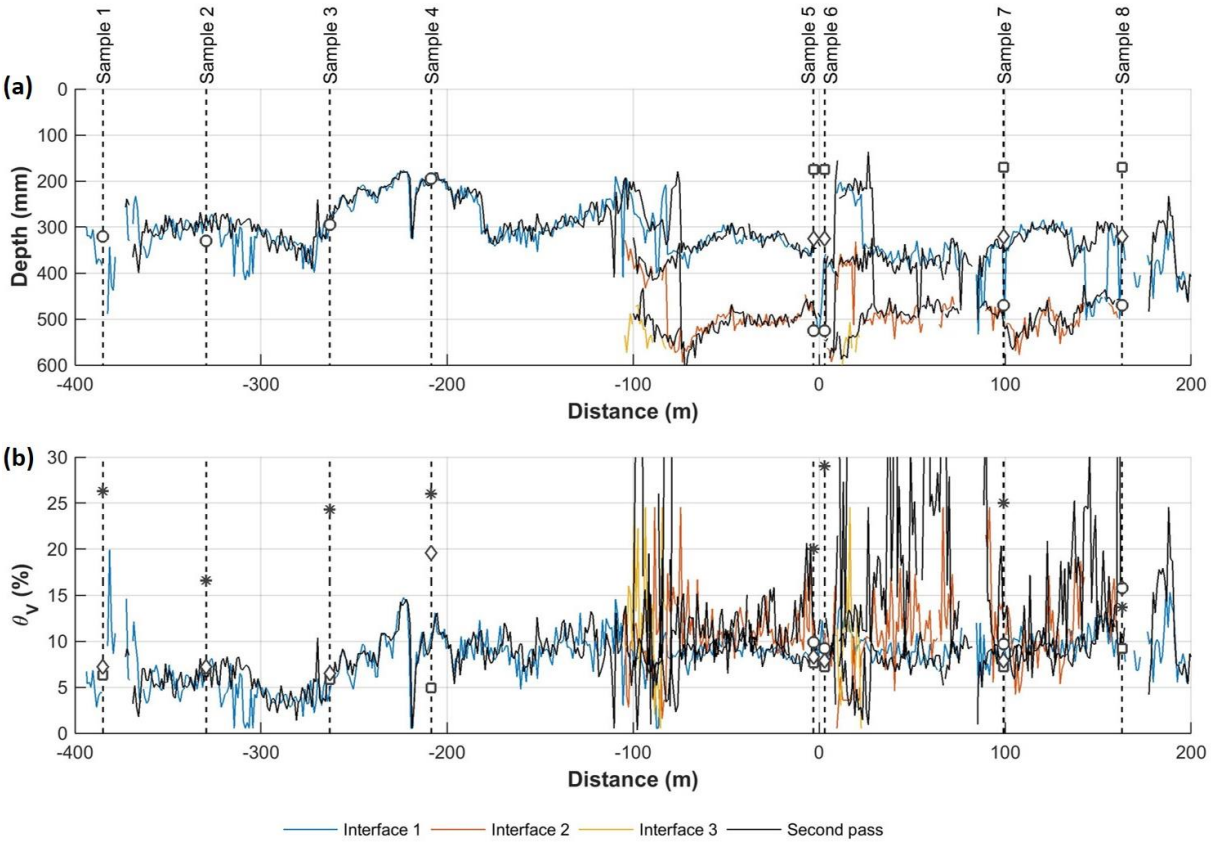

Figure 11: (a) Layer depths and (b) Moisture Content determined from two passes of the site during Site Visit 2 (first pass = coloured lines; second pass = black lines)

5.5. Other potential sources of error

As the RM-S approach relies on accurate tracking of interface reflections between near-transmitter receivers it tended to work best where these reflections were clear and consistent and became less reliable where interface reflections were intermittent, varied significantly across the array or were too closely spaced in time. In some instances the algorithm mistakenly

tracked an interface reflection from one WARR gather to a reverberation of another interface in the next WARR gather. At times it over-corrected a permittivity estimate in a lower layer due to an erroneous upper-layer result. Such errors or inaccuracies also compound, leading to the observed increase in variability for lower layer predictions. The assumption of constant permittivity across the array in the RM-S1 approach is also a potential source of error, as travel time variations across the array are interpreted as a sloping interface but may instead be due to a permittivity differential. Furthermore, the RM-S1 variant would not be well suited where there is an abrupt change in pavement cross-section across the lane, for example a pavement repair in the outer wheel path. Nonetheless, in the majority of cases for the site studied the algorithm successfully managed to fit the ray-path model and produced relatively consistent results that matched well with validation measurements.

5.6. Benefits, limitations and potential uses of the approach

A key benefit of the RM-S approach is that enables quasi-continuous permittivity calibration of pavement layers. It therefore provides an alternative to surface-reflection based methods with the benefit of calibrations based on measurements through the full depth of existing pavement layers. As a result this approach should be more reliable for calibrating the depth of pavement layers for older or more variable pavement materials, however further field testing will be required to verify this. Another benefit is that it largely follows the steps of conventional common-offset investigations, requiring little or no additional effort by the operator. The analysis spacing can be adjusted, enabling highly detailed project level investigations or quicker and more widely spaced analyses. As the data can also be collected at traffic speeds network level investigations should also be possible, however as layers need to be identified and tracked this would most likely be based on spot assessments at intervals along the road. One limitation of the approach compared to surface-reflection based methods is that tracking along the road has to be undertaken before the permittivity of layers can be calculated. In addition the approach can only be used down to the lowest coherent interface, which is usually the subgrade. As a result embedded TDR or other sensors would still be required to monitor subgrade moisture.

The RM-S technique has a number of potential applications. One use would be in combination with the Traffic Speed Deflectometer (TSD). While visual comparisons of TSD and NM-GPR data have previously been demonstrated [50, 53], the ability to calibrate layer depth estimates

and estimate pavement moisture content may be useful for relating the amount of pavement moisture to its influence on structural response. Use in combination with TDR monitoring stations may also be advantageous, enabling the temporal sampling benefits of TDR to be enhanced by improved spatial coverage. The approach may also be useful for forensic investigations of pavement failures by confirming and better quantifying suspected moisture ingress problems. It may also be useful for assessing or monitoring moisture change within flood-affected or new UBG pavements without the need for embedded sensors or physical sampling.

6 Conclusion

This study presents an initial field validation of the ray-path modelling-semblance (RM-S) approach which enables easier and more efficient analysis of multi-offset GPR data collected continuously along the road using 3D GPR equipment. The approach was successfully applied to predict the depth and volumetric moisture content of pavement layers along a recently-constructed site. Predictions using this approach matched well with physical measurements of layer depth and the moisture content of pavement layers. Permittivity predictions using the approach also followed similar trends over time compared to embedded TDR sensors and common-offset GPR measurements of buried reflectors, however those methods produced slightly lower permittivity values. Use of the approach to monitor pavement moisture along the site was demonstrated as was the reproducibility of results using the analysis procedure. The new approach enables quasi-continuous calibration of the permittivity of pavement layers based on multi-offset measurements and as a result may enable more reliable estimates of layer depth for older and more variable pavements. It may also be useful for a number of pavement moisture investigation and monitoring applications, a few examples of which have been suggested.

7 Acknowledgment

This work was funded under the National Asset Centre of Excellence (NACOE) program of research by the Department of Transport and Main Roads. The author expresses his sincere thanks to Dr. Bryan Reeves and Dr-Ing. Alexander Scheuermann for their assistance during this work and also to Habibullah Bhuyan for collecting the TDR measurements. This paper

contributes to the work of COST Action TU1208 ‘Civil Engineering applications of Ground Penetrating Radar’.

8 References

1. Oliver, J., *The Performance of Sprayed Seals*. 1999, ARRB Transport Research.
2. Martin, T., *Structural deterioration of sealed granular pavements in Australia.* Road & Transport Research, 2005. **14**(2): p. 3-15.
3. Charlier, R., et al., *Water influence on bearing capacity and pavement performance: Field observations*, in *Water in road structures: Movement, drainage and effects*, A. Dawson, Editor. 2009, Springer Science+Business Media B.V.: Nottingham. p. 175-192.
4. Lekarp, F., U. Isacsson, and A. Dawson, *State of the Art. 1: Resilient response of unbound aggregates.* Journal of Transportation Engineering, 2000. **126**(1): p. 66-75.
5. Austroads, *APRG Technical Note 13: Control of moisture in pavements during construction*. 2003, ARRB Transport Research: Sydney.
6. Robinson, D.A., et al., *Soil moisture measurement for ecological and hydrological watershed-scale observatories: A review.* Vadose Zone Journal, 2008. **7**(1): p. 358-389.
7. Vereecken, H., et al., *On the value of soil moisture measurements in vadose zone hydrology: A review.* Water Resources Research, 2008. **44**(W00D06): p. 1-21.
8. Dobriyal, P., et al., *A review of the methods available for estimating soil moisture and its implications for water resource management.* Journal of Hydrology, 2012. **458-459**: p. 110-117.
9. Huisman, J.A., et al., *Measuring soil water content with Ground Penetrating Radar: A review.* Vadose Zone Journal, 2003. **2**(4): p. 476-491.
10. Baran, E., *Use of time domain reflectometry for monitoring moisture changes in crushed rock pavements*, in *Symposium and workshop on time domain reflectometry in environmental, infrastructure and mining applications*. 1994, United States Bureau of Mines: Evanston, USA. p. 349-356.
11. Diefenderfer, B., I. Al-Qadi, and A. Loulizi, *Laboratory calibration and in situ measurements of moisture by using time-domain reflectometry probes.* Transportation Research Record: Journal of the Transportation Research Board, 2000. **1699**: p. 142-150.

12. Ekblad, J. and U. Isacsson, *Time-domain reflectometry measurements and soil-water characteristic curves of coarse granular materials used in road pavements.* Canadian Geotechnical Journal, 2007. **44**(7): p. 858-872.

13. Jiang, Y.J. and S.D. Tayabji, *Evaluation of in situ moisture content at long-term pavement performance seasonal monitoring program sites.* Transportation Research Record: Journal of the Transportation Research Board, 1999. **1655**: p. 118-126.

14. Richter, C.A., *Seasonal Variations in the Moduli of Unbound Pavement Layers*, in *Long-Term Pavement Performance Program*. 2006, Federal Highways Administration (FHWA), USA: McLean, USA.

15. Wright, W.C., et al., *Calibration of five-segment Time Domain Reflectometry probes for water content measurement in high density materials.* Geotechnical Testing Journal (GTJODJ), 2001. **24**(2): p. 172-184.

16. Elseifi, M., et al., *Performance of geocomposite membrane as pavement moisture barrier.* Transportation Research Record: Journal of the Transportation Research Board, 2001. **1772**: p. 168-173.

17. Berthelot, C., et al., *Use of structural asset management to evaluate road substructure drainage systems.* Transportation Research Record: Journal of the Transportation Research Board, 2009. **2101**: p. 44-52.

18. Walubita, L.F., et al., *Non-destructive testing technologies: Application of the Ground Penetrating Radar (GPR) to perpetual pavements.* Road Materials and Pavement Design, 2009. **10**(2): p. 259-286.

19. Topp, G.C., J.L. Davis, and A.P. Annan, *Electromagnetic determination of soil water content: Measurements in coaxial transmission lines.* Water Resources Research, 1980. **16**(3): p. 574-582.

20. Al-Qadi, I.L., S. Lahouar, and A. Loulizi, *GPR: From the state-of-the-art to the state-of-the-practice*, in *Non-Destructive Testing in Civil Engineering (NDT-CE 2003)*. 2003, NDT.net: Berlin.

21. Lahouar, S., et al., *Approach to determining in situ dielectric constant of pavements - Development and implementation at Interstate 81 in Virginia.* Transportation Research Record, 2002 (1806): p. 81-87.

22. Saarenketo, T. and T. Scullion, *Road evaluation with ground penetrating radar*. Journal of Applied Geophysics, 2000. **43**(2-4): p. 119-138.

23. Plati, C. and A. Loizos, *Estimation of in-situ density and moisture content in HMA pavements based on GPR trace reflection amplitude using different frequencies.* Journal of Applied Geophysics, 2013. **97**: p. 3-10.

24. Al-Qadi, I.L., et al., *Effective Approach to Improve Pavement Drainage Layers.* Journal of Transportation Engineering, 2004. **130**(5): p. 658-664.

25. Chanzy, A., et al., *Soil water content determination using a digital ground-penetrating radar*. Soil Science Society of America Journal, 1996. **60**(5): p. 1318-1326.

26. Du, S. and P. Rummel, *Reconnaissance studies of moisture in the subsurface with GPR*, in *5th International conference on Ground Penetrating Radar (GPR'94)*. 1994, Waterloo Centre for Groundwater Research, University of Waterloo: Kitchener, Canada. p. 1241-1248.

27. Gerhards, H., et al., *Continuous and simultaneous measurement of reflector depth and average soil-water content with multichannel ground-penetrating radar.* Geophysics, 2008. **73**(4): p. J15-J23.

28. Greaves, R.J., et al., *Velocity variations and water content estimated from multi-offset, ground-penetrating radar.* Geophysics, 1996. **61**(3): p. 683-695.

29. Sperl, C., H. Stanjek, and A. Berktold, *On-site measurement of the spatial distribution of soil water content with ground-penetrating radar*, in *Field Screening Europe: Proceedings of the first international conference on strategies and techniques for the investigations and monitoring of contaminated sites*, J. Gottleib, et al., Editors. 1997, Kluwer Academic Publishers. p. 157-160.

30. Steelman, C.M. and A.L. Endres, *Assessing vertical soil moisture dynamics using multi-frequency GPR common-midpoint soundings.* Journal of Hydrology, 2012. **436–437**: p. 51-66.

31. Emilsson, J., P. Englund, and J. Friborg, *Simple method for estimation of water content of roadbeds using multi-offset GPR*, in *9th International Conference on Ground Penetrating Radar (GPR-2002)*, K. Steven and L. Hua, Editors. 2002, SPIE: Santa Barbara, USA. p. 422-426.

32. Grote, K., et al., *Evaluation of infiltration in layered pavements using surface GPR reflection techniques.* Journal of Applied Geophysics, 2005. **57**(2): p. 129-153.

33. Hamrouche, R. and T. Saarenketo, *Improvement of a coreless method to calculate the average dielectric value of the whole asphalt layer of a road pavement*, in *15th International Conference on Ground Penetrating Radar (GPR-2014)*. 2014, IEEE: Brussels. p. 899-902.

34. Leng, Z. and I.L. Al-Qadi, *An innovative method for measuring pavement dielectric constant using the extended CMP method with two air-coupled GPR systems.* NDT&E International, 2014. **66**: p. 90-98.

35. De Pue, J., M. Van Meirvenne, and W.M. Cornelis, *Accounting for surface refraction in velocity semblance analysis with air-coupled GPR.* IEEE Journal of selected topics in applied earth observations and remote sensing, 2016. **9**(1): p. 60-73.

36. Zhao, S. and I.L. Al-Qadi, *Development of an analytic approach utilizing the extended common midpoint method to estimate asphalt pavement thickness with 3-D ground-penetrating radar.* NDT&E International, 2016. **78**: p. 29-36.

37. Dix, C.H., *Seismic velocities form surface measurements.* Geophysics, 1955. **20**(1): p. 68-86.

38. Fauchard, C., et al., *GPR performances for thickness calibration on road test sites.* NDT&E International, 2003. **36**(2): p. 67-75.

39. Liu, H. and M. Sato, *in situ measurement of pavement thickness and dielectric permittivity by GPR using an antenna array.* NDT&E International, 2014. **64**: p. 65-71.

40. Davis, J.L., et al., *Quantitative measurement of pavement structures using radar*, in *5th International conference on Ground Penetrating Radar*. 1994, Waterloo Centre for Groundwater Research: Kitchener, Canada. p. 319-334.

41. Reeves, B., *Noise Modulated GPR: Second generation technology*, in *15th International Conference on Ground Penetrating Radar (GPR-2014)*. 2014, IEEE: Brussels. p. 708-713.

42. Muller, W.B., A. Scheuermann, and B. Reeves, *Quantitative moisture measurement of road pavements using 3D GPR*, in *14th International Conference on Ground Penetrating Radar (GPR-2012)*. 2012, IEEE: Shanghai. p. 517-523.

43. Muller, W., *Self-correcting pavement layer depth estimates using 3D multi-offset ground penetrating radar (GPR)*, in *15th International Conference on Ground Penetrating Radar (GPR-2014)*. 2014, IEEE: Brussels. p. 887-892.

44. Muller, W. and X. Dérobert, *A comparison of phase-shift and one-port coaxial cell permittivity measurements for GPR applications*, in *7th International Workshop on Advanced Ground Penetrating Radar (IWAGPR-2013)*. 2013, IEEE: Nantes. p. 1-6.

45. Muller, W. and A. Scheuermann, *Optimising a modified free-space permittivity characterisation method for civil engineering applications.* Journal of Geophysics and Engineering, 2016. **13**(2016): p. S9-S18.

46. Muller, W., *Permittivity characterization of unbound granular pavement materials using a modified free-space approach.* Transportation Research Record: Journal of the Transportation Research Board, 2578, 93-101, Washington, D.C., 2016.

47. Department of Transport and Main Roads, *MRTS05 Unbound Pavements*, in *Transport and Main Roads Specifications*, Brisbane.

48. Muller, W.B., H. Bhuyan, and A. Scheuermann, *A comparison of modified free-space (MFS), GPR and TDR techniques for permittivity characterisation of unbound granular pavement materials.* Near Surface Geophysics, Accepted 13 July 2016. In press.

49. Burger, H.R., A.F. Sheehan, and C.H. Jones, *Introduction to Applied Geophysics: Exploring the shallow subsurface*. 2006, New York: W.W. Norton & Company Inc.

50. Muller, W.B., *A comparison of TSD, FWD and GPR field measurements*, in *International Symposium Non-Destructive Testing in Civil Engineering (NDT-CE 2015)*. 2015: Berlin.

51. Stork, C., *Reflection tomography in the postmigrated domain.* Geophysics, 1992. **57**(5): p. 680-692.

52. Department of Transport and Main Roads, *Material testing manual, 4th edition*, Brisbane.

53. Muller, W. and B. Reeves, *Comparing Traffic Speed Deflectometer and Noise-Modulated Ground Penetrating Radar data for rapid road pavement investigations*, in *14th International Conference on Ground Penetrating Radar (GPR-2012)*. 2012, IEEE: Shanghai. p. 502-509.